

# **OPTIMAL SYNTHESIS OF LINKAGES FOR KNEE JOINT SUPPORTING DEVICES**

**Ph.D. Thesis**

**RAMANPREET SINGH**

ID No. 2014RME9063



**DEPARTMENT OF MECHANICAL ENGINEERING  
MALAVIYA NATIONAL INSTITUTE OF TECHNOLOGY JAIPUR**

**October, 2018**

# **Optimal Synthesis of Linkages for Knee Joint Supporting Devices**

*Submitted in  
fulfillment of the requirements for the degree of*

*Doctor of Philosophy*

by

**Ramanpreet Singh**

ID:2014RME9063

Under the Supervision of  
Prof. Himanshu Chaudhary

and

Dr. Amit Kumar Singh



**DEPARTMENT OF MECHANICAL ENGINEERING  
MALAVIYA NATIONAL INSTITUTE OF TECHNOLOGY JAIPUR  
October, 2018**

© Malaviya National Institute of Technology Jaipur - 2018.

All rights reserved.

# DECLARATION

I, **Ramanpreet Singh**, declare that this thesis titled, “**OPTIMAL SYNTHESIS OF LINKAGES FOR KNEE JOINT SUPPORTING DEVICES**” and the work presented in it, are my own. I confirm that:

- This work was done wholly or mainly while in candidature for a research degree at this university.
- Where any part of this thesis has previously been submitted for a degree or any other qualification at this university or any other institution, this has been clearly stated.
- Where I have consulted the published work of others, this is always clearly attributed.
- Where I have quoted from the work of others, the source is always given. With the exception of such quotations, this thesis is entirely my own work.
- I have acknowledged all main sources of help.
- Where the thesis is based on work done by myself, jointly with others, I have made clear exactly what was done by others and what I have contributed myself.

Date: 31-10-2018

Ramanpreet Singh  
2014RME9063

## Certificate

This is to certify that the thesis entitled **Optimal Synthesis of Linkages for Knee Joint Supporting Devices** being submitted by **Mr. Ramanpreet Singh** to the Malaviya National Institute of Technology Jaipur for the award of the degree of **Doctor of Philosophy** is a bonafide record of original research work carried out by him under our supervision in conformity with rules and regulations of the institute.

The results contained in this thesis have not been submitted, in part or in full, to any other University or Institute for the award of any Degree or Diploma.

**Dr. Amit Kumar Singh**

Assistant Professor

Mechanical Engineering Department

Malaviya National Institute of

Technology Jaipur

Jaipur-302017, India

**Prof. Himanshu Chaudhary**

Professor

Mechanical Engineering Department

Malaviya National Institute of

Technology Jaipur

Jaipur-302017, India

## Acknowledgements

*“mayraa kee-aa kachhoo na ho-ay.  
kar hai raam ho-ay hai so-ay.”*

*‘I cannot do anything by my own actions.*

*Whatever the Lord does, that alone happens. ’-(Sri Guru Granth Sahib Ji)*

I am highly indebted to express extreme gratefulness to Almighty God for his immense grace on me by granting me the wisdom, health, and strength to undertake and complete this research task.

It is a great pleasure and privilege for me to express sincere gratitude to my thesis supervisors, Prof. Himanshu Chaudhary and Dr. Amit Kumar Singh, for their meticulous guidance and encouragement during the study. Expression of a deep sense of gratefulness is beyond words in front of the inspiring attitude of Dr. Himanshu Chaudhary. He showed me different ways to approach a research problem and the need to be persistent to accomplish any goal. Without his encouragement and constant guidance, I could not have finished this thesis. He is an excellent teacher and his logical way of thinking has been of great value for me.

I also take this opportunity to express my heartfelt thanks to the members of Departmental Research Evaluation Committee (DREC), Dr. T. C. Gupta and Dr. Dinesh Kumar, who spared their valuable time and experiences to evaluate my research plan and the synopsis.

I am thankful to Prof. Dilip Sharma, Head of the Mechanical Engineering Department, and his office team for providing facilities and conducive environment in the department throughout the study.

I extend my thanks to my senior research colleague Kailash Chaudhary, who with a keen interest accorded me advice and help at every step, whenever it was needed. Last, but not the least, my humble thanks goes to all colleagues and friends, Vimal Pathak, NRVN Gowaripathi Rao, Prem Singh, Prashant Athanker, Devesh Sharma, Manoj Gupta, Chitresh Nayak for their constant motivation and for believing in me. Finally, I cannot refrain myself from giving thanks to my parents, wife Rasmeet and daughter Harsirat who have surrendered their priority and time for me.

Ramanpreet Singh

Department of Mechanical Engineering

Malaviya National Institute of Technology Jaipur

## Abstract

Defect-free and gait-inspired linkage syntheses using optimization methodology are proposed in this study. The proposed method is applied to path generating four-bar and Stephenson III six-bar mechanisms for realistic applications. The applications are posed as optimization problems which are subjected to defect-specific constraints. It is well established that during synthesis of linkages kinematic defects are encountered. These defects are eliminated during synthesis by posing constraints which are presented and formulated in simplified form, for multiloop linkages. Using the proposed methodology, a defect-free four-bar linkage is designed and developed for the human knee supporting device. The device is validated for one gait cycle. Besides the design of four-bar linkage, a refinement scheme is proposed to reduce the computational effort which is appended to teaching–learning-based optimization (TLBO) for the first time. For Stephenson III six-bar linkage, a new loop-by-loop method for defect rectification is proposed, in which constraints are formulated for Loop I and Loop II, separately. The effectiveness of the proposed methodology is checked by considering the benchmark problem of straight line trajectory. Then, it is applied to design a six-bar linkage for human knee joint supporting device followed by its development as a solid model.

The gait–inspired linkage synthesis procedure is based on the human gait. The methodology is presented separately for assumed and natural human gait trajectories. When assumed gait is considered, the gait is divided into two stages; namely, the swing and the stance stages. The trajectories are derived with respect to the frame fixed to the ground. The swing stage minimized the Euclidean distance between the desired and generated swing limb trajectories; whereas, in the stance stage the Euclidean distance between the desired and generated stance limb trajectories is minimized. In this regard, a two-stage optimization problem is formulated. To solve the optimization problem, the proposed hybrid teaching-learning-particle swarm optimization (HTLPSO) and genetic algorithm (GA) is used. For natural trajectories, the two stages are linkage and position syntheses stages. Linkage is designed using the proposed methodology and solid models are developed for the designed linkages followed by stick diagrams for the whole gait cycle. The proposed synthesis method can be applied for synthesizing walking linkages that can be embedded in gait rehabilitation devices, exoskeleton, bipeds, etc. In addition, a novel shape is designed for the supporting knee joint device for persons with the injured knee in which the proposed four-bar linkage is embedded on the lateral and the medial sides of the knee joint while thigh and shank attachments are common to both the linkages. The proposed model can be used for providing support to the surrounding ligaments, tendons, and muscles of the injured knee.

# Contents

Declaration	i
Certificate	ii
Acknowledgements	iii
Abstract	iv
Contents	v
List of Figures	x
List of Tables	xviii
List of Symbols and Abbreviations	xx
<b>Chapter 1 Introduction</b>	<b>1</b>
1.1 Linkage synthesis	4
1.2 Nature-inspired algorithm	6
1.3 Contributions of the Research	8
1.4 Thesis Organization	8
1.5 Summary	10
<b>Chapter 2 Literature Survey</b>	<b>11</b>
2.1 Exoskeletons and Assistive Devices	11
2.1.1 Treadmill-Based Exoskeletons	11
2.1.2 Mobile Base Over-Ground Exoskeletons	15
2.1.3 Portable Exoskeletons	19
2.1.4 Assistive Devices	21
2.2 Walking Linkages	25
2.3 Planar Linkage Synthesis	29
2.3.1 Analytical Linkage Synthesis	31



2.3.2	Optimal Linkage Synthesis	35
2.3.2.1	Objective Functions	35
2.3.2.2	Local Optimization Algorithms	37
2.3.2.3	Global Optimization Algorithms	38
2.3.2.4	Hybrid Optimization Algorithms	39
2.4	Defect-Rectification	41
2.5	Summary	46
<b>Chapter 3</b>	<b>Analytical Synthesis of Planar Linkages</b>	49
3.1	Mathematical Modeling Using Complex-Number	49
3.1.1	Synthesis of Path Generating Four-Bar Linkage for Two Precision Points	53
3.1.2	Synthesis of Path Generating Four-Bar Linkage for Three Precision Points	54
3.1.3	Synthesis of Path Generating Four-Bar Linkage for Four Precision Points	55
3.2	Numerical Examples	58
3.2.1	Three Precision Point Synthesis	58
3.2.2	Four Precision Point Synthesis	61
3.3	Summary	63
<b>Chapter 4</b>	<b>Nature-Inspired Optimization Algorithms</b>	65
4.1	Teaching-Learning-Based Optimization (TLBO)	65
4.1.1	Teacher Phase	66
4.1.2	Learner Phase	66
4.2	Particle Swarm Optimization	69
4.3	Hybrid-Teaching Learning Particle Swarm Optimization (HTLPSO)	72
4.4	Numerical Examples	74

4.5	Application- Path Synthesis of Four-Bar Linkage	79
4.5.1	Case 1: Straight Line Trajectory	82
4.5.2	Case 2: Semi-Circular Trajectory	87
4.5.3	Case 3: Circular Trajectory	90
4.6	Summary	94
<b>Chapter 5</b>	<b>Optimal Linkage Synthesis</b>	<b>95</b>
5.1	Four-Bar Linkage Synthesis	96
5.1.1	Position Analysis of Four-Bar Linkage	96
5.1.2	Optimization Problem Formulation	97
5.1.3	Constraint Formulation	97
5.2	Six-Bar Linkage Synthesis	99
5.2.1	Position Analysis of Stephenson III Six-Bar Linkage	100
5.2.2	Optimization Problem Formulation for Six-Bar	101
5.2.3	Loop-by-Loop Constraint Formulation	101
	5.2.3.1 Formulation of Order, Circuit, and Branch Constraints	103
5.3	Optimization Algorithm	106
5.4	Numerical Examples	108
5.4.1	Example 1: Four-Bar Linkage for Straight Line Trajectory	108
5.4.2	Example 2: Four-Bar Linkage for Four-Bar Linkage for Knee Supporting Device	111
5.4.3	Example 3: Six-Bar for Straight Line Trajectory	118
5.4.4	Example 4: Six-Bar for Human Knee Supporting Device	125
5.5	Summary	129
<b>Chapter 6</b>	<b>Gait-Inspired Linkage Synthesis</b>	<b>131</b>

6.1 Gait-Inspired Linkage with Assumed Trajectories	133
6.1.1 Modeling of Exoskeleton Leg	133
6.1.2 Trajectory for LLE in Swing phase	136
6.1.3 Trajectory for HLL in Stance phase	137
6.1.4 Trajectory for HLL in Swing phase	137
6.1.5 Trajectory for LLE in Stance phase	138
6.1.6 Optimization Problem Formulation	138
6.1.6.1 First Stage- When Swing Limb Trajectory of LLE is Considered	139
6.1.6.2 Second Stage- When Roles of Swing- and Stance-Limbs are Exchanged	140
6.2 Gait-Inspired Linkage with Natural Trajectories	141
6.2.1 Kinematic Modeling of Four-Link Exoskeleton	142
6.2.2 Two-Stage Optimization Problem Formulation	144
6.3 Numerical Examples	147
6.3.1 Four-Bar Linkage with Assumed Trajectories	147
6.3.2 Four-Bar Linkage with Natural Trajectories	152
6.4 Summary	159
<b>Chapter 7 Topology Optimization of Supporting Device</b>	<b>161</b>
7.1 Design Specifications	161
7.2 Mechanism Analyses	162
7.2.1 Position Analysis	162
7.2.2 Static Force Analysis	163
7.3 Topology Optimization of Supporting Device	167
7.4 Results	168
7.5 Summary	173

<b>Chapter 8</b>	<b>Conclusions</b>	175
	<b>References</b>	179
<b>Appendix A</b>	Position Analysis of Planar Linkages	197
<b>Appendix B</b>	Refinement Scheme for TLBO	199
<b>Appendix C</b>	MATLAB® code for HTLPSO algorithm	205
<b>Appendix D</b>	Sagittal Position Analysis of Five-Link Robot: A Case Study	211
	Papers published based on this work	221
	Brief Bio-data of the author	223

## List of Figures

Fig. 1.1	Treadmill based robotic gait rehabilitation devices	2
Fig. 1.2	Over ground rehabilitation devices	2
Fig. 1.3	Portable rehabilitation devices (Chen et al., 2016)	3
Fig. 1.4	Functional knee brace (Paluska et al., 2007)	3
Fig. 1.5	Graphical synthesis for 3 precision positions (Hartenberg et al., 1964)	5
Fig. 1.6	Teardrop trajectory (Tsuge et al., 2016)	6
Fig 1.7	Swarm behavior in 2D space for nature-inspired algorithm (Saremi et al., 2017)	7
Fig. 2.1	ReoAmbulator™ (Courtesy Motorika USA Inc. )	12
Fig. 2.2	Driven gait orthosis (Colombo et al., 2000)	12
Fig. 2.3 a)	Lokohelp (Freivogel et al., 2008)	13
Fig. 2.3 b)	ALEX (Banala et al., 2009)	13
Fig. 2.3 c)	LOPES (Veneman et al., 2007)	13
Fig. 2.3 d)	PAM and POGO (Reinkensmeyer et al., 2002)	13
Fig. 2.4	a) Robotic Orthosis of University of Auckland b) Kinematic diagram of the robotic orthosis (Hussain et al., 2012)	14
Fig. 2.5	Robotic gait rehabilitation system (Seo et al., 2014)	15
Fig. 2.6	UCI gait mechanism (Tsuge and McCarthy, 2016)	15
Fig. 2.7	Conceptual model of gait rehabilitation system developed at NJIT Newark (Ji and Manna, 2008)	15
Fig. 2.8 a)	EXPOS developed by Sogang University (Kong and Jeon, 2006)	17
Fig. 2.8 b)	SUBAR developed by Sogang University (Kong et al., 2009)	17
Fig. 2.8 c)	LEER developed by SJTU (Guo et al., 2012)	17
Fig. 2.8 d)	NaTure-gaits (Wang et al., 2011)	17
Fig. 2.9	Parallelogram mechanism at ankle joint of WalkTrainer™ (Stauffer et al., 2009)	18
Fig. 2.10	Linkage mechanisms of MLLRE (Guo et al., 2014)	18
Fig. 2.11	Linkage gait trainer device (Kora et al., 2017)	18
Fig. 2.12 a)	ReWalk™ (Courtesy ReWalk Robotics, Inc)	20

Fig. 2.12 b)	Powered Orthosis of Vanderbilt University (Quintero et al., 2011)	20
Fig. 2.12 c)	Hybrid assistive limb (Kawamoto et al., 2009)	20
Fig. 2.12 d)	Modified motor-powered gait orthosis (Ohta et al., 2007)	20
Fig. 2.13	Powered gait orthosis (PGO)(Ruthenberg et al., 1997)	21
Fig. 2.14	Knee module of knee-ankle-foot robot(Chen et al., 2016)	21
Fig. 2.15 a)	Knee brace (Butler et al., 1983)	22
Fig. 2.15 b)	OAdjuster Osteoarthritis Knee Brace (Draganich et al., 2006)	22
Fig. 2.15 c)	Knee brace with geared hinge (Greenfield et al., 2017)	22
Fig. 2.15 d)	Adjustable Unloader Knee Brace (Hangalur et al., 2018)	22
Fig. 2.16	Knee-ankle-foot-orthosis (Jonathan et al., 2009)	23
Fig. 2.17	Linkage orthosis (Berkelman et al., 2007)	23
Fig. 2.18	Robot KAFO (Kawasaki et al., 2017)	24
Fig. 2.19	KAFO with actuator (Guo et al., 2011)	24
Fig. 2.20	Four-bar linkage knee actuator (Kim et al., 2015)	24
Fig. 2.21	Schematic of ERNIE knee actuator with spring attached in parallel (Yang et al., 2008)	25
Fig. 2.22	Series Compliant Articulated Robotic Leg (Hutter et al., 2011)	25
Fig. 2.23	Robot RAMone (Smit-Anseeuw et al., 2017)	25
Fig. 2.24	Planar bipedal testbed MABEL (Sreenath et al., 2011)	25
Fig. 2.25 a)	Single DOF planar biped (McKendry et al., 2008)	27
Fig. 2.25 b)	Stephenson III leg mechanism (Batayneh et al., 2013)	27
Fig. 2.26	a)Klann Linkage b)Klann linkage implemented in quadruped robot (Sheba et al., 2017)	27
Fig. 2.27	Stephenson II leg mechanism (Plecnik and McCarthy, 2016)	28
Fig. 2.28	Theo Janeson linkage used in the leg of wind beast (Giesbrecht et al., 2012)	28
Fig. 2.29	Eight-bar leg linkage for walking and stair climbing (Liu et al., 2017)	28
Fig. 2.30	Human-like eight-bar leg mechanism (Al-Araidah et al., 2011)	28
Fig. 2.31	Mechanism analysis and synthesis	29

Fig. 2.32	Construction of a) center point curve b) circle point curve (Hartenberg et al., 1964)	32
Fig. 2.33	Representation of a dyad (Erdman, 1981)	32
Fig. 2.34	Representation of triad at two precision positions (Subbian and Flugrad, 1994)	33
Fig. 2.35	Representation of RR chain for algebraic modeling (McCarthy et al., 2006)	34
Fig. 2.36	Combined paths a) rectilinear segment and a circular arc b) rectilinear segment, a circular arc, and a slanting line segment (Bulatovic and Orđevic, 2012)	36
Fig. 2.37	Circuits defect in four-bar mechanism	41
Fig. 2.38	Inversions of Stephenson six-bar mechanism a) Stephenson I b) Stephenson II c) Stephenson III	42
Fig. 3.1	Complex-vector representation of single bar during pure rotation	50
Fig. 3.2	Dyad representation of a four-bar linkage	50
Fig. 3.3	Schematic of Dyad for k consecutive positions	51
Fig. 3.4	Path generating four-bar linkage for two-precision points	53
Fig. 3.5	Path generating four-bar linkage for three-precision points	55
Fig. 3.6	Geometric construction of the compatibility linkage	57
Fig. 3.7	Synthesized four-bar linkage for three precision points	60
Fig. 3.8	Deviation of generated trajectory from desired trajectory	60
Fig. 3.9	Synthesized four-bar linkage for four precision-points	62
Fig. 3.10	Deviation between desired points and generated trajectory	62
Fig. 4.1	Algorithm for teaching-learning-based optimization	69
Fig. 4.2	Algorithm for particle swarm optimization	72
Fig. 4.3	Flowchart of hybrid-teaching learning particle swarm optimization (HTLPSO) algorithm	74
Fig. 4.4	Convergence of the best objective function values with respect to the number of function evaluations for a) Benchmark 1 b) Benchmark 2 c) Benchmark 3 d) Benchmark 4 e) Benchmark 5	78
Fig. 4.5	Comparison of standard deviation for all benchmark function	80

	using different algorithms	
Fig. 4.6	Four-bar linkage and definition of various notations	80
Fig. 4.7	Convergence between a) Best function values and number of function evaluations, b) Average function values and number of function evaluations for Case 1	83
Fig. 4.8	Generated trajectory and prescribed points	87
Fig. 4.9	Convergence between a) Best function values and number of function evaluations, b) Average function values and number of function evaluations for Case 2	88
Fig. 4.10	Generated trajectory and prescribed points	90
Fig. 4.11	Convergence between a) Best function values and number of function evaluations, b) Average function values and number of function evaluations for Case 3	91
Fig. 4.12	Generated trajectory and prescribed points	93
Fig. 5.1	Four-bar linkage and definition of various notations	96
Fig. 5.2	a) Linkage has no circuit defect b) Linkage has circuit defect	98
Fig. 5.3	Stephenson III six-bar path generator mechanism	100
Fig. 5.4	Accessible region of the external dyad of Stephenson III mechanism and coupler curve of constituent four-bar	102
Fig. 5.5	Toggle when angle between adjacent links a) $180^0$ b) $0^0$	104
Fig. 5.6	Description of circuit defect in Loop II	104
Fig. 5.7	Description of branch defect in Loop II	105
Fig. 5.8	Scheme for loop-by-loop defect rectification algorithm using optimization technique	107
Fig. 5.9	Convergence of the best objective function value in PSO, GA, and TLBO	109
Fig. 5.10	Convergence of average value in PSO, GA, and TLBO	109
Fig. 5.11	Generated trajectory and desired points of crank-rocker linkage	111
Fig. 5.12	Error between the desired and generated points	111
Fig. 5.13	Satisfaction of order constraint	111
Fig. 5.14	Satisfaction of circuit constraint	111



Fig. 5.15	Convergence of the best objective function value in PSO, GA, and TLBO	113
Fig. 5.16	Convergence of average function values in PSO, GA, and TLBO	113
Fig. 5.17	Defect-free crank-rocker mechanism designed using TLBO	114
Fig. 5.18	Prototype of human knee exoskeleton developed for the designed crank-rocker linkage	115
Fig. 5.19	Generated and desired trajectories of knee flexion/extension	115
Fig. 5.20	Error between the desired and generated points	115
Fig. 5.21	Simulation of the crank-rocker mechanism a) 1st position b) 3rd position c) 8th position d) 14th position	116
Fig. 5.22	Satisfaction of order constraint	117
Fig. 5.23	Satisfaction of circuit constraint	117
Fig. 5.24	Experimental validation of designed crank-rocker linkage for human knee exoskeleton	118
Fig. 5.25	Convergence of algorithm for unconstrained problem	119
Fig. 5.26	Convergence of algorithm for constrained problem	119
Fig. 5.27	Synthesized Stephenson III mechanism demonstrates a) circuit defect b) branch defect	121
Fig. 5.28	Synthesized Stephenson III mechanism with branch defect	122
Fig. 5.29	Defect-free Stephenson III mechanism	124
Fig. 5.30	Stick diagram of Stephenson III mechanism	125
Fig. 5.31	Satisfaction of transmission angle constraint	125
Fig. 5.32	Satisfaction of order constraint	125
Fig. 5.33	Synthesized defect free Stephenson III linkage	127
Fig. 5.34	Stick diagram of Stephenson III mechanism	128
Fig. 5.35	Satisfaction of transmission angle constraint	129
Fig. 5.36	Satisfaction of order constraint	129
Fig. 6.1	Contact points generated while rolling and gliding motion, when femur moves relative to tibia	133
Fig. 6.2	Lower limb exoskeleton model as four-bar linkage	134
Fig. 6.3	Various definitions of HLL and LLE, when LLE is in swing phase	134

Fig. 6.4	Various definition of LLE and HLL, when HLL is in swing phase	136
Fig. 6.5	Two-stage optimization formulation for position synthesis of exoskeleton lower limb	141
Fig. 6.6	a) Four-link exoskeleton for lower limb b) Various definitions for four-link exoskeleton	142
Fig. 6.7	Scheme of two-stage optimization problem	145
Fig. 6.8	Convergence of the function value in HTLPSO and GA for swing phase	149
Fig. 6.9	Convergence of the function value in HTLPSO and GA for support phase	150
Fig. 6.10	Comparison of foot trajectories in swing phase	150
Fig. 6.11	Comparison of hip-trajectories in support phase	151
Fig. 6.12	Stick diagram of a healthy lower limb and exoskeleton lower limb for one gait cycle	151
Fig. 6.13	CAD model of the designed linkage when embedded in an orthotic device	152
Fig. 6.14	a) Curve fitting of the Trajectory Data b) Marker indicating hip and ankle positions	153
Fig. 6.15	Scheme for selection of precision points	154
Fig. 6.16	Convergence of best objective function v/s number of function evaluations	155
Fig. 6.17	Generated trajectory and desired points of hip joint P during the first stage using PSO	155
Fig. 6.18	Tracking of precision points on the hip trajectory	156
Fig. 6.19	Convergence of best objective function v/s number of function evaluations	157
Fig. 6.20	Generated trajectory and desired points of hip point P during the second stage using PSO	157
Fig. 6.21	Four-bar linkage lower limb tracking 5 precision points on the hip trajectory	157
Fig. 6.22	Stick diagram of four-bar linkage lower limb exoskeleton for one gait cycle	158

Fig. 6.23	Conceptual design of four-bar knee exoskeleton	159
Fig. 7.1	Biomechanics of human knee joint a) joint angle b) joint torque	162
Fig. 7.2	Schematic diagram of the four-bar linkage for the knee exoskeleton	163
Fig. 7.3	Various definitions of four-bar linkage	164
Fig. 7.4	Free body diagram of four-bar linkage	165
Fig. 7.5	Base model of thigh attachment used for shape synthesis of knee exoskeleton	167
Fig. 7.6	Crank model for knee exoskeleton	168
Fig. 7.7	Rocker model for knee exoskeleton	168
Fig. 7.8	Base model of shank attachment used for shape synthesis of knee exoskeleton	168
Fig. 7.9	Schematic diagram for shape synthesis of knee exoskeleton	169
Fig. 7.10	Comparison between required actuating force of proposed knee linkage with literature	170
Fig. 7.11	Reaction forces in the knee exoskeleton for one gait cycle a) $F_{21x}$ and $F_{21y}$ b) $F_{32x}$ and $F_{32y}$ c) $F_{43x}$ and $F_{43y}$ d) $F_{14x}$ and $F_{14y}$	170-71
Fig. 7.12	Simulated model of thigh attachment	172
Fig. 7.13	Simulated model of crank	172
Fig. 7.14	Simulated model of shank attachment	172
Fig. 7.15	Simulated model of rocker	173
Fig. 7.16	CAD model of the supporting device with four-bar linkage	174
Fig. B.1	Scheme of the TLBO algorithm for defect-free synthesis of crank-rocker mechanism	201-02
Fig. D.1	Five link biped	211
Fig. D.2	Complete gait cycle	212
Fig. D.3	Various definitions for five link biped in DSP	216
Fig. D.4	x-displacement of hip and feet a) When $V_{h1} = V_{h2} = 2.4$ m/s b) When $V_{h1} = V_{h2} = 1.4$ m/s	217
Fig. D.5	Hip and lower limb trajectories when $V_{h1} = 0.4$ and $V_{h2} = 0.3$ m/s	218

Fig. D.6	Lower limb trajectories	218
Fig. D.7	Joint angle profiles	219
Fig. D.8	Stick diagram	219

## List of Tables

Table 3.1	Desired points for knee flexion (Sancibrian et al., 2016)	59
Table 4.1	Performance of PSO, TLBO,APSO, MFO,WOA, and HTPLSO	76
Table 4.2	Percentage of number of function evaluations require for HTLPSO in comparison with other algorithms	76
Table 4.3	Comparison of HTLPSO with various algorithms used in literature, for case 1	84
Table 4.4	Comparison of HTLPSO with various algorithms used in literature, for case 2	87
Table 4.5	Comparison of HTLPSO with various algorithms used in literature, for case 3	91
Table 4.6	Comparison of HTLPSO with TLBO in terms of number of function evaluations	93
Table 5.1	Desired points for vertical straight line (Acharyya and Mandal, 2009)	108
Table 5.2	Optimized parameters for the crank-rocker linkage	110
Table 5.3	Error between the desired and generated points	111
Table 5.4	Desired points for knee flexion (Sancibrian et al., 2016)	111
Table 5.5	Optimum design of crank-rocker mechanism using GA, PSO and TLBO	113
Table 5.6	Error between the desired and generated points	115
Table 5.7	The results of Stephenson III mechanism with and without constraints	123
Table 5.8	The results of Stephenson III mechanism when constraints are imposed	126
Table 6.1	Desired foot and hip trajectories (Mu and Wu, 2003; Appendix D for illustration)	147
Table 6.2	Optimized values of design variables of the first stage of optimization	148
Table 6.3	Optimized values of design variables of the second stage of optimization	148
Table 6.4	Selected precision points on the fitting curve	153- 54
Table 7.1	Dimensions of four-bar linkage	163

Table 7.2	Max value of forces in one gait cycle	171
Table 7.3	Weight of the components of knee supporting device	173
Table D.1	SSP and DSP geometric relations	215- 16

## List of Symbols and Abbreviations

$r_1$	<i>length of the stationary link</i>
$r_2$	<i>length of the crank</i>
$r_3$	<i>length of the coupler</i>
$r_4$	<i>length of the follower</i>
$l$	<i>length of AP in the direction of angle <math>\beta</math> with respect to coupler vector <math>\mathbf{r}_3</math> from A to B</i>
$A_x$	<i>x- coordinate of pivot <math>O_2</math></i>
$A_y$	<i>y- coordinate of pivot <math>O_2</math></i>
$\theta_1$	<i>angular position of the stationary link at any instant with respect to the X-axis</i>
$\theta_2^k$	<i>angular position of the crank corresponding to the <math>k^{\text{th}}</math> position of the coupler</i>
$\beta$	<i>coupler angle</i>
$P_x$	<i>x- coordinate of a point on the generated trajectory</i>
$P_y$	<i>y- coordinate of a point on the generated trajectory</i>
$P_{xd}$	<i>x- coordinate of a point on the desired trajectory</i>
$P_{yd}$	<i>y- coordinate of a point on the desired trajectory</i>
$L_i$	<i>lower bound on the <math>i^{\text{th}}</math> design variable</i>
$U_i$	<i>upper bound on the <math>i^{\text{th}}</math> design variable</i>
$k$	<i><math>k^{\text{th}}</math> position of the coupler</i>
$B_m$	<i>Boolean Function</i>
$p^m$	<i>constants with a high value of <math>10^4</math> to penalize the objective function, where <math>m = 1, \dots, 3</math></i>
$p$	<i>number of learners, i.e., population size</i>
$x_i$	<i><math>i^{\text{th}}</math> design variable, i.e., course offered to learner</i>
$n$	<i>number of design variables</i>
$x_{ij}$	<i>marks in the <math>i^{\text{th}}</math> course for <math>j^{\text{th}}</math> learner</i>
$t$	<i><math>t^{\text{th}}</math> iteration, i.e., a teaching-learning cycle</i>
$\mu_i$	<i>mean of the <math>i^{\text{th}}</math> course for whole class of learners</i>

$M_i$	<i>marks of the <math>i^{\text{th}}</math> course whose objective function value is minimum</i>
$f_j$	<i>objective function value of the <math>j^{\text{th}}</math> learner</i>
<i>rand</i>	<i>Any random number in the range of 0 and 1</i>
SCI	<i>Spinal Cord Injury</i>
ACL	<i>Anterior Cruciate Ligament</i>
TLBO	<i>Teaching-Learning-Based Optimization</i>
PSO	<i>Particle Swarm Optimization</i>
HTLPSO	<i>Hybrid Teaching-Learning Particle Swarm Optimization</i>
WOA	<i>Whale Optimization Algorithm</i>
MFO	<i>Moth Flame Optimization Algorithm</i>
GOA	<i>Grasshopper Optimization Algorithm</i>
TE	<i>Tracking error</i>
BWS	<i>Body-Weight System</i>
HLL	<i>Healthy lower limb</i>
LLE	<i>Lower limb exoskeleton</i>
SSP	<i>Single support phase</i>
DSP	<i>Double support phase</i>
$\{XOY\}$	<i>Used for frame</i>



**Introduction**

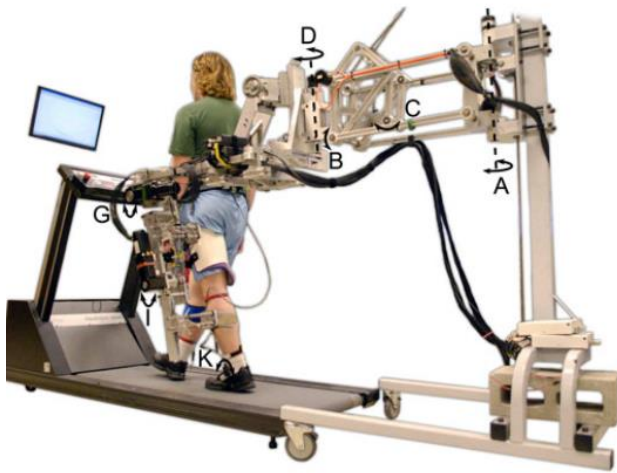
Aging is the natural process which can be seen around the world. It changes the body composition, muscle strength, and reduces capacity to perform routine activities efficiently. Furthermore, the elderly are more prone to diseases such as strokes, arthritis, central nervous system disorder, etc. According to the *Indian Aging Report 2017* (Giridhar G, 2017), arthritis and stroke cases amongst elderly may increase up to 55.9 million and 1.9 million, respectively, by 2030. These diseases may cause severe knee pain, gait disorder, loss of mobility, and dysfunctional lower limb. To provide relief to the patients, case-specific measures are taken such as manual physical therapy, use of robotic rehabilitation device/exoskeleton, supporting device/brace, etc.

The manual physical therapy is helpful for the patients to regain control over the lost functions. However, it is labor intensive and challenging for both the patients and the therapists. Besides, irregularities in the training sessions may not recover the patients' ambulation, and lost functions. Moreover, the therapy is not optimal because training time is limited and gait trajectories of the patients are not reproducible.

In contrast, robotic rehabilitation devices/exoskeletons may be used, as depicted in Figs 1.1-1.3. The exoskeleton may be considered as a device that can augment the functional performance of an able-bodied person (Dollar et al., 2008). The robotic exoskeletons/rehabilitation devices help the therapists to engage with patients, intervening in the therapy, and assessing the outcome of the therapy. In addition, it provides active and repetitive movements in a controlled manner that helps the patients in recovering ambulation (Dollar et al., 2008). In these devices, actuators are attached to the patient's legs that provide desired movement. Furthermore, these systems may include the hip and the knee degree of freedoms for providing motion to the patient's foot (Hesse et al., 2000). However, there are limitations in a number of rehabilitation devices such as they are bulky, complex, and expensive. Besides, they operate in confined areas and require special training to operate that makes them less amiable to therapists and small clinics.

The exoskeletons/devices are categorized as, treadmill-based, portable lower-limb, and over-ground rehabilitation devices, according to their type functions. The over-ground and portable rehabilitation robots include mechanical braces and computer-controlled actuators that allows the patients to experience realistic walking. However, the portable exoskeleton requires crutches for balancing. As opposed,

treadmill based-exoskeletons require a body-weight support system for balancing while exoskeleton provides support during leg movement. These devices are meant for patients with spinal cord injury, and dysfunctional lower limb.

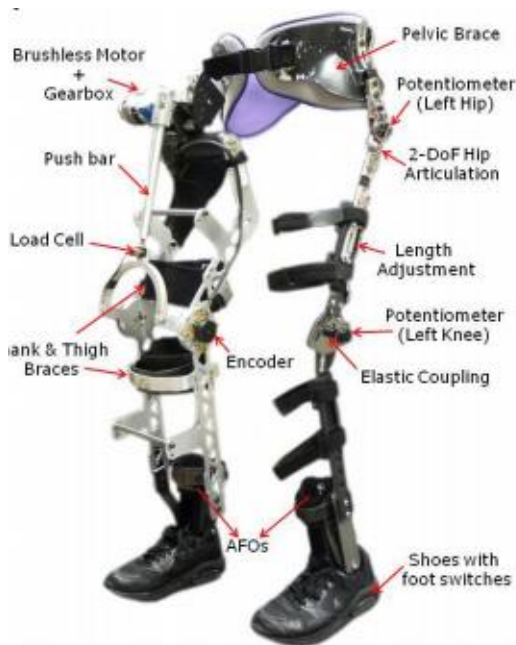


*a) ALEX II (Stegall et al., 2013)*



*b) (Kubo et al., 2011)*

**Fig. 1.1** Treadmill based robotic gait rehabilitation devices



*a) (Unluhisarcikli et al., 2011)*



*b) (Allemand et al., 2009)*

**Fig 1.2** Over ground rehabilitation devices



**Fig 1.3** Portable rehabilitation devices (Chen et al., 2016)

Deficient/reconstructed anterior cruciate ligaments (ACL) are considered as the essential factors at the beginning of knee osteoarthritis. Typically, orthotic devices/assistive devices are recommended for patients who have deficient or reconstructed ACL. Passive orthotic devices are used to prevent the knee injuries, instability in the knee, and uncontrolled motion of knee. Active orthoses are typically used to increase the ambulatory ability of a person. Sometimes, the term exoskeleton can be also used for referring assistive devices (Dollar et al., 2008). Figure 1.4 shows the functional knee orthotic devices/ braces which is typically preferred for reducing the knee instability. The knee orthotic/assisting devices are categorized as: prophylactic, functional, rehabilitative, and patella-femoral knee devices (Paluska et al., 2007).



**Fig 1.4** Functional knee brace (Paluska et al., 2007)

Linkage synthesis, associated actuator, and control are considered important factors for the feasibility and efficiency of the robotic exoskeletons and assistive devices. There are several methods to synthesize a linkage; thus selection, or,

determination of an accurate synthesis procedure, and the synthesized linkage that can be embedded in both the exoskeleton/ assistive devices are two distinct problems, besides control and actuator design.

The synthesis of linkages for the exoskeletons/assistive devices is a challenging task because these devices are attached to human lower limb to provide assistance. The lower limb has complex and rhythmic nature of gait that makes the synthesis task difficult. Furthermore, the kinematic defects such as change of circuit, branch, and order are some common challenges during synthesis of linkages (Guo et al., 2004 and Chase et al., 2006).

In this research work, several linkages are considered for the path synthesis task. For synthesizing the linkages, an optimization problem is formulated. The optimization problem minimizes the tracking error between the desired and the generated trajectories. Besides, defect-specific constraints are formulated to avoid defects that may occur during linkage synthesis. Additionally, for the multi-loop mechanism, i.e., six-bar, constraints are formulated, and a new loop-by-loop defect-rectification procedure is introduced.

There are several nature-inspired optimization algorithms available to solve the optimization problems. Among the nature-inspired algorithms, Teaching-Learning-Based Optimization algorithm (TLBO) and Particle Swarm Optimization algorithm (PSO) are explored for the linkage synthesis problems. The nature-inspired algorithms find a near-optimum solution and they do not require initial guess solution. A refinement scheme is presented for TLBO to increase its computational effort during optimization. Further, both the TLBO and PSO algorithms are merged to explore the effectiveness of the new hybrid algorithm which is named as Hybrid-Teaching Learning Particle Swarm Optimization algorithm (HTLPSO). The new algorithm is applied to synthesize the linkage for demonstrating the effectiveness of the proposed algorithm.

### **1.1 Linkage Synthesis**

Kinematic synthesis is the process of designing linkages to achieve the desired motion specification; Erdman and Sandor defined it as “the process of designing a mechanism to accomplish the desired task” (Erdman et al., 1984). The tasks in the kinematic synthesis are categorized as motion-, path-, and function-generation. In path-generation, a point on the floating link moves through the desired precision points, whereas, the floating link is guided through desired positions in motion generation. The functional relationship needs to be satisfied with the input and output link in case of function

generation. In addition, the areas of synthesis are grouped into two categories, namely, *type synthesis* and *dimensional synthesis*. The type synthesis deals with the type of mechanism, the number of links in the mechanism, the degree of freedom of the mechanism, etc., whereas dimensional synthesis deals in the determination of the significant dimensions and the starting position of the mechanism to accomplish the desired task. The methods for linkage synthesis are classified as, graphical, analytical, and numerical.

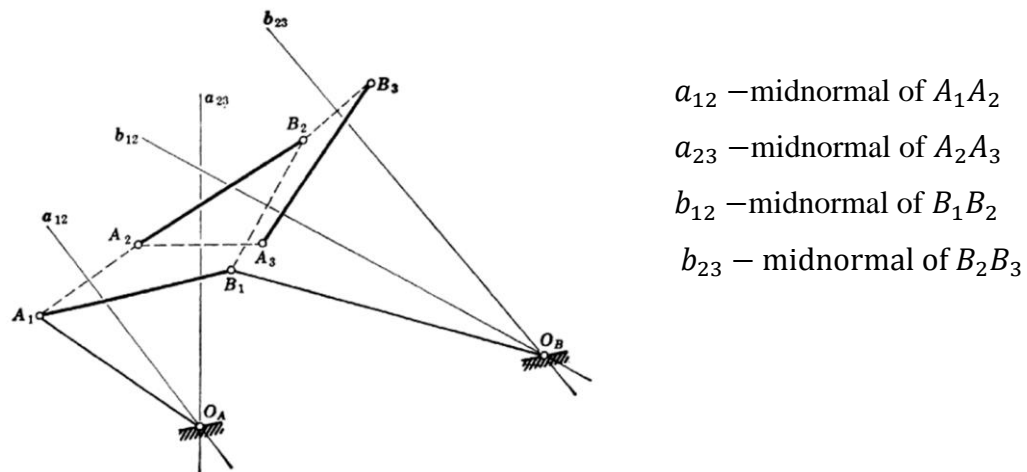


**Fig 1.5** Graphical synthesis for 3 precision positions (Hartenberg et al., 1964)

Figure 1.5 shows the graphical synthesis of four-bar linkage for 3 precision positions. The accuracy of graphical methods is restricted due to the drawing errors, though they are straightforward and quick. The synthesis process may have to repeat several times to achieve desirable results (Erdman et al., 1984). Alternatively, in case of four-bar linkage synthesis, the analytical method can be used; however, the number of desired precision points cannot be more than nine (Kim et al., 2016) and eleven for six-bar function generation synthesis (Plecnik et al., 2016). The numerical method may be used to solve this issue. Two types of numerical methods are reported. One method is to utilize the Atlas of coupler curves along with the Fourier series method (Ullah et al., 1997). The other method is to obtain the solution numerically by minimizing the optimization parameters. Typically, the tracking error (TE) is used as the objective function. It is the sum of the square of the Euclidean distance between the desired and the generated points, by the floating link.

The numerical method can be used for the linkage synthesis of exoskeleton /assistive device for gait rehabilitation. Typically, mechanisms for gait rehabilitation or

assistive devices are designed by taking an ankle trajectory in shape of a “teardrop,” as shown in Fig 1.6. This happens by transforming the coordinates of ankle joint relative

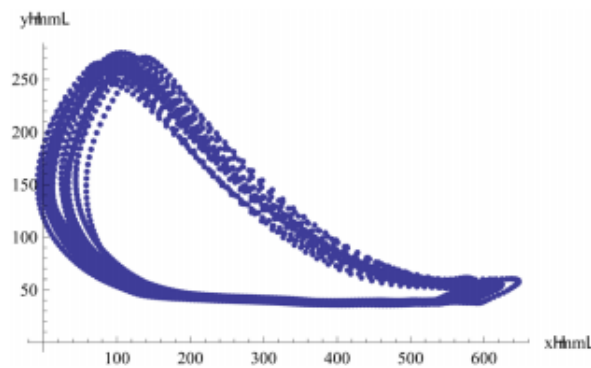


**Fig 1.6** Teardrop trajectory (Tsuge et al., 2016)

to the hip joint because it is believed that the synthesis procedure requires the hip joint to be stationary (Tsuge et al., 2016), and involves the solution of complex equations. Other methods to synthesize the knee joint supporting linkages are discussed in Chapter 2.

Besides, TE can be used as the objective function that may be subjected to specific constraints to avoid kinematic defects during linkage synthesis. Additionally, an optimization algorithm can be used to solve the optimization problem. There are various algorithms available, and not all kinds of algorithms can perform equally well in solving all optimization problems. This indicates that some optimizers may perform well for some set of problems while they fail to perform equally well for a different set of problems.

## **1.2 Nature-Inspired Algorithm**

One of the crucial element for the linkage synthesis using numerical method is to use an optimization algorithm. There are two types of the optimization algorithms available, namely, local optimization and global optimization algorithms. The local optimization algorithms such as exact gradient, primal-dual interior point, exact differentiation, etc., can be used. However, there is a non-zero probability of obtaining global optimum in classical optimization methods, and complexity is involved in calculating derivatives and Hessians. Thus, to refrain these problems, nature-inspired algorithms may be used.

The nature-inspired algorithms have become more popular for solving various non-linear problems in different fields, including path synthesis. There are various nature-inspired algorithms available that are used in distinct applications. One such algorithm is the genetic algorithm (GA) that can be used for solving highly nonlinear

problems to find the optimum solutions, and its efficiency may be increased by modifying its selection- and crossover procedure. Artificial bee colony (ABC), the teaching-learning-based optimization (TLBO) algorithm, the binary genetic algorithm (BGA), whale optimization algorithm (WOA), moth-flame optimization (MFO), and simulated annealing (SA) are among other algorithms that can be used for linkage synthesis. Figure 1.7 shows the behavior of swarms in 2D space for grasshopper optimization algorithm (GOA) which is a nature-inspired algorithm.

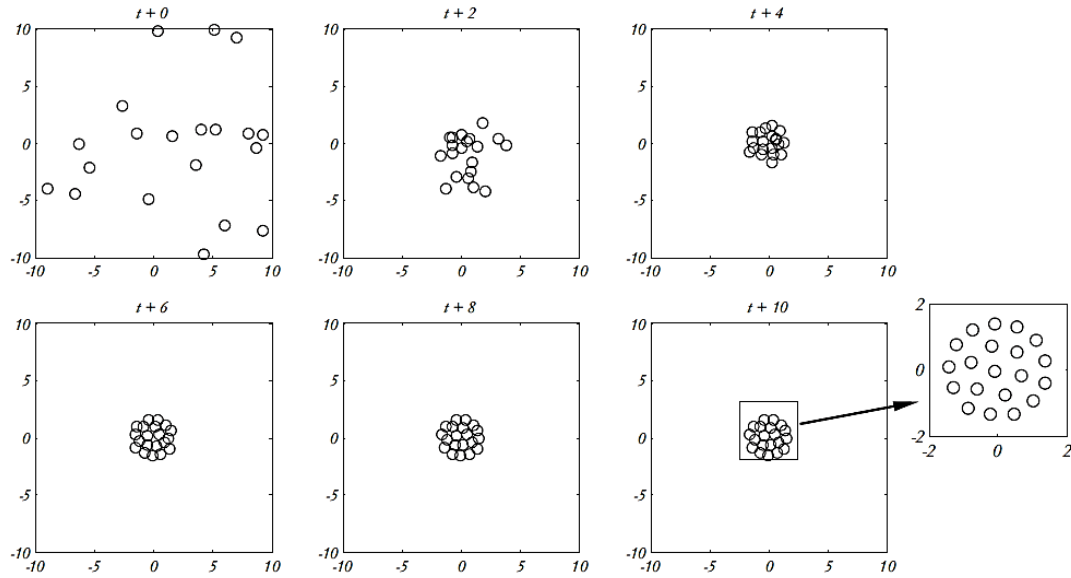


**Fig 1.7** Swarm behavior in 2D space for nature-inspired algorithm (Saremi et al., 2017)

These are population-based metaheuristic algorithms that work in two phases, namely, exploration phase and exploitation phase. Promoting any one of the exploration or exploitation may degrade the results of the other. A right balance between the two is required for the accurate approximation of the global optimum.

The optimization algorithms are applied to the teardrop trajectory of the ankle for one gait cycle while the hip joint remains stationary during linkage synthesis (Tsuge et al., 2016), that may lead to the complex form of equations. The change of circuit, branch, and order are some of the common defects that occur during linkage synthesis. Besides, single nature-inspired algorithms have used for synthesis. This motivates to develop a methodology that designs the linkage and then position, using the natural gait trajectories, which simultaneously rectify the kinematic defects occurring during linkage synthesis. Additionally, it also inspires to develop an algorithm that has the right

balance of exploration and exploitation, and refinement scheme to reduce the computational effort.

In this thesis, the mechanism synthesis principles are used to synthesize planar single- and multi-loop linkages and constraints are applied to rectify the kinematic defects. A new gait-based methodology for linkage synthesis, a hybrid optimization algorithm, and refinement schemes are among the other contributions of this research work.

### **1.3 Contributions of the Research**

The contributions of this research work are discussed below.

1. Defect-free synthesis of four- and six bar linkages is proposed in this study.
2. Reduced number of necessary and sufficient constraints are proposed to get a defect-free crank-rocker four-bar linkage.
3. An optimization problem for the synthesis of knee supporting linkage using a reduced number of necessary and sufficient constraints is proposed.
4. A new loop-by-loop defect-rectification procedure for the optimal synthesis of the Stephenson III path generator is proposed, and verified by synthesizing the Stephenson III mechanisms for knee supporting linkage.
5. A novel gait-inspired procedure to synthesize a four-bar knee supporting linkage to guide the walking movement is proposed.
6. In addition, refinement scheme is applied to well-established TLBO algorithm to reduce the computational effort.
7. A new hybrid-teaching learning particle swarm optimization (HTLPSO) algorithm is proposed for the path synthesis of the linkages.
8. A new design of the four-bar linkage knee supporting device based on required torque is proposed. In this design, the required peak force is significantly reduced.
9. Static force analysis of the proposed linkage is presented, and a procedure for the shape synthesis of the knee supporting device is proposed.

### **1.4 Thesis Organization**

The thesis contains eight chapters and five appendices, and is structured as follows:

#### **Chapter 1: Introduction**

The motivation and scope of the linkage synthesis for knee supporting devices and the nature-inspired algorithms are presented in this chapter. The linkage synthesis and



nature-inspired algorithms approaches are introduced. Besides, the significant contributions of the research work and structure of the thesis are outlined in this chapter.

## **Chapter 2: Literature Survey**

Research work on various methods of the analytical synthesis of planar and multi-loop linkages, optimal synthesis of linkages, defect-rectification, nature-inspired algorithms, hybrid algorithms is critically surveyed. Moreover, numerous types of supporting and gait rehabilitation devices are also explored to comprehend the feasibility of mechanism in these devices.

## **Chapter 3: Analytical Synthesis of Planar Linkages**

This chapter introduces the analytical synthesis techniques for planar linkages. Analytical synthesis approaches for three- and four-precision points are discussed for path generation task. Besides, the method to synthesize the supporting knee linkage for three- and four-precision points is demonstrated in this chapter.

## **Chapter 4: Nature-Inspired Optimization Algorithms**

In this chapter, traditional and nature-inspired optimization algorithms are discussed. It distinguishes the algorithmic and control parameters required to explore and exploit the entire design space to obtain an optimum solution, for the nature-inspired algorithms. The two algorithms, namely, particle swarm optimization algorithm (PSO) and teaching-learning-based optimization algorithm (TLBO) are explained, and their applications are discussed. Additionally, a new hybrid-teaching learning particle swarm optimization algorithm (HTLPSO) is proposed and applied to the path synthesis of linkages.

## **Chapter 5: Optimal Linkage Synthesis**

In this chapter, an optimization problem for the synthesis of knee supporting linkage using the reduced number of necessary and sufficient constraints to prevent kinematic defects is presented. Further, for the multi-loop mechanism, i.e., Stephenson III path generator, a new loop-by-loop defect-rectification procedure is proposed and its effectiveness is demonstrated by synthesizing the Stephenson III mechanisms for knee supporting linkage.

## **Chapter 6: Gait-Inspired Linkage Synthesis**

This chapter deals with the foot and the hip trajectories which are derived in the global frame of reference, for the stance and the swing phases. The synthesis problem is posed as a two-stage linkage synthesis problem. Based on the gait-inspired procedure, a knee supporting linkage is designed using the natural trajectories.

## **Chapter 7: Topology Optimization of Supporting Device**

This chapter demonstrates the static force analysis of the proposed four-bar linkage. A solid model of the knee supporting device which contains two four-bar linkages is prepared. The solid model is optimized using a CAD/CAE software to obtain the new shapes. The links' shapes of the thigh and the shank attachments of the knee supporting device are proposed.

## **Chapter 8: Conclusions**

This chapter briefs the significant results obtained in the research work and addresses the contributions of the present work. Based on the results, the future scope of the research work is also discussed.

## **Appendix A: Position Analysis of Planar Linkages**

In order to formulate the tracking error objective function for the optimum synthesis of linkages, coupler curve trajectories of the linkages are required. The solution of the loop-closure equation for the planar and the multi-loop linkages are explained in this appendix.

## **Appendix B: Refinement Scheme for TLBO**

In this appendix, refinement scheme is proposed and appended to the teaching-learning-based optimization algorithm.

## **Appendix C: MATLAB® code for HTLPSO algorithm**

In this appendix, MATLAB® codes for the hybrid teaching-learning particle swarm optimization algorithm are provided.

## **Appendix D: Sagittal Position Analysis for a Gait Cycle: A Case Study**

In this appendix, sagittal walking is completely analyzed for one gait cycle, by considering five-links. The methodology of position analysis while walking and results are presented for one gait cycle.

## **1.5 Summary**

This chapter describes the necessity and motivation of the present thesis. The kinematic synthesis of planar linkages and nature-inspired optimization algorithms are introduced. Besides, the significant contributions of this thesis are outlined, and brief information on the thesis structure is also provided in this chapter. This thesis contains eight chapters and five appendices to provide additional information.

## Literature Survey

This chapter deals with the review of the rehabilitation exoskeletons, assistive devices, and linkages used in them. The various methods for the synthesis of planar single and multiloop linkages along with the methods for defect-rectification are explored. Further, it also includes a critical review of the local, global, and hybrid optimization algorithms used in the synthesis of linkages.

### 2.1 Exoskeletons and Assistive Devices

The exoskeletons are used for augmenting the able-bodied and rehabilitation of physically challenged humans. The research on the exoskeleton for humans began in the late 1960s in the United States and Yugoslavia. The United States mainly focused on developing exoskeletons for able-bodied humans whereas Yugoslavia intended to develop exoskeletons for physically challenged humans (Dollar and Herr, 2008). The scope of this review is restricted to the rehabilitation exoskeletons and assistive devices. The exoskeletons can be categorized as treadmill-based exoskeletons, over-ground exoskeletons, and portable exoskeletons.

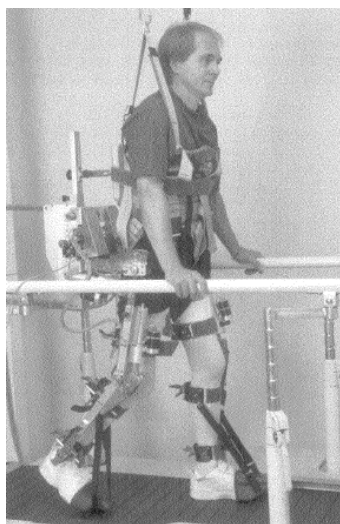
#### 2.1.1 Treadmill-Based Exoskeletons

The treadmill-based exoskeletons contain a treadmill, a body-weight system (BWS), and a leg orthoses. This type of exoskeletons is also known as immobile robots. They allow gait training in the confined areas. However, they are considered effective in gait recovery because they reduce gravitational forces on the legs (Chen et al., 2013). Various treadmill-based exoskeletons have been explored over the years. Typically, these are multi-degree of freedom devices that contain mechanisms, actuators, and control technology for manipulating users' lower limb motion while walking. Some of the treadmill-based rehabilitation devices are discussed here. The ReoAmbulator™ is commercialized by Motorika USA Inc. and powered to lift a patient from a wheelchair and transports the patient over the treadmill (West, 2004), shown in Fig 2.1. LOKOMAT is developed from the prototype of driven gait orthosis and is provided with virtual reality environment along with audio and visual biofeedback which is commercially available (Riener et al., 2005). The driven gait orthosis shown in Fig 2.2 (a) is a treadmill-based exoskeleton that actuates hip and knee, while the parallelogram linkage is used as an attachment for the trunk, shown in Fig 2.2 (b) The setup with parallelogram linkage allows controlled movement of legs in sagittal plane, and it does

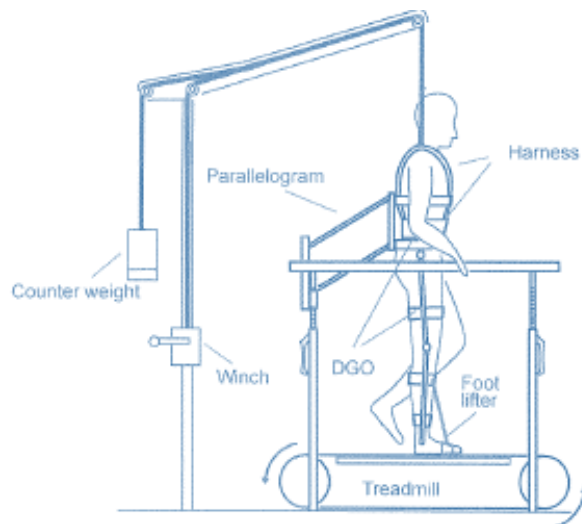
not restrict the patients to keep their trunk in vertical position themselves (Colombo et al., 2000).



**Fig. 2.1** ReoAmbulator™ (Courtesy Motorika USA Inc. )



**a)**



**b)**

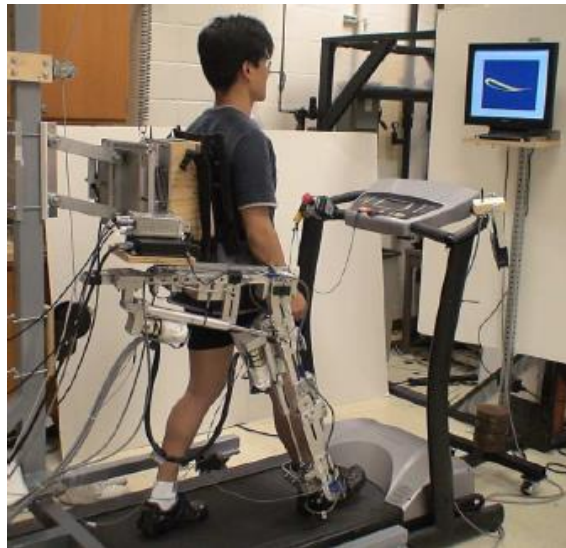
**Fig. 2.2** Driven gait orthosis (Colombo et al., 2000)

Besides, it utilizes a revolute joint between the thigh and lower leg attachments to allow the anterior-posterior motion of the leg. The LokoHelp is another treadmill-based exoskeleton that is fixed onto the powered treadmill to transmit the motion of the treadmill to the levers positioned on its both sides. These levers imitate the swing and the stance phases in the desired manner and guide the walking movement in a natural manner. Also, it consists of BWS located over the device, and orthoses which are attached to the levers, as shown in Fig 2.3(a). The ALEX (Active leg exoskeleton) is

another rehabilitation device that consists of a walker, trunk orthosis, thigh segment, shank segment, and foot segment as shown in Fig 2.3(b). Herein shank segment maintains one degree of freedom (DOF) with respect to the thigh segment while walking. Linear actuators are used at the hip and the knee joints, and force field controller is used for assisting the patients (Banala et al., 2007).



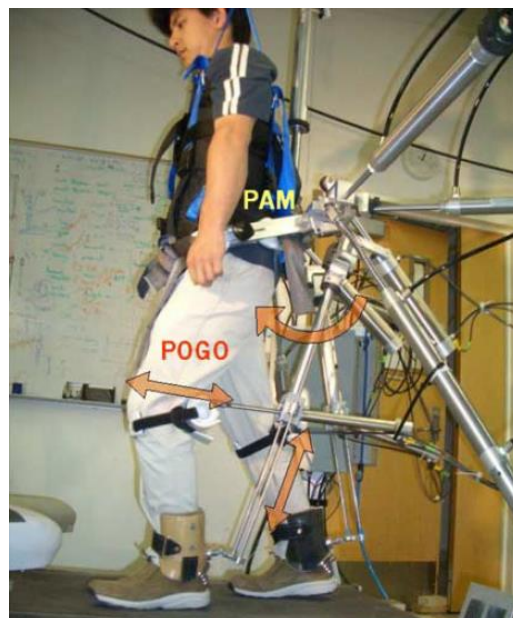
*a)*



*b)*



*c)*



*d)*

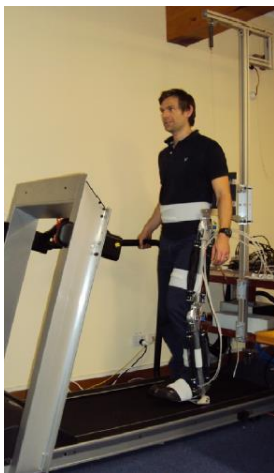
**Fig 2.3** Treadmill-based exoskeletons *a)* Lokohelp (Freivogel et al., 2008)

*b)* ALEX (Banala et al., 2009)

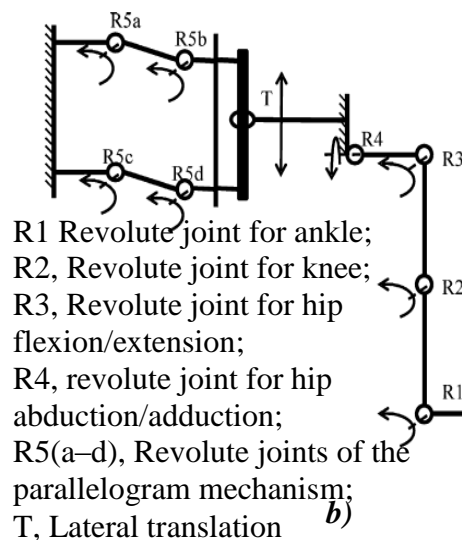
*c)* LOPES (Veneman et al., 2007)

*d)* PAM and POGO (Reinkensmeyer et al., 2002)

The LOPES (Lower extremity powered exoskeleton) exoskeleton is also used for gait rehabilitation which contains two rotational actuated joints at the hip joint and one at the knee joint. In this exoskeleton, no additional DOF or motion ranges are required to track patient's motion because the exoskeleton moves parallel to the legs of the patient (Veneman et al., 2007). Figure 2.3(c) shows the LOPES exoskeleton wherein thigh, and shank segments are connected by a revolute joint. The Pelvic Assist Manipulator (PAM) controls natural pelvic motion, and the Pneumatically Operated Gait Orthosis (POGO) which is attached to PAM uses linear actuators to move patient's pelvis and legs for training over the treadmill, shown in Fig 2.3(d) (Reinkensmeyer et al., 2002). In contrast, a compliant robotic orthosis developed at the University of Auckland used pneumatic muscles actuator to actuate the hip and knee joints in the sagittal plane as shown in Fig 2.4 (a). Besides, the orthosis allows vertical and lateral translations of the trunk through passive mechanisms as shown in Fig 2.4 (b). Like other exoskeletons, this orthosis also uses a revolute joint for knee flexion/extension in the sagittal plane (Hussain et al., 2012). The robotic gait rehabilitation systems are also developed for patients suffering from hemiplegia. This system supports the torque of the weak limb of the patient. Figure 2.5 shows the robotic gait rehabilitation system that has actuators at the hip and knee joints. Also, the system has 3 DOFs for each leg; the revolute joint is considered at the knee of the system (Seo et al., 2014).



a)



b)

**Fig. 2.4** a) Robotic Orthosis of University of Auckland b) Kinematic diagram of the robotic orthosis (Hussain et al., 2012)

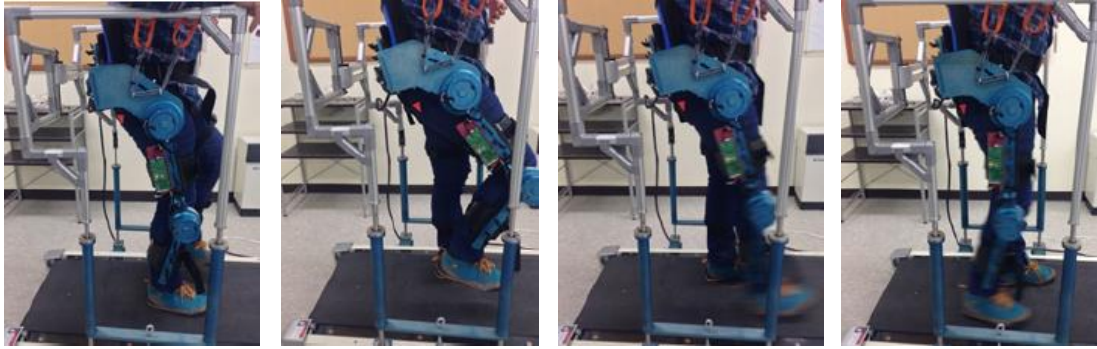


**Fig. 2.5** Robotic gait rehabilitation system (Seo et al., 2014)

These treadmill-based gait rehabilitation systems have multi-degree of freedom; however, they use a single-axis revolute joint at the knee which allows only rotational motion. Therefore, to select the best mechanism, it is vital to comprehend the biomechanics of the knee joint and its coordination with the hip and ankle joints. Besides, the mechanisms for these devices are designed using ‘tear-drop’ trajectory in which the hip joint is considered stationary. As opposed to these exoskeletons, UCI gait mechanism (Tsuge and McCarthy, 2016), Fig 2.6, and NJIT gait rehabilitation system (Ji and Manna, 2008), Fig 2.7, have six- and four-bar linkages, respectively, which are utilized for the whole limb. In addition, the treadmill-based exoskeletons are bulky, and they are often used in rehabilitation centers and hospitals. The other categories of exoskeletons are over-ground and portable exoskeletons.

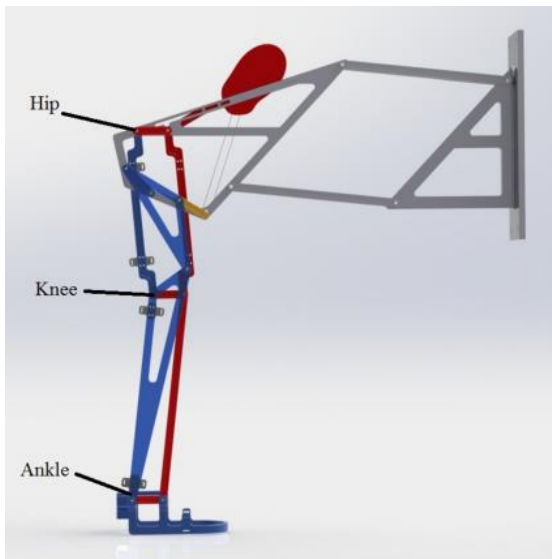


**Fig. 2.6** UCI gait mechanism (Tsuge and McCarthy, 2016)

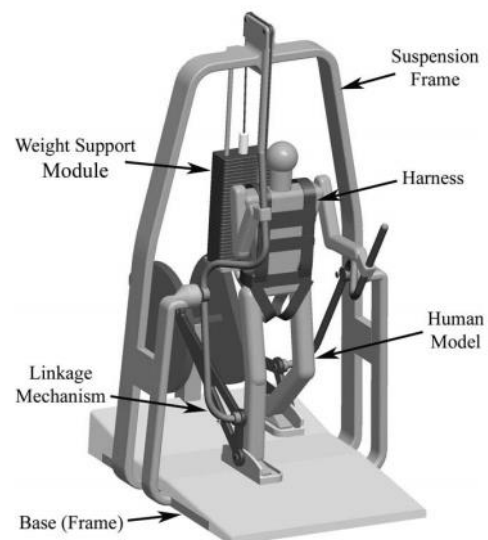


**Fig. 2.7** Conceptual model of gait rehabilitation system developed at NJIT Newark (Ji and Manna, 2008)

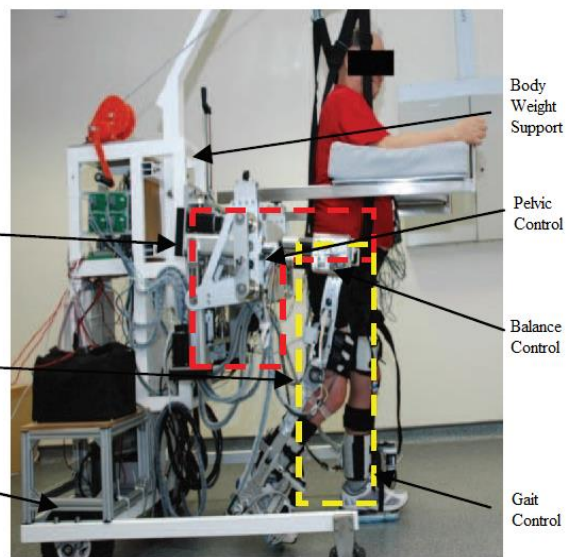
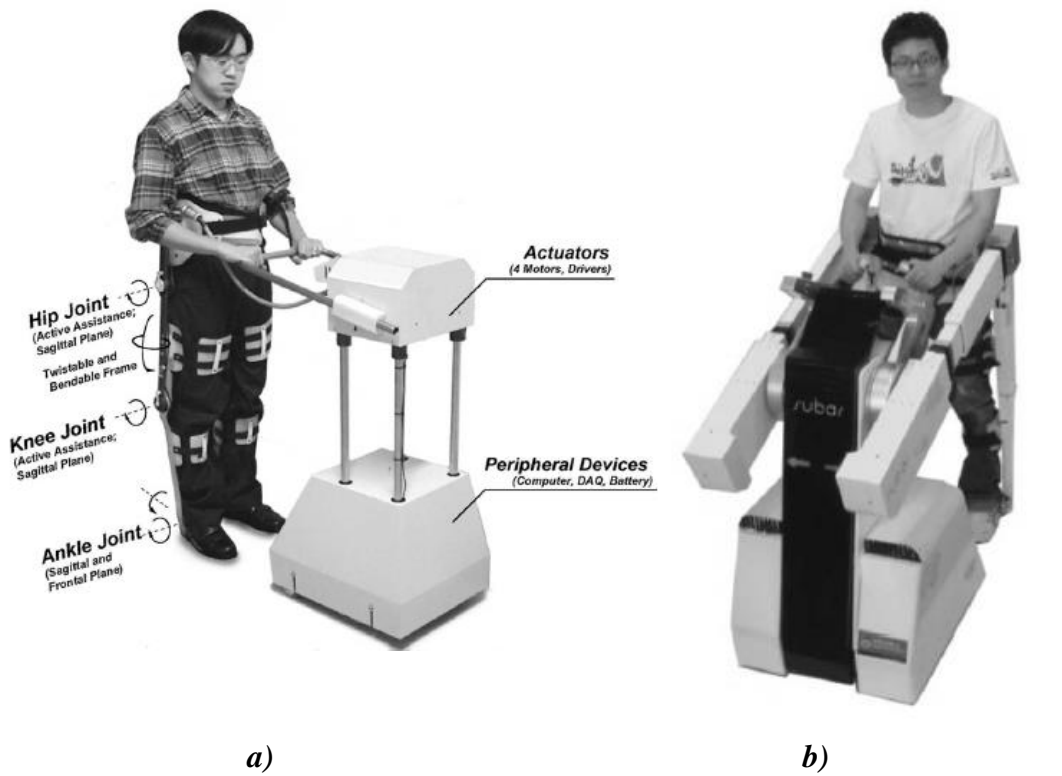
## 2.1.2 Mobile Base Over-Ground Exoskeletons

The mobile base over-ground rehabilitation exoskeletons may consist of a mobile base, a BWS, and joint level assistance to provide comfort to the patients for rehabilitation. They do not restrict training to the treadmill or a confined area rather they allow patients to regain their natural walk. In addition, the patients move voluntarily despite considering a predetermined pattern for moving. Some of the over-ground exoskeletons are explored to identify the mechanism used for the joints.

EXPOS is developed by Sogang University, as shown in Fig 2.8 (a), especially for the elderly and the patients'. It is an over-ground exoskeleton that contains a caster walker for balancing during rehabilitation training. It is a multi-DOF device which uses four actuators for driving the wheels of the caster walker to aid the patient's motion; while the hip and knee joints are actively assisted by servo motor controls and ankle joint is passively assisted by shock absorbers. The device pneumatically actuates the handle of caster walker for synchronizing the up and down motions during walking on the levelled ground. Moreover, the EXPOS has air bladders that are wrapped by the braces and attached on the muscle. The pressure sensors are attached to those braces for measuring any change in the pressure of the air bladder with the muscle movement (Kong and Jeon, 2006). Another version of the EXPOS which is known as SUBAR (Sogang University biomedical assistive robot), as shown in Fig 2.8 (b), may also be used for over-ground rehabilitation. This version of the exoskeleton has improved transmission mechanism and actuating power for providing effective assistance (Kong et al., 2009). LEER (Lower Extremity Exoskeleton Robot), NatTure-gaits, WalkTrainer<sup>TM</sup>, and Kine Assist robotic device are among other rehabilitation devices which may also be used.

Figure 2.8 (c) shows the LEER device developed by a group of researchers at Shanghai Jiao Tong University in China. The device contains a mobile platform, BWS, powered hip and knee joints embedded in orthoses. The joint's movement in the device is assisted by force provided by the exoskeleton which also assists the weaker muscle to complete the desired movement (Guo et al., 2012). This device also uses revolute joints at knee and ankle. Another exoskeleton with the mobile platform is NaTure-gaits (natural and tunable rehabilitation gait system) as shown in Fig 2.8 (d) can also be used. One of its notable features is, it provides 6 DOF for assisting pelvic motion which is





**a)** *EXPOS* developed by Sogang University (Kong and Jeon, 2006)

**b)** *SUBAR* developed by Sogang University (Kong et al., 2009)

**c)** *LEER* developed by SJTU (Guo et al., 2012)

**d)** *NaTUre-gaits* (Wang et al., 2011)

important in clinical rehabilitation (Wang et al., 2011). The same feature is observed in WalkTrainer™ developed at Laboratoire des Systemes Robotiques (Ecole Polytechnique Federale de Lausanne) for gait rehabilitation. The system contains a deambulator, a BWS, a pelvis orthosis, electrostimulator, and two leg orthoses. Besides, the thigh and leg segments are connected through revolute joint, and ankle joint is actuated through powered parallelogram mechanism as shown in Fig 2.9 (Bouri et al., 2006; Stauffer et al., 2009). KineAssist may also be used for rehabilitation that contains a trunk and pelvis mechanism for allowing the natural walk and balance exercises (Peshkin et al., 2005). A compact mobile lower limb robotic exoskeleton (MLLRE) and linkage design gait trainer (LGT) are among other mobile exoskeletons that use linkage

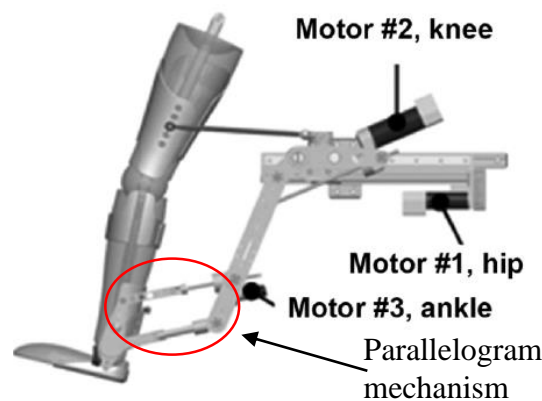


**Fig. 2.9** Parallelogram mechanism at ankle joint of WalkTrainer™ (Stauffer et al., 2009)

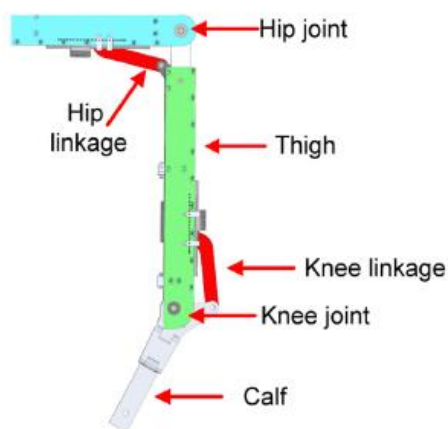


**Fig. 2.10** Linkage mechanisms of MLLRE (Guo et al., 2014)



**Fig. 2.11** Linkage gait trainer device (Kora et al., 2017)

mechanisms at joints and lower limb, respectively. The linkage mechanism used in MLLRE use offset slider-crank mechanisms for actuating the hip and knee joints, as shown in Fig 2.10 (Guo et al., 2014). In contrast, a passive linkage mechanism can also be used for the whole lower limb in the caster walker to rehabilitate gait, shown in Fig 2.11 (Kora et al., 2017).

It is found that the over-ground exoskeletons with mobile base have multi DOFs, and they use single axis revolute joint between the thigh and lower leg segments of the exoskeleton. Further, in some of the devices, robotic orthoses provide motion to hip, knee, and ankle joints in the sagittal plane; while some exoskeletons use linkage mechanism for actuating joints. The linkages are designed based on the “teardrop” trajectory which is obtained by making the hip joint stationary.

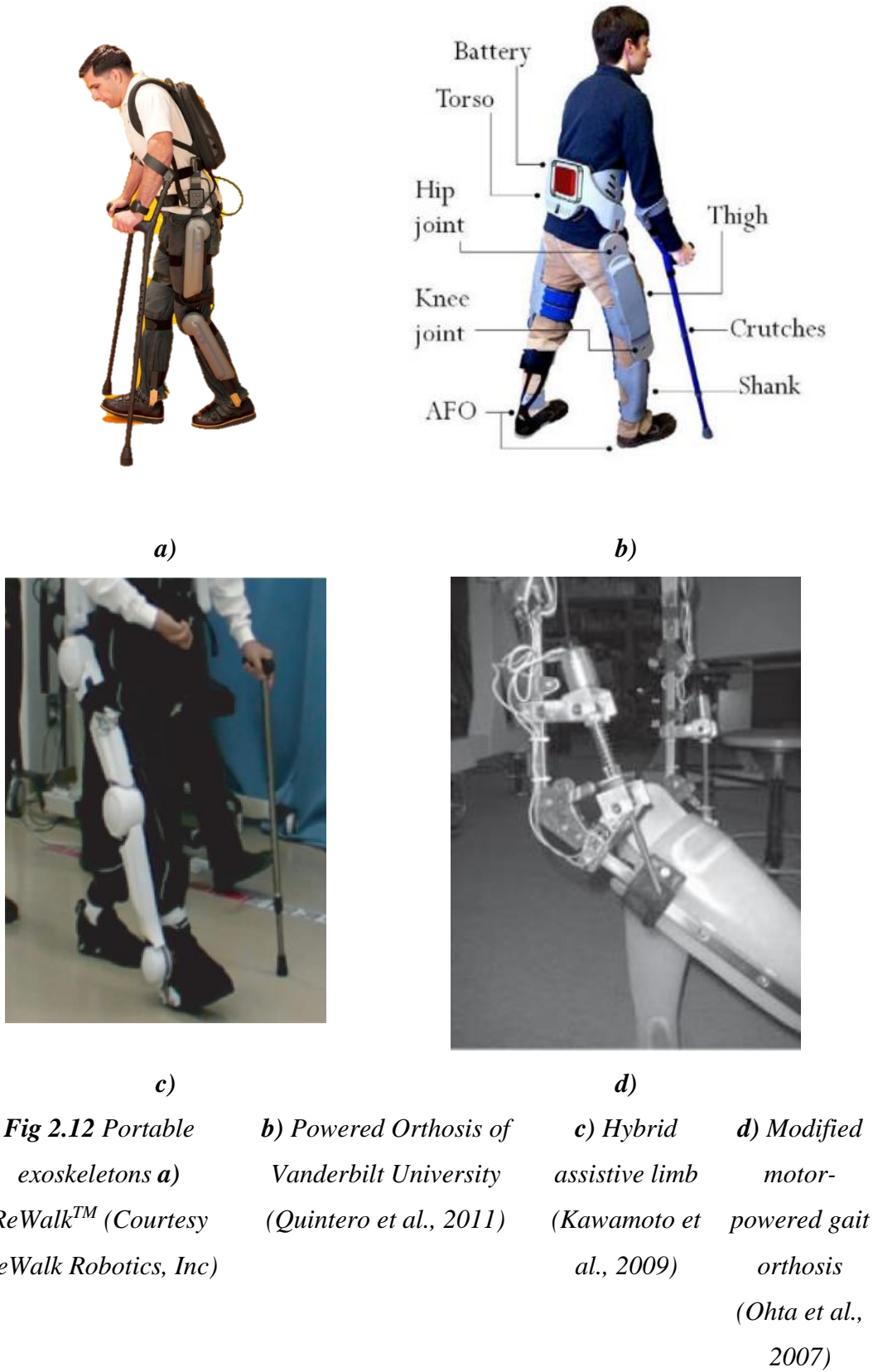
### **2.1.3 Portable Exoskeletons**

These exoskeletons are mobile and do not require any base or treadmill. As opposed to treadmill-based exoskeletons, they are lightweight and easy to don and doff. Their simple and small structure makes them relatively more comfortable in comparison with treadmill-based and mobile-based overground exoskeletons. Besides, one of the most notable features of the portable exoskeletons is that they allow natural walking and the power source is attached to the exoskeleton for actuating the joints. In addition, the users require crutches along with the exoskeleton during walking because of their impaired physical ability. Some of these portable multi-DOF exoskeletons are explored here.

ReWalk, Indego, and HAL are some of the commercially available portable exoskeletons that can be used with crutches for rehabilitation. The ReWalk<sup>TM</sup> exoskeleton is developed by ReWalk Robotics Inc., for paralyzed patients to assist them in standing and walking, shown in Fig 2.12 (a). It contains motorized joints, a rechargeable battery, sensors to measure the joint angle, ground contact, etc., and a backpack comprised of the control system. The device has bilateral thigh and leg segments that are hinged at the knee (Zeilig et al., 2012). Another commercialized exoskeleton developed at Vanderbilt University can also be used for treating paralyzed patients. It consists of joint-level controllers which are controlled by a control structure. Moreover, the hip and knee joints are powered by direct current (DC) motors, and brakes are included as a safety measure, shown in Fig 2.12 (b). The exoskeleton is proposed to use with forearm crutches for stability (Quintero et al., 2011; Ha et al., 2016). A single leg version of hybrid assistive limb (HAL) may be used for the patients of hemiplegia. Figure 2.12 (c) shows the exoskeleton of the HAL in which the hip, knee,

and ankle joints have single-axis joints in the sagittal plane (Kawamoto et al., 2009).

Linkage



**a)** Portable exoskeletons *ReWalk™* (Courtesy ReWalk Robotics, Inc)

**b)** Powered Orthosis of Vanderbilt University (Quintero et al., 2011)

**c)** Hybrid assistive limb (Kawamoto et al., 2009)

**d)** Modified motor-powered gait orthosis (Ohta et al., 2007)

mechanisms, for actuating the hip and knee joints, can be incorporated in the robotic orthoses for improving the gait speed, step length, and dynamic cosmesis of walking (Ohta et al., 2007). Figure 2.12 (d) shows the modified form of the advanced reciprocating gait orthosis (AGRO) which uses linear actuator, at knee joint, to form a four-bar linkage and the same mechanism is used at hip joint for actuation. This makes it a two DOF robotic orthoses. However, a single DOF mechanism may be used to actuate hip and knee, simultaneously, shown in Fig 2.13. The four-bar mechanism can be used to actuate the hip joint which in turn actuates the knee joint through cam modulated mechanism (Ruthenberg et al., 1997). The motion can be achieved in the sagittal plane using revolute joints as a connection between the thigh and lower leg segments. Besides, a compliant series elastic actuator can also be used for actuating the knee and ankle joints through a slider-crank linkage as shown in Fig 2.14 (Chen et al., 2016; Skelton et al., 2013).

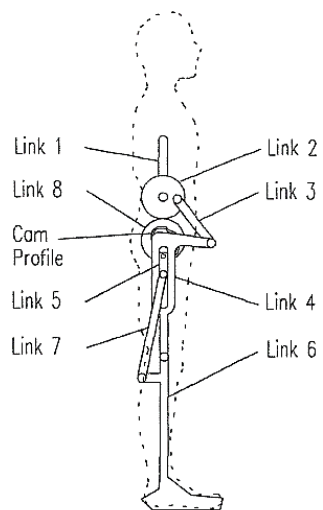


**Fig. 2.13** Powered gait orthosis (PGO)(Ruthenberg et al., 1997)

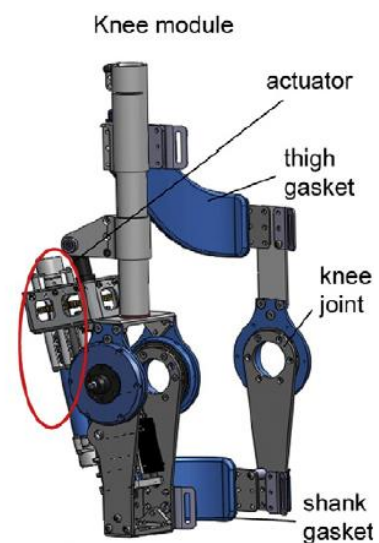


**Fig. 2.14** Knee module of knee-ankle-foot robot(Chen et al., 2016)

Various portable gait rehabilitation devices have been explored and it is observed that revolute joint is used to articulate the thigh and leg segments. The exoskeletons reported in this section have multi DOFs, however, only PGO is found to have single DOF for actuating hip and knee simultaneously. Linkage mechanisms play a vital role in the actuation of mechanism, gait speed, step length, etc.

#### 2.1.4 Assistive Devices

It is worthwhile to investigate the area of assistive devices or orthosis for knee joint while synthesizing a mechanism for supporting an injured knee, or gait rehabilitation.

The orthosis is defined as an “externally applied device used to modify the structural and functional characteristics of the neuromuscular and skeletal systems,” as per International Organization for Standardization (ISO) guidelines. Typically, it is used to correct the functions of physically impaired patients. Some of the important features of an orthosis are restraining joint mobility, correcting limb malformations, assistance in ambulation, stability, etc., (Masiero et al., 2018). Various orthoses that are used for assisting an injured knee or rehabilitating gait are explored. The orthosis/knee brace use

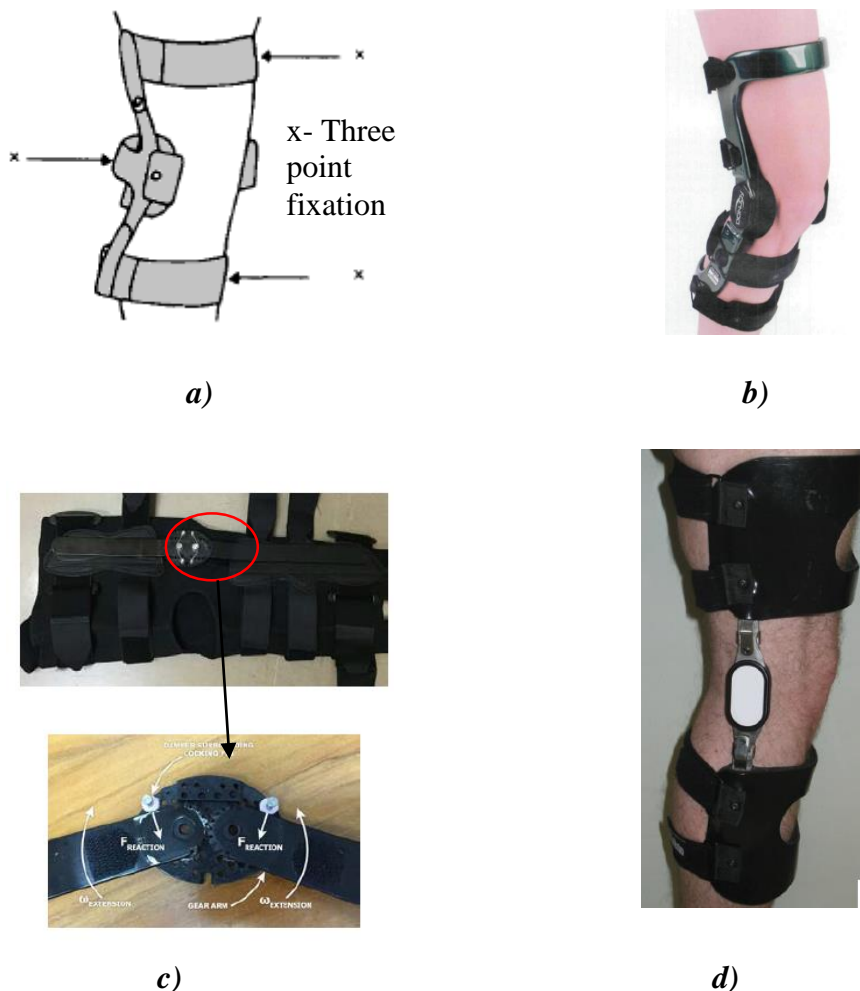


**Fig 2.15 a) Knee brace (Butler et al., 1983)**      **b) OAdjuster Osteoarthritis Knee Brace (Draganich et al., 2006)**      **c) Knee brace with geared hinge (Greenfield et al., 2017)**      **d) Adjustable Unloader Knee Brace (Hangalur et al., 2018)**

three-point fixation system as shown in Fig 2.15 (a), to avoid hyperextension and effectively control hyperextension. Figure 2.15 (b) shows an off-the-shelf knee brace

with a hinge between the thigh and shank which can be used by the osteoarthritis patients (Draganich et al., 2006). An important feature of the hinged knee brace is to control flexion/extension. The joint between the thigh and shank segments can be a revolute joint, or it can also be a double gear mechanism, as shown in Fig 2.15 (c), which can imitate the rotation motion of the synovial knee joint naturally (Greenfield et al., 2017). Another orthosis which can be used for providing relief to osteoarthritis patients can be an adjustable unloader knee brace which uses a polycentric joint between thigh and leg segments, as shown in Fig 2.15 (d). In addition, this novel knee brace does not require straps for providing the needed moment (Hangalur et al., 2018).

Besides, the orthoses can be extended to ankle, and foot and those type of orthoses are called knee-ankle-foot orthoses (KAFO). Figure 2.16 shows a KAFO with a cam mechanism with friction rings and lock that enable the KAFO to lock the knee joint at any position to assist the patients with knee flexion contractures (Jonathan Kofman et al., 2009; Tian et al., 2015). Figure 2.17 shows another KAFO that uses four-bar linkage for coupling the knee and ankle movement (Berkelman et al., 2007). Other

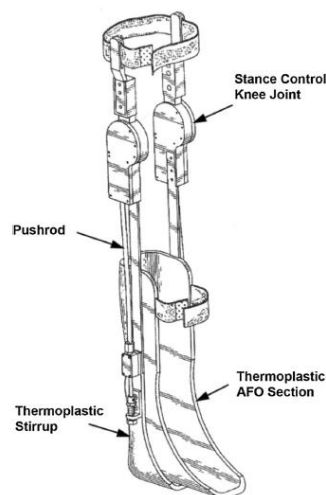


**Fig. 2.16** Knee-ankle-foot-orthosis (Jonathan et al., 2009)      **Fig. 2.17** Linkage orthosis (Berkelman et al., 2007)

types of KAFO use motors or actuators at the knee and ankle joints, for example, Robot KAFO, KAFO with an actuator, exoskeleton with 4-bar linkage actuator, etc. Figure 2.18 shows a Robot KAFO in which an accelerometer at the hip joint identifies the gait phase, and the actuator at the knee joint generates the torque required for assistance (Kawasaki et al., 2017); whereas KAFO with actuator uses a four-bar linkage for actuating the knee joint, the linkage is formed by two steel cables, a metal bar as shown in Fig 2.19 (Guo et al., 2011). In addition, actuators with linkage mechanism at the knee

joints are also found. Figure 2.20 shows a four-bar linkage actuator for knee assisting device that can be used to mimic the motion of the human knee joint for rehabilitation of hemiplegic patients (Kim et al., 2015).



**Fig. 2.18** Robot KAFO (Kawasaki et al., 2017)

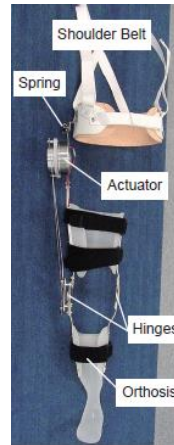


**Fig. 2.19** KAFO with actuator (Guo et al., 2011)

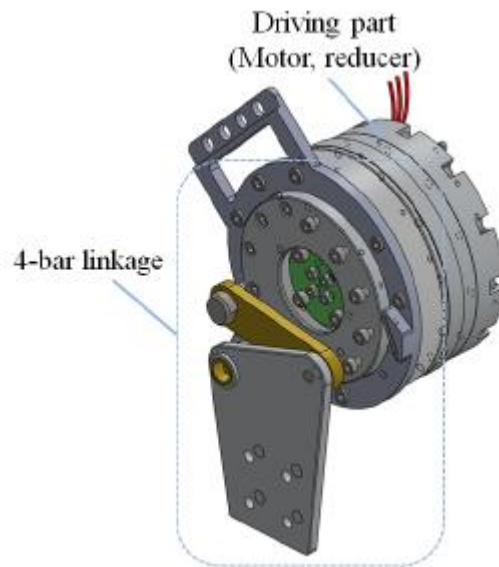


**Fig. 2.20** Four-bar linkage knee actuator (Kim et al., 2015)

It is observed that single-axis joint, gear, and cam mechanisms are normally used at the knee joint of the assisting devices. Devices which couple the knee and ankle movement through linkage mechanisms and those with linkage mechanisms for actuation are among others. Thus the mechanisms play a vital role in the functioning of the exoskeleton and assistive devices. A mechanism can be employed in the rehabilitation devices, bipeds, exoskeletons, etc., to benefit the society. Besides,



exoskeletons and assistive devices, it is equally important to investigate the linkage mechanisms used in the walking robots.

## 2.2 Walking Linkages

While designing an assisting device for rehabilitation, it is worth mentioning that the linkages and joints are used among the walking robots. Various walking robots have been explored to find their walking mechanisms. ERNIE, a bipedal robot that contains five links with motion limited to the sagittal plane can be used as shown in Fig 2.21.

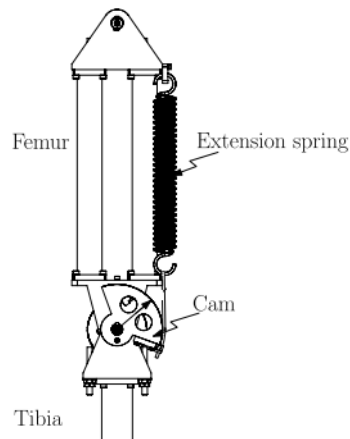


**Fig. 2.21** Schematic of ERNIE knee actuator with spring attached in parallel (Yang et al., 2008)

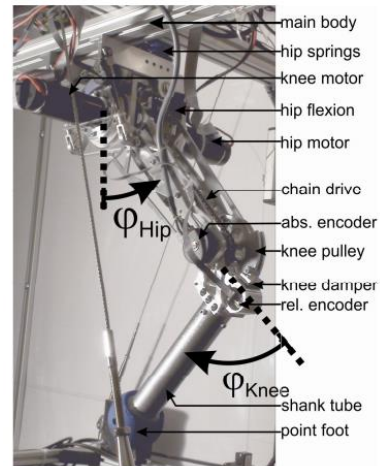


**Fig. 2.22** Series Compliant Articulated Robotic Leg (Hutter et al., 2011)



**Fig. 2.23** Robot RAMone (Smit-Anseeuw et al., 2017)



**Fig. 2.24** Planar bipedal testbed MABEL (Sreenath et al., 2011)

Revolute joints can be used at the knee and an extension spring may be attached in parallel to the knee actuator for improving the energy efficiency of walking (Yang et al., 2008). *BIRT* (Biped Robot with Three Legs) being another biped robot which has a total six actuated DOF and revolute knee and hip joints can also be used (Schmiedeler

et al., 2005). *ScarLETH* (Series Compliant Articulated Robotic Leg developed at ETH Zurich) and *RAMone* are among other robots that can be used. They can use high compliant series elastic actuators (SEA) for connecting the body and thigh at hip joint; whereas SEA may be used to connect the thigh and the shank at the knee joint. The actuators may be placed directly at the hip joint by using a miniature chain and pulley system to allow hip and knee flexion/extension, shown in Fig 2.22 (Hutter et al., 2011; Smit-Anseeuw et al., 2017). Additionally, *RAMone* can be mounted on a planarizer to restrict its motion in the sagittal plane as shown in Fig 2.23. Alternatively, *MABEL*, shown in Fig 2.24, which contains a torso, two legs with revolute knee joints along with four actuators can be used. Its locomotion agility and energy efficiency can be improved by connecting its two actuators in series with large springs. These walking robots have multi-DOF and most of them use revolute joint for connecting thigh and shank segments.

Single degree of freedom walking mechanism is another area in which researchers are working actively. Various synthesis techniques and mechanisms have been explored for designing them. A cam driven mechanism in which cam system attached to the body frame connects feet of the robot through pantograph mechanism can be used (Zhang et al., 2017). A single-DOF mechanism can be used in the planar biped as shown in Fig 2.25 (a). A six-bar linkage can be used to approximate the femur and tibia motions while a third leg can be included to ensure the frontal stability (McKendry et al., 2008). Alternatively, a six-bar Stephenson III mechanism can be used for designing a walking linkage, shown in Fig 2.25 (b). The mechanism can be synthesized in two stages; four-bar linkage that generates the inverted gait should be synthesized in the first stage followed by the synthesis of dyad that inverts and magnify the gait (Batayneh et al., 2013). Another six-bar linkage, i.e., Klann linkage (shown in Fig 2.26 (a)) can also be used for producing a variety of gaits. It can be utilized as a walking mechanism in the quadruped robots as shown in Fig 2.26 (b) (Sheba et al., 2017). Furthermore, a novel mechanism named as Atlas which is a six-bar Watt I mechanism may be synthesized using an optimization technique to generate desired gait (Selvi et al., 2017). Besides, other inversions of the six-bar such as Stephenson II and Stephenson III may be used as function generators for controlling an RR chain to obtain the desired trajectory. Figure 2.27 demonstrates the Stephenson II leg mechanism which can be implemented in walkers (Plecnik and McCarthy, 2016).

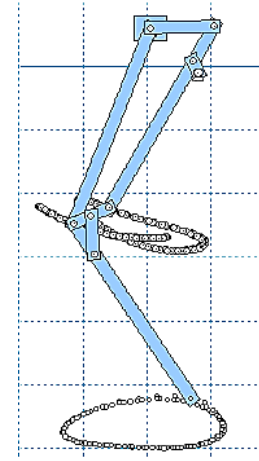
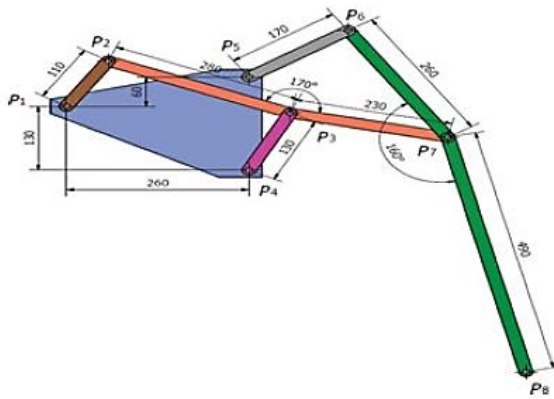


**Fig 2.25 a)** Single DOF planar biped  
(McKendry et al., 2008)

**b)** Stephenson III leg mechanism  
(Batayneh et al., 2013)



a)

b)

**Fig. 2.26 a)** Klann Linkage **b)** Klann linkage implemented in quadruped robot  
(Sheba et al., 2017)

Another single-DOF mechanism which is developed by Theo Janeson can be optimized to minimize energy input and maximize stride length. Two of its four-bar mechanisms can be synthesized for function generation followed by the synthesis of parallel mechanism to generate the path, shown in Fig 2.28. Further, the optimized eight-bar linkage can be implemented in the kinematic sculpture “wind beast” (Giesbrecht et al., 2012). An eight-bar linkage can be used to perform walking and stair climbing simultaneously using counterweight slider for adjusting the center of gravity of the walking/climbing robot, shown in Fig 2.29. The synthesis of such a multi-legged robot can also be performed by minimizing the distance between the “teardrop” ankle trajectory and the generated trajectory (Liu et al., 2017). Alternatively, an eight-bar



**Fig. 2.27** Stephenson II leg mechanism  
(Plecnik and McCarthy, 2016)

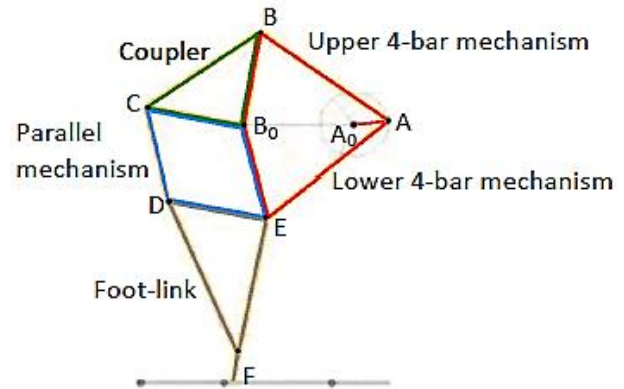


**Fig. 2.28** Theo Janeson linkage used  
in the leg of wind beast (Giesbrecht  
et al., 2012)

linkage can be synthesized analytically for four-precision points using the complex number technique. Dimensional synthesis of the linkage may be performed by considering four loops which yield a total of 24 independent nonlinear equations that can be solved in MATLAB®. An eight-link human-like lower limb linkage is shown in

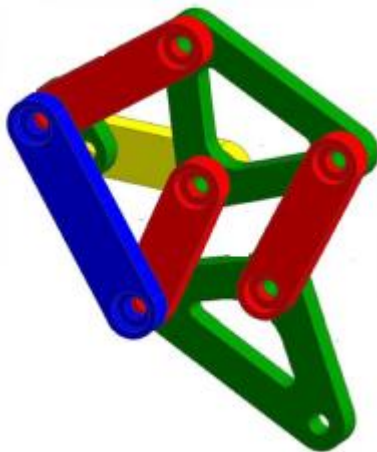


**Fig. 2.29** Eight-bar leg linkage for  
walking and stair climbing (Liu et al.,  
2017)

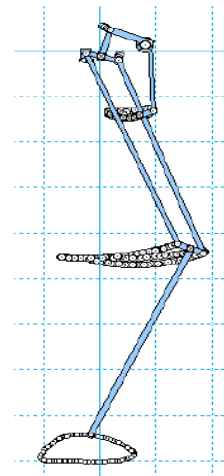


**Fig. 2.30** Human-like eight-bar leg  
mechanism (Al-Araidah et al., 2011)

Figure 2.30 which illustrates that the linkage is capable of tracking the desired ankle trajectory (Al-Araidah et al., 2011). Besides, a ten-link mechanism can be synthesized for the same purpose. It may be possible by designing a 3R chain that matches the human leg dimensions and which is constrained through two separate four-

bar linkages to tracking ankle and toe trajectory (Tsuge and McCarthy, 2015). However, the synthesized mechanism may be complex and bulky due to a large number of links.

Various type of mechanisms have been explored and it is found that four-bar and six-bar mechanisms are typically used in the leg mechanisms. Besides a conventional method of tracking a ‘teardrop’ ankle trajectory is used while synthesizing any mechanism. In addition, a complex set of equations that involve huge computational effort is required for synthesis. In contrast, cable-driven mechanism may be another interesting area to explore because of its advantages such as: 1) It does not require link adjustment 2) It does not restrict natural DOF 3) It is lighter in comparison with the rigid link mechanism (Mao and Agrawal, 2012).

### 2.3 Planar Linkage Synthesis

A collection of rigid bodies such as cams, gears, and links which are interconnected to transform motion is known as a mechanism. A linkage may be defined as an assemblage of interconnected rigid or resistant bodies that are separately called links. They are connected by a physical connection called joints. A joint also known as a kinematic pair can be formed by the direct contact between two components (McCarthy, 2000). It can be categorized according to the type of contact between the members or the number of degrees of freedom allowed for a joint (Norton, 2011). However, our discussion is limited to the rotary hinge or the revolute joints for planar linkages that allows only one degree of freedom movement between two components.

The study of mechanisms’ motions and their design procedure is defined as kinematics. The motion study of mechanisms is kinematic analysis whereas kinematic synthesis is the process of designing linkages to achieve the desired motion specification (Erdman and Sandor, 1984). In kinematic analyses, the positions

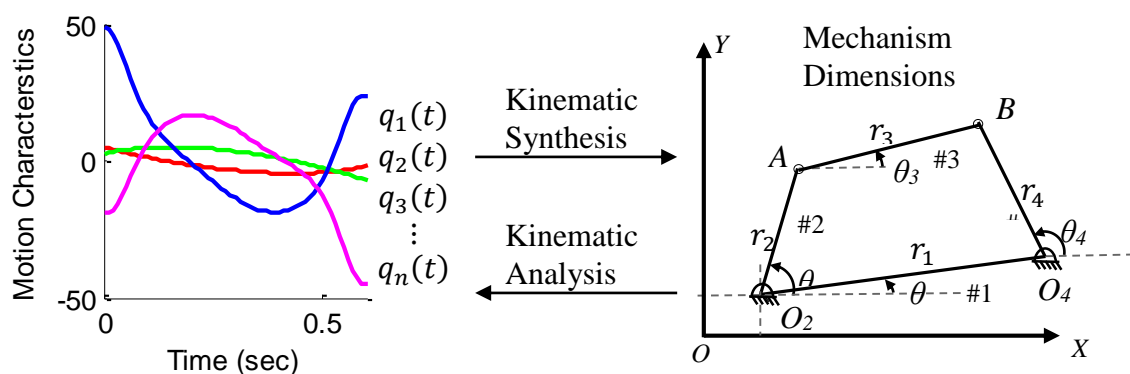


**Fig. 2.31** Mechanism analysis and synthesis

, velocities, and accelerations of the mechanism are determined while the dimensions of the mechanism are known. It deals with comprehending the kinematic behaviour of the mechanism. In contrast, mechanism dimensions are determined from the known set of motion in kinematic synthesis<sup>1</sup> (Russell et al., 2013). Figure 2.31 demonstrates the above definitions of the mechanism analysis and synthesis.

The kinematic synthesis of linkages is divided into two classes, namely, type synthesis and dimensional synthesis. The type of mechanism, the number of links in the mechanism, the degree of freedom of the mechanism, etc., come under type synthesis whereas the significant dimensions and the starting position of the mechanism to accomplish the desired task are determined during dimensional synthesis (Erdman and Sandor, 1984). In addition, kinematic synthesis of linkages is further divided into three sub-categories based on the type of tasks which are path generation, motion generation, and function generation. A point on the floating link traces the series of points on the desired path in the path generation (Waldron and Stevensen, 1979). In the event, if path points correlation with the time or input-link positions is required, then the task is considered as path generation with prescribed timing. When the entire rigid body of linkage is moved through the desired motion sequence then the process is termed “rigid body guidance” by Suh, 1968 and “motion generation” by Erdman et al., 1984. Waldron and Stevensen (1979) define function generation as the process of coordinating the rotation angles of the driving link with that of the follower links. Besides several tasks, various techniques of kinematic synthesis of linkages have been explored.

Some of the techniques of kinematic linkage synthesis are geometrical construction or graphical, analytical and numerical techniques (Norton, 2011). They can be broadly classified as precision point methods and optimal synthesis methods. A path to be tracked by a coupler point of a mechanism is depicted by the number of precision or accuracy points. The generated trajectory passes exactly through the desired points however trajectory between consecutive desired points may differ with the points on the generated trajectory. The geometrical or graphical construction is relatively quick and straightforward technique of linkage synthesis. The notion of pole and rotation angle as constraints (PRC) can be used for the synthesis of mixed motion, point and function generation four-bar linkage problems (Zimmerman, 2017). Using the graphical approach, Hrones et al., 1951 developed an atlas of coupler curves of four-bar linkage

---

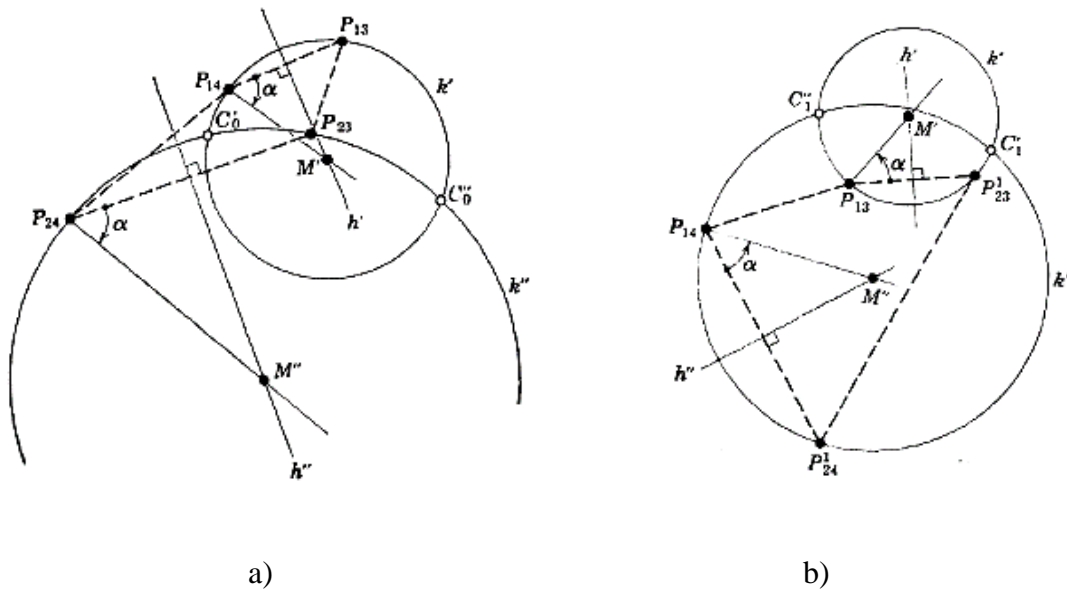
<sup>1</sup> Since the determined output parameters in kinematic synthesis are mostly mechanism dimensions, therefore, kinematic synthesis can also be called as dimensional synthesis

which contains around 7000 curves. However, it only provides an approximate solution which needs to be refined further. Subsequently, a similar type of atlas of coupler curves is developed for five-bar geared linkage (Zhang et al., 1984). This method is not accurate, and the designer may have to perform many iterations until the final design (Erdman and Sandor, 1984). However, it is used as an introductory tool for kinematic synthesis (Lee and Russell, 2017). In contrast, analytical techniques are accurate and most suitable for computer simulation. Furthermore, there are other approaches that involve analytical and numerical solutions which are explored in the subsequent subsections.

### **2.3.1 Analytical Linkage Synthesis**

Various analytical techniques for the synthesis of planar four-bar and six-bar linkages have been used for desired finitely separated points. A four-bar linkage can be formed by rigidly connecting two two-revolute jointed open chains. The linkage can be synthesized by separately designing each open chain such that its floating link reaches the desired motion sequence. These open chains are called  $RR$  chains where  $R$  denotes a revolute joint. This process of designing a four-bar linkage is termed as rigid body guidance (Suh and Radcliffe, 1967). The researchers in the field of kinematic synthesis gave birth to the celebrated Burmester theory to designing mechanisms for four finite positions. The theory reports that the points on the moving plane can form a circle about a point in the fixed plane at the specified precision positions that can be used to identify mechanisms between two planes. As a circle can pass through three points, a point on the fixed plane can be found corresponding to the three points on the moving plane. Furthermore, it is found that if the angle of the moving plane is prescribed at each position, a cubic curve of these points on moving plane may exist for four precision positions, simultaneously a cubic curve will also exist for their corresponding centers. These curves are named as circle point and center point curves (Burmester, 1888). This notion of Burmester curves can be applied to linkage synthesis when the focus is to design the  $CC$  chains rather than  $RR$  chains, where  $C$ -denotes the cylindrical joint (Roth et al., 1967). The center points can be generated by three different techniques. The first technique is the graphical construction which utilizes the notion of pole triangle and opposite pole quadrilateral (Hartenberg and Denavit, 1964). Figure 2.32 (a) depicts the construction of center points while circle points construction is shown in Fig 2.32 (b). The geometrical or graphical construction may be utilized for generating the mathematical model for the analytical synthesis. The second technique applies a

constant curvature condition to coordinate transformations and uses a single equation for coordinates of the curves (Suh et al., 1978). The third technique for generating the locus of points is



$P_{ij}$  Poles;  $h', h''$  are mid normals;  $k', k''$  circles,  $M', M''$  circle centers,  $C_0', C_0''$  center points ;  $C_0', C_0''$  circle points

**Fig. 2.32** Construction of a) center point curve b) circle point curve (Hartenberg et al., 1964)

developed by Sandor in 1959 which is a complex number method to form a set of loop displacement equations (Erdman and Sandor, 1984). This method allows modeling of the vector pairs, better known as dyads, for motion-, path- and function-generation tasks. Figure 2.33 depicts the dyad representation in the form of vectors in which  $W$  and  $Z$  represent the links,  $\beta_i$  represent the angular rotation of vector  $W$  from the first to

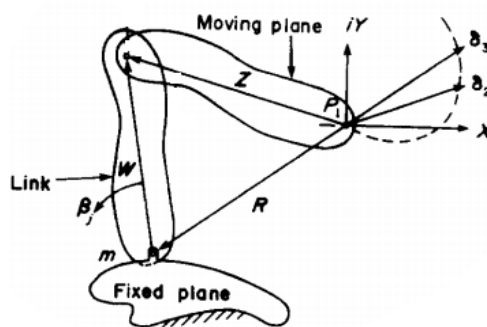


**Fig. 2.33** Representation of a dyad (Erdman, 1981)



the  $i$ th position, the distance between the precision points  $P_1P_2$  and  $P_2P_3$  is represented by  $\delta_2, \delta_3$ , respectively, and the fixed point  $m$  is located by the vector  $\mathbf{R}$ . The analytical model can be explored in detail in Ref (Erdman, 1981). However, mere dyad modeling may be inadequate for the function generation synthesis of four-bar linkages. In such cases, tracer point is not certain; therefore, three moving links cannot be modeled through dyad modeling. In contrast, the generic triad model that describes the motion of tracer point may be synthesized through relative precision position using the complex number formulation, shown in Fig 2.34. The triad synthesis technique can be used for the synthesis of linkages for function generation task, and to synthesize complex planar mechanisms (Chase et al., 1987). Various mechanisms such as geared five-bar, six-bar, and eight-bar mechanisms have been synthesized using triads for six and seven precision positions (Subbian and Flugrad, 1994).

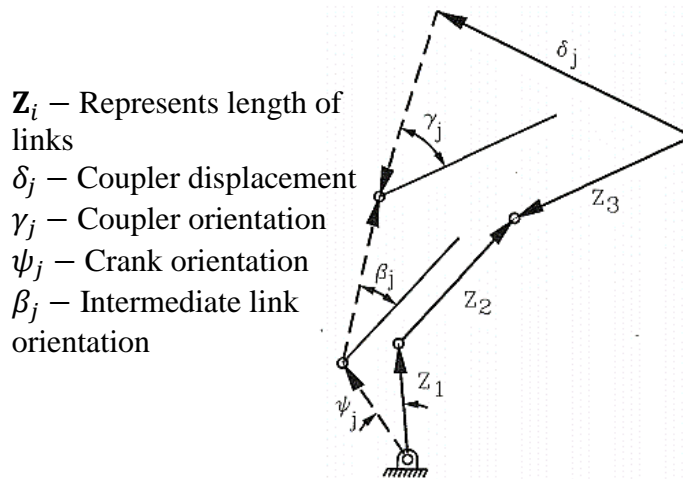


**Fig. 2.34** Representation of triad at two precision positions (Subbian and Flugrad, 1994)

The position-wise loop closure equations can be formed for three finitely separated positions using the complex-number formulations to generate circle-point and center-point circles. Furthermore, a *standard form* of equation can be used for planar four-bar linkage synthesis, shown in Eq (2.1).

$$\mathbf{W}(e^{i\beta_j} - 1) + \mathbf{Z}(e^{i\alpha_j} - 1) = \delta_j \quad (2.1)$$

Alternatively, the planar open  $RR$ ,  $PR$ , and  $RP$  chains can be designed algebraically using geometric approach. This method utilizes the constraint equations for each chain to characterize the positions it can track. Figure 2.35 represents an  $RR$

open chain at two positions  $M_1$  and  $M_2$  in which  $\mathbf{G}(x, y)^T$  represent the fixed revolute joint,  $\mathbf{W}^i(\lambda, \mu)^T$  represent the  $i$ th position of the joint moving around  $\mathbf{G}$ ,  $\alpha_{1i}$  is the

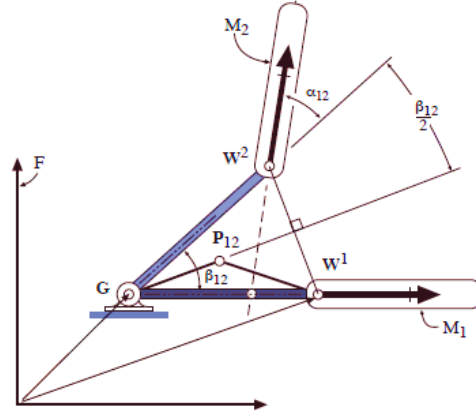


**Fig. 2.35** Representation of  $RR$  chain for algebraic modeling (McCarthy et al., 2006)

rotation of  $M_i$  about  $\mathbf{W}^1$ ,  $\beta_{1i}$  is the rotation about  $\mathbf{G}$ , and  $\mathbf{P}_{1i}$  is the pole. The algebraic equation for the design of  $RR$  chain can be formed as shown in Eq (2.2) (McCarthy et al., 2006):

$$(\mathbf{G} - \mathbf{P}_{1i}) \cdot [A(\phi_{1i}) - I](\mathbf{W}^1 - \mathbf{P}_{1i}) = 0, \quad i = 2, \dots, n \quad (2.2)$$

The equation can be used to design an  $RR$  chain for two-, three-, four-, and five-precision positions. The chains synthesized using the design equation can be used to construct chains that allow the coordinated movement of input and output links. This methodology can be used for function generation linkage synthesis. Additionally, this methodology can be utilized in the synthesis of multi-loop linkages. A  $3R$  serial chain can be constrained using a planar  $RR$  chain to obtain a six-bar linkage. There are several ways to add  $RR$  constraints to a  $3R$  serial chain which can be explored in Ref (Soh et al., 2006). Likewise, an eight-bar linkage can be designed using  $4R$  serial chain by adding an  $RR$  constraint. It is worthwhile to note that  $PR$  and  $RP$  are among the other constraints which can be used for synthesizing a linkage (Sonawale and McCarthy, 2016). As opposed to these methods, an algebraic equation of coupler curve may be used for four-bar linkage synthesis (Bleichschmidt and Uicker, 1986). The equation is of the order of sixth-degree that can be derived from analytic geometry and it is tricircular sextic (Hartenberg and Denavit, 1964). In addition, these equations are very complex which make the synthesis process very tedious. Besides, the four-bar linkage

can be synthesis for a combined task of path-point and path-point with orientation using the numerical algebraic geometry (Brake et al., 2016).

It is observed that ‘Standard form’ of the equation can be developed for the synthesis of mechanisms which yield closed-form solutions for 2–4 precision points and extendable to 5 points. Furthermore, the standard-form equations can be solved analytically up to 5 precision points for four-bar linkage. Although, the maximum number of precision points can be nine for analytical path synthesis of four-bar linkage (Wampler et al., 1992). The standard-form equations cannot be solved easily for 6–9 precision points. When these nonlinear equations are solved using numerical methods there may be problems causing convergence to singular or imaginary solutions (Norton, 2011). Another approach is to use coupler curve equation instead of vector-loop or standard form equation for synthesis. However, it involves complexity and iterations are required. For a large number of precision points, the path synthesis problem becomes over-constrained and exact trajectory cannot be obtained. Additionally, complexity and computational efficiency of these synthesis methods increase with the increase in the number of precision points. Thus, it is noteworthy to investigate the linkage synthesis techniques using the optimization methodology.

### **2.3.2 Optimal Linkage Synthesis**

Another approach which has gained popularity among the linkage synthesis techniques is the use of optimization methodology. It consists of two distinct parts, namely, formulation of objective function along with the constraints (if required) and algorithm to solve it. Various objective functions for synthesizing the linkage are explored followed by the optimization algorithms.

#### **2.3.2.1 Objective Functions**

The sum of the square of Euclidean distance also known as tracking error (TE) between the generated- and desired points is the most widely used objective function (Chi-Yeh, 1966). Another objective is the minimization of the deviations of the shape and position functions that can be used for linkage synthesis, represented in Eq (2.3) in which  $\xi$  is shape function,  $\eta$  is position function,  $g_1$ , and  $g_2$  are Grashof and transition and of dyad constraint. The objective can be created for combined paths such as rectilinear segment and a circular arc, and rectilinear segment, a circular arc, and a slanting line segment, shown in Fig 2.36 (Bulatovic and Orđevic, 2012). Although the formulation is complex,

however, it can be applied to a large number of precision points. The deviation of orientation of the fixed link, in four-bar linkage, with the coupler

$$f(X) = \sum_{j=1}^S \left( k \cdot \sum_{i=1}^{N_j} [\xi_{ij}^2 + \eta_{ij}^2] + k_1 \cdot g_{1j}^2 + k_2 \cdot g_{2j}^2 \right) \quad (2.3)$$

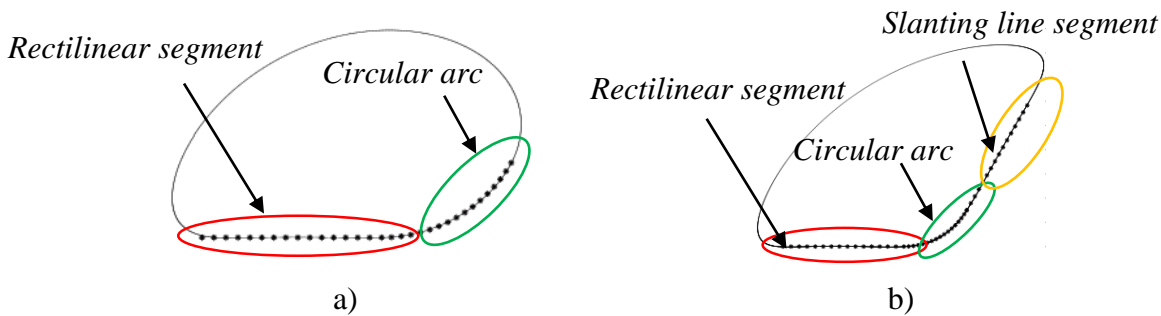


**Fig. 2.36** Combined paths a) rectilinear segment and a circular arc b) rectilinear segment, a circular arc, and a slanting line segment (Bulatovic and Orđevic, 2012)

trajectory can be used as “orientation structural error” objective function (Zhou and Cheung, 2001). The angular bend in the coupler curve can be expressed in function of relative arc length and its Fourier series expanded form can be utilized to evaluate the shape difference (Ullah and Kota, 1997). The finite-element-based error function is another objective function that can be used for linkage synthesis (Fernández-Bustos et al., 2005). The deviation in the trajectory of the moving pivots of the linkage from their desired path can also be used as an objective function. It can be used in the path generation synthesis of slider-crank, four-bar linkages, and linkage with slotted links (Buśkiewicz, 2015). The closeness of a group of points to a circular curve may be measured from the circular proximity tool (CFP). It identifies a circle which has the maximum closeness to the points that can also be considered as minimization objective function while synthesizing a four-bar linkage (Hadizadeh and Nahvi, 2015).

Alternatively, multi-objective functions can also be used for the synthesis of path or motion generating mechanisms. For example, minimization of tracking error (TE) and transmission angle (TA) deviation from  $90^\circ$  may be considered together for better path tracking, and minimum torque requirement (Nariman-Zadeh et al., 2009). Likewise, three objective functions, namely, TE, TA deviation from  $90^\circ$ , and Maximum Angular Velocity Ratio (MAVR) can also be used to improve the kinematic performance of a mechanism (Khorshidi et al., 2011). Combination of Euclidean distance with an error in coupler angular displacement, and “normalized pole position error” with “normalized angular displacement error,” are among the other objective

functions that can be used to synthesize four-bar linkages (Gogate and Matekar, 2012). Another noteworthy objective function consists of hybrid tasks for synthesis (Penunuri et al., 2011). There are various optimization algorithms used for solving the formulated problem.

### **2.3.2.2 Local Optimization Algorithms**

The optimization algorithms that are applied to the linkage synthesis problem are loosely classified into two broad areas, namely, local and global optimization algorithms. Various local optimization algorithms are explored first. A nonlinear goal programming technique is used for the synthesis of the planar mechanism through multiple objectives (Krishnamurty and Turcic, 1992). Newton-Raphson's method is another technique which is also used for the linkage synthesis; however, it requires second order derivative for both the objective function and the constraints (Angeles and Callejas, 1984). An unconstrained nonlinear synthesis problem can be investigated using the Newton-Gauss algorithm (Angeles et al., 1988). The Fletcher's Line Search (FLS) may be augmented in Broyden-Fletcher-Goldfarb-Shanno (BFGS) to solve the synthesis problem. Nevertheless, for finding the gradients, the finite-difference method should be used because of the complexity of the synthesis problem (Nokleby and Podhorodeski, 2001).

'Exact Gradient Method' is one such local optimization method which is free from finite difference approximation methods that render inaccurate results. A notable feature of this algorithm is its flexibility to use it for different classes of synthesis problems (Mariappan and Krishnamurty, 1996). Extension of the primal-dual infeasible interior algorithm may be used for the linearly constrained convex nonlinear programming problem (Zhang et al., 2000). Another technique for the synthesis of the planar mechanism for different tasks may be exact differentiation that also improves the quality of search direction (Sancibrian et al., 2006). Gauss constrained method (Paradis and Willmert, 1983), generalized reduced gradient method (Fallahi et al., 1981), gradient projection method (Rosen, 1960), and a state space approach (Sohoni and Haug, 1982) are among other algorithms which can also be used. These are some of the local optimization techniques which may be used for optimal synthesis. However, these techniques involve calculation of derivatives and Hessians, and there also exist non-zero probability of obtaining a global optimum solution. In contrast to the classical optimization methods, nature-inspired (global) optimization methods can be used for getting a global optimum solution (Kunjur and Krishnamurty, 1997).

### 2.3.2.3 Global Optimization Algorithms

Recently, these algorithms have been used for the optimum synthesis of mechanism, as they are expected to converge at global optimum. They have become more popular for solving various non-linear problems in different fields including linkage synthesis. One such nature-inspired algorithm is Genetic Algorithm (GA). GA could be used for solving highly nonlinear problems to find the optimum solutions, and its efficiency may be increased by modifying its selection- and crossover- procedure (Kunjur and Krishnamurty, 1997; Nishad et al., 2014; Acharyya and Mandal, 2009). Alternatively, particle swarm optimization (PSO) and differential evolution (DE) algorithms may be used for path synthesis of four-bar linkage for tracking more than five precision points. Moreover, some refinement schemes can also be applied to the initial population which increases the computational efficiency (Acharyya and Mandal, 2009). These algorithms may be used for synthesizing four-bar linkages with and without clearance at all joints and serial concatenation of four-bar linkages (Sardashti et al., 2013; Nishad et al., 2014). Nature-inspired algorithms such as artificial bee colony (ABC), the binary genetic algorithm (BGA) (Ettfagh et al., 2013), whale optimization algorithm (WOA) (Mirjalili and Lewis, 2016), moth-flame optimization (MFO) (Mirjalili, 2015), and simulated annealing (SA) (Martínez-Alfaro, 2007) can also be used for the same purpose. While, a modified form of the KH algorithm (Bulatović, 2016), and MUMSA (Malaga University Mechanism Synthesis Algorithm) (Bataller, 2016) which deals with Differential Algorithm are among other algorithms for the dimensional synthesis of a four-bar linkage to generate the path. Synthesis of different mechanisms other than four-bar, such as five-bar mechanism with non-circular gears (Mundo et al., 2009), six-bar mechanisms (Bataller, 2016) and cam-linkage mechanisms (Mundo et al., 2006) can also be carried out using these algorithms.

However, these algorithms require tuning of algorithmic parameters, for example, GA requires crossover probability, mutation rate (Cabrera et al., 2002); PSO requires inertia or weighting factor, social parameters; ABC requires limit value (Ettfagh et al., 2013); whereas, DE needs crossover constant and scaling factor (Acharyya and Mandal, 2009). Unlike these techniques, teaching-learning-based optimization (TLBO) algorithm does not require algorithm parameters which make TLBO implementation easier (Rao et al., 2011; Rao, 2016). It uses the best solution of iteration to change the existing solution, which results in fast convergence. TLBO algorithm is used in different fields such as design optimization of spur gear train, plate

fin heat sink, minimization of shaking force and shaking moment for various linkages etc., (Chaudhary and Chaudhary, 2015; Daniali et al., 2015; Chaudhary and Chaudhary, 2016).

The efficiency of an algorithm may be improved by merging it with another algorithm or incorporating another search algorithm in the well-established algorithm. Thus, it is worthwhile to investigate the area of hybrid optimization algorithms to synthesize planar linkages.

#### **2.3.2.4 Hybrid Optimization Algorithms**

In contrast to the single-nature inspired algorithms, merging of two or three algorithms taking their distinct proficiencies can be an option to obtain an efficient algorithm. Various hybridized (merged) techniques have been explored in the past for unconstrained functions (Lai and Zhang, 2009; Lin, 2010), and path-synthesis problems (Lin, 2010; Kim et al., 2016). Linkage synthesis may be performed by appending an adaptive local search to GA that helps in generating relatively better and distinct solutions (Khorshidi et al., 2011). Likewise, gradient search is combined with the ant colony optimization (ACO) to the synthesis of linkages for hybrid tasks (Smaili and Diab, 2007).

In addition, hybrid algorithms can be applied to numerous real-life applications. For example, PSO-GA hybrid algorithm is used for closed-loop supply chain network design in large-scale networks to obtain superior results in comparison with GA (Soleimani and Kannan, 2015). The exploration tendency of the Biography based optimization (BBO) are improved by incorporating the modified PSO velocity and position update mechanism of the particles (Yogesh et al., 2017). This hybrid form of PSO, i.e., PSOBBO has been applied to improve the feature selection problem in emotion and stress recognition from a speech signal. An interesting variant of PSO is used for sustainable integrated dynamic ship routing and scheduling optimization (De et al., 2016; De et al., 2015), and maritime inventory routing to satisfy demand at different ports (De et al., 2017). It is known as composite particle PSO (PSO-CP). This variant of PSO has addressed an important issue of premature convergence. The improved sterling quality of PSO-CP helps to escape the local optima and provides near optimal results. Another variant of PSO which is named as modified particle form optimization (MPSO) can also be used (Pathak et al., 2017). In this variant, the improved particles (candidate solutions) are generated using the difference between the global and local best positions. Additionally, a greedy selection is also appended to this

algorithm to improve its robustness. It can be applied to the form error evaluation which contributes significantly to the production of mechanical components (Pathak et al., 2017). PSO can also be hybridized by combining with adaptive crossover and mutation rates (Masrom, 2013) or by combining PSO with ant colony optimization (ACO) for convex and non-convex economic load dispatch (ELD) problem of the small-scale thermal power system (Santra, 2016). Also, a cooperative PSO (CPSO) is applied for solving function approximation and classification problems with improved accuracy (Alexandridis, 2016). This algorithm uses two swarms for the same problem (dismantled into two parts) and both the swarms work in a cooperative manner to achieve an improved solution. There are several metaheuristics available in the literature; therefore, it is important to anticipate if more algorithms are required. The answer to this problem is presented in Wolpert and Macready, 1997. ‘No-free-lunch’ theorem has proved that not all kind of algorithms can perform equally well to solve all optimization problems (Wolpert and Macready, 1997). This indicates that some optimizers may perform well for some set of problems while they fail to perform equally well for a different set of problems. The theorem allows the proposal of new hybrid algorithms which can solve the wider range of problems or some specific unsolved problems.

For any population-based metaheuristic optimization algorithm, search process involves two stages, namely, exploration and exploitation stages, irrespective of their nature. The operators should be included to explore search space globally with the randomized movements (as many perturbations of design variables as possible). This stage is known as the exploration that explores the search space to get a better solution. The exploitation stage is followed by the exploration stage that identifies and searches locally in the promising areas identified during exploration in the search space. Promoting anyone of the exploration or exploitation may degrade the results of the other. A right balance between the two is required for the accurate approximation of the global optimum. This balance between exploration and exploitation is a challenging task for developing a metaheuristic algorithm because of its stochastic nature.

These algorithms play an essential role in the synthesis of linkages, however, during linkage synthesis several defects such as circuit, branch, order, etc., are encountered every so often. Therefore, the techniques to rectify the defects during linkage synthesis is another area to explore.



## 2.4 Defect-Rectification

It has been observed that circuit, branch, order (CBO), and Grashof's defects frequently occur during kinematic linkage synthesis. These defects are common to both precision point, and optimal synthesis methods and they may be avoided by imposing proper constraints (Hwang and Chen, 2008; Sardashti et al., 2013).

Circuit and branch defects were discussed under the name of branch defect prior to the improved definition of the circuit/branch. Any synthesized four-bar mechanism was said to have branch defect if all possible orientations of links cannot be realized without dismantling the mechanism (Chase et al., 1985; Krishnamurty and Turcic, 1988). Confusion in the usage of the terms branch and circuit has been stamped out, and improved definitions are: A circuit of a mechanism is defined as all possible orientations of the links which can be attained without dismantling any joint while a branch is continuous series of positions of mechanism between two stationary configurations on a circuit. Elimination of circuit defect is necessary otherwise it would render the

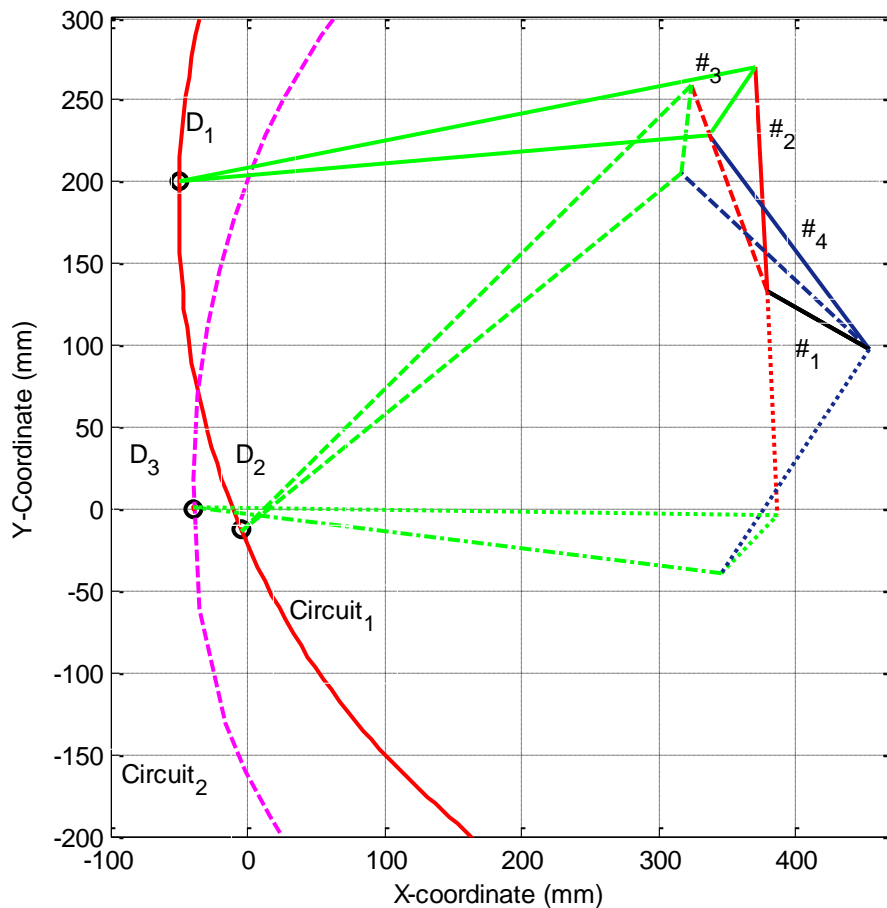


**Fig. 2.37** Circuits defect in four-bar mechanism

mechanism unusable (Chase and Mirth, 1993). The definition is illustrated with the help of Fig 2.37, that depicts the four-bar linkage having circuit defect will not trace all the desired positions with its single circuit. The two design positions  $D_1$  and  $D_2$  fall on  $Circuit_1$  whereas  $D_3$  fall on  $Circuit_2$ . Therefore, the mechanism has to be dismantled to move from  $D_2$  to  $D_3$ . Other defects such as Grashof defect occurs when there is a frequent need of fully rotating the design linkage while order defect occurs when rotation (clockwise or counter-clockwise) of design linkage is not in the desired order (Waldron and Stevensen, 1979).

Multi-loop mechanisms are more likely to suffer these defect problems. Moreover, the synthesis of multi-loop mechanisms is not straightforward due to circuit, branch, and order defects encountered during drivability, and they may render the mechanisms useless (Chase and Mirth, 1993). Circuit defect is considered as the worst problem that may occur during six-bar linkage synthesis (Mirth and Chase, 1995a). A six-bar linkage which satisfies the Grubler's criterion can constitute only four binary and two ternary links. The linkage has two topologically different configurations, namely, Watt and Stephenson linkages. In Watts linkage, ternary links are directly connected to each other, whereas, they are connected by binary links in Stephenson linkage (McCarthy, 2000). Inversion of the Watt linkage yields Watt I and Watt II mechanisms; whereas, inversion of the Stephenson linkage are Stephenson I, Stephenson II, and Stephenson III mechanisms as shown in Fig 2.38. Stephenson six-bar mechanism can have up to six circuits, which remain unaffected by the inversion of the kinematic chain (Guo and Chu, 2004). Typically, Stephenson III is considered for circuit analysis because it allows decomposition of six-bar into a simple four-bar and a dyad (Mirth and Chase, 1995). Various methods for defect identification and rectification in four- and six-bar linkages have been discussed for a long time.

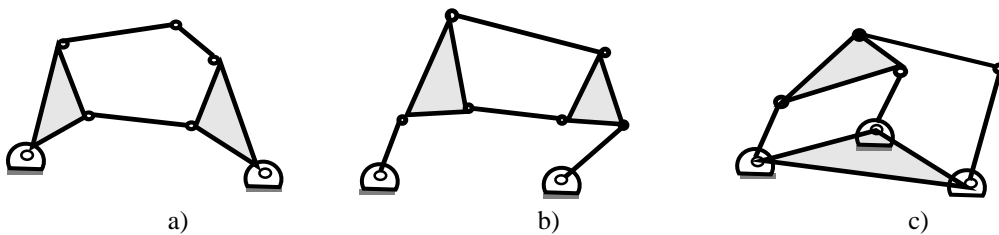


**Fig. 2.38** Inversions of Stephenson six-bar mechanism a) Stephenson I b) Stephenson II c) Stephenson III

It is worth mentioning that some of the identification and solution rectification techniques that have been used for four-bar mechanisms (Cabrera et al., 2002; Balli and Chand, 2002; Chase et al., 1985; Krishnamurty and Turcic, 1988). Prior to the exploration of techniques, comprehension of the defects elimination in the four-bar mechanisms, the identification of defects in the distinct classes of four-bar is required. In the Crank-Rocker/Double-Crank, an in-line or toggle position is possible for dyad (crank+coupler); whereas, dyad (coupler+rocker) cannot reach in-line position on either of the two possible circuit (Chase et al., 1985; Krishnamurty and Turcic, 1988; Waldron and Stevensen, 1979; Chase and Mirth, 1993). The Rocker-Crank/Double-Rocker can reach two collinear positions on each of two possible circuits. Hence, either branch or circuit defect or both may be present. While Triple-Rocker has only one circuit, so it is free from circuit defect; however, branch defect may be present. As crank-rocker and double crank have no branch defects (Chase and Mirth, 1993), transmission angles can be used to eliminate the circuit defect while the same is not true for rocker-crank and double-rocker. The circuit defect in crank-rocker can also be identified by the change in sign of the crank and coupler angle (Sardashti et al., 2013). The angle between the driving link and base link may be used to determine the presence of circuit defect for rocker-crank and double-rocker linkages (Bawab and Li, 1997). In case of triple rocker, sign change of the Jacobian determinant may indicate a change in the branch.

The defects can be eliminated through graphical and optimal synthesis techniques. The defects problem can be investigated graphically for finitely, infinitesimally, and combination of two, i.e., multiply separated positions in four-bar Burmester synthesis (Waldron, 1977; Waldron and Stevensen, 1979). The graphical procedure to eliminate the defects may be used (Filemon et al., 1972) whereas, Waldron's three-circle diagram on the center-point plane can be drawn for eliminating the circuit defect in the motion generation synthesis of four-bar linkage (Russell et al., 2013). The Filemon's construction and Waldron's circle diagrams may be used simultaneously for avoiding defects while synthesizing four-bar linkage using three positions and two velocities specification in design equations (Robson and McCarthy, 2010). The circuit defect in the four-bar linkage obtained through Burmester curve can be eliminated by removing the portion of the Burmester curve that yields circuit defect (Balli and Chand, 2002). Complex number equivalent to pole based order rectification

can be used to identify the desired regions of the Burmester curves for eliminating the order defects (Chase and Fang, 1991).

Grashof defect may be eliminated by selecting only those linkages that satisfy Grashof's rule (Balli and Chand, 2002). The solution rectification of branch and circuit depends on the relationship among geometric inversions, circuits, and branches of the linkage. An interesting approach is to prescribe the range of motion constraint to prevent circuit defect in the synthesis of the slider-crank mechanism for function generation. Besides, a constraint may be used such that the prescribed precision points fall on the lower circuit of the linkage (Almandeel et al., 2015). The control of transmission angle is another method which is used for the synthesis of slider-crank linkages (Wilhelm et al., 2017). In addition, the defects can also be eliminated through constraints during the optimal synthesis of mechanisms.

The optimal synthesis method is another way to synthesize a mechanism (Tinubu and Gupta, 1984) in which an optimization problem may be formulated using single or a multi-objective function. Typically, the sum of squares of the structural error is used as an objective function for mechanism synthesis (Yan and Chiou, 1987). The displacement analysis of Stephenson six-bar mechanisms can be performed using the sixth order equation, and its results can be used to generate the coupler trajectory for tracking error (Watanabe and Funabashi, 1984). Also, maximum transmission quality may be used in combination with minimum least-square design error as a multi-objective function for the synthesis of four-bar linkage (Angeles and Bernier, 1987). However, these objective functions are subjected to defect-specific constraints for defect elimination. A detailed study on the identification and elimination of the Grashof-, circuit-, order-, and branch- defect for mechanism synthesis can be found in Ref. (Balli and Chand, 2002). It is observed that four-bar linkage rectification is a prerequisite for defect-free Watt (Mirth and Chase, 1993; Mirth and Chase, 1995b) and Stephenson six-bar linkage synthesis (Mirth and Chase, 1995a).

Constraints such as rotation of driving link, sign on transmission angle, etc., play a vital role in the elimination of defects while synthesizing a mechanism. The sign of Sub-Jacobian matrices is used to identify circuits present in the mechanism. The circuit defect can be eliminated by maintaining the same sign of determinant values of the Sub-Jacobian matrices. This method is suited for planar multi-loop mechanisms, and it is preferable to implement within an optimization process (Krishnamurty and Turcic, 1988). The improved definitions for circuits and branches are proposed by Chase et al.,

1993, and definition of dyad configuration is also suggested, that is a key to identification and elimination of circuit and branch defects in four-bar and Stephenson six-bar mechanisms (Chase and Mirth, 1993). The sign of transmission angle may be maintained to avoid branch defect, whereas, the sign of the angle between the driving link and the coupler can be used to eliminate circuit defects (Sardashti et al., 2013). Also, the transmission angle constraints can be used for eliminating the defects in slider-crank mechanisms (Wilhelm et al., 2017). Inequality constraint based on the product of the cross product of the follower link length and diagonal distance between follower pivot and the crank moving point is another way to eliminate circuit defects (Shen et al., 2015). The constraint for clockwise or counter-clockwise rotation of driving link can be used for the elimination of order defect.

Some of the methods for the defect identification, analysis, and rectification, in the six-bar mechanisms are discussed here. Defects in the Stephenson-type mechanisms can be identified by mapping the domains of motion on the four number lines (Watanabe and Katoh, 2004). Alternatively, automatic identification algorithm to detect the circuits and defects in the Stephenson six-bar chains can be used (Guo and Chu, 2004a). It can also be used to synthesize a Stephenson six-bar mechanism computationally. Also, its feature point loop method can be used to identify order defect in the six-bar mechanism (Guo and Chu, 2004b). Besides, a two-part test for checking whether a linkage designed as a 3R constrained chain using Burmester theory is usable. The first part is to check the linkage configuration at each task position followed by checking numerical solution between each task position. The linkage which maintains the same configuration at all task positions is considered as usable (Parrish and McCarthy, 2013). Detailed circuit analysis of six-bar Watt chain mechanisms is demonstrated by Mirth and Chase, 1993, and all pin-jointed Watt mechanisms are presented in chart form to detect any change of circuit during synthesis. The chart can be exploited to identify any change in the circuit that causes circuit defect. Based on that, the segments of Burmester curve of first constituent four-bar are eliminated followed by the second constituent four-bar (Hwang and Chen, 2008). Geometric constraint programming (GCP) to design the six-bar linkages can also be used for verifying the linkage motion during its synthesis (Mirth, 2012). It is necessary to comprehend the causes of circuit defects for its elimination. Mirth and Chase, 1995b, quantified the causes of circuit defect and developed a generalized procedure for synthesizing a Stephenson six-bar mechanism free from circuit defect. The designer can identify the segments of the Burmester curves to

eliminate them if they have defected. Alternatively, defect-specific constraints can be used such as constraints for circuit, branch, and order (CBO) defects in the optimal synthesis of Stephenson III mechanism for motion generation (Hwang and Chen, 2008).

From the literature review on four- and six-bar linkages, it is found that, in the kinematic synthesis of linkages, any mechanism that needs to be disassembled and reassembled to move between two desired positions is useless. However, the drivability problems may occur in the mechanisms which have branch defect. Various solution rectification techniques have been discussed extensively. Relatively, less work has been reported in defect elimination in the optimal synthesis of the four-bar mechanism for path generation. Besides, it is observed that CBO defects can be avoided by identifying and applying the constraint for each cause of the defect. The rectification procedure can be applied to Burmester curves while analytically synthesizing a mechanism for five or fewer precision points. Alternatively, GCP can be applied to modify the geometry till an acceptable solution is found that can pass through all the precision points smoothly. Lastly, constraints can be formulated for N-precision point optimal synthesis of a mechanism. It is found that constraints formulated for eliminating the CBO defects in six-bar consider three precision points simultaneously that increases complexity. Other methods either removes the Burmester segment which consists of the defect or provides the geometric model for eliminating the defects. Thus, there is a need to develop a simplified method which should also provide a mathematical model of the constraints to eliminate CBO defects.

## **2.5 Summary**

In this thesis, several synthesis procedures are explored and documented to synthesize a single degree of freedom planar linkage for supporting knee joint. The linkage synthesis procedure is proposed after exploring various techniques. Various knee supporting and gait rehabilitation devices have been reviewed in Section 2.1. It is observed that the devices use the single-axis joint, gear, and cam mechanisms at the knee of the assisting devices. Likewise, gait rehabilitation devices also use a single-axis, revolute joint at the knee. Devices which couple the knee and ankle movement through linkage mechanisms and which use linkage mechanisms for actuation are among others. Moreover, the mechanisms are synthesized using a “tear-drop” ankle trajectory in which the hip joint is considered stationary. The walking linkages are found to use the four-bar and six-bar mechanisms for imitating the whole lower limb. However, a complex set of equations is used that requires substantial computational effort for synthesis. The

literature review regarding the linkages used for walking is presented in Section 2.2 that reflects the importance of linkages in imitating walk. Therefore, linkage synthesis techniques for walking are explored. The literature review based on the synthesis procedures using geometrical, analytical, and optimization techniques is presented in Section 2.3. It is found that geometrical or graphical construction is relatively quick and straightforward; however, the designer may have to perform many iterations until the final design. In contrast, the ‘standard form’ of the equation is used to analytically synthesize mechanisms up to nine precision points. However, it is difficult to solve these equations when the precision points are between six and nine; their solutions converge to singular or imaginary solutions. Other approaches involve complexity, and a large number of iterations are required. The complexity may increase if the number of precision points becomes large. Another approach which is reviewed alongside analytical synthesis is optimal linkage synthesis technique, which is divided into three sub-sections, namely, local, global, and hybrid optimization techniques. It is concluded that local optimization techniques may be used for the synthesis; however, they involve calculation of derivatives and Hessians, and there also exist non-zero probability of obtaining a global optimum solution. In contrast, global optimization techniques may be used. However, refinement schemes may be applied, and algorithms may be merged to improve its computational effort. Various defects are encountered during synthesis of linkages; therefore, multiple techniques for defect identification and elimination are reviewed in Section 2.4. It is concluded that relatively less work has been reported in constraint formalism for the synthesis of defect-free four- and six-bar linkages to generate the path. Also, more than the required number of constraints are used, and constraints formulated for rectifying defects in six-bar that considers three precision points simultaneously involves complexity. The research gap is justified through the limitations of the approaches discussed.





## Analytical Synthesis of Planar Linkages

A planar linkage can be synthesized by geometrical or graphical construction, analytical, and optimal synthesis methods. The synthesis can be performed for either one or combination of function, motion, and path generation tasks. Various mathematical techniques to model planar linkages can be matrix, algebraic, and complex number methods. Among these, complex number technique is considered as the most versatile technique for the linkage synthesis. In this chapter, complex number modeling technique is explained for three- and four-precision points. Besides modeling technique, two distinct nontrivial numerical examples are considered to illustrate the path synthesis of the four-bar linkage.

### 3.1 Mathematical Modeling Using Complex-Number

The planar linkage can be modeled easily using the complex-vector formulation. Figure 3.1 represents a single-rigid bar in pure rotation with respect to complex coordinate system. The position of the point  $B_j^k$  on the  $j^{\text{th}}$  rigid bar,  $AB_j^k$ , at  $k^{\text{th}}$  rotation with respect to the global reference frame  $\{XAiY\}$  is represented by  $\mathbf{P}_j^k$ . Note the length of rigid bar does not change, therefore, the modulus of  $\mathbf{P}_j^k$  will be written as  $P_j$  for any orientation. The position vector at the initial or first position can be expressed in the complex-number form as follows:

$$\begin{aligned}\mathbf{P}_j^1 &= P_j e^{i\theta_1} \\ \mathbf{P}_j^1 &= P_j (\cos \theta_1 + i \sin \theta_1)\end{aligned}\quad (3.1)$$

where,  $\theta_1$  is the angle rotated by the rigid bar in the counter-clockwise direction when measured from real axis, i.e.,  $X$ , of the global reference frame  $\{XAiY\}$ , and,  $\beta_k$ , is the rotation angle of the rigid bar from position 1 to the  $k^{\text{th}}$  position.

If the rigid bar is further rotated by an angle,  $\beta_k$ , with respect to its previous position, then the  $k^{\text{th}}$  position of the  $AB_j^k$  in the pure rotation can be expressed as:

$$\mathbf{P}_j^k = P_j e^{i(\theta_1 + \beta_k)} \quad (3.2)$$

$$\beta_k = \theta_k - \theta_1 \quad (3.3)$$

$e^{i(\beta_k)}$  in Eqs (3.1) and (3.2) is called as the rotational operator that is responsible for rotating the vector between two positions by an angle,  $\beta_k$ .

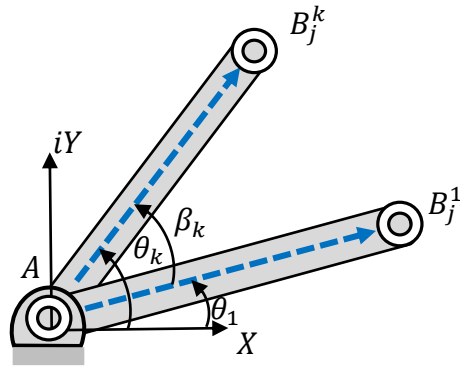


**Fig. 3.1** Complex-vector representation of single bar during pure rotation

The planar linkages are typically considered as the combination of two or more vector pairs which are also known as dyads. Fig 3.2 depicts a four-bar linkage as a combination of two dyads. The vector pair  $\mathbf{W}$  and  $\mathbf{Z}$  represent the left dyad whereas the right dyad is represented by the vector pair  $\mathbf{W}'$  and  $\mathbf{Z}'$ . The coupler point  $C$  moves along the point on the prescribed trajectory defined by the vector,  $\mathbf{R}_1$ , with respect to the reference frame as shown in Fig 3.2<sup>2</sup>. The coupler length  $\mathbf{BD}$  and the distance between the grounded points, i.e.,  $\mathbf{AE}$  can be determined by vector addition, when both dyads are synthesized.

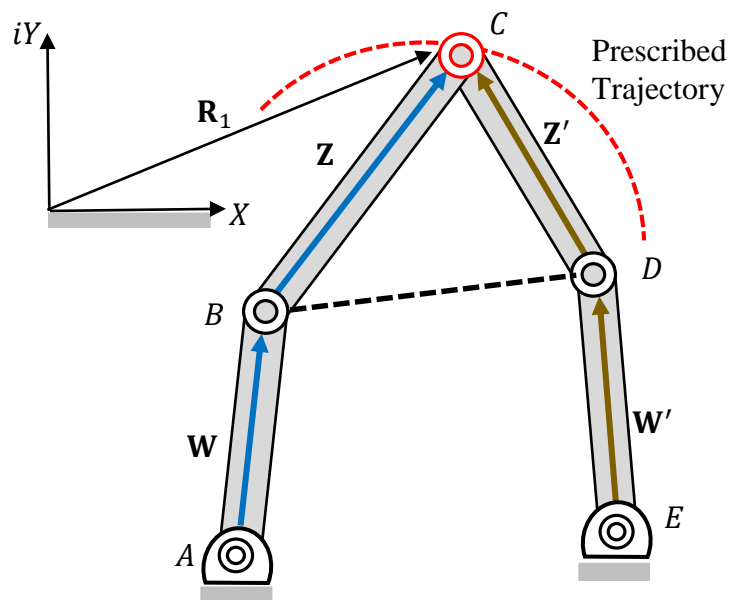


**Fig. 3.2** Dyad representation of a four-bar linkage

<sup>2</sup> BDC depicts a coupler link

The four-bar linkage can be designed by synthesizing the two dyads separately. A standard-form of the equation can be used for the synthesis in which angles are measured from an initial position in the counter-clockwise direction. Figure 3.3 represents the schematic of a dyad for  $k$  consecutive rotation angles corresponding to precision points. Vector  $\mathbf{W}$  rotates by angles,  $\beta_2, \beta_3 \dots \beta_k$ , corresponding to prescribed

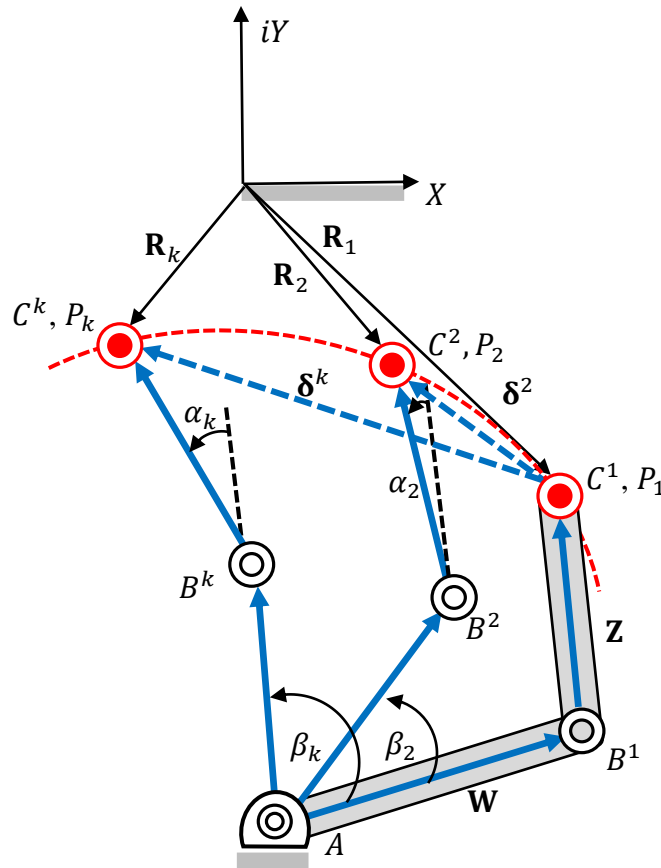


**Fig. 3.3** Schematic of Dyad for  $k$  consecutive positions

precision points  $P_2, P_3 \dots P_k$ . Likewise,  $\alpha_k$  are the rotation angles of the vector  $\mathbf{Z}$  from its initial to the  $k^{th}$  precision point. Based on the above definitions, the standard form of equation can be derived for a dyad,  $\mathbf{W} - \mathbf{Z}$ . Note, in this work, only path synthesis cases are considered. Details on the standard form of the equation for motion- and function-generation cases can be found in Ref., Erdman and Sandor, (1984). In the path-generation synthesis of a dyad,  $\mathbf{R}_1, \mathbf{R}_2, \dots, \mathbf{R}_k$ , is prescribed whereas  $\beta_2, \beta_3, \dots, \beta_k$  and  $\alpha_2, \alpha_3, \dots, \alpha_k$  can be considered as free choices for determining the unknown initial position of the dyad,  $\mathbf{W} - \mathbf{Z}$ . The loop-closure equation can be formed

by vector addition (clockwise sense) of the vectors forming the loops,  $AB^1C^1C^2B^2A, \dots, AB^1C^1C^k B^k A$ , etc.

When the dyad moves from first precision point,  $P_1$ , to second precision point,  $P_2$ , the first loop,  $AB^1C^1C^2B^2A$ , is formed and its loop-closure equation can be formed as follows:

$$\mathbf{W}e^{i\beta_2} + \mathbf{Z}e^{i\alpha_2} - \boldsymbol{\delta}^2 - \mathbf{Z} - \mathbf{W} = 0 \quad (3.4)$$

Likewise, other loop-closure equations for remaining  $k - 1$  loops can be formulated as:

$$\mathbf{W}e^{i\beta_3} + \mathbf{Z}e^{i\alpha_3} - \boldsymbol{\delta}^3 - \mathbf{Z} - \mathbf{W} = 0 \quad (3.5)$$

⋮

$$\mathbf{W}e^{i\beta_k} + \mathbf{Z}e^{i\alpha_k} - \boldsymbol{\delta}^k - \mathbf{Z} - \mathbf{W} = 0 \quad (3.6)$$

where  $\boldsymbol{\delta}^k = \mathbf{R}_k - \mathbf{R}_1$ , it is a displacement vector between the initial and  $k^{th}$  precision point.

Equation (3.6) can be simplified to form the ‘standard form’ of the equation which is expressed as:

$$\mathbf{W}(e^{i\beta_k} - 1) + \mathbf{Z}(e^{i\alpha_k} - 1) = \boldsymbol{\delta}^k \quad k = 2, 3, \dots, n \quad (3.7)$$

Using Eqs. (3.4)-(3.6) the left dyad,  $\mathbf{W} - \mathbf{Z}$ , of the four-bar linkage can be synthesized for  $k$  prescribed points. Similarly, the right dyad,  $\mathbf{W}' - \mathbf{Z}'$ , can be synthesized in which  $\alpha_k$  selected for the left dyad are considered as the prescribed values and  $\beta_k$  are replaced by  $\sigma_k$ .

The number of equations contained in the standard form equation depends on the number of prescribed precision points. There are two independent scalar equations which are referred as real and imaginary parts of the equation for two prescribed precision points. A total of six unknowns is present in these scalar equations which are  $W_x, W_y, Z_x, Z_y, \beta_2$ , and  $\alpha_2$ . These equations can be solved if four out of the six unknowns are chosen randomly. Therefore, there can be infinite choices for each unknown in the equation. In case of three precision points, two loop-closure equations are formed that results in four scalar equations. There are eight unknowns  $W_x, W_y, Z_x, Z_y, \beta_2, \beta_3, \alpha_2$ , and  $\alpha_3$  present in these scalar equations. To solve these equations four of the eight unknowns should be selected arbitrarily. Likewise, in case of four-precision points, three loop-closure equations are formed. These equations have six scalar equations that contain a total of ten unknowns,  $W_x, W_y, Z_x, Z_y, \beta_2, \beta_3, \beta_4, \alpha_2, \alpha_3$  and  $\alpha_4$ , therefore, the equations can only be solved if four of the ten unknowns are selected randomly. Thus

there are infinities of solutions in two, three, and four precision point synthesis for path generation. Another important task is the selection of the potential solution from infinities of solution. That can be achieved by developing an analytical model of the linkage. For three precision point path synthesis, a graphical search may be performed to get initial solutions for use in kinematic synthesis (Erdman and Sandor, 1984). In case of four precision points, the selection of linkage from the Burmester curve may be performed by eliminating the defected segments using Filemon's construction (Russell et al., 2013). The selected linkage may be analyzed to check its performance.

### 3.1.1 Synthesis of Path Generating Four-Bar Linkage for Two Precision Points

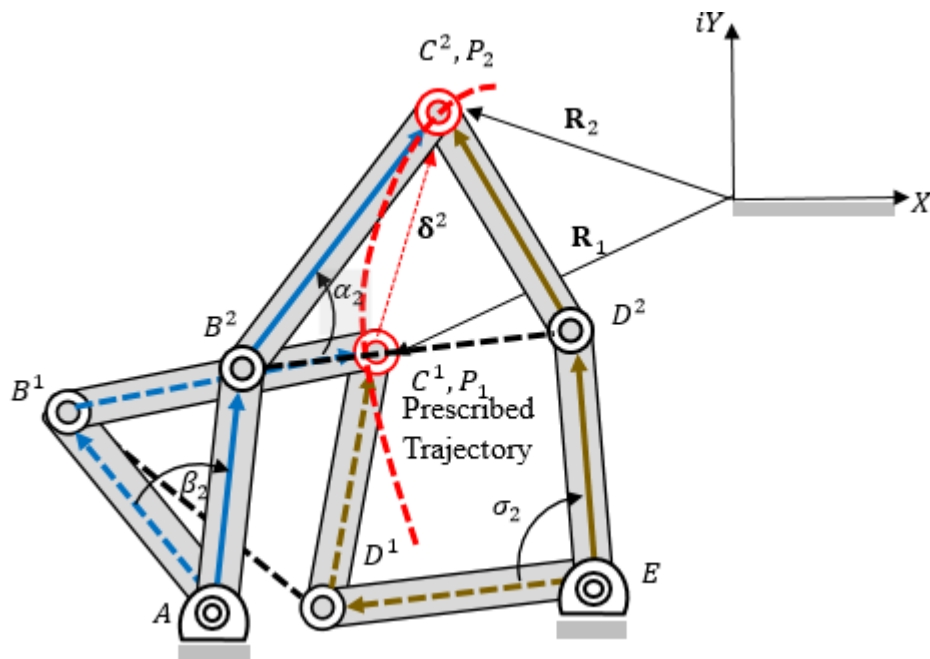


*Fig. 3.4 Path generating four-bar linkage for two-precision points*

Figure 3.4 shows the configuration of the four-bar linkage at two prescribed precision points. The points  $A$  and  $E$  are the ground or fixed pivots which are also known as center points; whereas, the moving pivots such as  $B^k$  and  $D^k$  are known as circle points. The circle point in any dyad connects the path point on the coupler link to the center point or the ground pivot. A four-bar can be synthesized using ‘standard form’ of the equation for two precision points. This can be done by separately synthesizing the ‘left-hand dyad’ and the ‘right-hand dyad.’ The notion of standard form of the equation, Eq. (3.7), presented in the previous section can be utilized as:

For left dyad:

$$\mathbf{W}(e^{i\beta_2} - 1) + \mathbf{Z}(e^{i\alpha_2} - 1) = \delta^2 \quad (3.8)$$

For right dyad:

$$\mathbf{W}'(e^{i\sigma_2} - 1) + \mathbf{Z}'(e^{i\alpha_2} - 1) = \delta^2 \quad (3.9)$$

where  $\delta^2$  is prescribed,  $\alpha_2, \beta_2, Z_x, Z_y$  are considered as free choices, and  $W_x, W_y$  are considered as unknowns. Equation (3.8) can be further simplified as:

$$\mathbf{W} = \frac{\delta^2 - \mathbf{Z}(e^{i\alpha_2} - 1)}{(e^{i\beta_2} - 1)} \quad (3.10)$$

$$\mathbf{W}' = \frac{\delta^2 - \mathbf{Z}'(e^{i\alpha_2} - 1)}{(e^{i\sigma_2} - 1)} \quad (3.11)$$

Eqs. (3.10) and (3.11) can be used for the synthesis of left- and right-hand dyad, respectively, to generate path while prescribing two precision points. The remaining two linkage vectors are determined by vector additions as:

$$\mathbf{B}^1\mathbf{D}^1 = \mathbf{Z} - \mathbf{Z}' \quad (3.12)$$

$$\mathbf{AE} = \mathbf{W} + \mathbf{B}^1\mathbf{D}^1 - \mathbf{Z}' \quad (3.13)$$

### 3.1.2 Synthesis of Path Generating Four-Bar Linkage for Three Precision Points

The loop-closure equations can be utilized for the synthesis of four-bar linkage for three precision points. Figure 3.5 depicts the configurations of the four-bar linkage at three precision points. The loop-closure equation can be formed as:

For left dyad:

$$\mathbf{W}(e^{i\beta_2} - 1) + \mathbf{Z}(e^{i\alpha_2} - 1) = \delta^2 \quad (3.14)$$

$$\mathbf{W}(e^{i\beta_3} - 1) + \mathbf{Z}(e^{i\alpha_3} - 1) = \delta^3 \quad (3.15)$$

For right dyad:

$$\mathbf{W}'(e^{i\sigma_2} - 1) + \mathbf{Z}'(e^{i\alpha_2} - 1) = \delta^2 \quad (3.16)$$

$$\mathbf{W}'(e^{i\sigma_3} - 1) + \mathbf{Z}'(e^{i\alpha_3} - 1) = \delta^3 \quad (3.17)$$

where  $\delta^2, \delta^3$  are prescribed,  $\alpha_2, \alpha_3, \beta_2, \beta_3, \sigma_2, \sigma_3$ , are considered as free choices, and  $W_x, W_y, Z_x, Z_y, W'_x, W'_y, Z'_x, Z'_y$  are considered as unknowns for both dyads. The complex system of equations, Eqs. (3.14)-(3.17), with known coefficients can be solved using Cramer's rule as follows:

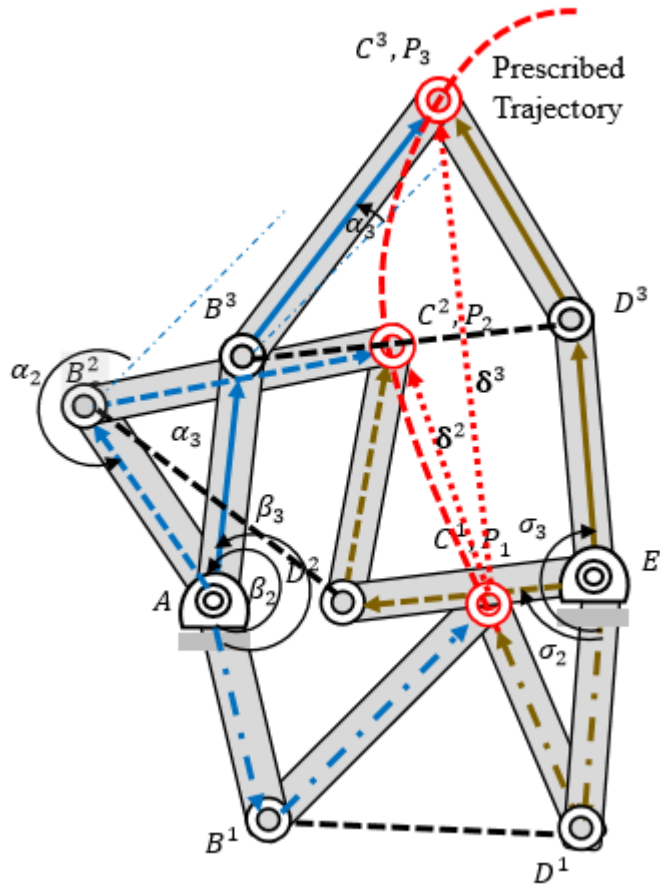


**Fig. 3.5** Path generating four-bar linkage for three-precision points

$$\mathbf{W} = \frac{\begin{vmatrix} \delta^2 & e^{i\alpha_2-1} \\ \delta^3 & e^{i\alpha_3-1} \end{vmatrix}}{\begin{vmatrix} e^{i\beta_2-1} & e^{i\alpha_2-1} \\ e^{i\beta_3-1} & e^{i\alpha_3-1} \end{vmatrix}} \quad (3.18)$$

$$\mathbf{Z} = \frac{\begin{vmatrix} e^{i\beta_2-1} & \delta^2 \\ e^{i\beta_3-1} & \delta^3 \end{vmatrix}}{\begin{vmatrix} e^{i\beta_2-1} & e^{i\alpha_2-1} \\ e^{i\beta_3-1} & e^{i\alpha_3-1} \end{vmatrix}} \quad (3.19)$$

$$\mathbf{W}' = \frac{\begin{vmatrix} \delta^2 & e^{i\alpha_2-1} \\ \delta^3 & e^{i\alpha_3-1} \end{vmatrix}}{\begin{vmatrix} e^{i\sigma_2-1} & e^{i\alpha_2-1} \\ e^{i\sigma_3-1} & e^{i\alpha_3-1} \end{vmatrix}} \quad (3.20)$$

$$\mathbf{Z}' = \frac{\begin{vmatrix} e^{i\sigma_2-1} & \delta^2 \\ e^{i\sigma_3-1} & \delta^3 \end{vmatrix}}{\begin{vmatrix} e^{i\sigma_2-1} & e^{i\alpha_2-1} \\ e^{i\sigma_3-1} & e^{i\alpha_3-1} \end{vmatrix}} \quad (3.21)$$

### 3.1.3 Synthesis of Path Generating Four-Bar Linkage for Four Precision Points

The four-bar linkage as shown in Fig 3.5 can be synthesized for four-precision points to generate the path. The standard form of the equation derived in Section 3.1 can be utilized here; however, the prescribed angles and unknowns are different as compared to those used for three precision points. For four precision points,  $\delta^4$  is prescribed besides  $\delta^2$  and  $\delta^3$ ; whereas  $\beta_4, \alpha_4, \alpha_2, \alpha_3, \beta_2, \beta_3$  are considered as free choices, for **W-Z** dyad. The system of complex equations, Eqs. (3.4)-(3.6), of one dyad **W-Z** can be utilized for four precision points as:

$$\mathbf{W}(e^{i\beta_2} - 1) + \mathbf{Z}(e^{i\alpha_2} - 1) = \delta^2 \quad (3.22)$$

$$\mathbf{W}(e^{i\beta_3} - 1) + \mathbf{Z}(e^{i\alpha_3} - 1) = \delta^3 \quad (3.23)$$

$$\mathbf{W}(e^{i\beta_4} - 1) + \mathbf{Z}(e^{i\alpha_4} - 1) = \delta^4 \quad (3.24)$$

The method proposed by Erdman and Sandor, 1984 can be used for solving the Eqs. (3.22)-(3.24). The equations can be represented in matrix form as:

$$\begin{bmatrix} e^{i\beta_2} - 1 & e^{i\alpha_2-1} \\ e^{i\beta_3} - 1 & e^{i\alpha_3-1} \\ e^{i\beta_4} - 1 & e^{i\alpha_4-1} \end{bmatrix} \begin{bmatrix} \mathbf{W} \\ \mathbf{Z} \end{bmatrix} = \begin{bmatrix} \delta^2 \\ \delta^3 \\ \delta^4 \end{bmatrix} \quad (3.25)$$

The compatibility relations of the coefficient of the equations have to be satisfied if one of the three complex equations linearly depends upon remaining equations, then the Eqs. (3.22)-(3.24) have simultaneous solutions for **W** and **Z**. Therefore to have simultaneous solutions of Eq. (3.25), an augmented matrix is formed by adding right-hand matrix,  $\delta^k$ , to the coefficients of the left hand matrix and the determinant of the augmented matrix should be zero.

$$\det \begin{bmatrix} e^{i\beta_2} - 1 & e^{i\alpha_2-1} & \delta^2 \\ e^{i\beta_3} - 1 & e^{i\alpha_3-1} & \delta^3 \\ e^{i\beta_4} - 1 & e^{i\alpha_4-1} & \delta^4 \end{bmatrix} = 0 \quad (3.26)$$

The determinant, Eq (3.26), can be expanded about its first column as:

$$\Delta_2 e^{i\beta_2} + \Delta_3 e^{i\beta_3} + \Delta_4 e^{i\beta_4} + \Delta_1 = 0 \quad (3.27)$$

$$\Delta_1 + \Delta_2 + \Delta_3 + \Delta_4 = 0 \quad (3.28)$$

where,

$$\begin{aligned} \Delta_2 &= \begin{vmatrix} e^{i\alpha_3-1} & \delta^3 \\ e^{i\alpha_4-1} & \delta^4 \end{vmatrix} \\ \Delta_3 &= - \begin{vmatrix} e^{i\alpha_2-1} & \delta^2 \\ e^{i\alpha_4-1} & \delta^4 \end{vmatrix} \\ \Delta_4 &= \begin{vmatrix} e^{i\alpha_2-1} & \delta^2 \\ e^{i\alpha_3-1} & \delta^3 \end{vmatrix} \end{aligned} \quad (3.29)$$

Since  $\alpha_k$  and  $\delta^k$  are known, therefore,  $\Delta_i$  is known for  $i = 1, \dots, 4$ . The sets of  $\beta_2, \beta_3$ , and  $\beta_4$  for randomly selected  $\beta_2$  that satisfies Eq. (3.27) will make the system



of Eqs. (3.22)-(3.24) compatible. Thus Eq. (3.27) is known as compatibility equation in which unknowns are expressed in the form of exponents of the exponential function. A graphical procedure is adapted for calculating range of values of  $\beta_3$  and  $\beta_4$  for a prescribed range of  $\beta_2$ . For an arbitrary choice of  $\beta_2$ ,  $\beta_3$  and  $\beta_4$  can be easily calculated through an algorithm based on geometrical construction (Erdman and Sandor, 1984). Equation (3.27) reveals that  $\Delta_2$ ,  $\Delta_3$  and  $\Delta_4$  are multiplied by rotational operators  $e^{i\beta_2}$ ,  $e^{i\beta_3}$ , and  $e^{i\beta_4}$ , respectively, which indicates the rotation of  $\Delta_2$ ,  $\Delta_3$  and  $\Delta_4$  by angles  $\beta_2$ ,  $\beta_3$  and  $\beta_4$ , respectively, while they are in closed loop with  $\Delta_1$ . Therefore Eq. (3.27) can be considered as a loop-closure equation of a compatibility linkage with four links, namely,  $\Delta_1$  (fixed link), and  $\Delta_i$  movable links,  $i = 2,3,4$ . Figure 3.6 represents the geometric construction of the compatibility linkage that can be used to forming an

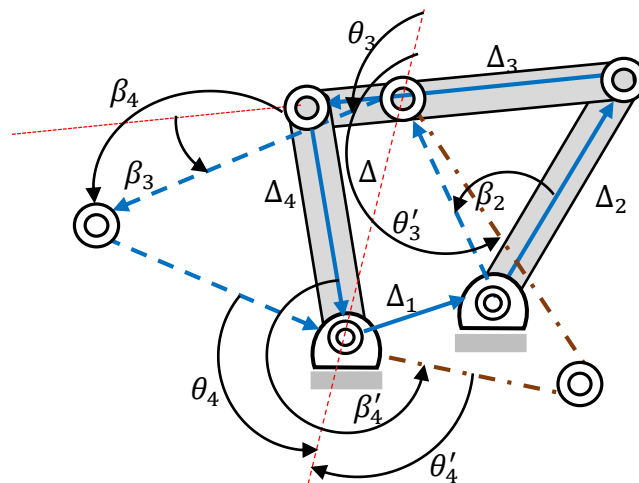


**Fig. 3.6** Geometric construction of the compatibility linkage

analytical solution. Equation (3.27), can be simplified for determining the rotation angles of driving link  $\beta_3$  and  $\beta_4$  for the prescribed range of  $\beta_2$ . An algorithm proposed by Erdman and Sandor, (1984), is presented for solving the compatibility equation based on the geometric construction.

$$\Delta_3 e^{i\beta_3} + \Delta_4 e^{i\beta_4} = -\Delta \quad (3.30)$$

$$\Delta = \Delta_2 e^{i\beta_2} + \Delta_1 \quad (3.31)$$

An algorithm for solving the compatibility equation (Erdman and Sandor, 1984; Russell et al., 2013)

$$\Delta = \Delta_2 e^{i\beta_2} + \Delta_1$$

$$\cos \theta_3 = \frac{\Delta_4^2 - \Delta_3^2 - \Delta^2}{2\Delta_3\Delta}$$

$$\sin \theta_3 = \left| \sqrt{1 - \cos^2 \theta_3} \right| \geq 0, \text{ Then, use } \text{atan2}^3(\sin \theta_3, \cos \theta_3)$$

$$\beta_3 = \arg \Delta + \theta_3 - \arg \Delta_3$$

$$\theta_3' = 2\pi - \theta_3$$

$$\beta_3' = \arg \Delta + \theta_3' - \arg \Delta_3$$

$$\cos \theta_4 = \frac{\Delta_3^2 - \Delta_4^2 - \Delta^2}{2\Delta_4\Delta}$$

$$\sin \theta_4 = \left| \sqrt{1 - \cos^2 \theta_4} \right| \geq 0 \text{ Then, use } \text{atan2}(\sin \theta_4, \cos \theta_4)$$

$$\beta_4 = \arg \Delta - \theta_4 - \arg \Delta_4$$

$$\beta_4' = \arg \Delta + \theta_4 - \arg \Delta_4 + \pi$$

According to mobility limits of the compatibility linkage, the range of  $\beta_2$  may be selected to obtain the corresponding values of  $\beta_3$ ,  $\beta_4$ ,  $\beta_3'$ , and  $\beta_4'$ . This enables the user to select  $\beta$ 's from the sets  $\beta_2$ ,  $\beta_3$ ,  $\beta_4$  and  $\beta_2$ ,  $\beta_3'$ ,  $\beta_4'$ . This information is sufficient to solve any two of the three Eqs. (3.22)-(3.24) simultaneously to determine  $\mathbf{W}$  and  $\mathbf{Z}$ , as shown in the previous section. The circle point and center points can be generated using  $\mathbf{W}$  and  $\mathbf{Z}$ .

$$\mathbf{k}_1 = \mathbf{R}_1 - \mathbf{Z} \quad (3.32)$$

$$\mathbf{m} = \mathbf{k}_1 - \mathbf{W} \quad (3.33)$$

Two sets of center and circle points forming two curves can be generated for a selected range of  $\beta_2$ . Any point on the center point curve may be regarded as a ground pivot that can be linked to its conjugate point on the circle point curve in that particular set. In this way, a dyad is formed on that  $\mathbf{k}_1 - \mathbf{m}$  pair that may be combined with another dyad to form a path generating four-bar linkage.

### 3.2 Numerical Examples

In this section, the four-bar linkage is considered as a typical case to synthesize for three- and four-precision points using the theory explained above (Erdman and Sandor, 1984). Two numerical examples are discussed here for three- and four-precision syntheses and analyses of a path generating four-bar linkage.

#### 3.2.1 Three Precision Point Synthesis

---

<sup>3</sup> atan2 is a MATLAB® function

A nontrivial four-bar linkage is designed for flexion/extension movement of a human knee joint. Three points are on the known flexion/extension trajectory of a healthy human knee joint, shown in Table 3.1 (Sancibrian et al., 2016) are selected as desired points. The prescribed points are taken here at an apparently equal interval. The points 1, 7, and 14 are selected from the given points.

**Table 3.1** Desired points for knee flexion (Sancibrian et al., 2016)

Desired Points	1	2	3	4	5	6	7	8	9	10	11	12	13	14
$P_{xd}$	-50	-16	10	14	6	0	-5	-10	-15	-20	-25	-30	-35	-40
$P_{yd}$	200	150	100	60	18	0	-12	-19	-21.5	-22	-21	-18	-11	0

The values of  $\delta$ 's are prescribed indirectly in the form of given coordinates  $\mathbf{P}_i$  for  $i = 1, 2, 3$ .

$$\delta^k = \mathbf{R}_1 - \mathbf{R}_k$$

Here, prescribed values are:

$$\mathbf{R}_1 = -50 + i200; \mathbf{R}_2 = -5 - i12; \mathbf{R}_3 = -40 + i0$$

$$\delta^2 = -45 + i212; \delta^3 = -10 + i200$$

Randomly selected values:

$$\alpha_2 = -70^\circ; \alpha_3 = -90^\circ; \beta_2 = 50^\circ; \beta_3 = 90^\circ; \sigma_2 = 50^\circ; \sigma_3 = 240^\circ$$

Using Eqs. (3.18)-(3.21), the following results are obtained:

$$\mathbf{W} = -1.8446 - i91.7490$$

$$\mathbf{Z} = 186.75 + i103.16$$

$$\mathbf{W}' = -25.1821 - i16.1446$$

$$\mathbf{Z}' = 129.91 + i116.12$$

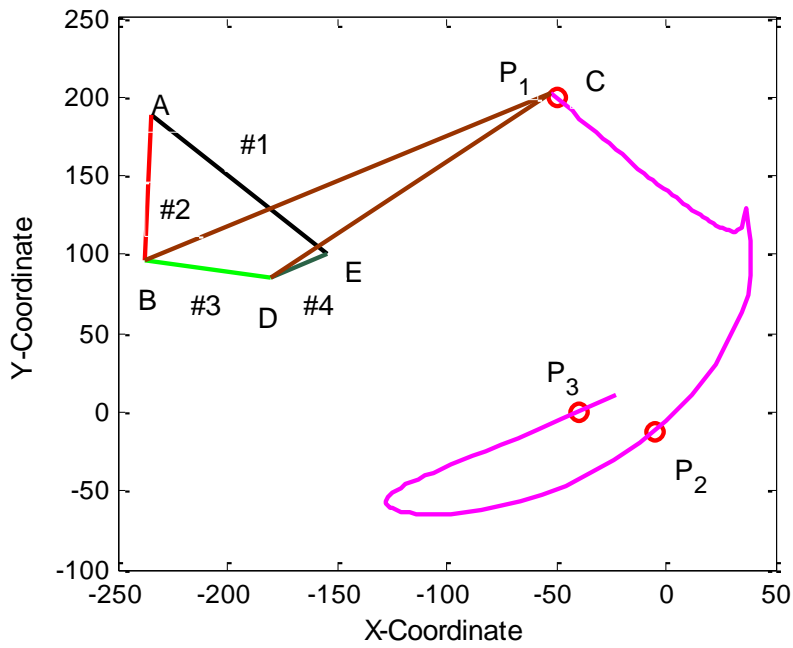


**Fig. 3.7** Synthesized four-bar linkage for three precision points

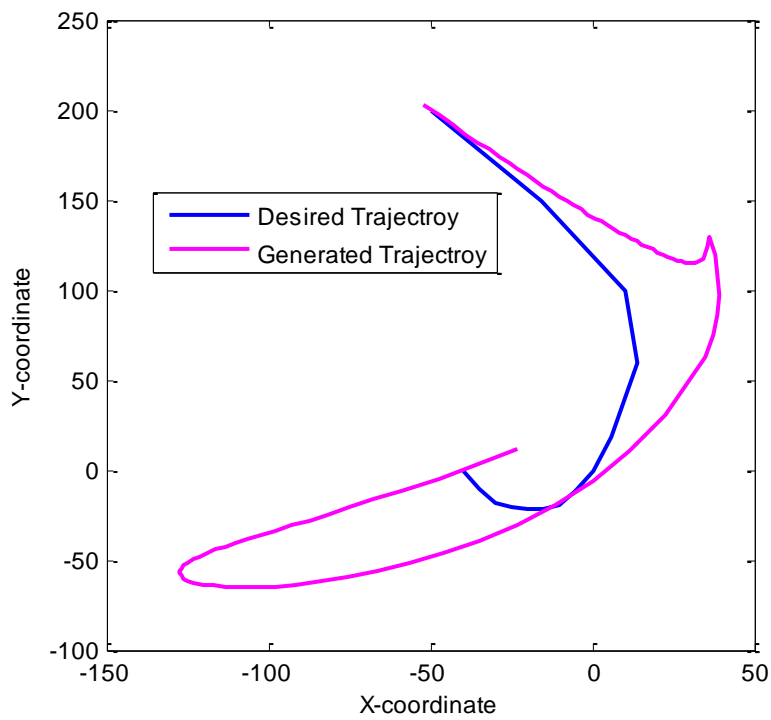


**Fig. 3.8** Deviation of generated trajectory from desired trajectory

Coordinates of moving and fixed centers can be determined using Eqs. (3.22) and (3.33) as:

$$\mathbf{B} = \mathbf{R}_1 - \mathbf{Z}; \mathbf{A} = \mathbf{B} - \mathbf{W}; \mathbf{D} = \mathbf{R}_1 - \mathbf{Z}'; \mathbf{E} = \mathbf{D} - \mathbf{W}'$$

$$\mathbf{B} = -236.75 + i96.845; \quad \mathbf{A} = -234.90 + i188.59; \quad \mathbf{D} = -179.91 + i83.883; \quad \mathbf{E} = -154.73 + i100.03$$

It is found that synthesized four-bar linkage can track the desired three precision-points accurately, shown in Fig 3.7 and Fig 3.8. However, the generated trajectory between any two precision points deviates from the prescribed trajectory. Thus, the number of desired precision points is increased to four for synthesis and analyses of a path generating four-bar linkage.

### 3.2.2 Four Precision Point Synthesis

A nontrivial four-bar linkage is designed for landing gear through four precision-points. In this section, instead of considering three points on the desired trajectory, four precision points are considered, shown in (Russell et al., 2013). The prescribed points  $P_{xd}$  and  $P_{yd}$  for landing gear (Russell et al., 2013) are as follows:

$$(1,0); (0.292,0.734); (0.251,1.227); (0.299,1.461)$$

Here, prescribed values are (Russell et al., 2013):

$$\mathbf{R}_1 = 0 + i0; \mathbf{R}_2 = 0.292 + i0.734; \mathbf{R}_3 = 0.251 + i1.227; \mathbf{R}_4 = 0.299 + i1.461$$

$$\delta^2 = -0.292 - i0.734; \delta^3 = -0.251 - i1.227; \delta^4 = -0.299 - i1.461$$

Randomly selected values:

$$\alpha_2 = -51.7124^\circ; \alpha_3 = -66.9732^\circ; \alpha_4 = -84.9734^\circ; \text{Range of } \beta_2 = 170^\circ - 270^\circ$$

Using Eqs. (3.26)-(3.33), the following results are obtained:

$$\mathbf{W} = -0.3857 + i1.3019$$

$$\mathbf{Z} = -1.1528 - i2.3842$$

$$\mathbf{W}' = -0.3476 + i1.4557$$

$$\mathbf{Z}' = -1.2158 - i2.5354$$

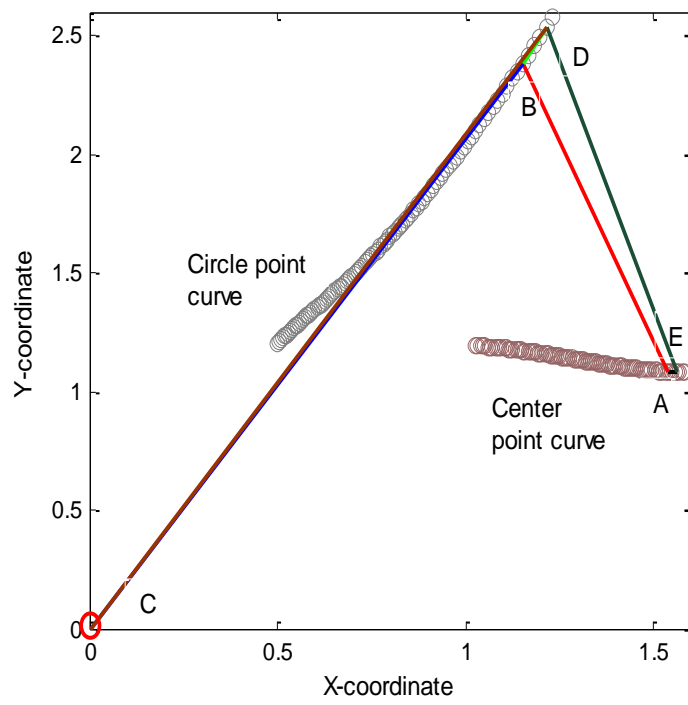


**Fig. 3.9** Synthesized four-bar linkage for four precision-points

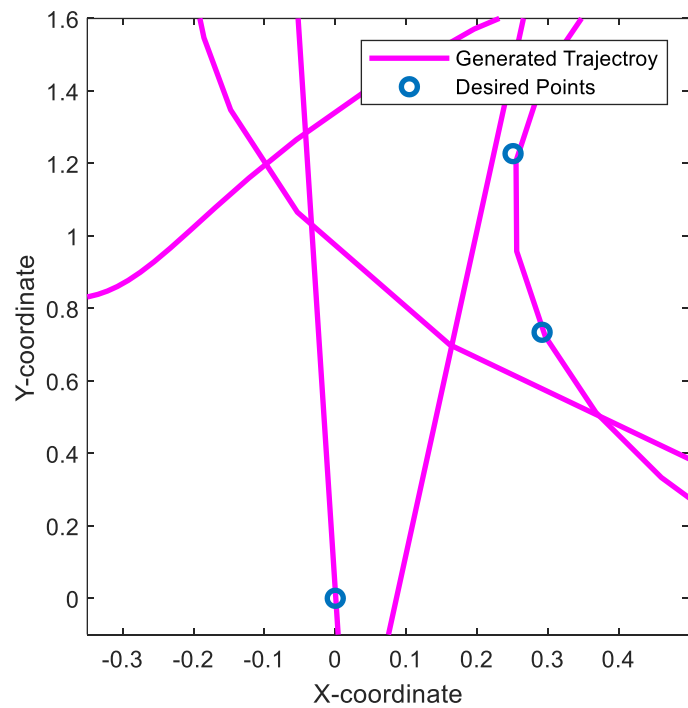


**Fig. 3.10** Deviation between desired points and generated trajectory

Coordinates of moving and fixed centers can be determined using Eqs. (3.22) and (3.33) as:

$$\mathbf{B} = \mathbf{R}_1 - \mathbf{Z}; \mathbf{A} = \mathbf{B} - \mathbf{W}; \mathbf{D} = \mathbf{R}_1 - \mathbf{Z}'; \mathbf{E} = \mathbf{D} - \mathbf{W}'$$

$$\mathbf{B} = 1.1528 + i2.3842; \mathbf{A} = 1.5385 + i1.0823; \mathbf{D} = 1.2158 + i2.5354; \mathbf{E} = 1.5634 + i1.0797$$

It is observed that four-bar linkage designed using the above approach can track all the desired precision-points accurately, shown in Figs 3.9 and 3.10. However, the generated trajectory between any two precision points may deviate from the actual trajectory. Besides, in this synthesis procedure, infinite solutions are obtained, and all solutions are not feasible. In the above example, a sample solution is chosen in which the frame link and coupler link lengths are relatively small in comparison with other links. Hence, it is left for the designer to select the four-bar linkage accordingly. In contrast, the synthesis may be performed optimally to consider more desired precision points for synthesizing path generating four-bar linkage. Furthermore, analytical methods are usually preferred when accuracy is a major concern. They design linkages which precisely pass through the desired points (Erdman, 1981; Freudenstein, 2010). However, in exoskeletons, trajectory shapes are preferred over precision points that makes optimization-based methods a more suitable choice for dimensional synthesis (Shen et al., 2018).

### 3.3 Summary

This chapter discusses the analytical synthesis of planar four-bar linkage for three and four precision points. The complex number based synthesis procedure is presented in detail for path generating linkages for three and four precision points. Besides, two distinct realistic numerical examples of the human knee and landing gear are presented and explained to synthesize a path generating four-bar linkage for three and four-precision points, respectively. In case of three-precision point example, the desired points overlap on the generated trajectory; however, there is a finite deviation between the desired and generated trajectories. In contrast, the deviation is huge in case of four-precision point example, but the generated trajectory precisely passes through the desired points.





## Nature-Inspired Optimization Algorithms

In this chapter, a hybrid-teaching learning particle swarm optimization algorithm (HTLPSO) is proposed which merges two well-established algorithms, namely, TLBO and PSO. It is observed that PSO provides result very quickly, but its ability to solve the optimal solutions especially for real-life problems is insufficient (Gao and Xu, 2011). Also, the new solution replaces the old solution instead of considering the best solution which reflects its explorative tendency, and it lacks exploitation (Rao and Savasani, 2012). The only exploration of search space may avoid an algorithm for finding the accurate approximation of the optimum solution. In contrast to PSO, the TLBO algorithm incorporates both exploration and exploitation in the teaching, and learning phases. The TLBO and PSO are combined in HTLPSO which uses the explorative tendency of PSO with the explorative and exploitation tendency of teaching phase-TLBO. The combination appends the exploration of PSO and Teaching-Learning phases of TLBO. This is due to the use of extra updating mechanisms of swarms of PSO and learners of TLBO in HTLPSO.

This chapter proposes a novel optimization algorithm which merges the explorative tendency of PSO with the Teacher phase of TLBO to generate a new population. This population is used in Learner phase of TLBO and final population obtained after Learner phase ends one iteration. Hence, this algorithm is named as hybrid-teaching learning particle swarm optimization (HTLPSO) algorithm. By merging these two algorithms, the HTLPSO generates better results than either method alone. The proposed algorithm is applied for path synthesis problem of linkages. Five constrained benchmark functions are considered here to validate the algorithm proficiency. The feasibility and limitations of the new algorithm are suggested by analyzing the results of the single and hybridized algorithms.

### 4.1 Teaching-Learning-Based Optimization (TLBO)

TLBO is a population-based nature-inspired algorithm that does not require tuning of parameters. Parameter tuning is to find good values for the parameter before running the algorithm, and subsequently, the values remain constant for the whole process (Eiben et al., 1999). Therefore, the implementation of TLBO is the simplest among nature-inspired algorithms. It works on the philosophy of natural teaching-learning process. Here, each learner is offered a set of courses in which grades are awarded. The grade set of all learners collectively is called population set. The class is analogous to

the population set in any nature-inspired algorithm while the set of courses offered to the learners is considered as design variables and numeric grades obtained by learners are considered as values of design variables. Furthermore, learners' result is akin to objective function value of optimization problem. The algorithm works in two phases, namely, teacher phase and learner phase for each iteration.

#### **4.1.1 Teacher Phase**

Learners in the teachers' phase learn through the teacher. A teacher is considered as the most learned and knowledgeable person of a course. Therefore, a learner with the best grade qualifies for the teacher. The teacher improves the mean result of his class, which depends on the quality of himself and learners. In this phase, course grades of all learners are updated based on the course grade of the best learner, who qualified as a teacher. This step acts as the explorative tendency of the teacher phase. Subsequently, a greedy selection between initial and updated grades is exploitation. In greedy selection, learners with better results are kept along with their course grades and the new class is formed. Thus, teacher phase uses both explorative and exploitation tendencies. The teacher phase ends with the formation of a new class, which is treated as initial population for the Learner phase of the algorithm.

#### **4.1.2 Learner Phase**

Learning is possible in two ways: one through teacher and other by mutual interaction among learners. Here, learners learn through mutual interactions. This phase starts with the new class formed at the end of teacher phase. In this phase also, both exploration and exploitation exist. In order to improve the grades, learners interact with at least one other learner in the class. The grade of the learners is improved if another learner has a better grade in the corresponding course. Exploration is followed by greedy selection as in teacher phase with formation of a new class. This ends the Learner phase and first iteration (teaching-learning cycle). The new class formed by greedy selection is used for next iteration in teacher phase.

Various parameters used in this algorithm are described below:

- $p$  = population size, i.e., number of learners in a class
- $d$  = number of design variables, i.e., number of courses offered to learners
- $L_i, U_i$  = lower and upper limit on  $i^{th}$  design variable, i.e., minimum and maximum numeric grade in the  $i^{th}$  course

$t$  =  $t^{th}$  iteration  
 $c$  = the number of classes in a teaching-learning cycle  
 $f_j^c$  = the objective function value of  $j^{th}$  learner of  $c^{th}$  class  
 $\mu_i$  = Mean of  $i^{th}$  course grades of whole class  
 $G_i$  = Grade of the  $i^{th}$  course whose objective function value is minimum  
 $g_{ji}^q$  = Grade of the  $i^{th}$  course of the  $j^{th}$  learner and for  $q^{th}$  class,  $q = 1 \dots c$   
 $I$  = Number of iterations  
 $rand$  = Random number between 0 and 1

Note that class term is used here for population set ( $p \times d$ ).

---

**Algorithm begins :**

Input: population size, i.e.,  $p$   
 number of courses offered to learners, i.e.,  $d$   
 lower and upper limit for all the courses, i.e.,  $L_i$  and  $U_i$  where  
 $i = 1, \dots, d$  course  
 number of iterations,  $I$

**% Start of Teacher phase**

Initialize: % Initialize course grades for all learners and this is class one  
 for  $j = 1 \dots p$  % whole class  
     for  $i = 1 \dots d$  % all courses  
         % Grade of the  $i^{th}$  course of the  $j^{th}$  learner  
          $g_{ji}^1 = L_i + rand(U_i - L_i)$   
     end loop  
 $c_1 = \{g_{ij}^1; j = 1, \dots, p; i = 1, \dots, d\}$   
 % here class one is created with all course grades  
 % From result of all learners identify the best learner grade for  
 $i^{th}$  course,  $G_i$   
 end loop  
 % Start of  $t^{th}$  iteration  
 % Mean of  $i^{th}$  course grade of whole class  

$$\mu_i = \frac{\sum_{j=1}^p g_{ji}^1}{p}$$

---

```

% Update course grade for whole class
for j = 1 ... p      % whole class
    for i = 1 ... d  % all courses
         $g_{ji,t}^2 = g_{ji}^1 + \text{rand}(G_i - \mu_i)$     % for  $t^{\text{th}}$  iteration
    end loop
 $c_2 = \{g_{ij}^2; j = 1, \dots, p; i = 1, \dots, d\}$ 
% Compare and compute the values of objective functions for first
and second class, i.e.,  $f_j^1$  and  $f_j^2$ 
% Greedy selection for better result
if  $f_j^1 < f_j^2$ 
     $g_{ji,t}^3 = g_{ji,t}^1$ 
else
     $g_{ji,t}^3 = g_{ji,t}^2$ 
end
end loop
 $c_3 = \{g_{ij}^3; j = 1, \dots, p; i = 1, \dots, d\}$ 
% End of Teacher Phase

% Start of Learner phase
% Compare results of two learners j and l from the third class
of learners
for j = 1 ... l ... p      and  $j \neq l$ 
    if  $f_j^3 < f_l^3$ 
        for i = 1 ... d
             $g_{ji,t}^4 = g_{ji}^3 + \text{rand}(g_{ji,t}^3 - g_{li,t}^3)$ 
        end loop
    else
        for i = 1 ... d
             $g_{ji,t}^4 = g_{ji}^3 + \text{rand}(g_{li,t}^3 - g_{ji,t}^3)$ 
        end loop
    end
 $c_4 = \{g_{ij}^4; j = 1, \dots, p; i = 1, \dots, d\}$ 

```

---

```

% Greedy selection for better result between third and fourth
class
    if  $f_j^3 < f_j^4$ 
        % Update course grades
         $g_{ji,t}^5 = g_{ji}^3$ 
    else
         $g_{ji,t}^5 = g_{ji}^4$ 
    end
end loop
% Check limits on the course grades
for  $j = 1 \dots p$  % whole class
    for  $i = 1 \dots d$  % all courses
         $g_{ji,t}^5 = \max(g_{ji,t}^5, L_i)$ 
         $g_{ji,t}^5 = \min(g_{ji,t}^5, U_i)$ 
    end loop
end loop
 $c_5 = \{g_{ij}^5; j = 1, \dots, p; i = 1, \dots, d\}$ 
% End of Learner phase
% End of  $t^{\text{th}}$  iteration

```

**Algorithm ends**

**Fig. 4.1** Algorithm for teaching-learning-based optimization

Figure 4.1 shows the detailed algorithm for teaching-learning-based optimization. In this algorithm, five classes, namely,  $c_1, \dots, c_5$ , are formed in each iteration and the fifth class obtained after Learner phase is treated as the first class of learners for next iteration. A cycle of Teacher-Learner phase completes one iteration.

#### 4.2 Particle Swarm Optimization (PSO)

PSO is a nature-inspired algorithm, and it exhibits common nature-inspired algorithm attributes such as random population initialization and optimum value search by updating generations. It is inspired by the simulation of environmental conditions. The main focus is to simulate graphically its smooth but unpredictable choreography of a bird flock. Potential solutions are called particles, which track their coordinates in the problem space corresponding to best fitness (solution) achieved so far. The value

obtained is known as ‘*pBest*’ while the location (value) obtained corresponding to overall best value is called ‘*gBest*.’ In PSO, velocity changes (i.e., accelerating) at each step towards its ‘*pBest*’ and ‘*gBest*’ locations. Acceleration is weighted by two separate random numbers towards ‘*pBest*’ and ‘*gBest*’ locations. Following equations are used for updating velocity and position:

$$V_{i+1} = wV_i + c_{1a}r_1(pBest_i - X_i) + c_{2a}r_2(gBest_i - X_i) \quad (4.1)$$

$$X_{i+1} = X_i + V_{i+1} \quad (4.2)$$

where  $V_{i+1}$  denotes a new velocity for each particle based on its previous velocity,  $X_{i+1}$  denotes the updated particle’s position,  $r_1$  and  $r_2$  are two random numbers generated in the range  $[0, 1]$ ,  $w$  is the constant parameter (inertia weight);  $c_{1a}$  and  $c_{2a}$  are the acceleration constants in which  $c_{1a}$  represents confidence of particle in itself while  $c_{2a}$  represents confidence of particle in swarm. Thus, the low and high values of these constants allow the particles to flow far from the target before being pulled back and abrupt movement towards, or past, the target, respectively (Rao and Savasani, 2012; Dong et al., 2005). In contrast to GA, PSO does not require a special genetic operator. Here, evolution focuses only on the best solution and all the particles tends to converge to the best solution. The algorithm for PSO is shown in Fig 4.2.

**Algorithm begins :**

Input :                      population size, i.e.,  $p$   
                                   number of particles, i.e.,  $d$   
                                   lower and upper limit for all the particles, i.e.,  $L_i$  and  $U_i$  where  
                                    $i = 1, \dots, d$   
                                   number of iterations,  $I$   
                                   inertia weight,  $w$   
                                   acceleration factor,  $c_{1a}$   
                                   acceleration factor,  $c_{2a}$

*%Particle Swarm optimization initialization*

*for j = 1 ... p                      % whole population*

*for i = 1 ... d                % all particles*

*$x_{j,i}^0 = L_i + rand(U_i - L_i)$  % Initial position*

*end loop*

*end loop*

```

 $x = x^0$  % Current position
 $v^0 = 0.1x^0$  % Current velocity
% Compute objective function value  $f^0$  using current position
pBest ( $x^0$ ) and find gBest (value of  $x_{ji}^0$  for which objective
function value is minimum)

%Particle Swarm optimization algorithm starts, Start of Iteration
% Update velocity using Eq. (4.1)
for j = 1 ... p
    for i = 1 ... d
         $v_{j,i}^1 = wv_{j,i}^0 + c_{1a} * rand(pBest_{j,i} - x_{j,i}) + c_{2a}$ 
            * rand(gBest_{j,i} - x_{j,i})
    end loop
end loop
% Update position using Eq. (4.2)
for j = 1 ... p
    for i = 1 ... d
         $x_{j,i}^1 = x_{j,i}^0 + v_{j,i}^1$ 
    end loop
end loop
% Handling boundary constraints
for j = 1 ... p
    for i = 1 ... d
        if  $x_{j,i}^1 < L_i$ 
             $x_{j,i}^1 = L_i$ 
        elseif  $x_{j,i}^1 > U_i$ 
             $x_{j,i}^1 = U_i$ 
        end
    end loop
end loop
% Compute fitness  $f^1$  for the updated position
% Update the pBest and fitness

```

```

for j = 1 ... p
    if  $f_j^1 < f_j^0$ 
        % Update pBest corresponding to better fitness
         $f_j^0 = f_j^1$ 
    end
end loop
% Now, update gBest and fitness similarly
% End of PSO, End of Iteration

```

**Algorithm Ends**

**Fig. 4.2** Algorithm for particle swarm optimization

### 4.3 Hybrid-Teaching Learning Particle Swarm Optimization (HTLPSO)

HTLPSO is a hybridized technique developed by merging PSO and TLBO. This merging makes the new algorithm useful for finding the optimum solution in the lesser number of function evaluations. The flowchart in Fig. 4.3 illustrates HTLPSO technique. HTLPSO begins with the initialization of the population randomly. Simultaneously, initialization of PSO algorithm parameters is also done. The population so generated is treated as initial population for teacher phase in TLBO and PSO. The best half of the population obtained in teacher phase is merged with the best half obtained in PSO. The resulting population will be of the same size as the size of the initial population. This population is used in the learner phase of TLBO, where established learner phase technique is applied. The final population obtained after learner phase will be treated as the initial population for the next iteration. The size of the final population is same as the size of the population, which is initialized randomly. This completes one iteration of HTLPSO. This combination of established techniques takes care of the drawback of exploitation tendency of PSO and provides better results.

Various notations used for HTLPSO algorithm are:

- $p_{TLBO}$  = best half of the population selected after teacher phase
- $p_{PSO}$  = best half of the population selected after PSO
- $p_l$  = best population selected for learner phase
- $p_{new}$  = final population selected after each iteration



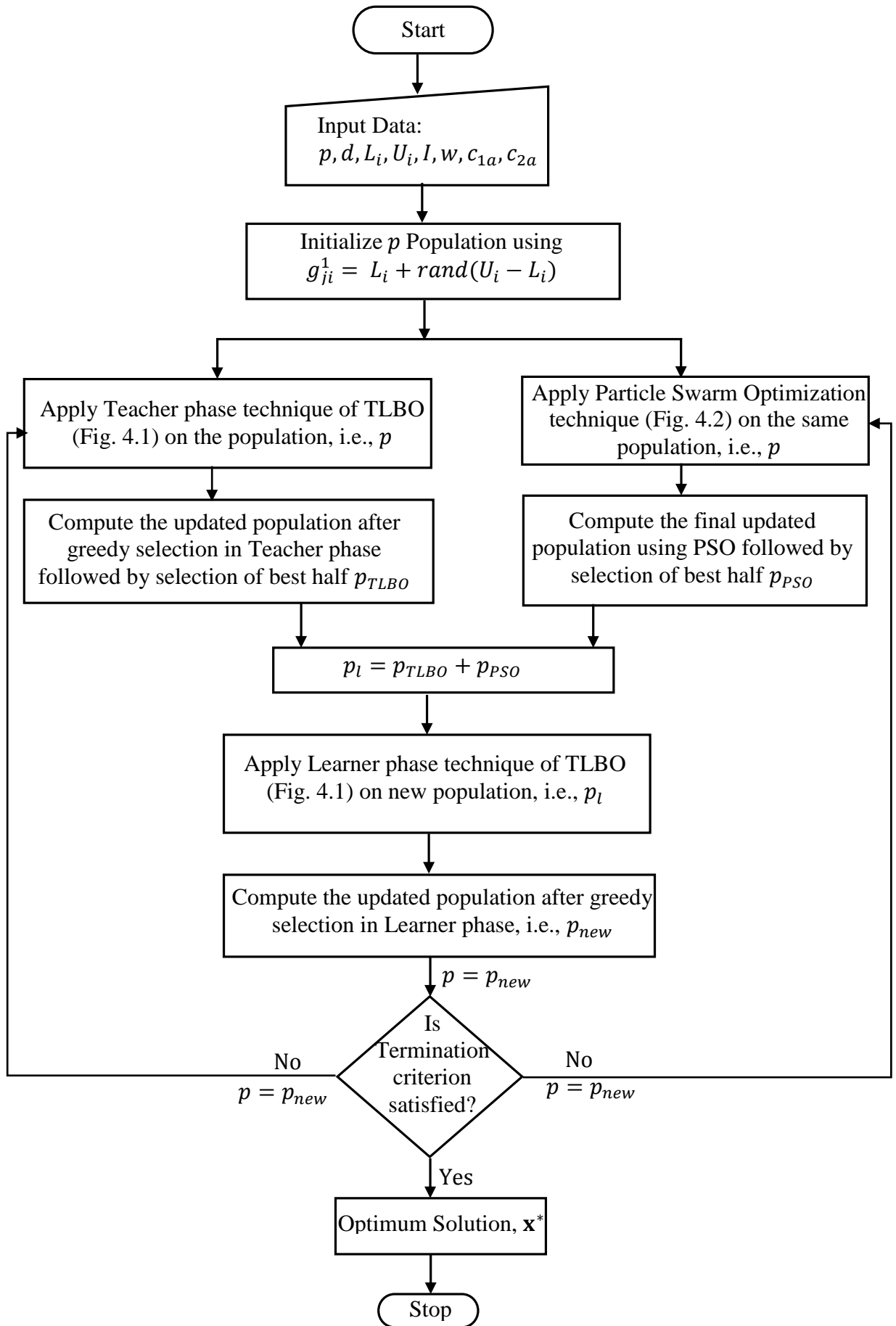


**Fig.4.3** Flowchart of hybrid-teaching learning particle swarm optimization (HTLPSO) algorithm

#### 4.4 Numerical Examples

In this section, validation of the proposed HTLPSO algorithm is demonstrated. The results of HTLPSO are compared with those obtained using TLBO, PSO, whale optimization algorithm (WOA), moth-flame optimization (MFO), and accelerated particle swarm optimization (APSO) technique. For PSO,  $c_1$  and  $c_2$  both are taken as 2,  $w = w_{max} - (w_{max} - w_{min}) * (1/l)$  where,  $w_{max} = 0.9$  and  $w_{min} = 0.4$  are taken, default settings are used for other algorithms, whereas, TLBO does not require algorithmic parameters. Five constrained benchmark functions are used to compare the performance of each algorithm. All these functions are to be minimized. These benchmark functions (Rao, 2016; Rao and Savasani, 2012) are defined as follows:

##### 1. Benchmark function 1

$$\text{minimize } f_1 = (x_1 - 10)^3 + (x_2 - 20)^3$$

subject to:

$$g_1 = -(x_1 - 5)^2 - (x_2 - 5)^2 + 100 \leq 0$$

$$g_2 = (x_1 - 6)^2 + (x_2 - 5)^2 - 82.81 \leq 0$$

$$13 \leq x_1 \leq 100, 0 \leq x_2 \leq 100$$

The global minimum value of function is **-6961.814** (Rao and Patel, 2012).

##### 2. Benchmark function 2

$$\text{minimize } f_2 = 5.3578547(x_3)^2 + 0.8356891x_1x_5 + 37.293239x_1 - 40792.141$$

subject to:

$$g_1 = 85.334407 + 0.005685x_2x_5 + 0.0006262x_1x_4 + 0.0022053x_3x_5 \leq 0$$

$$g_2 = -85.334407 - 0.005685x_2x_5 - 0.0006262x_1x_4 - 0.0022053x_3x_5 \leq 0$$

$$g_3 = 80.512499 + 0.0071317x_2x_5 + 0.002995x_1x_2 + 0.0021813x_3^2 - 110 \leq 0$$

$$g_4 = -80.51249 - 0.0071317x_2x_5 - 0.002995x_1x_2 - 0.0021813x_3^2 + 90 \leq 0$$

$$g_5 = 9.300961 + 0.0047026x_3x_5 + 0.0012547x_1x_3 + 0.0019085x_3x_4 - 25 \leq 0$$

$$g_6 = -9.300961 - 0.0047026x_3x_5 - 0.0012547x_1x_3 - 0.0019085x_3x_4 + 20 \leq 0$$

$$\text{Lower limit} = [78 \ 33 \ 27 \ 27 \ 27]$$

$$\text{Upper limit} = [102 \ 45 \ 45 \ 45 \ 45]$$

The global minimum value of function is **-30665.539** (Rao and Patel, 2012).

### 3. Benchmark function 3

$$\text{minimize } f_3 = (x_1 - 10)^2 + 5(x_2 - 12)^2 + x_3^4 + 3(x_4 - 11)^2 + 10x_5^6 + 7x_6^2 + x_7^4 - 4x_6x_7 - 10x_6 - 8x_7$$

subject to:

$$g_1 = -127 + 2x_1^2 + 3x_2^4 + x_3 + 4x_4^2 + 5x_5 \leq 0$$

$$g_2 = -282 + 7x_1 + 3x_2 + 10x_3^2 + x_4 - x_5 \leq 0$$

$$g_3 = -196 + 23x_1 + x_2^2 + 6x_6^2 - 8x_7 \leq 0$$

$$g_4 = 4x_1^2 + x_2^2 - 3x_1x_2 + 2x_3^2 + 5x_6 - 11x_7 \leq 0$$

Where,  $-10 \leq x_i \leq 10$  ( $i = 1, \dots, 7$ )

The global minimum value of function is **680.63** (Rao and Patel, 2012).

### 4. Benchmark function 4

$$\text{minimize } f_4 = -\frac{\sin x^3(2\pi x_1) \sin(2\pi x_2)}{x_1^3(x_1+x_2)}$$

subject to:

$$g_1 = x_1^2 - x_2 + 1 \leq 0$$

$$g_2 = 1 - x_1 + (x_2 - 4)^2 \leq 0$$

Where,  $0 \leq x_i \leq 10$  ( $i = 1, 2$ )

The global minimum value of function is **-0.095825** (Rao and Savasani, 2012).

### 5. Benchmark function 5

$$\text{minimize } f_5 = (x_1^2 + x_2 - 11)^2 + (x_1^2 + x_2^2 - 7)^2$$

subject to:

$$g_1 = 26 - (x_1 - 5)^2 - x_2^2 \geq 0$$

$$g_2 = 20 - 4x_1 - x_2 \geq 0$$

Where,  $-5 \leq x_1 \leq 10, -10 \leq x_2 \leq 5$

The global minimum value of the function is **0** (Rao, 2016).

The performance of any new optimization algorithm on the benchmark functions should be checked with known global optima. Therefore, the same practice is adopted here to test the performance of HTLPSO algorithm. Since the metaheuristics are stochastic optimization techniques, for each benchmark function, the HTLPSO algorithm is run 30 times to obtain reasonable results. The same process is followed for

**Table 4.1** Performance of PSO, TLBO, APSO, MFO, WOA, and HTLPSO

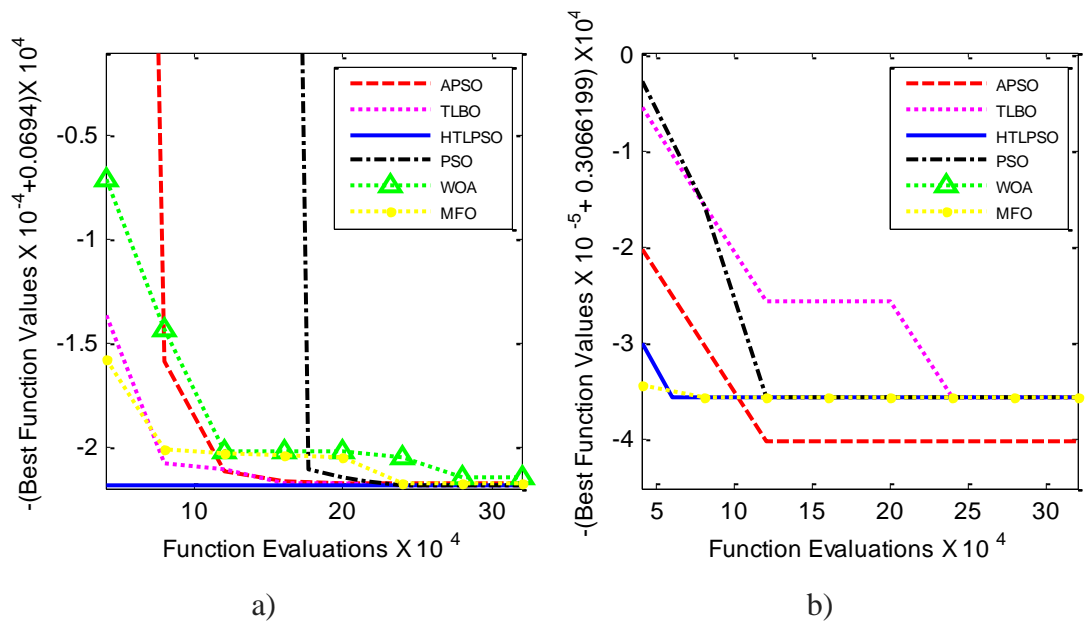
Benchmark Function	Performance parameters	PSO	TLBO	APSO	MFO	WOA	HTLPSO
1	Best Value	-6961.813	-6961.806	-6961.8	-6961.736	-6961.4234	-6961.814
	Mean Value	-6961.804	-6961.778	-6961.8	-6.96E+03	-6448.6547	-6961.814
	Standard Deviation	0.00875	0.02388	.000506	2.13E+02	3.27E+02	0.002056
	Number of Function Evaluations	240000	240000	240000	240000	280000	48000
2	Best Value	-30665.54	-30665.54	-30666	-30665.538	-30668.7873	-30665.54
	Mean Value	-30665.38	-30665.54	-30666	-30665.515	-30234.1062	-30665.54
	Standard Deviation	0.00011	5.561e-7	4.72E-07	4.49E-02	2.34E+02	2.283e-9
	Number of Function Evaluations	120000	240000	280000	80000	320000	60000
3	Best Value	680.6408	680.6326	680.6308	680.6595	686.440	680.6308
	Mean Value	680.6734	680.6358	680.6668	680.8062	706.936	680.6334
	Standard Deviation	0.03060	0.00204	0.092	0.125689	22.061508	0.003073
	Number of Function Evaluations	240000	240000	320000	120000	120000	120000
4	Best Value	-0.095825	-0.095825	-0.0958247	-0.0958250	-0.09582504	-0.095825
	Mean Value	-0.095825	-0.095825	-0.0958125	-0.0958169	-0.09582417	-0.095825
	Standard Deviation	2.458e-8	1.911e-8	1.15E-05	1.14E-05	1.78E-06	1.075e-8
	Number of Function Evaluations	8000	8000	28000	16000	8000	4800
5	Best Value	0.000000	9.0381e-5	0.000013	8.70E-05	7.93E-07	1.6983e-6
	Mean Value	3.8680e-4	0.004552	0.0444	2.16E-02	1.16E-02	9.6176e-4
	Standard Deviation	0.00211	0.00407	0.0384	2.36E-02	0.0195802	0.00143
	Number of Function Evaluations	800	6400	6400	8000	4000	4800

**Table 4.2** Percentage of number of function evaluations require for HTLPSO in comparison with other algorithms

Benchmark Function	PSO	TLBO	APSO	MFO	WOA
1	80	80	80	80	83
2	50	75	79	25	82
3	50	50	100	100	100
4	40	40	70	70	40
5	180	25	40	40	20

all the algorithms used in this study. The objective function value corresponding to each iteration is recorded. To verify the performance of HTLPSO, its results are compared with the well-established single, nature-inspired, modified variant, and hybrid algorithms. Table 4.1 summarizes the statistical results (i.e., the average objective function value, corresponding standard deviation) for HTLPSO and other algorithms used in this study to solve the benchmark problems. It is observed that HTLPSO algorithm outperforms all the algorithms in terms of efficiency (ability to locate the global optimum in less number of function evaluations) for four benchmark functions; however, the HTLPSO takes more function evaluations for fifth benchmark function to

reach global optimum but provides best mean results. A reduction of 17–80% in the number of function evaluations is observed in the comparison of other algorithms as shown in Table 4.2. These superior results are obtained through the combination of two well-established algorithms. The combination appends the exploration of PSO and teaching-learning phases of TLBO. This is due to the use of extra updating mechanisms of swarms of PSO and learners of TLBO used in HTLPSO, as shown in Fig 4.2 and Fig 4.1, respectively. These updating mechanisms of teaching phase widen the exploration in the search space. However, the only exploration may avoid reaching the optimal solution; therefore, it is followed by exploitation (greedy selection of best solutions), which identifies the promising areas of the solution. PSO operator of updating mechanism is applied in parallel to further explore the area for the optimal solution, but PSO lacks exploitation, therefore to widen the TLBO search capability and to compensate the lacking exploitation of PSO both these algorithms are combined. Hence, the search space is explored widely and refined; thereafter, the best half population from both the results are selected. The well-established learning technique is then applied to the selected population to explore and exploit the search space to find the accurate approximation of the optimal solution. In this way, a right balance between the exploration and exploitation is created which gives superior results in comparison with the single nature-inspired algorithms used here.



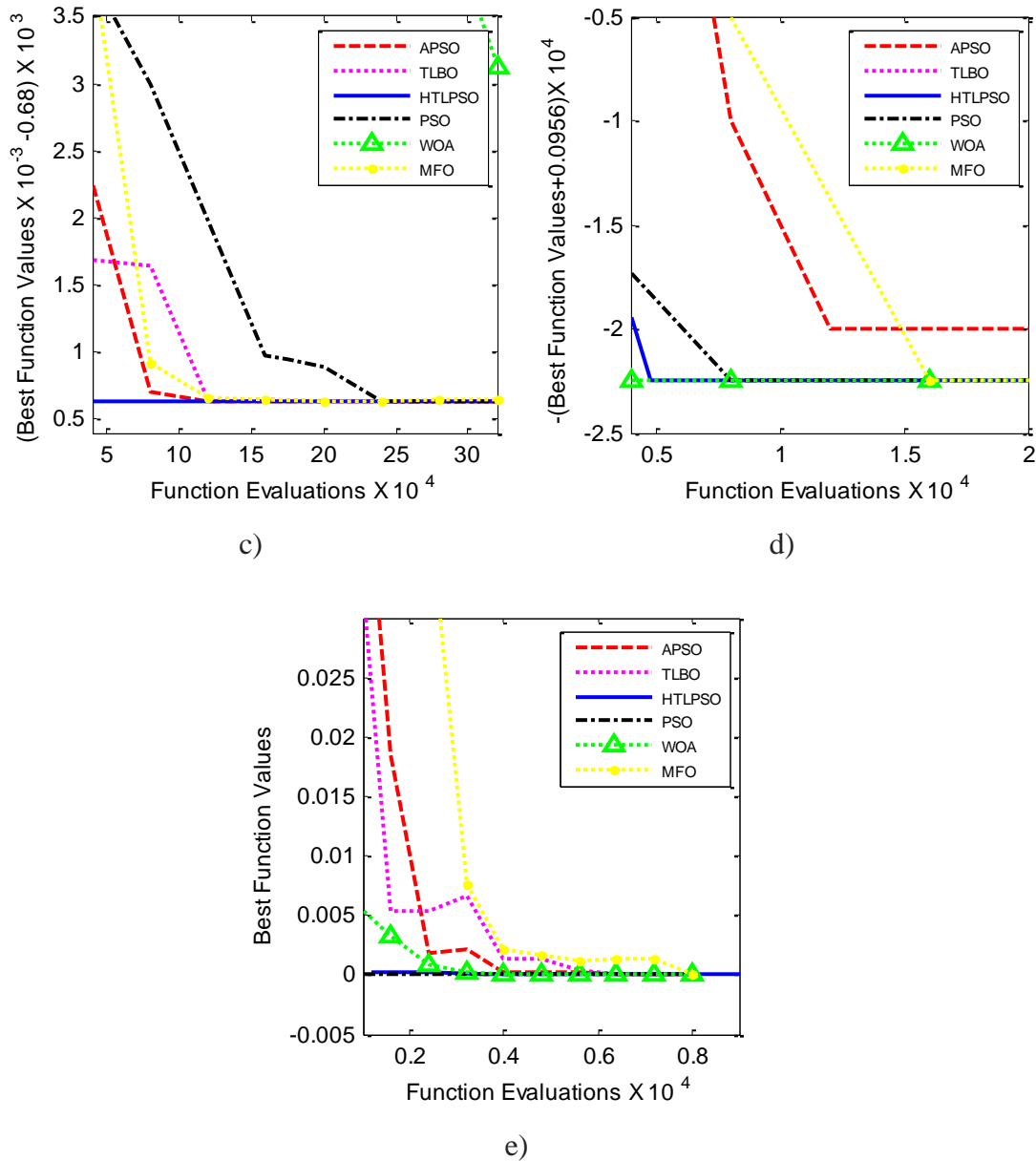


**Fig. 4.4** Convergence of the best objective function values with respect to the number of function evaluations for a) Benchmark 1 b) Benchmark 2 c) Benchmark 3 d) Benchmark 4 e) Benchmark 5

In order to illustrate the results lucidly, the best objective function values are plotted with the number of function evaluations for all the benchmark functions as shown in Fig 4.4. It is observed that HTLPSO's learners and swarms tend to explore the promising regions of search space, simultaneously, exploits the best region. Initially, the population (learners and swarms) changes abruptly and thereafter converges to an optimum point. This behavior of the population-based algorithms is shown by

convergence curve Fig 4.4. It is found that HTLPSO is more competitive in comparison with all the other well-established metaheuristic algorithms.

From Fig 4.4 three different trends in convergence are observed. Firstly, the convergence of the algorithm occurs rapidly after initial steps of iterations. This behaviour is seen for the HTLPSO (benchmark functions-(1-5)), WOA (benchmark functions-(4, 5)), MFO (benchmark functions-(2, 3)), PSO (benchmark function-(5)), APSO (benchmark function-(3)), and TLBO (benchmark function-(3)). Only HTLPSO shows this trend in the convergence of the best values of the objective function in all the Benchmark Functions because of a good balance of exploration and exploitation that helps HTLPSO to find the global minimum. This also ensures the high success rate of HTLPSO in solving the wide range of problems. Secondly, the convergence of algorithm occurs when the maximum number of function evaluations are reached. This trend is observed for the WOA (Benchmark Functions-(1-3)), MFO (Benchmark Functions-(1, 4, 5)), PSO (Benchmark Functions-(1, 3)), and TLBO (Benchmark Functions-(2, 4)). The convergence trend may be due to the failure of the algorithm in finding the promising solution for exploitation in the initial steps. Therefore, algorithms keep on exploring the search space to find good solutions. The third case is when the algorithm converges in an accelerated fashion. This trend is observed in the APSO (Benchmark Functions-(1, 2, 4, 5)), PSO (2, 4), and TLBO (1, 5). This behaviour is observed due to the operators used in the algorithm that helps in exploring the promising regions of the search space, thereafter converging rapidly after almost half of the maximum number of the function evaluations. Overall, it is found that HTLPSO converges fast in comparison with the other algorithms used here.

Figure 4.5 shows the standard deviation of the objective function value for all the benchmark functions using six metaheuristic algorithms. It is found that standard deviation for HLPSO is the least in comparison with all the other algorithms. This shows that solution obtained by HTLPSO is more reliable than the other algorithms used here.

#### **4.5 Application- Path Synthesis of Four-Bar Linkage**

The HTLPSO algorithm developed in section 2 is applied to solve a four-bar path synthesis problem. Figure 4.6 shows various design parameters of a four-bar linkage.  $\{XOY\}$  represent a global reference frame; a coupler point  $P$  is defined by vectors  $\mathbf{AC}$  and  $\mathbf{CP}$ , where  $\mathbf{AC}$  is along  $\mathbf{AB}$  and  $\mathbf{CP}$  is normal to  $\mathbf{AB}$  and passing to point  $P$ . The

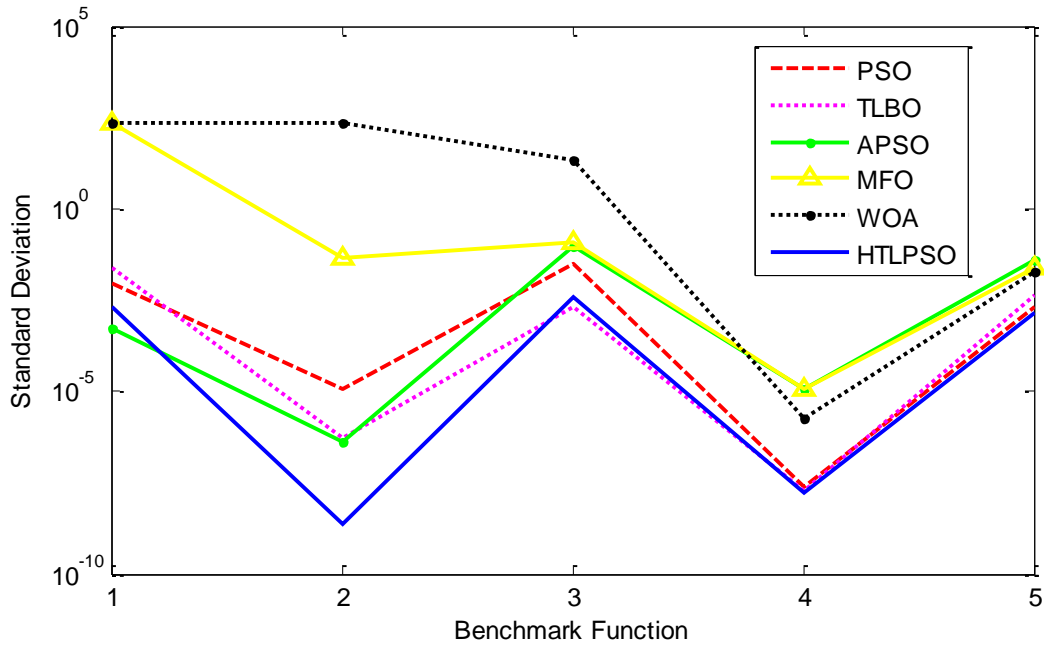


**Fig. 4.5** Comparison of standard deviation for all benchmark function using different algorithms

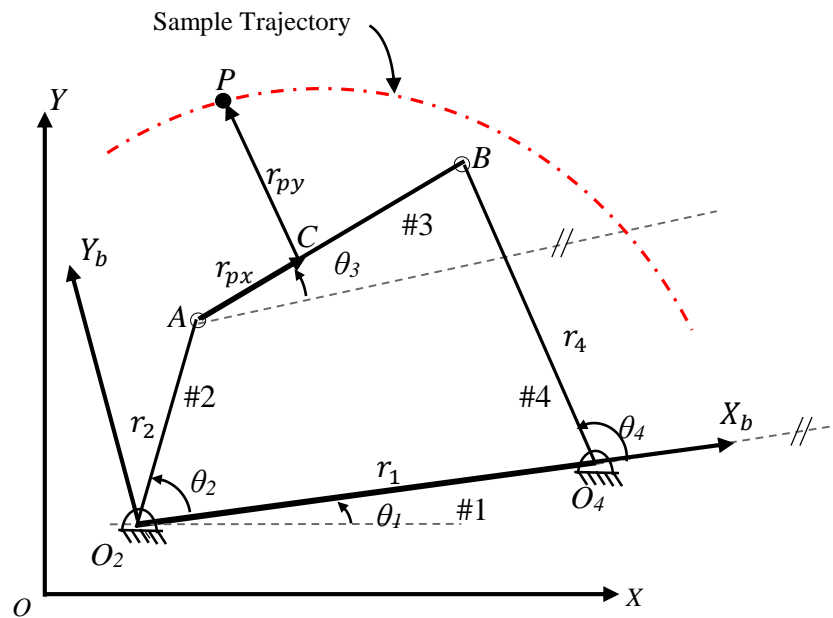


**Fig. 4.6** Four-bar linkage and definition of various notations

length between joints is used to define link length as shown in Fig 4.6. A frame  $\{X_b O_2 Y_b\}$  is defined to measure the orientation of links with respect to link #1. It is fixed to link #1, and its  $X$ -axis is aligned along link #1. Now, orientations of link #2, link #3 and link #4 are given by angles  $\theta_2$ ,  $\theta_3$ , and  $\theta_4$ , respectively, with respect to the axis  $X_b$ .



The orientation of link #1 is defined by angle  $\theta_1$  with respect to the fixed axis  $X$ . The coordinates of coupler point  $P$  in frame  $\{X_b O_2 Y_b\}$  are given as follows:

$$P_{xb} = r_2 \cos \theta_2 + r_{px} \cos \theta_3 - r_{py} \sin \theta_3 \quad (4.3)$$

$$P_{yb} = r_2 \sin \theta_2 + r_{px} \sin \theta_3 + r_{py} \cos \theta_3 \quad (4.4)$$

The coupler point coordinates in fixed reference frame  $\{XOY\}$  given are obtained as follows:

$$P_x = O_{2x} + P_{xb} \cos \theta_1 - P_{yb} \sin \theta_1 \quad (4.5)$$

$$P_y = O_{2y} + P_{xb} \sin \theta_1 + P_{yb} \cos \theta_1 \quad (4.6)$$

where  $O_{2x}$  and  $O_{2y}$  are the coordinates of the  $O_2$  in the frame  $\{XOY\}$ .

Equations (4.5) and (4.6) represent the coordinates of any point on the path traced by the coupler point  $P$ . Link lengths  $r_1, r_2, r_3$  and  $r_4$ , Orientation  $\theta_1$  of the link#1,  $N$  positions of link#2 defined by  $\theta_2^1, \theta_2^2, \dots, \theta_2^N$ , and lengths  $|AC|$  ( $r_{px}$ ) and  $|CP|$  ( $r_{py}$ ) are to be determined for prescribed trajectory of point  $P$ . These  $N + 9$  unknown parameters are considered as design variables to synthesize the linkage:

$$\mathbf{x} = [r_1, r_2, r_3, r_4, r_{px}, r_{py}, O_{2x}, O_{2y}, \theta_1, \theta_2^1, \theta_2^2, \dots, \theta_2^N] \quad (4.7)$$

where  $N$  represents the number of desired points for the coupler trajectory, and the design variables are defined in Fig 4.6. The other parameters  $\theta_3$ , and  $\theta_4$  can be determined by loop closure equation of the mechanism (Acharyya and Mandal, 2009).

Normally, for path generation problem, the position error is considered as the square root of the sum of the square of the Euclidean distances between each coupler-point position  $P$  and the corresponding desired point  $P_d$ . Then, the position error is the objective function to be minimized for the synthesis problem and is expressed as follows:

$$f(\mathbf{x}) = \sum_{k=1}^N \sqrt{(P_x^k - P_{xd}^k)^2 + (P_y^k - P_{yd}^k)^2} \quad (4.8)$$

where  $P_{xd}, P_{yd}$  are the  $x$  and  $y$  coordinates of desired points and  $P_x, P_y$  are the  $x$  and  $y$  coordinates of the coupler point trajectory. Superscript  $k$  represents the  $k^{th}$  position of the coupler.

A four-bar linkage is expected to achieve this objective, such that crank can rotate completely in sequence, either clockwise or counter-clockwise, and values of design variables should lie within the prescribed range. The following constraints are imposed to get feasible four-bar linkage.

a) *Grashof constraint:*

$$g_1(\mathbf{x}) = r_1 + r_2 - r_3 - r_4 < 0 \text{ if } (r_2 < r_3 < r_4 < r_1) \quad (4.9)$$

b) *Order constraint:*

$$g_2(\mathbf{x}) = \theta_2^k - \theta_2^{k+1} < 0 \quad k = 1, \dots, N \quad (4.10)$$

c) *Range of variables:*

$$L_i \leq x_i \leq U_i$$

where  $L_i$  and  $U_i$  are the lower and upper limits for the  $i^{\text{th}}$  design variable. Thus using, Eqs. (4.7-4.10), the problem is completely stated as follows:

$$\begin{aligned} \text{minimize} \quad & f(\mathbf{x}) = \sum_{k=1}^N \sqrt{(P_x^k - P_{xd}^k)^2 + (P_y^k - P_{yd}^k)^2} \\ \text{subject to} \quad & g_1(\mathbf{x}) = r_1 + r_2 - r_3 - r_4 < 0 \quad (r_2 < r_3 < r_4 < r_1) \\ & g_2(\mathbf{x}) = \theta_2^k - \theta_2^{k+1} < 0 \quad k = 1, \dots, N \\ & L_i \leq x_i \leq U_i \end{aligned} \quad (4.11)$$

Now, the constrained optimization problem defined by Eq. (4.11) is transformed into an unconstrained problem for obtaining a feasible and optimum solution. This is achieved by penalizing the objective function for any constraint violation. A large value of order  $10^4$  is added to the objective function, which assures that infeasible solution has function value greater than the feasible solution. This eliminates all the infeasible solution and promotes the algorithm convergence towards optimum solution. Finally, the original problem is transformed into an unconstrained problem which is expressed as follows:

$$\text{minimize } f(\mathbf{x}) = \sum_{k=1}^N \sqrt{(P_x^k - P_{xd}^k)^2 + (P_y^k - P_{yd}^k)^2} + \sum_{m=1}^2 B_m(P^m) \quad (4.12)$$

$$\text{range of variables } L_i \leq x_i \leq U_i$$

where  $P^m$  ( $m = 1, 2$ ) are the constants with value ( $10^4$ ) for penalizing the objective function if the constraints are violated and  $B_m$  is the Boolean Function (Mundo et al., 2009) expressed as:

$$B_m = \begin{cases} 0, & \text{if } g_m(\mathbf{x}) \leq 0 \\ 1, & \text{otherwise} \end{cases} \quad (4.13)$$

The optimization problem formulated in, Eq. (4.12), is solved considering three different cases: straight line, semi-circular and elliptical path generations as case 1, case 2 and case 3, respectively.

#### 4.5.1 Case 1: Straight Line Trajectory

This case illustrates path generation without prescribed timing for four-bar linkage (Acharyya and Mandal, 2009). In this case, the vertical straight line is to be tracked which is composed of 6 prescribed points. The coordinates of prescribed points and limit on the design variables are as follows:

$$P_d^k = [(20,20), (20, 25), (20, 30), (20, 35), (20, 40), (20, 45)]$$

$$r_1, r_2, r_3, r_4 \in [5, 60]; r_{px}, r_{py}, O_{2x}, O_{2y} \in [-60, 60]; \theta_1 \in [0, 2\pi]$$

To find out the optimal solution for this case, five algorithms are used as solvers, and their results are compared with those established algorithms in the literature (Ettefagh et al., 2013; Cabrera et al., 2002), as shown in Table 4.3. The comparison shows that HTLPSO performs better than those of single nature-inspired algorithms whereas, HTLPSO cannot find the better solution in comparison of HTRCA. However, the difference between function value obtained through HTLPSO and HTRCA is negligible.

The rate of convergence for the best and average objective function against the number of function evaluations is shown in Fig 4.7. Figure 4.8 shows the generated trajectories and prescribed points for the four-bar linkage using various optimization algorithms, for case1. HTLPSO reports the error of 0.0812 which is better in comparison with the single nature-inspired algorithms.

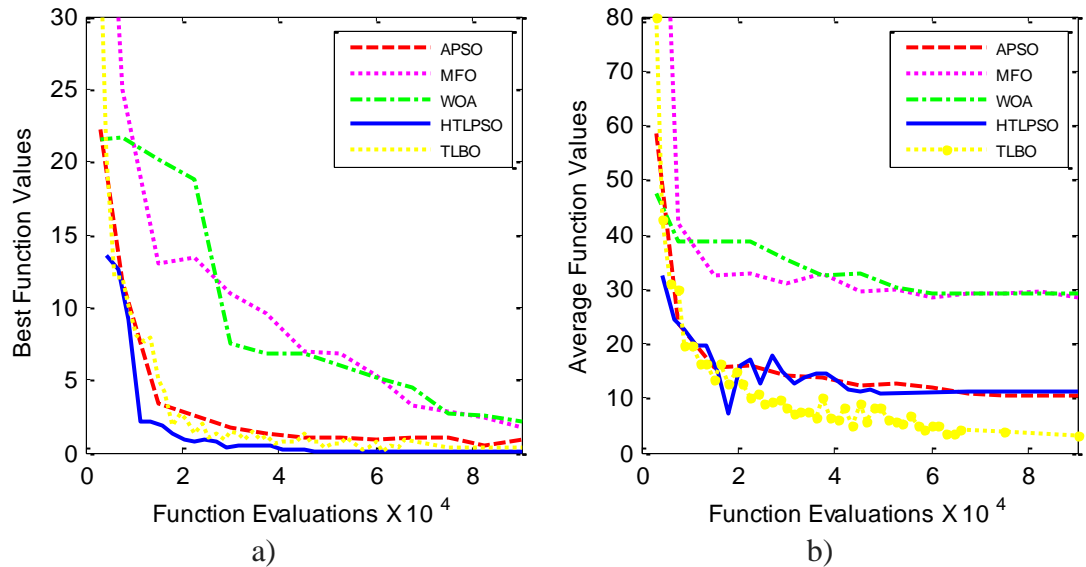
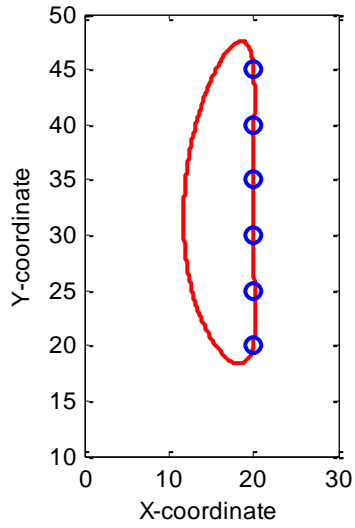


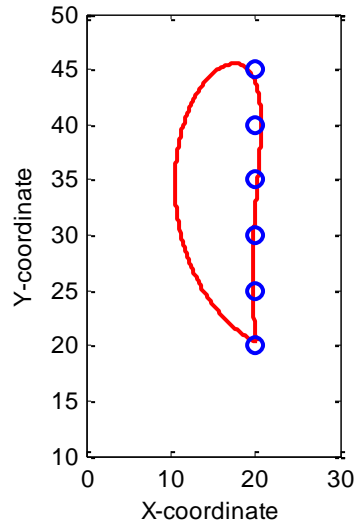
**Fig. 4.7** Convergence between a) Best function values and number of function evaluations, b) Average function values and number of function evaluations for Case 1

**Table 4.3** Comparison of HTLPSO with various algorithms used in literature, for case 1

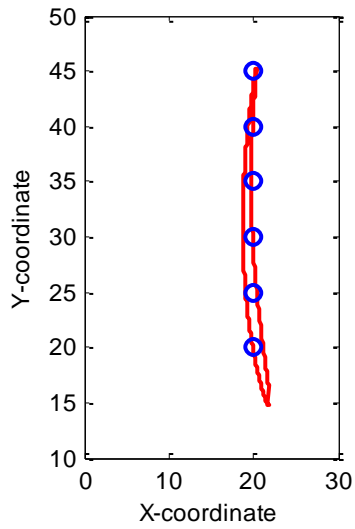
Design Variables	Gabrer <i>a et al.</i> 2002	GA (Achary ya and Mandal, 2009)	PSO (Acharya and Mandal, 2009)	DE (Aacharya a and Mandal, 2009)	ABC (Etefag h et al., 2013)	BGA (Etefagh et al., 2013)	TLBO	APSO	MFO	WOA	HTRC A (Kim et al., 2016)	HTLPSO
$r_1$	39.466 29	28.7713 3	31.15501 3	35.02074 3	16.3446	25.2613	27.972	36.94 83	60.0000	59.9267	18.42	58.7357
$r_2$	8.5629 12	5.00000 0	5.000000 0	6.404196 0	18.5965	8.3871	7.6705	5.000 0	5.0000	48.2787	35.14	5.9847
$r_3$	19.094 86	35.3654 8	23.84561 8	31.60722 8	50.0000	16.1828	26.533	13.30 14	24.8464	52.7064	56.42	8.3028
$r_4$	47.838 86	59.1368 1	45.80352 1	50.59949 1	48.5635	30.2151	27.746	29.92 04	60.0000	59.9221	49.99	56.5439
$r_{cx}$	13.385 56	0.00000 0	39.00066 0	20.80324 0	-	22.5806	43.221	39.71 05	36.7826	44.4886	55.08	-12.1993
$r_{cy}$	12.219 61	14.8503 7	18.50846 7	41.54364 7	50.0000	-22.4633	18.037	12.65 25	-	42.1151	-59.52	-0.6693
$O_{2x}$	29.722 55	29.9132 9	59.99999 9	60.00000 9	-	-3.57771	-17.50	5.208 4	6.2832	6.2830	-25.92	26.2198
$O_{2y}$	23.454 54	32.6022 8	17.91696 8	18.07791 8	47.1614	24.5902	59.359	16.63 45	-	32.9165	42.12	28.3434
$\theta_1$	6.2016 27	5.28747 4	0.419837 4	0.000000 4	4.35100	5.65057	4.2524	31.80 82	8.9630	42.1844	5.931	4.9605
$\theta_1^1$	6.1193 71	6.28318 5	4.842412 5	6.283185 5	3.34008	3.18152	1.4000	2.956 9	3.2796	6.0715	2.347	0.7235
$\theta_2^2$	0.1930 40	0.31820 5	0.404684 5	0.264935 5	3.57682	4.18879	2.2466	3.780 4	4.0727	6.1220	2.584	1.1004
$\theta_2^3$	0.4408 30	0.63852 0	0.657415 0	0.500377 0	3.87317	4.717	3.2219	4.146 7	4.5149	6.1695	2.847	1.4408
$\theta_2^4$	0.6846 74	0.97995 0	0.922086 0	0.735321 0	4.24872	5.08551	2.7538	4.514 2	4.9172	6.1947	3.117	1.7913
$\theta_2^5$	0.9583 51	1.41273 2	1.247066 2	0.996529 2	4.78717	5.50316	3.6999	4.934 6	5.3601	6.2203	3.377	2.2021
$\theta_2^6$	1.3553 31	2.07625 4	2.298727 4	1.333549 4	5.26775	6.08664	4.2484	5.608 6	6.2832	6.2427	3.612	2.9409
Function Value	0.1904 7	1.10169 7	0.546461 6	0.122738 6	0.9898	2.3319	0.1047	0.868 3	1.7585	2.1253	0.005 6	0.0812



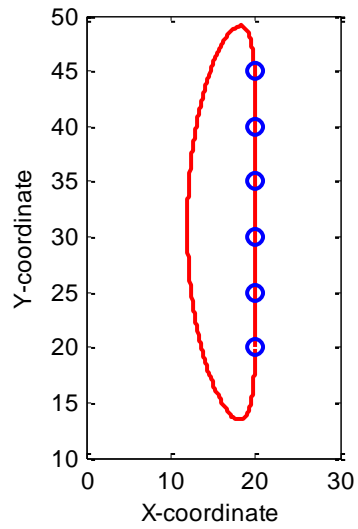
Result from literature (Cabrera et al., 2002)



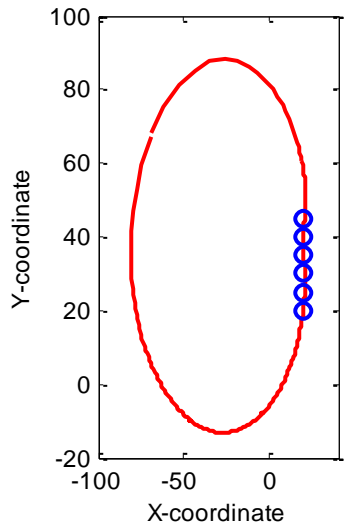
GA (Acharyya and Mandal, 2009)



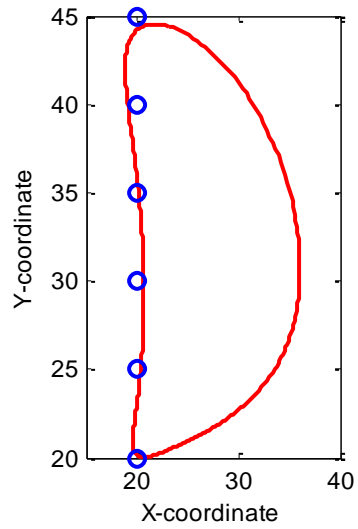
PSO (Acharyya and Mandal, 2009)



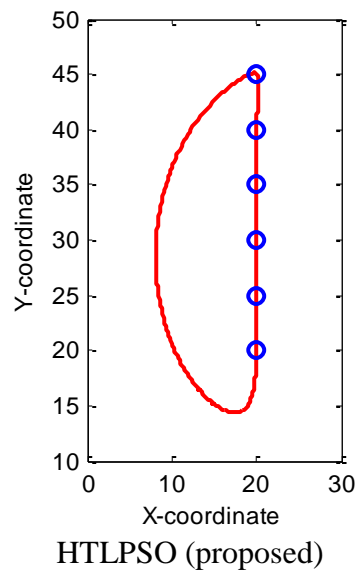
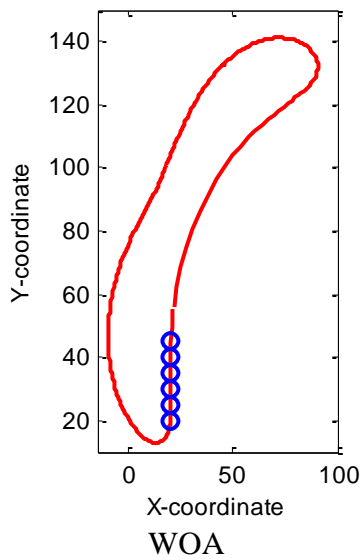
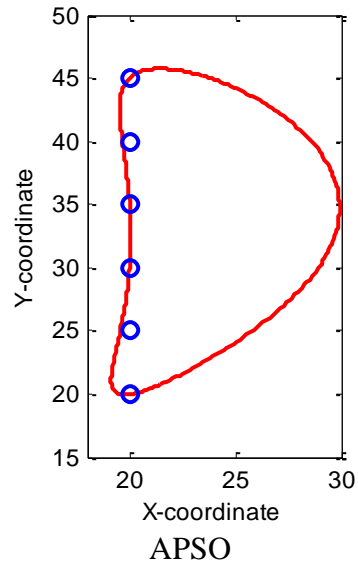
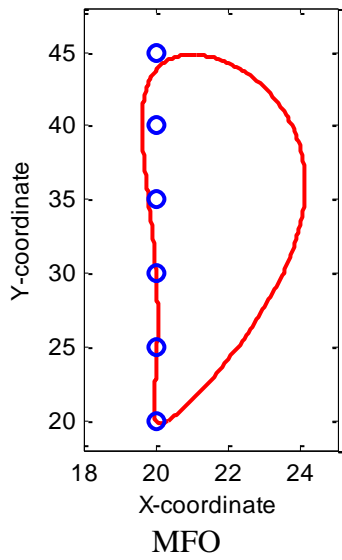
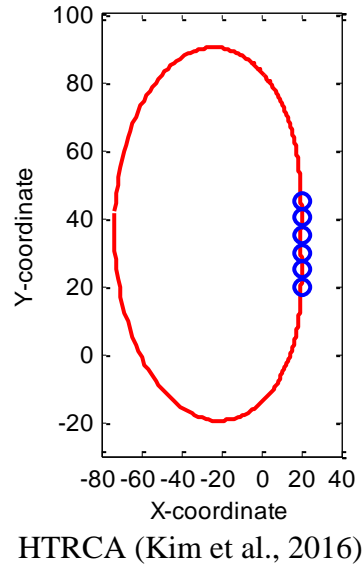
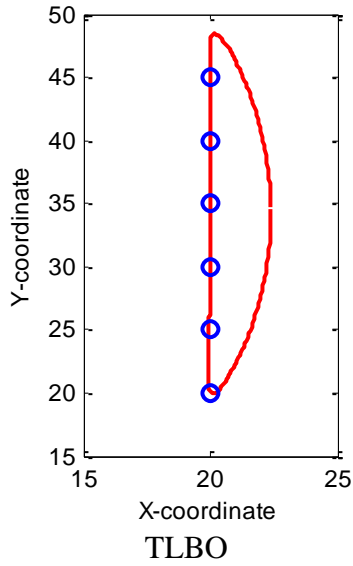
DE (Acharyya and Mandal, 2009)



ABC (Ettfagh et al., 2013)



BGA (Ettfagh et al., 2013)



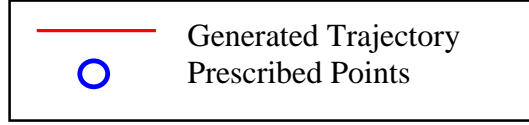


**Fig. 4.8** Generated trajectory and prescribed points

#### 4.5.2 Case 2: Semi-Circular Trajectory

This case illustrates path generation with prescribed timing for four-bar linkage (Acharyya and Mandal, 2009). Here, four-bar linkage generates a semi-circular trajectory similar to the prescribed trajectory. The coordinates of prescribed points on the path and limit on the design variables are as follows:

$$P_d^k$$

$$= [(0,0), (1.9098, 5.8779), (6.9098, 9.5106), (13.09, 9.5106), (18.09, 5.8779), (20, 0)]$$

$$r_1, r_2, r_3, r_4 \in [5, 50]; r_{px}, r_{py}, O_{2x}, O_{2y} \in [-50, 50]; \theta_1 \in [0, 2\pi]$$

In this problem, the angle of the link is provided. Therefore, there are only nine design variables.

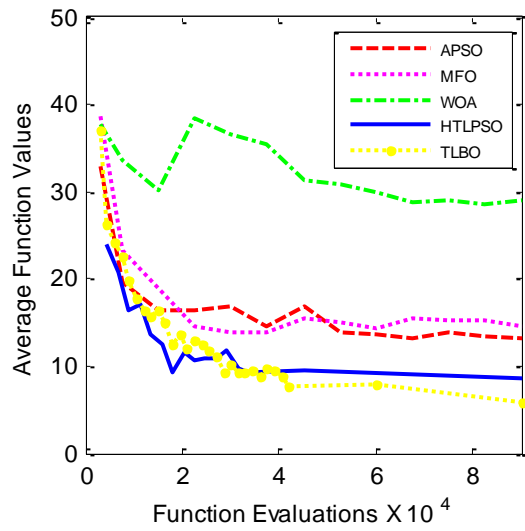
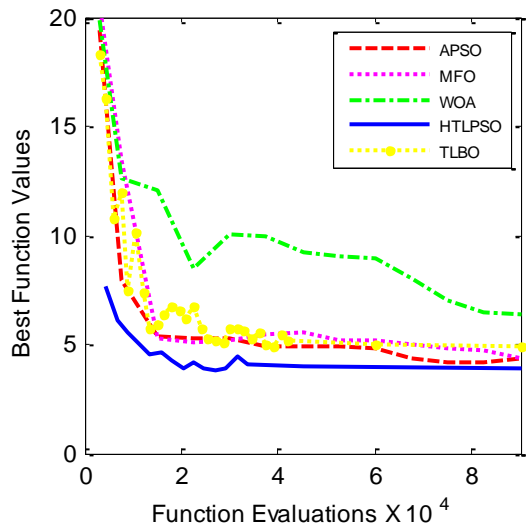
$$\mathbf{x} = [r_1, r_2, r_3, r_4, r_{px}, r_{py}, O_{2x}, O_{2y}, \theta_1],$$

$$\theta_2^k = \left[ \frac{\pi}{6}, \frac{\pi}{3}, \frac{\pi}{2}, \frac{2\pi}{3}, \frac{5\pi}{6}, \pi \right]$$

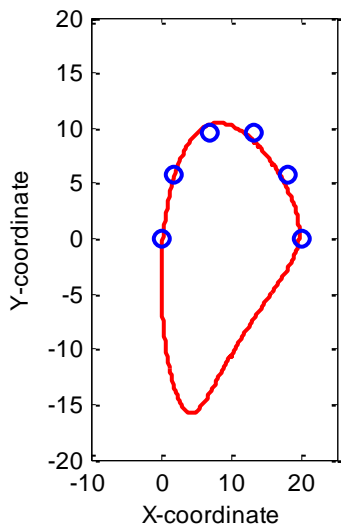
Objective function, Eq. (4.12), is minimized to get a feasible solution. Figure 4.9 shows the convergence for the best and average objective function with the number of function evaluations for case 2. Table 4.4 shows the result comparison of the proposed algorithm with the other established algorithms. The generated and prescribed trajectories of case 2 are shown in Fig 4.10.

**Table 4.4** Comparison of HTLPSO with various algorithms, for case 2

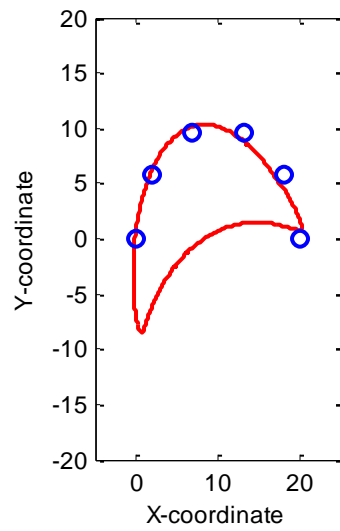
Design Variables	GA (Acharyya and Mandal, 2009)	PSO (Acharyya and Mandal, 2009)	DE (Acharyya and Mandal, 2009)	TLBO	MFO	WOA	APSO	HTRCA (Kim et al., 2016)	HTLPSO
$r_1$	50.00000	49.994859	50.00000	50.000	50.0000	49.1672	54.5605	49.46	50.0000
$r_2$	9.164414	5.0000000	5.000000	5.9278	5.0000	8.3843	8.1548	5.405	5.00000
$r_3$	16.85808	5.9156430	5.905345	9.2490	8.8532	17.7921	19.9956	8.015	7.31650
$r_4$	50.00000	49.994867	50.00000	50.000	46.4047	40.8881	45.2836	47.165	48.0298
$r_{cx}$	38.45887	18.925715	18.81931	25.110	17.9879	32.8107	40.6120	17.90	19.9172
$r_{cy}$	0.090117	0.0000000	0.000000	-6.1922	20.3398	20.2363	22.7522	15.30	9.74970
$O_{2x}$	32.32828	14.472475	14.37377	22.204	12.8609	29.7055	33.2163	12.00	14.7515
$O_{2y}$	-29.53705	-12.49441	-12.4442	-17.704	-22.0471	-30.7715	-38.0495	-18.7	-16.5078
$\theta_1$	0.877212	0.467287	0.463633	0.9123	6.2832	0.7773	0.7787	6.2832	0.31140
Function Value	3.171063	2.35529	2.349649	4.9439	4.3587	6.3559	4.2199	3.571	3.766



a) b)  
**Fig. 4.9** Convergence between a) Best function values and number of function evaluations, b) Average function values and number of function evaluations for Case 2

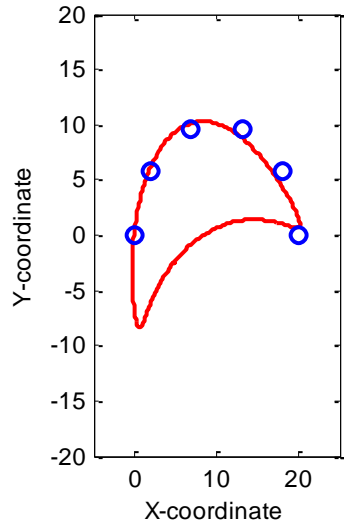


GA (Acharyya and Mandal, 2009)

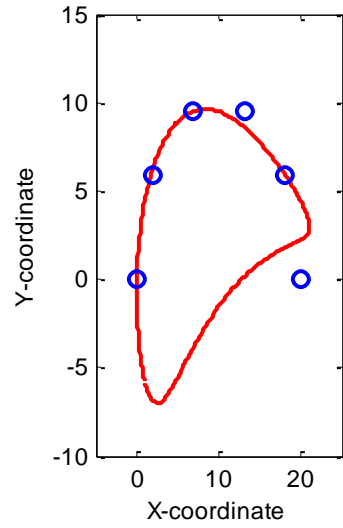


PSO (Acharyya and Mandal, 2009)

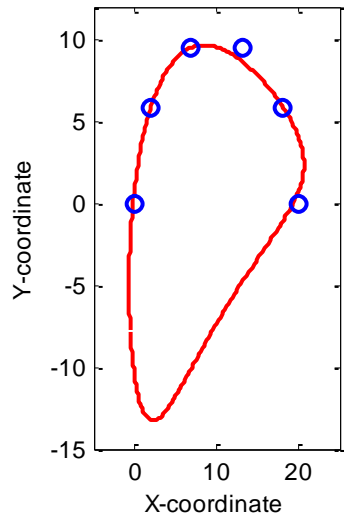




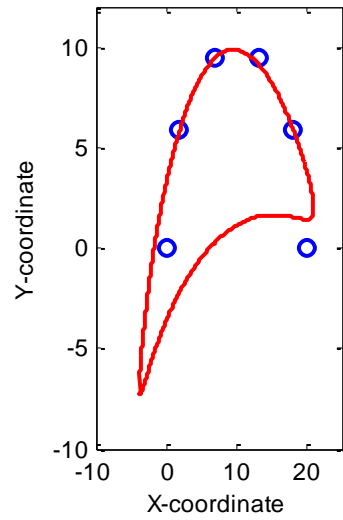
DE (Acharyya and Mandal, 2009)



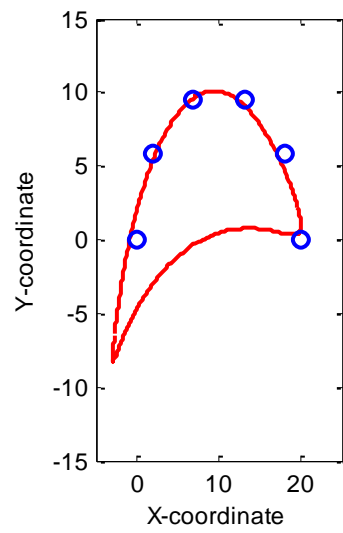
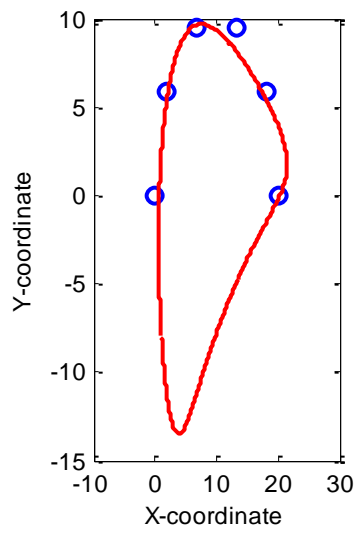
TLBO



APSO



MFO



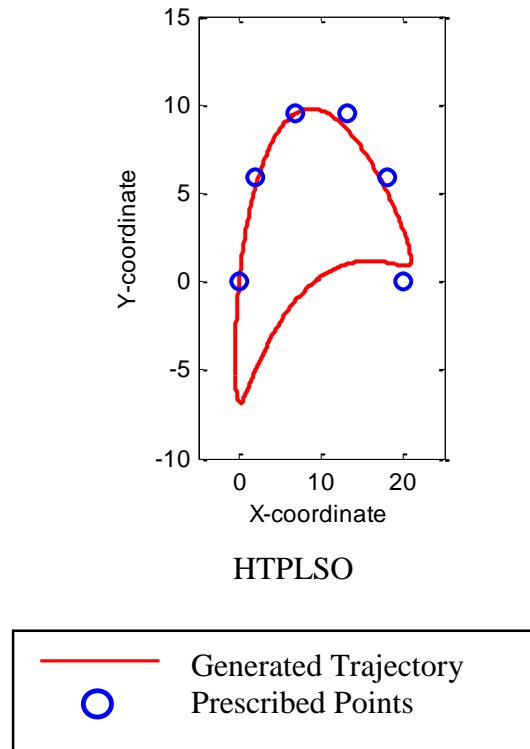


*Fig. 4.10* Generated trajectory and prescribed points

### 4.5.3 Case 3: Circular Trajectory

This case illustrates path generation of four-bar linkage without prescribed timing. Here, total ten prescribed positions are given to track an elliptical trajectory. The trajectory is expressed as follows:

Prescribed points:

$$P_d^k = \left[ \begin{array}{l} (20,10), (17.66, 15.142), (11.736, 17.878), (5, 16.928), (0.60307, 12.736), \dots, \\ (0.60307, 7.2638), (5, 3.0718), (11.736, 2.1215), (17.66, 4.8577), (20, 10) \end{array} \right]$$

Limits of the design variables:

$$r_1, r_2, r_3, r_4 \in [5, 80]; r_{px}, r_{py}, O_{2x}, O_{2y} \in [-80, 80]; \theta_1 \in [0, 2\pi]$$

The results obtained using HTLPSO are compared with other algorithms and shown in Table 4.5. Figure 4.12 shows the plots of the generated trajectory and prescribed points, for case 3. The convergence of the best and average objective function is shown in Fig. 4.11. In this case, HTLPSO obtains the function value of 0.3729 which is much better than those by single nature-inspired algorithms used here. The HTLPSO algorithm cannot find the better solution than that by the HTRCA

algorithm, but the difference in values between the HTLPPO and HTRCA algorithm used here is thought to be negligible. It is observed that HTLPPO gives the best solution compared with the other algorithms while using lesser function evaluations, as shown in Table 4.6.

**Table 4.5** Comparison of HTLPPO with various algorithms, for case 3

Design Variables	GA (Acharyya and Mandal, 2009)	PSO (Acharyya and Mandal, 2009)	DE (Acharyya and Mandal, 2009)	TLBO	MFO	WOA	APSO	HTRCA (Kim et al., 2016)	HTLPPO
$r_1$	79.981513	52.53516	54.36089	75.9859	80.0000	79.4190	59.9306	54.875	80.0000
$r_2$	9.1099930	8.687886	8.683351	8.2946	5.0000	20.9035	8.3158	9.725	8.75920
$r_3$	72.936511	36.15508	34.31863	39.1410	63.0691	77.8578	32.2771	49.925	48.3073
$r_4$	80.000000	80.000000	79.99617	48.2598	79.9922	78.4010	44.6219	23.375	50.2142
$r_{cx}$	0.0000000	0.000000	0.000187	-1.4864	-80.0000	58.1669	-3.3149	7.8400	1.6448
$r_{cy}$	0.0000000	1.481055	1.465250	-7.4652	-12.0492	77.8962	-7.6757	-4.320	-10.0785
$O_z$	10.155966	11.00212	10.95434	7.5190	-28.7214	30.2928	6.9639	1.440	3.92080
$O_y$	10.000000	11.09559	11.074534	17.0350	80.0000	-73.7423	17.5758	12.16	18.0160
$\theta_1$	0.0261490	1.403504	2.12965	6.2831	0.7605	6.0956	0.0002	6.1135	6.1526
$\theta_2^1$	6.2831850	6.282619	6.283185	0.0001	0.0000	0.0000	0.0000	0.148283	0.0192
$\theta_2^2$	0.6007450	0.615302	0.616731	0.6301	0.0637	0.0000	0.6275	0.825611	0.7348
$\theta_2^3$	1.3728120	1.305421	1.310254	1.3420	0.5793	0.0000	1.3088	1.520531	1.4363
$\theta_2^4$	2.2105750	2.188053	2.193570	2.0459	1.1008	0.0000	2.0291	2.236814	2.1357
$\theta_2^5$	2.8626390	2.913049	2.917170	2.7347	1.5800	0.0000	2.6835	2.906602	2.8222
$\theta_2^6$	3.4205470	3.499313	3.490746	3.4154	2.0584	5.9025	3.3994	3.565079	3.4994
$\theta_2^7$	4.0726110	4.125586	4.132017	4.0876	3.4290	5.9680	4.0763	4.295185	4.1961
$\theta_2^8$	4.9103730	4.919977	4.922075	4.7858	3.9938	6.0654	4.7637	5.021522	4.8998
$\theta_2^9$	5.6824400	5.685021	5.695372	5.4909	4.5198	6.1583	5.4510	5.718955	5.5955
$\theta_2^{10}$	6.283185	6.282323	6.28297	6.1974	5.0146	6.2832	6.1877	0.148283	6.2832
Function Value	2.281273	1.971004	1.952326	0.7701	22.3829	65.3812	1.873	0.1649	0.3729

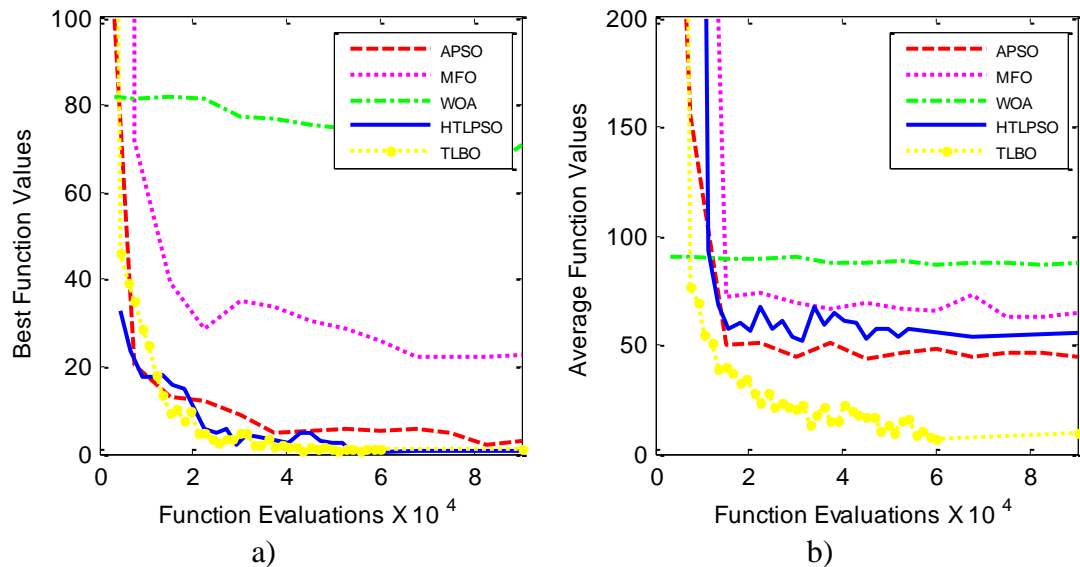
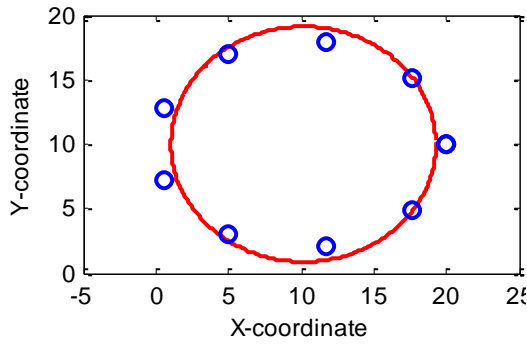
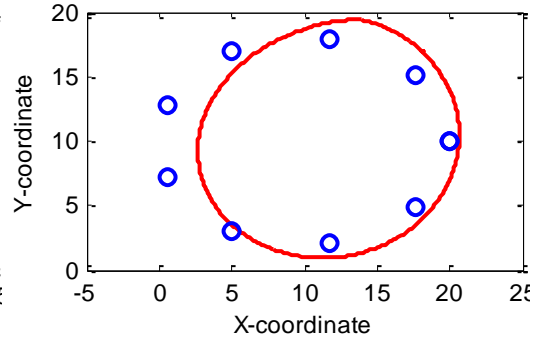


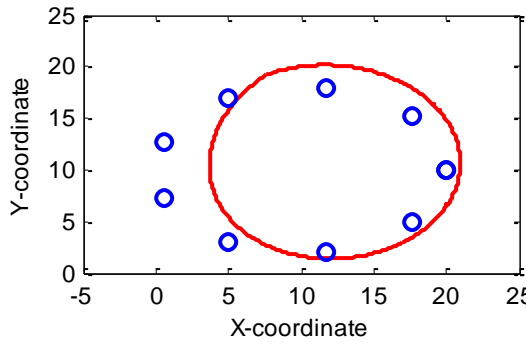
**Fig. 4.11** Convergence between a) Best function values and number of function evaluations, b) Average function values and number of function evaluations for Case 3



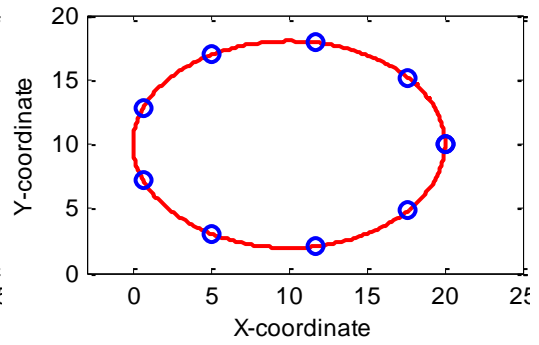
GA (Acharyya and Mandal, 2009)



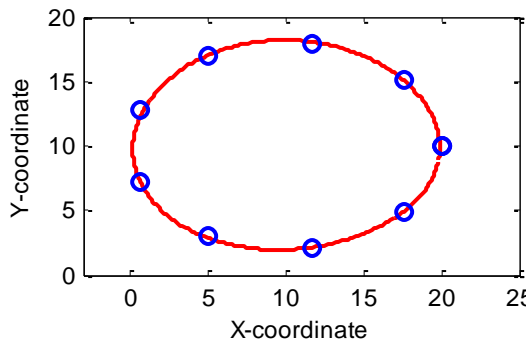
PSO (Acharyya and Mandal, 2009)



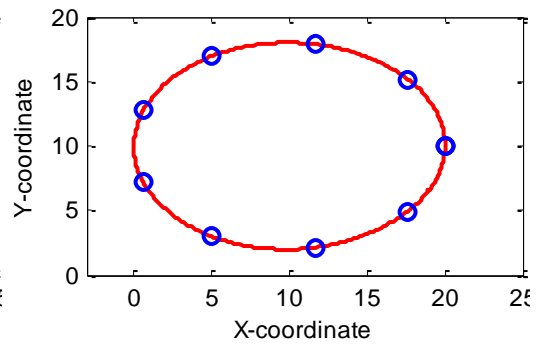
DE (Acharyya and Mandal, 2009)



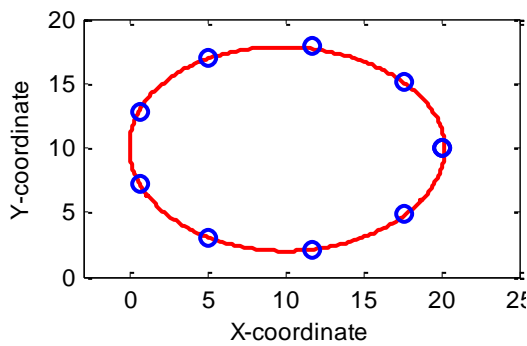
TLBO



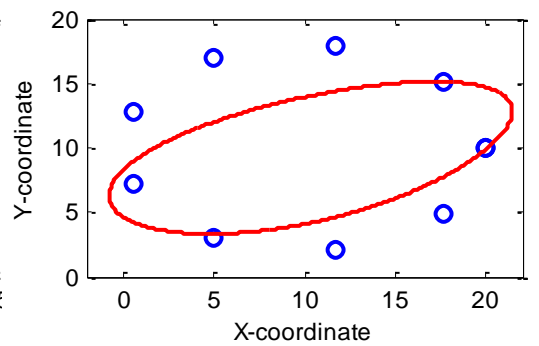
HTRCA (Kim et al., 2016)



HTLPSO (proposed)



APSO



MFO

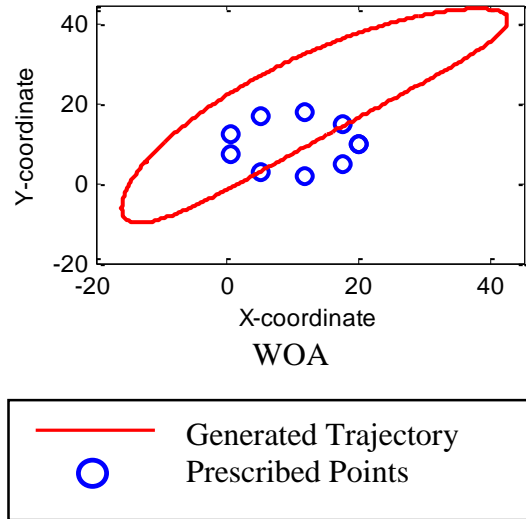


**Fig. 4.12** Generated trajectory and prescribed points

**Table 4. 6** Comparison of HTLPSO with TLBO in terms of number of function evaluations

Case No.	Number of Function Evaluations				
	HTLPSO	TLBO	WOA	MFO	APSO
1	47250	60000	90000	90000	60000
2	24750	39000	90000	90000	75000
3	54000	55500	82500	82500	82500

The application of HTLPSO on these cases proved that the HTLPSO algorithm is more robust in comparison with the other algorithms used here. HTLPSO can find optimal global value in all the cases while MFO and WOA could not find the near approximation to the global optimal solution in case 3, and the TLBO takes more function evaluations to converge. This means that merging of PSO with TLBO assists in escaping the local optima successfully. This merging has also improved the effectiveness of the algorithm. Now, HTLPSO algorithm can find optimal values for all the cases in a lesser number of function evaluations for the algorithms used here. Note that, the number of function evaluations of the other algorithms for the path synthesis cannot be accessed. Hence, only the comparison of the proposed algorithm with APSO, TLBO, MFO, and WOA in terms of the number of function evaluations is performed.

Lastly, HTLPSO can find more accurate optimal values than all the recent metaheuristic and benchmark algorithms used here. Therefore, HTLPSO can be considered as an efficient algorithm for solving the wide range of problems.

The results of HTLSPO algorithm are found to be competitive and superior over the conventional and new single nature-inspired algorithms used here for comparison.

However, compared to HTRCA, the HTLPSO algorithm cannot find the better solution. Nevertheless, the difference in results of HTLPSO and HTRCA are negligible. Also, the result of HTLPSO in case 2 is worse than other algorithms except for TLBO, WOA, MFO, and APSO. The tracking error of all algorithms in case 2 lies in the range 2.349–4.943 which is greater than benchmark single-nature inspired algorithm (GA, PSO, and DE (Acharyya and Mandal, 2009)). However, the results are superior to the recent single nature-inspired algorithms used here (MFO, WOA). This implies that hybrid algorithms (HTRCA and HTLPSO) cannot obtain optimal solutions compared to GA, PSO, DE (Acharyya and Mandal, 2009) for the case of path synthesis with prescribed timing. From the above discussion, it is found that performance of HTLPSO is superior to that of other metaheuristics used here. However, using a different operator for exploitation to improve the performance of HTLPSO in prescribed timing (Case 2) case may be the subject of future studies.

#### **4.6 Summary**

This chapter proposed an HTLPSO using two established single nature-inspired algorithms, namely, TLBO and PSO. Both the established algorithms are also demonstrated along with a flowchart for the proposed algorithm. In this algorithm, the initial population is simultaneously fed into teacher phase of TLBO and PSO. Then, the best half of population obtained after PSO and teacher phase are merged, and resulting population is fed into learner phase. The final population obtained after learner phase is used as initial population for PSO and teacher phase. This cycle is repeated for each iteration. To validate the proposed algorithm, five constrained benchmark functions, and a path generation problem for four-bar linkage is considered. The WOA, MFO, and APSO are among other algorithms apart from TLBO and PSO which are used for comparing the results with HTLPSO. It is found that proposed algorithm performs better than single nature-inspired algorithms such as PSO, MFO, WOA, APSO and TLBO for all the five benchmark functions. It also finds the better solution for path generation cases without prescribed timing. However, the HTLPSO cannot find near optimal solution for path synthesis cases with prescribed timing. However, HTLPSO finds reasonable optimal solutions in comparison to the other algorithms. Hence, HTLPSO may prove to be an important tool for wide range of problems including path synthesis of four-bar linkages.

## Optimal Linkage Synthesis

A linkage can be synthesized for several single and hybrid tasks using graphical, analytical, and optimal synthesis techniques. The graphical technique to synthesize linkages is discussed in Chapter 2; whereas, analytical linkage synthesis is explained using complex number formulation in Chapter 3. However, these techniques are typically preferred for a fewer number of prescribed precision points. Also, selecting a defect-free linkage among a considerable number of solutions, eliminating defects, and use of a simplified model that requires less computational effort for syntheses are three distinct problems. Parameter homotopy requires large computational effort for solving the polynomial equations and selecting the defect-free successful design out of millions of linkage solutions. Other methods either removes the Burmester segment which consists of the defect or provides the geometric model for eliminating the defects. In contrast, the defect-free linkage can be synthesized for  $N$ -precision points using optimization techniques. However, few researchers (Caberera et al., 2002; Acharyya and Mandal, 2009; Ettefagh et al., 2013) have applied necessary constraints to eliminate only order defects while others used more constraints than it is required (Sardashti et al., 2013). The constraints can be formulated to eliminate defects during  $N$ -precision point optimal syntheses. It is found that constraints formulated for eliminating the CBO defects in six-bar consider three precision points simultaneously that increases complexity. There is a need to develop a simplified method which should also provide a mathematical model of the constraints to eliminate CBO defects in multiloop linkages.

In this chapter, the use of a reduced number of necessary and sufficient constraints for CBO defect elimination for  $N$ -precision points of the four-bar crank-rocker linkage is proposed. Based on the reduced constraints, an optimization problem is formulated to minimize the error between the desired and generated trajectories. This optimization problem is solved using a well-established TLBO algorithm. A refinement scheme is applied to this algorithm to reduce its computational effort. Further, the performance of this refined algorithm is compared with those of GA and PSO in terms of the number of function evaluations and the structural error. The proposed refinement scheme is reported first time in this study. Besides, a new loop-by-loop method is proposed, and simplified constraints are formulated to identify and rectify the CBO defects for improved design reliability and efficiency, for Stephenson III six-bar

linkage. In addition, four numerical examples are considered for four- and six-bar linkage synthesis to generate the path. The two of four examples are benchmark problems in linkage synthesis that demonstrates the effectiveness of the proposed method and remaining two are nontrivial realistic examples of human knee flexion/extension. Also, a novel bilateral knee supporting device is fabricated in which designed four-bar linkage is embedded; and the device is experimentally validated.

## 5.1 Four-Bar Linkage Synthesis

In this section, a formalism to synthesize a defect-free four-bar linkage using the reduced number of necessary and sufficient constraints is presented. Besides, the use of reduced constraints to eliminate defects in the crank-rocker linkage is discussed.

### 5.1.1 Position Analysis of Four-Bar Linkage

The position analysis of four-bar linkage is presented in this section. The four-bar linkage along with various design parameters is shown in Fig 5.1. Here,  $\{XOY\}$  represents the global coordinate system. The angular positions of the links at any instant with respect to the X-axis are  $\theta_1, \theta_2, \theta_3$ , and  $\theta_4$  and  $r_1, r_2, r_3$  and  $r_4$  represent the lengths of the stationary link (#1), crank (#2), coupler (#3) and follower (#4), respectively. Coupler point is defined at length  $l$  in the direction of angle  $\beta$  with respect to coupler vector  $\mathbf{r}_3$  from  $B$  to  $D$  as shown in Fig 5.1.

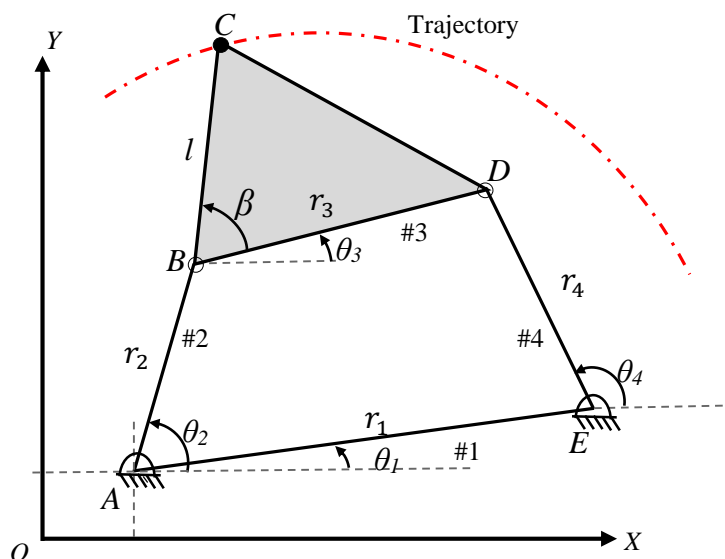


**Fig. 5.1** Four-bar linkage and definition of various notations

For position analysis of the four-bar linkage, loop-closure equation, Eq. (5.1), can be used (See Appendix A for illustration).



$$\mathbf{r}_2 + \mathbf{r}_3 - \mathbf{r}_1 - \mathbf{r}_4 = \mathbf{0} \quad (5.1)$$

The coordinates of coupler point  $C$  are then given by

$$C_x = A_x + r_2 \cos \theta_2 + l \cos(\theta_3 + \beta) \quad (5.2)$$

$$C_y = A_y + r_2 \sin \theta_2 + l \sin(\theta_3 + \beta) \quad (5.3)$$

Note that in the four-bar mechanism, the position of pivot  $A$  is fixed and the trajectory is tracked whereas here, the position of  $A$  is considered as a variable. Equations (5.2) and (5.3) give the coordinates of any point on the path traced by the coupler point  $C$ . Link lengths  $r_1, r_2, r_3$  and  $r_4$ , orientation  $\theta_1$  of the link#1,  $N$  positions of link#2 defined by  $\theta_2^1, \theta_2^2, \dots, \theta_2^N$ , coupler angle  $\beta$ , and length  $l$  are to be determined for the prescribed trajectory of the point  $C$ ; these parameters are unknowns. The other parameters  $\theta_3$  and  $\theta_4$  can be determined by the loop-closure equation of the linkage.

### 5.1.2 Optimization Problem Formulation

#### *Design variables*

For path generation without prescribed timing, the unknown parameters are identified as design variables and are expressed in the vector form as:

$$\mathbf{x} = [r_1, r_2, r_3, r_4, l, \theta_1, A_x, A_y, \theta_2^1, \theta_2^2, \theta_2^3, \dots, \theta_2^N, \beta]^T \quad (5.4)$$

in which,  $N$  represents the number of desired points on the trajectory.

#### *Objective function*

In optimal synthesis problem, both the linkage dimensions and its kinematics play an important role. The performance criteria deal with the dimensions. Hence, the linkage should be kept as small as possible. Therefore, the objective function is formulated as a position error function. Typically, for path generation problems, Euclidean distance between the generated trajectory  $(C_x, C_y)$  and desired trajectory  $(P_{xd}, P_{yd})$  is considered as an error function and is given by

$$f(\mathbf{x}) = \sum_{k=1}^N \sqrt{(P_{xd}^k - C_x^k)^2 + (P_{yd}^k - C_y^k)^2} \quad (5.5)$$

### 5.1.3 Constraint Formulation

Normally four constraints are used in the literature for obtaining defect free crank-rocker mechanism (Sardashti et al., 2013). These are Grashof, circuit, branch, and order constraints. Moreover, it is not necessary to impose all the four constraints to get defect free mechanism. In this section, use of the following three constraints is proposed.

*Constraint for avoiding Grashof defect in constituent four-bar:* If any link in the mechanism is capable of rotating fully, the mechanism is termed as Grashof mechanism.

If any link is unable to rotate fully, the mechanism does have Grashof defect. To avoid the Grashof (crank) defect, the mechanism should satisfy Grashof condition. Accordingly, the constraint to avoid Grashof defect can be expressed as follows:

$$g_1(\mathbf{x}) = r_2 + r_1 - r_3 - r_4 < 0 \quad (5.6)$$

*Constraint for preventing order defects:* The order defect never occurs in the path generation problem if the input angles are prescribed in a sequence (Waldron and Stevensen, 1979). Therefore to avoid order defects, the angular positions of the driving link must be specified in the increasing or decreasing order. Then, the constraints can be expressed as:

$$g_2(\mathbf{x}) = \theta_2^k - \theta_2^{k+1} < 0, \quad k = 1, \dots, N - 1 \quad (5.7)$$

*Constraint for preventing circuit defects:* The mechanism suffers circuit defect if the sign of one of the two interior angles opposite to the shortest link changes while moving from first precision position to second (Waldron, 1976), as shown in Fig 5.2. The interior angle is termed as ‘test angle,’  $\emptyset$ , to check the presence of circuit defect in the four-bar linkage. The sign of test angle is taken as positive when it is measured clockwise from the link, which is opposite to the shortest link, to the adjacent link. If the sign of test angle changes between any two adjacent positions that indicate the presence of circuit defect. Using this logic, the constraint can be modeled mathematically and can be expressed as:

$$g_3(\mathbf{x}) = \emptyset = \theta_3^k - \theta_4^k < 0, \quad k = 1, \dots, N \quad (5.8)$$

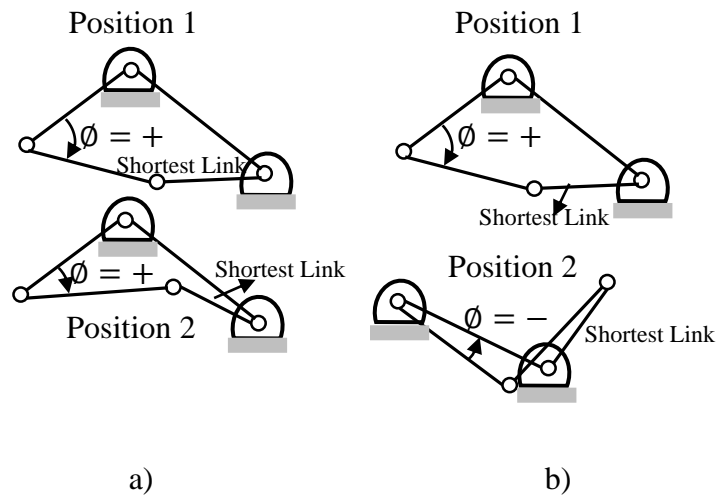


**Fig. 5.2** a) Linkage has no circuit defect b) Linkage has circuit defect

These three equations (5.6)-(5.8) are individually necessary and combinedly sufficient to optimally synthesize a CBO defect-free crank-rocker mechanism. Finally, the optimization problem is stated as:

$$\begin{aligned}
& \text{minimize } f(\mathbf{x}) = \sum_{k=1}^N \sqrt{(P_{xd}^k - C_x^k)^2 + (P_{yd}^k - C_y^k)^2} \\
& \text{subject to } \quad g_1(\mathbf{x}) = r_1 + r_2 - r_3 - r_4 < 0 \\
& \quad \quad \quad g_2(\mathbf{x}) = \theta_3^k - \theta_4^k < 0 \quad k = 1, \dots, N \\
& \quad \quad \quad g_3(\mathbf{x}) = \theta_2^k - \theta_2^{k+1} < 0 \quad k = 1, \dots, N - 1 \\
& \quad \quad \quad L_i \leq x_i \leq U_i \quad i = 1, \dots, n
\end{aligned} \tag{5.9}$$

in which,  $L_i$  and  $U_i$  are the lower and upper bounds on the  $i^{\text{th}}$  design variable,  $n$  represents the number of design variables, and superscript  $k$  represents the  $k^{\text{th}}$  position of the coupler.

To obtain an optimum solution, the constrained problem defined in Eq. (5.9) is transformed into an unconstrained problem (Sardashti et al., 2013; Mundo et al., 2009; Mundo et al., 2006). This transformation can be done using penalty formulation. For each constraint violation, a large value is added to the objective function which assures that infeasible solution has greater objective function value than the feasible solution. Hence, it promotes the algorithm convergence towards the global optimum while satisfying all the constraints. The original constrained problem is then posed as an unconstrained problem in which the first part is the objective function and the second part is the penalty function. Finally, the optimal synthesis problem is formulated as:

$$\text{minimize } f(\mathbf{x}) = \sum_{k=1}^N \sqrt{(P_{xd}^k - C_x^k)^2 + (P_{yd}^k - C_y^k)^2} + \sum_{m=1}^3 B_m(P^m) \tag{5.10}$$

$$\text{range of variables } L_i \leq x_i \leq U_i \text{ where } i = 1, \dots, n \tag{5.11}$$

in which,  $P^m$  ( $m = 1, 2, 3$ ) are the constants with the high value of order  $10^4$  to penalize the objective function if the constraints are violated and  $B_m$  is the Boolean Function (Mundo et al., 2009) expressed as:

$$B_m = \begin{cases} 0, & \text{if } g_m(\mathbf{x}) \leq 0 \\ 1, & \text{otherwise} \end{cases} \tag{5.12}$$

## 5.2 Six-Bar Linkage Synthesis

In this section, a new loop-by-loop defect rectification procedure to synthesize a defect-free Stephenson III six-bar linkage is proposed. Besides, constraint to eliminate defects are presented in simplified form.

### 5.2.1 Position Analysis of Stephenson III Six-Bar Linkage

Analytical expressions for the coordinates of a point on the intended floating link of a Stephenson III linkage are defined in this section. Figure 5.3 shows the Stephenson III six-bar linkage that can be considered as a combination of a four-link mechanism, Loop I ( $ABDEA$ ), a five-link mechanism, Loop II ( $ABCD_oE_oA$ ), and a dyad ( $CD_oE_o$ ). The links' parameters and their positions are defined in Fig 5.3. The global coordinate frame  $\{XOY\}$  (Fig 5.3) is used for the

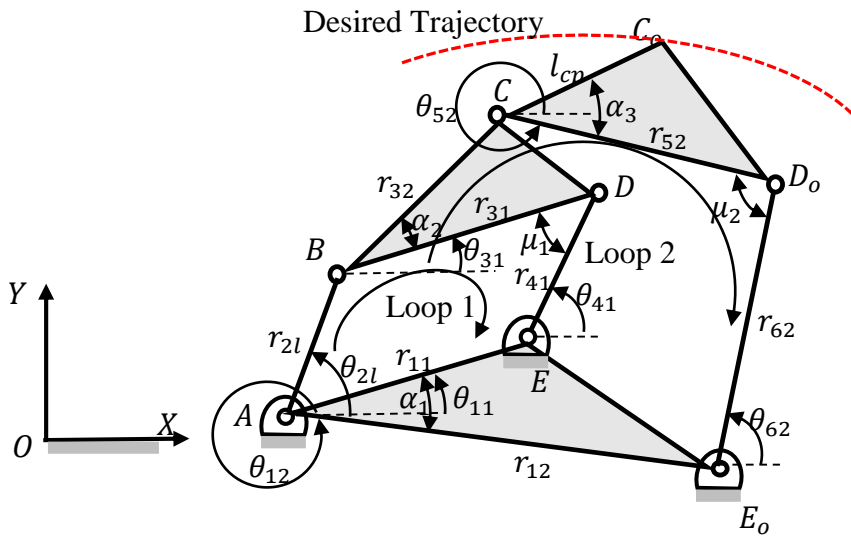


**Fig. 5.3** Stephenson III six-bar path generator mechanism

position analysis of the mechanism. The angular positions of the links in the Loop I are  $\theta_{11}$ ,  $\theta_{21}$ ,  $\theta_{31}$ , and  $\theta_{41}$  measured with respect to the  $X$  -axis, where subscript  $l$  is equal to 1 for Loop I and 2 for Loop II, respectively. The links' lengths in the Loop I are represented by  $r_{11}$ ,  $r_{21}$ ,  $r_{31}$ , and  $r_{41}$  whereas in the Loop II  $r_{12}$ ,  $r_{22}$ ,  $r_{32}$ ,  $r_{52}$ , and  $r_{62}$ . The floating link  $BCD$  of the constituent four-bar linkage is defined by arm lengths  $r_{31}$ , and  $r_{32}$ , and angle  $\alpha_2$  between them. Similarly, the floating link  $CC_oD_o$  is defined by lengths  $r_{52}$ , and  $l_{cp}$ , and angle  $\alpha_3$  between them. Note that  $AEE_o$  is fixed ternary link defined by arms  $r_{11}$  and  $r_{12}$ , and angle  $\alpha_1$ .

Now, the mechanism will satisfy the loop closure equations for Loops I and II

$$\mathbf{r}_{21} + \mathbf{r}_{31} - \mathbf{r}_{11} - \mathbf{r}_{41} = \mathbf{0} \quad (5.13)$$

$$\mathbf{r}_{22} + \mathbf{r}_{32} + \mathbf{r}_{52} - \mathbf{r}_{12} - \mathbf{r}_{62} = \mathbf{0} \quad (5.14)$$

When the angular positions of the link vector  $\mathbf{r}_{21}$  are specified, the loop-closure Eqs. (5.13)-(5.14), can be solved to find the orientations of the other links

$\mathbf{r}_{31}$ ,  $\mathbf{r}_{41}$ ,  $\mathbf{r}_{52}$ , and  $\mathbf{r}_{62}$ , as in Yan and Chiou, 1987. For ready reference, the details are presented in Appendix A. Then the coordinates of the coupler point  $P$  can be expressed in the global reference frame as:

$$C_{ox} = A_x + r_{21} \cos(\theta_{21}) + r_{32} \cos(\theta_{32}) + l_{cp} \cos(\theta_{52} + \alpha_3) \quad (5.15)$$

$$C_{oy} = A_y + r_{21} \sin(\theta_{21}) + r_{32} \sin(\theta_{32}) + l_{cp} \sin(\theta_{52} + \alpha_3) \quad (5.16)$$

Note that  $\theta_{32} = \theta_{31} + \alpha_2$ . The Stephenson III six-bar mechanism has four-assembly configurations (Hwang and Chen, 2008) of which two configurations belong to constituent four-bar, and other two belong to dyad  $CD_o$  and  $D_oE_o$ .

### 5.2.2 Optimization Problem Formulation for Six-Bar

In this section, an optimization problem is formulated to synthesize a defect-free Stephenson III six-bar mechanism defined in previous section, for path generation task. For eliminating defects, a new loop-by-loop defect rectification procedure is proposed here. The procedure formulates constraints for two loops, namely, Loop I and Loop II, respectively.

#### *Design variables*

All the unknown linkage parameters as defined in Fig 5.3 are identified as design variables and can be expressed in the vector form as:

$$\mathbf{x} = [r_{11}, r_{21}, r_{31}, r_{41}, r_{32}, r_{12}, r_{52}, r_{62}, l_{cp}, \alpha_2, \alpha_3, \theta_{11}, \theta_{12}, \theta_{21}^1, \dots, \theta_{21}^N, A_x, A_y]^T$$

where, the superscript  $N$  of  $\theta_{21}$  is the number of precision points to be traced. The design is evaluated for tracing the desired trajectory of point  $C_o$ . The criterion may be the minimum error between the desired and generated trajectories.

#### *Objective function formulation*

Designed Stephenson III six-bar linkage which can pass through all the desired points in sequence, without dismantling the linkage is evaluated for minimum structural error called the objective function. In this work, the objective function is formularized as the average of the Euclidean distance between the desired,  $(P_{xd}, P_{yd})$ , and generated points,  $(C_{ox}, C_{oy})$ , for  $N$  design points, i.e.,

$$f(\mathbf{x}) = \sum_{i=1}^N \sqrt{(C_{ox}^i - P_{xd}^i)^2 + (C_{oy}^i - P_{yd}^i)^2} \quad (5.17)$$

Moreover, constraints should be imposed to synthesize a defect-free mechanism. Such constraints are formulated in the next sub-section.

### 5.2.3 Loop-by-Loop Constraint Formulation

The constraints, namely, Grashof, circuit, branch, and order constraints are imposed to get defect-free mechanism. Identification of the defects would help in the formulation of the constraints; therefore, their identification, and procedure to eliminate them is the objective of this study.

The main causes of circuit defect in Stephenson III mechanism could be changes in the circuit of its constituent four-bar or disconnection of external dyad for any motion of constituent four-bar where the coupler curve of the constituent four-bar moves outside the accessible region (Mirth and Chase, 1995). To comprehend the defects, and to formulate the constraints, the Stephenson III mechanism may be decomposed into a constituent four-bar linkage ( $ABDEA$ ) and an external dyad ( $CD_oE_o$ ), as shown in Fig 5.3. In the conventional rectification procedures, constituent four-bar is rectified first thereafter its interaction with the external dyad is considered.

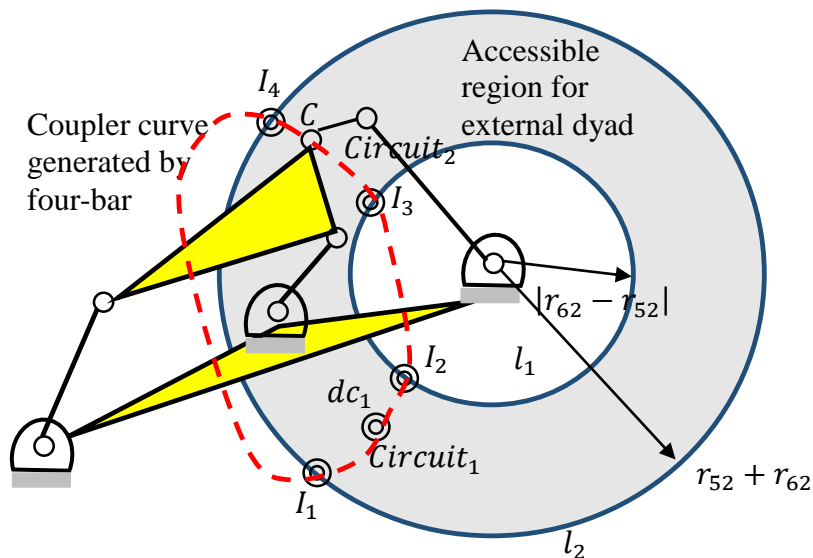


**Fig. 5.4** Accessible region of the external dyad of Stephenson III mechanism and coupler curve of constituent four-bar

Figure 5.4 shows a Stephenson III mechanism which consists of a constituent four-bar and an external dyad. The trajectory of coupler point  $C$  of the four-bar without external dyad is shown with dashed line in red color. The shaded area between the two concentric ‘limit circles’,  $l_1$  and  $l_2$ , traced by the external dyad with radii  $|r_{62} - r_{52}|$  and  $r_{52} + r_{62}$ , respectively, is the accessible region reachable by the dyad. The segment of the coupler curve of the constituent four-bar that lies within the accessible region is identified as a circuit. The points of intersection between the limit circles and the

coupler curve correspond to dead-center configurations (represented by two concentric circles in black color) where the external dyad become collinear, i.e., in the form extended and overlapping are  $I_1, I_2, I_3,$  and  $I_4$ .  $Circuit_1$  may contain dead-center configuration,  $dc_1$ , when coupler and follower in the constituent four-bar become collinear ( $\mu_1 = 0^\circ$  and  $\mu_1 = 180^\circ$ ).

Whereas, in  $Circuit_2$  the external dyad becomes collinear when  $\mu_2 = 0^\circ$  and  $\mu_2 = 180^\circ$ .

In literature (Mirth and Chase, 1995; Guo and Chu, 2004) constraints are formulated by considering Stephenson III as a constituent four-bar and an external dyad. However, as opposed to that conventional procedure, the Stephenson III mechanism is decomposed into Loop I and Loop II for constraint formulation. Later, the conventional procedure is used for verification.

### 5.2.3.1 Formulation of Order, Circuit, and Branch Constraints

The constraints for preventing defects in Loop I (four-bar) are formulated in the first stage, (See Section 4.2 for illustration):

*Constraint for avoiding Grashof defect in constituent four-bar:* The constraint to avoid Grashof defect can be expressed as follows:

$$g_1(\mathbf{x}) = r_{21} + r_{11} - r_{31} - r_{41} < 0 \quad (5.18)$$

*Constraint for preventing order defects:* The constraints can be expressed as:

$$g_2(\mathbf{x}) = \theta_{21}^{k+1} - \theta_{21}^k < 0, \quad k = 1, \dots, N - 1 \quad (5.19)$$

*Constraint for preventing circuit defects:* The constraint can be modeled mathematically and can be expressed as:

$$g_3(\mathbf{x}) = \emptyset = \theta_{31}^k - \theta_{41}^k < 0, \quad k = 1, \dots, N \quad (5.20)$$

*Constraint for preventing branch defects:* A toggle between two adjacent links within a linkage indicates a stationary position and it occurs when the two adjacent links align with one another. When a mechanism passes through a stationary configuration (dead center) while moving between two design positions, then the mechanism suffers from branch defect (Hang and Chen, 2008), as shown in Fig 5.5. The constraint to avoid toggle between two adjacent links, i.e., coupler and follower, can be formulated as:

$$g_4(\mathbf{x}) = \sin(\theta_{41}^k - \theta_{31}^k) > 0, \quad k = 1, \dots, N \quad (5.21)$$

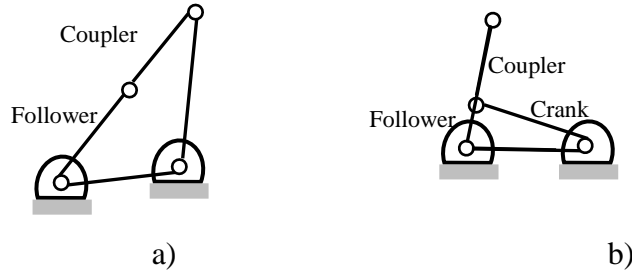


**Fig 5.5** Toggle when angle between adjacent links a)  $180^\circ$  b)  $0^\circ$

The constraints for preventing defects in Loop II (five-bar) are formulated in the second stage:

*Constraint for avoiding Grashof defect in five-bar:* The Grashof defect in a five-bar mechanism can be avoided by applying the five-bar Grashof criterion (Ting, 1986).

Accordingly, the constraints can be formulated as:

$$g_5(\mathbf{x}) = r_{22} + r_{12} + r_{32} - r_{52} - r_{62} < 0 \quad (5.22)$$

*Constraint for preventing circuit defects:* The circuit defect occurs in Loop II when all the design positions do not fall on the same segment of the constituent four-bar (Loop I) coupler curve which lies inside the accessible region, as shown in Fig 5.6. It occurs

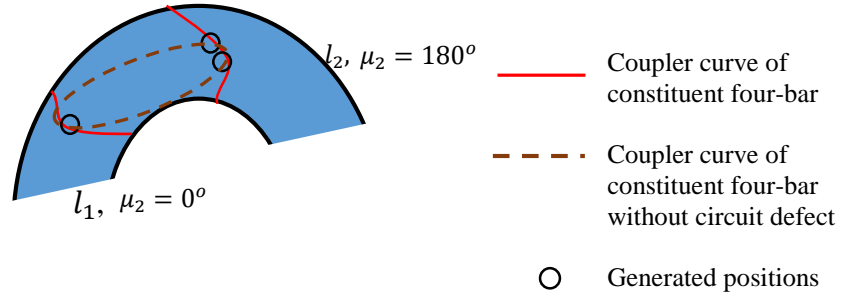


**Fig. 5.6** Description of circuit defect in Loop II

due to disconnection of point  $C$  in Loop II. However, if all the generated positions corresponding to design positions fall on the full curve inside accessible region as shown by dashed line (brown color), in that case, the mechanism is free from circuit defect. The circuit defect in the Loop II can be avoided by assigning the transmission angle in increasing or in decreasing order. The constraints are formulated as:

$$g_6(\mathbf{x}) = \theta_{62}^k - \theta_{52}^k < 0, \quad k = 1, \dots, N \quad (5.23)$$

*Constraint for preventing branch defects:* Figure 5.7 shows the motion of a mechanism consists of two segments  $s_s t_1$  and  $s_e t_2$  where  $s_s$ , and  $s_e$  are the starting and end



positions, respectively. If the toggle (dead center) positions  $t_1$  and  $t_2$  lie on  $l_2$  and are very close to each other, then the generated positions corresponding to prescribed design positions may lie anywhere over the curve which starts at  $s_s$  and terminates at  $s_e$ . That mechanism will have branch defect. Branch defect occurs when all the design positions do not fall on the same branch. The branch defect can be avoided by removing the toggle positions in the five-bar loop or avoiding  $\mu_2 = 180^\circ$  or  $0^\circ$ . Therefore, the constraints for eliminating branch defect can be expressed as:

$$g_7(\mathbf{x}) = \sin(\theta_{52}^k - \theta_{62}^k) > 0, \quad k = 1, \dots, N \quad (5.24)$$

Coupler curve of constituent four-bar

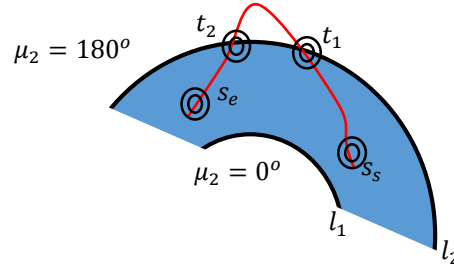


**Fig. 5.7** Description of branch defect in Loop II

The Eqs. (5.18)-(5.24) are required for avoiding all the defects in Stephenson III six-bar path generator mechanism. Finally, the optimization problem can be expressed as:

$$\text{minimize} \quad f(\mathbf{x}) = \sum_{i=1}^N \sqrt{(C_{ox}^i - P_{xd}^i)^2 + (C_{oy}^i - P_{yd}^i)^2} \quad (5.25)$$

$$\text{subject to} \quad g_1(\mathbf{x}) = r_{21} + r_{11} - r_{31} - r_{41} < 0 \quad (5.26)$$

$$g_2(\mathbf{x}) = \theta_2^{k+1} - \theta_2^k < 0, \quad k = 1, \dots, N - 1 \quad (5.27)$$

$$g_3(\mathbf{x}) = \theta_{31}^k - \theta_{41}^k < 0, \quad k = 1, \dots, N \quad (5.28)$$

$$g_4(\mathbf{x}) = \sin(\theta_{41}^k - \theta_{31}^k) > 0, \quad k = 1, \dots, N \quad (5.29)$$

$$g_5(\mathbf{x}) = r_{22} + r_{12} + r_{32} - r_{52} - r_{62} < 0 \quad (5.30)$$

$$g_6(\mathbf{x}) = \theta_{62}^k - \theta_{52}^k < 0, \quad k = 1, \dots, N \quad (5.31)$$

$$g_7(\mathbf{x}) = \sin(\theta_{52}^k - \theta_{62}^k) > 0, \quad k = 1, \dots, N \quad (5.32)$$

$$L_i < x_i < U_i, \quad i = 1, \dots, n \quad (5.33)$$

in which,  $L_i$  and  $U_i$  are the lower and upper limit, respectively, on the  $i^{th}$  design variable,  $n$  is the number of design variables, and superscript  $k$  represents the  $k^{th}$  position of the coupler.

Equations (5.25-5.33) represents a constrained optimization problem which is transformed into an unconstrained optimization problem (Mundo et al., 2009) to obtain an optimum solution. The transformation is executed by adding a penalty cost to the objective function for each violation of the constraint. Thereby, the original problem is framed as an unconstrained optimization problem wherein the first part is tracking error objective function and the second part is the penalty cost. Then the final optimization problem can be posed as:

$$\text{Minimize } f(\mathbf{x}) = \sum_{i=1}^N \sqrt{(C_{ox}^i - P_{xd}^i)^2 + (C_{oy}^i - P_{yd}^i)^2} + \sum_{m=1}^7 B_m (P)^m \quad (5.34)$$

$$\text{range of variables} \quad L_i < x_i < U_i, \text{ where } i = 1, \dots, n \quad (5.35)$$

in which,  $(P)^m$  ( $m = 1, \dots, 7$ ) are the penalty costs of high order ( $10^4$ ) which increase the objective function value if constraints are violated and  $B_m$  is the Boolean Function (Mundo et al., 2006) expressed as:

$$B_m = \begin{cases} 0, & \text{if } g_m(\mathbf{x}) \leq 0 \text{ for } 1 \leq m \leq 3 \\ 0, & \text{if } g_m(\mathbf{x}) > 0 \text{ for } m = 4 \text{ or } 7 \\ 1, & \text{otherwise} \end{cases} \quad (5.36)$$

### 5.3 Optimization Algorithm

Optimization problem formulated in the previous sections, Sections 4.1 and 4.2, can be solved either by conventional or nature-inspired optimization techniques. In classical or conventional optimization methods, complexity is involved in calculating derivatives and Hessians of the objective function. Moreover, there is a non-zero probability of obtaining global optimum, and its results depend upon starting point (Kunjur and Krishnamurty, 1997). An optimal solution is near to the initial guess point thereby produces a local optimum solution (Mariappan and Krishnamurty, 1996).

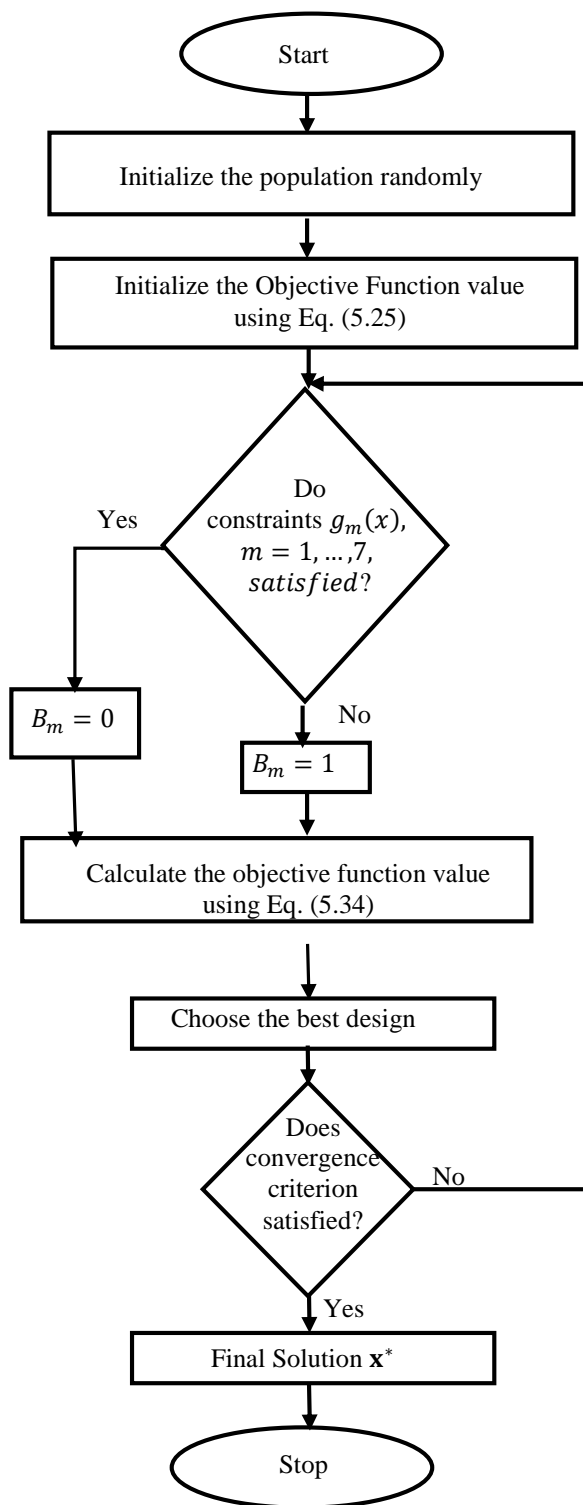


**Fig. 5.8** Scheme for loop-by-loop defect rectification using optimization technique

In contrast to conventional methods, nature-inspired optimization techniques do not require computation of derivatives and Hessians.

The Particle swarm optimization (PSO), the Genetic algorithm (GA), and Differential Evolution (DE) are some of the nature-inspired optimization techniques.

Although these nature-inspired techniques tend to converge to a global minimum, but there is no guarantee of global optimality of final solution (Arora, 2004). Furthermore, these algorithms require algorithm parameters that affect their performance. Even sometimes it becomes difficult to select these optimization parameters (Rao and Savsani, 2012; Rao, 2016). However, a teaching-learning-based optimization algorithm is a nature-inspired algorithm that does not require such algorithmic parameters, can be used. Figure 5.8 shows the scheme for loop-by-loop defect rectification using optimization technique. This is utilized here for defect-free synthesis of Stephenson III linkage; however, the objective function may be modified to use it for the synthesis of other inversions of Stephenson or Watt mechanisms. Besides, a refinement scheme is applied to TLBO algorithm to reduce its computational effort (See Appendix B for details).

## 5.4 Numerical Examples

There are no specific rules known for developing the guideline of the arbitrary single degree-of-freedom planar mechanisms. Therefore, it is essential to describe the motion of mechanisms on the case-by-case basis (Chase and Mirth, 1993). It is also required to check the rules that can be used for elimination of defect for a particular case. In this study, four- and six-bar linkages are considered as typical cases to synthesize. In all four numerical examples are discussed in this chapter to illustrate the proposed method and use of necessary and sufficient constraints required for defect elimination.

### 5.4.1 Example 1: Four-Bar Linkage for Straight Line Trajectory

In this section, a linkage is designed to track a vertical straight line trajectory. The desired points on the trajectory are shown in Table 5.1 (Acharyya and Mandal, 2009) which need to be tracked.

**Table 5.1** Desired points for vertical straight line (Acharyya and Mandal, 2009)

Desired Point	1	2	3	4	5	6
$P_{xd}$	20	20	20	20	20	20
$P_{yd}$	20	25	30	35	40	45

Using the proposed necessary and sufficient constraints and TLBO based algorithm (See Appendix, Fig B.1, for detail), an optimal synthesis of a planar crank-rocker mechanism is performed to obtain a defect-free mechanism that can track a straight line trajectory. Note that desired points  $N$  are 6 in this example and the limits on the design variables are taken as:

$$r_1, r_2, r_3, r_4, \in [5,60]; l \in [5,200]; \theta_1 \in [0,2\pi]; A_x, A_y \in [-60,60];$$

$$\theta_2^1, \dots, \theta_2^N, \beta \in [0,2\pi]$$

The optimization algorithm is coded in MATLAB®. The population size in all three techniques is taken as 150 while the number of iterations in TLBO is taken as half the corresponding number of iterations in any other (GA and PSO) algorithm. The best value of the objective function corresponding to the design variables and the average of all the function values are found for 30 independent runs corresponding to each iteration. This is followed by all three techniques and convergence plots are presented for comparing their computational efficiency. These algorithms (PSO and GA) are run for 300 iterations to find best objective function value where PSO reached to an optimum value of the objective function at 0.2239 after 87000 function evaluations, GA reached its optimum value at 0.6073 after 88500 function evaluations; whereas, optimum value of TLBO is found at 0.1482 after 82500 function evaluations. The convergence plots of the best and average objective function values are shown in Fig 5.9 and Fig 5.10, respectively.

Note: number of iterations depend upon convergence, population was taken as number of design variables×10.

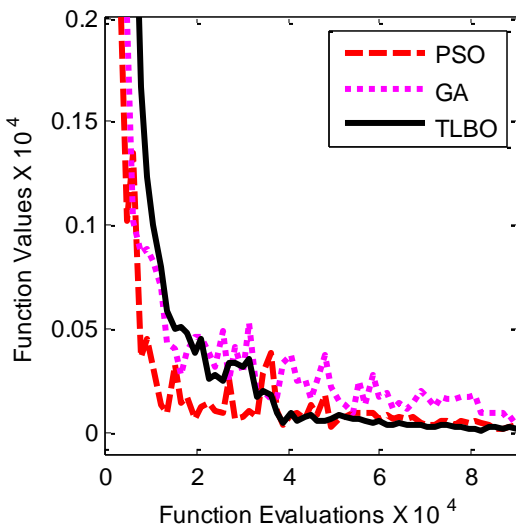


**Fig 5.9** Convergence of the best objective function value in PSO, GA, and TLBO

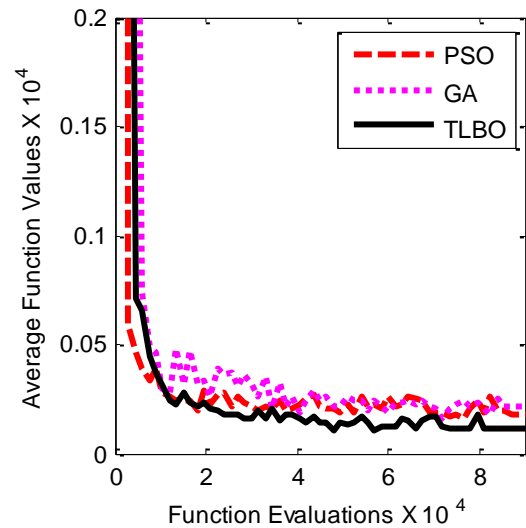


**Fig 5.10** Convergence of average value in PSO, GA, and TLBO

It is found that average function value as 11.0546 is obtained for TLBO which is very less as compared to GA (21.1489) and PSO (18.3275). Here, TLBO requires 5% and 7% fewer function evaluations as compared to those for PSO and GA, respectively. The synthesized optimum designs of crank-rocker using GA, PSO, and TLBO are shown in Table 5.2.

**Table 5.2** Optimized parameters for the crank-rocker linkage

Design Variables	GA	PSO	TLBO
$r_1$	50.7014	41.2974	60.0000
$r_2$	7.6397	7.1340	14.6488
$r_3$	27.1753	27.8342	47.6577
$r_4$	34.1741	36.3183	59.9128
$l$	59.7613	78.0690	92.1973
$\theta_1$	1.0509	4.5248	4.4871
$A_x$	-32.7301	-50.8317	-55.5544
$A_y$	16.8194	14.2660	1.8752
$\theta_2^1$	2.8082	3.0231	3.5408
$\theta_2^2$	3.9059	3.7070	3.9269
$\theta_2^3$	4.2404	4.0793	4.2133
$\theta_2^4$	4.5598	4.3985	4.4653
$\theta_2^5$	4.8942	4.7091	4.7052
$\theta_2^6$	5.2851	5.0471	4.9469
$\beta$	5.9634	5.5229	5.5222
$f(\mathbf{x}^*)$	0.6073	0.2239	<b>0.1482</b>

The plot of the desired points and generated trajectory by the optimized crank-rocker linkage is shown in the Fig 5.11; whereas, Fig 5.12 shows the errors. The constraints satisfaction are shown in Figs 5.13 and 5.14.

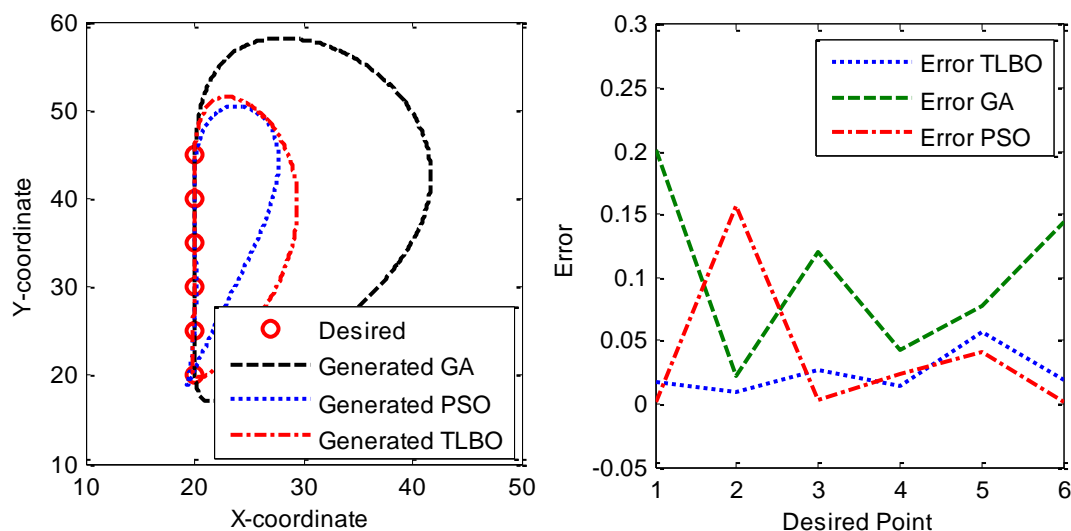


**Fig 5.11** Generated trajectory and desired points of crank-rocker linkage

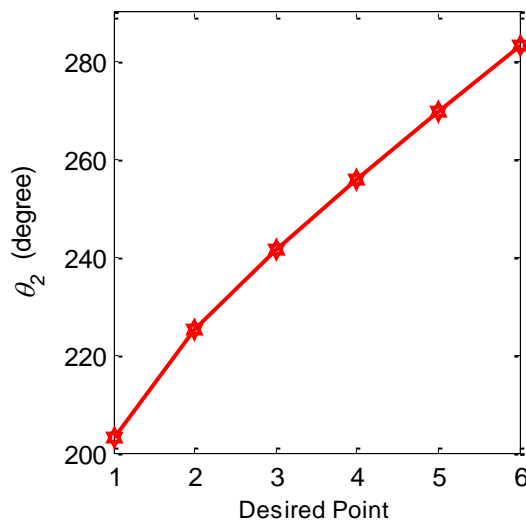


**Fig 5.13** Satisfaction of order constraint

**Fig 5.12** Error between the desired and generated points

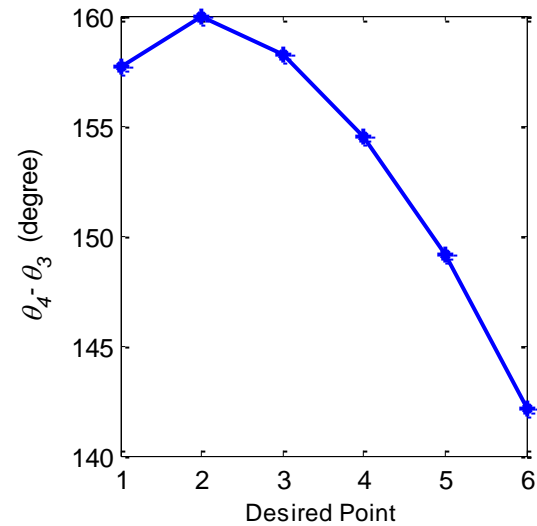


**Fig 5.14** Satisfaction of circuit constraint

**Table 5.3** Error between the desired and generated points

Error	PSO	GA	TLBO
Minimum	0.0015	0.0216	0.0102
Average	0.0379	0.1012	<b>0.0243</b>
Maximum	0.1565	0.2009	0.0570

From the Table 5.3, it is observed that average and maximum errors are minimum in TLBO algorithm. This indicates that TLBO provides more accurate results than those of GA and PSO, particularly for this numerical example.

#### 5.4.2 Example 2: Four-Bar Linkage for Knee Supporting Device

In this section, a nontrivial crank-rocker mechanism is designed for flexion/extension movement of a human knee supporting device. Flexion/extension trajectory of a healthy human knee shown in Table 5.4 (Sancibrian et al., 2016) is considered as points on the desired trajectory which needs to be tracked.

**Table 5.4** Desired points for knee flexion (Sancibrian et al., 2016)

Desired Points	1	2	3	4	5	6	7	8	9	10	11	12	13	14
$P_{xd}$	-50	-16	10	14	6	0	-5	-10	-15	-20	-25	-30	-35	-40
$P_{yd}$	200	150	100	60	18	0	-12	-19	-21.5	-22	-21	-18	-11	0

Using the necessary and sufficient constraints, and TLBO based algorithm (See Fig B.1 in Appendix B), an optimal synthesis of a planar crank-rocker mechanism is performed to obtain a defect-free mechanism. It is worth mentioning that presented

algorithm first checks population (class of learners) for Grashof and order constraints, and accordingly arranges the design variables (courses). In this way, a refined population (class of learners) is used in the subsequent part of the algorithm. Note that there are 14 desired points in this study, and the bounds on the design variables are taken as:

$$r_1, r_3 \in [20, 90]; r_2, r_4 \in [40, 170]; l \in [-1000, 1000]; \theta_1 \in [0, 2\pi];$$

$$A_x, A_y \in [-1500, 1500]; \theta_2^1, \dots, \theta_2^N \in [0, 2\pi]; \beta \in [0, \pi/3].$$

The algorithm is coded in MATLAB®. To compare the effectiveness of the algorithm, the same problem is solved using GA and PSO. The population size in all three techniques is taken as 230 while the number of iterations in TLBO is taken as half the corresponding number of iterations in any other (GA and PSO) algorithm. GA, PSO, and TLBO are run in succession with the increasing values of the iterations while the function values corresponding to the function evaluations are compared among themselves. The best value of the objective function corresponding to the design variables and the average of all the function values are found for 30 independent runs corresponding to each iteration. This is followed by all three techniques and convergence plots are presented for comparing their computational efficiencies. GA and PSO require tuning of parameters whereas TLBO is a parameter-less technique. Hence, default parameters were selected for both GA and PSO techniques. These algorithms are run for 220 iterations to find the best objective function value where PSO reached an optimum value of the objective function at 76.8973 after 48300 function evaluations, GA reached its optimum value at 343.8068 after 50600 function evaluations; whereas, optimum value of TLBO is found at 44.2845 after 34500 function evaluations as shown in Fig 5.15.

In addition, the average of objective function values is also reported as shown in Fig 5.16. It is found that minimum average function value as 330 is obtained for TLBO which is very less as compared to GA (3389) and PSO (3022.7). Thus, TLBO gives better results in comparison to those obtained in both GA and PSO. It requires 71% and 68% function evaluations in comparison to those for PSO and GA, respectively.



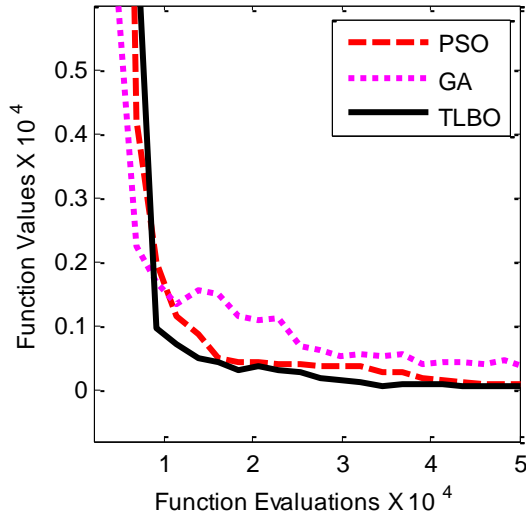


**Fig 5.15** Convergence of the best objective function value in PSO, GA, and TLBO

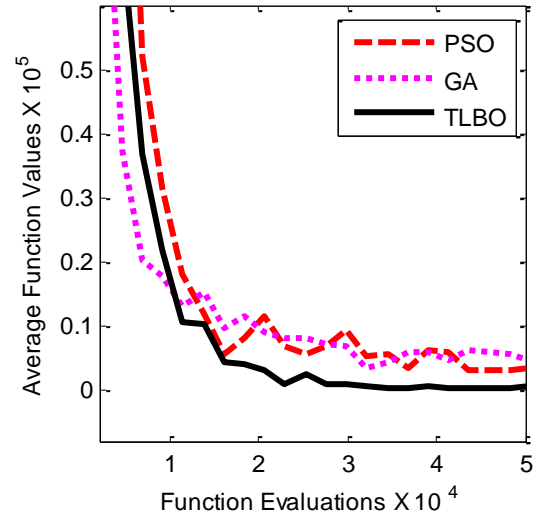


**Fig 5.16** Convergence of average function values in PSO, GA, and TLBO

An algorithm is considered efficient if it finds an optimum solution using lesser number of function evaluations. Thus, TLBO is computationally more efficient than GA and PSO for the mechanism synthesis. The synthesized optimum designs of crank-rocker using GA, PSO, and TLBO are shown in Table 5.5.

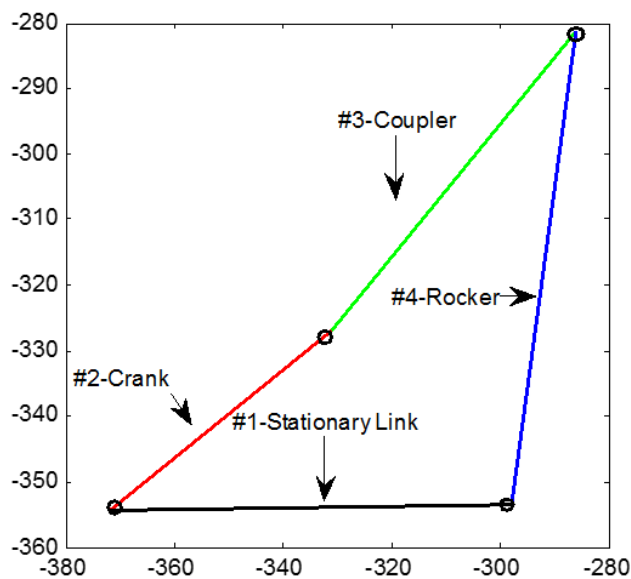
**Table 5.5** Optimum design of crank-rocker mechanism using GA, PSO and TLBO

Design Variables	GA	PSO	TLBO
$r_1$	89.8806	89.9242	81.7145
$r_2$	53.3663	54.4317	49.0499
$r_3$	64.5344	64.4317	64.1500
$r_4$	79.6841	80.8819	73.1816
$l$	207.8911	312.5359	459.4885
$\theta_1$	6.0948	5.8421	0.4431
$A_x$	-100.578	-229.081	-371.702
$A_y$	-306.618	-289.828	-354.478
$\theta_2^1$	0.4389	0.5378	0.594
$\theta_2^2$	0.7454	0.7669	0.7978
$\theta_2^3$	0.8898	1.2250	1.1131
$\theta_2^4$	1.7306	1.6552	1.4426
$\theta_2^5$	2.3481	2.0979	1.9198
$\theta_2^6$	2.6234	2.3187	2.1675
$\theta_2^7$	2.8507	2.4047	2.2808
$\theta_2^8$	2.9422	2.4059	2.4426
$\theta_2^9$	3.1746	2.5502	2.4978
$\theta_2^{10}$	3.2402	2.5858	2.6395
$\theta_2^{11}$	3.2841	3.3854	2.8410
$\theta_2^{12}$	3.3291	3.4065	2.9516
$\theta_2^{13}$	3.4193	3.4453	3.0363

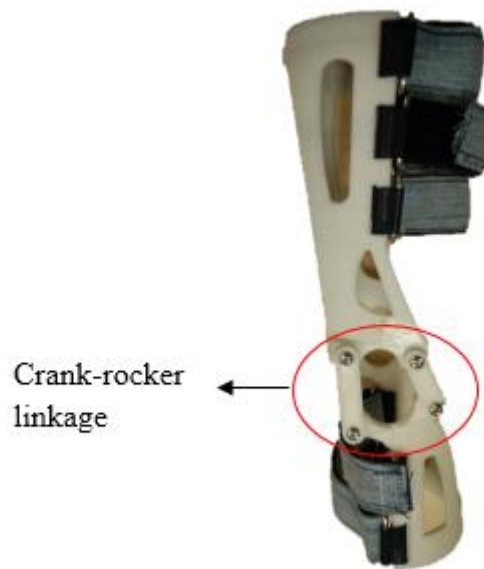
$\theta_2^{14}$	6.2826	3.4986	3.1664
$\beta$	0.2864	0.0081	0.0036
$f(\mathbf{x}^*)$	343.8068	76.8973	<b>44.2845</b>

Note that angles are in radian.

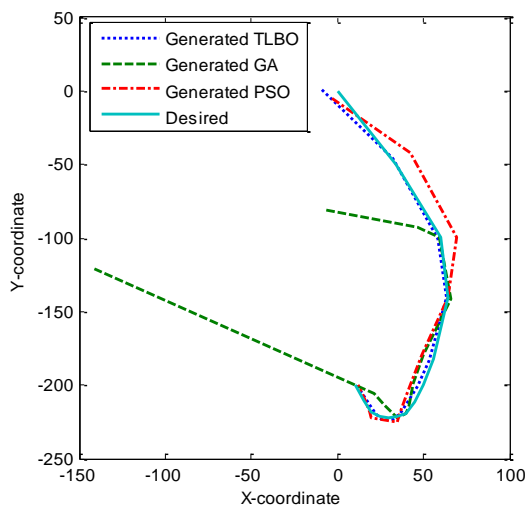
The design parameters obtained by TLBO algorithm with least objective function value are selected for the design of crank-rocker mechanism which is shown in Fig 5.17. A prototype of the designed crank-rocker linkage is developed for human knee exoskeleton which is shown in Fig 5.18. The designed mechanism for knee flexion/extension is capable of tracking all the desired points without any circuit, branch, and order defect. Figure 5.19 shows that generated trajectory matches the desired trajectory to a great extent while distances (error) between the generated and desired points is shown in Fig 5.20.



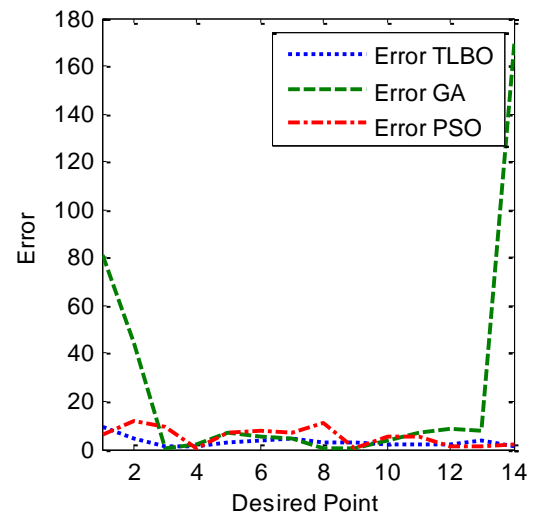
*Fig 5.17 Defect-free crank-rocker mechanism designed using TLBO*



**Fig 5.18** Prototype of human knee exoskeleton developed for the designed crank-rocker linkage



**Fig 5.19** Generated and desired trajectories of knee flexion/extension



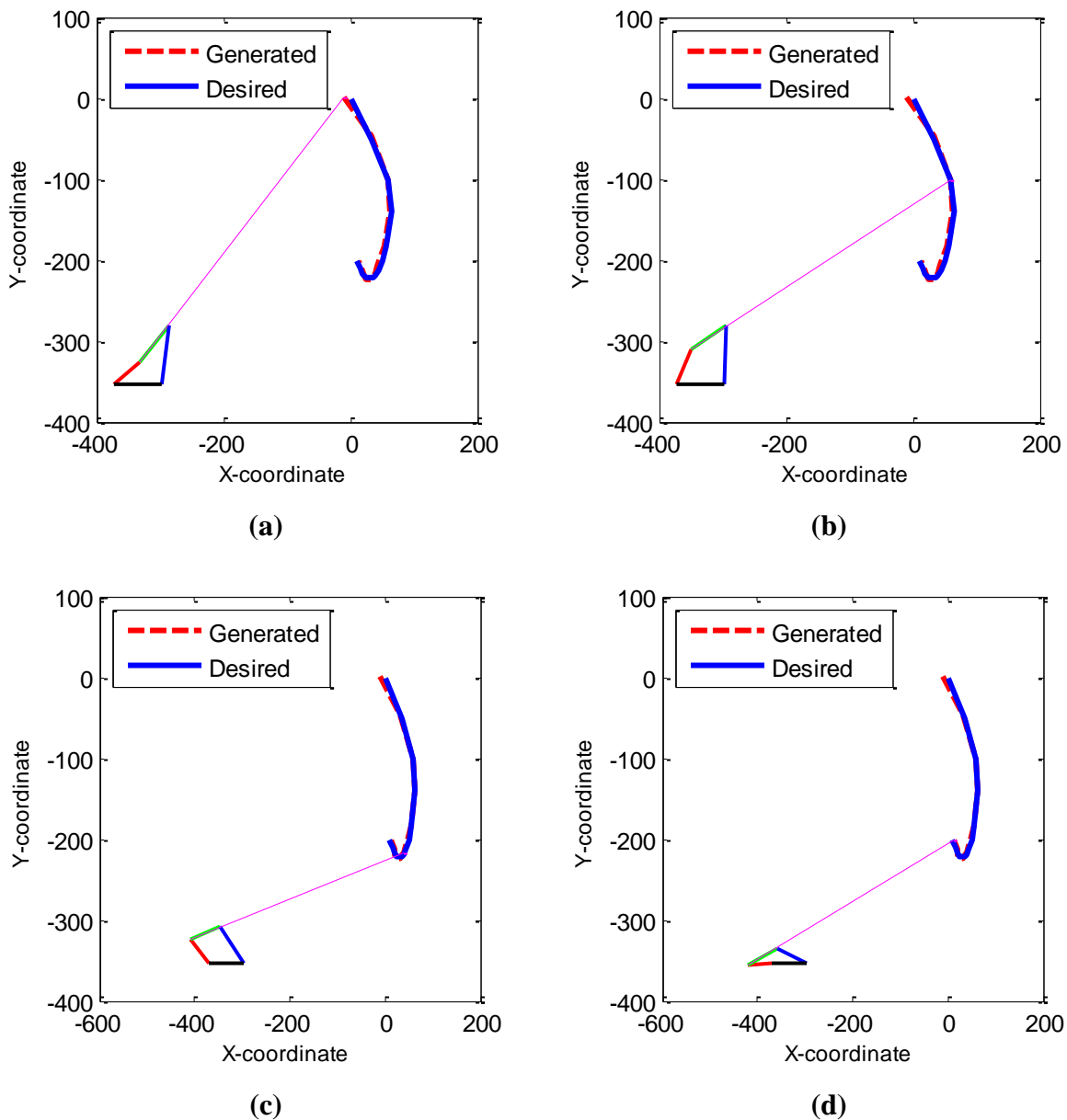
**Fig 5.20** Error between the desired and generated points

Table 5.6 provides the maximum, average, and minimum errors between desired and generated points for TLBO, GA, and PSO.

**Table 5.6** Error between the desired and generated points

Error	PSO	GA	TLBO
Minimum	0.0075	0.1876	0.8660
Average	5.4925	24.5582	3.2008
Maximum	11.4457	170.4722	9.2195

From Table 5.6, it is observed that average and maximum errors are minimum in TLBO algorithm. This indicates that TLBO provides more accurate results than those of GA and PSO, particularly for this numerical example.



**Fig 5.21** Simulation of the crank-rocker mechanism a) 1<sup>st</sup> position b) 3<sup>rd</sup> position c) 8<sup>th</sup> position d) 14<sup>th</sup> position

Simulation of the crank-rocker mechanism is also performed in MATLAB® environment to validate *defect-free* mechanism. Figure 5.21 represents four sequential positions of the mechanism for randomly selected crank angle  $\theta_2$ . This shows that the mechanism moves from the first position to the last position in sequence without any stationary configuration. Hence, circuit, branch, and order defects are rectified thereby

making the mechanism defect-free. Figure 5.21 shows that  $\theta_2^1 < \theta_2^2 < \dots < \theta_2^{14}$  for 14 sequential desired points which proves that constraint applied in Eq. (5.7) is satisfied and Fig 5.23 shows that  $\theta_3 < \theta_4$  is true for all the desired points which satisfy constraint in Eq.(5.8). The advantage of using necessary and sufficient constraints reduces the number of constraints from four to three for obtaining a defect-free mechanism. Moreover, change in the sign of transmission angle is used here for circuit defect rectification instead of the conventional use of change in sign of the crank and coupler angle (Sardashti et al., 2013).

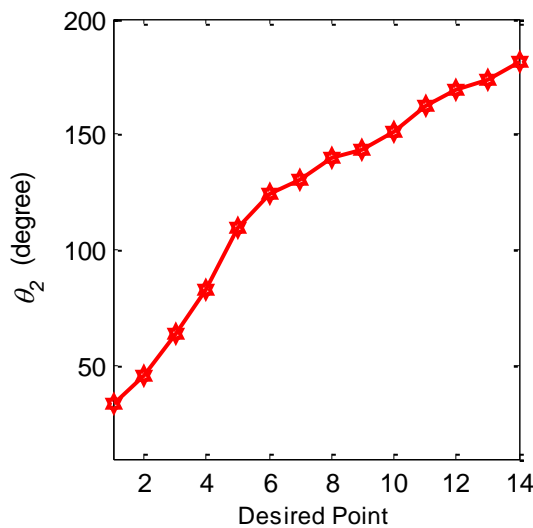


**Fig 5.22** Satisfaction of order constraint

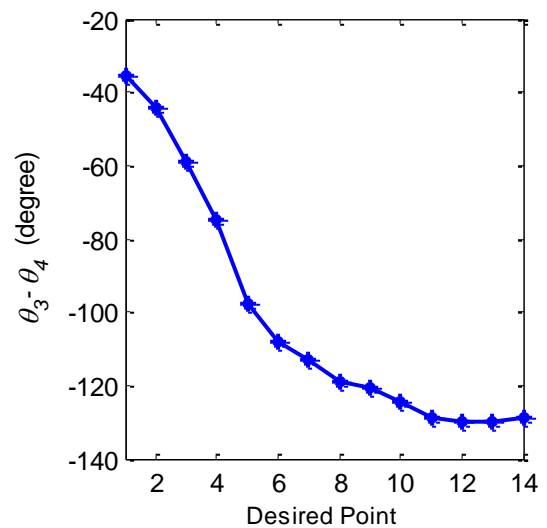


**Fig 5.23** Satisfaction of circuit constraint

### Validation

The prototype of proposed knee exoskeleton which consists of crank-rocker linkage has been developed to validate the results obtained through simulation in Fig 5.21. The prototype was donned by subject of height 6'16" and held tightly by velcros to support the knee. Then, the positions of crank-rocker linkage are observed for one complete gait cycle. It is observed that the subject was able to walk smoothly with knee exoskeleton, and the designed linkage was able to reach all the positions without dismantling. This proves that the designed mechanism is defect-free and it can be used in the knee of the exoskeletons, robots, etc., for walking. Figure 5.24 shows the positions reached by the prototype for one gait cycle.



*Fig 5.24 Experimental validation of designed crank-rocker linkage for human knee exoskeleton*

### **5.4.3 Example 3: Six-Bar for Straight Line Trajectory**

A planar Stephenson III six-bar mechanism free from circuit, branch, and order defects is to be designed for predefined positions as shown in Table 5.1. The mechanism is

expected to trace a predefined straight line path with six precision positions. The loop-by-loop method proposed in Section 4.2 can be solved by an optimization algorithm. Various algorithms such as genetic algorithm (GA) require algorithmic parameters which affect the algorithm performance. Alternatively, a teaching-learning-based-optimization algorithm (TLBO) which is a nature-inspired algorithm and it does not require any algorithmic parameter (Rao, 2016), is used to solve the problem in this study.

Ranges of design variables:

$$r_{11}, r_{21}, r_{31}, r_{41}, r_{32} \in [5, 60]; \alpha_2 \in [0, \frac{\pi}{2}]; \quad r_{12}, r_{52}, r_{62} \in [5, 100]; \alpha_3 \in [0, 2\pi];$$

$$l_{cp} \in [5, 200]; \theta_{11}, \theta_{21}^1, \dots, \theta_{21}^6 \in [0, 2\pi]; \quad \theta_{12} \in [0, \frac{\pi}{2}]; \quad A_x, A_y \in [-500, 500]$$

To demonstrate mechanism without defects, the optimization problem is solved first without imposing the constraints, i.e., Eqs (5.26)-(5.33). Thereafter, it is solved with constraints as posed in Eqs. (5.35)-(5.36). Figure 5.8 shows the scheme of the algorithm with constraints. The algorithm is run 30 times corresponding to each iteration for unconstrained and constrained problems denoted by WOC (without constraints) and WC (with constraints), respectively. The best results for both cases are obtained when the algorithm converges. Figures 5.25 and 5.26 shows that algorithm converges faster for constraint problem in comparison with that of the unconstrained problem.

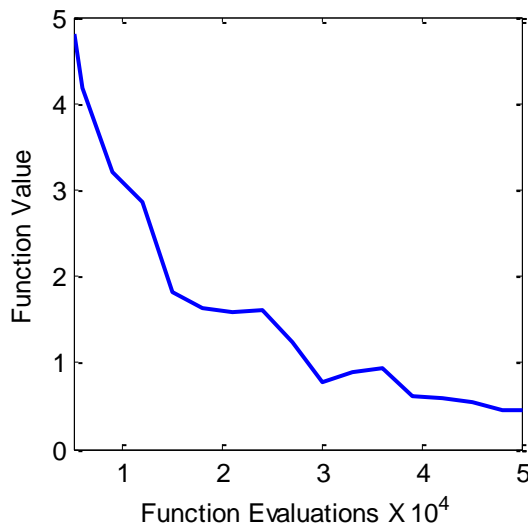


**Fig 5.25** Convergence of algorithm for unconstrained problem

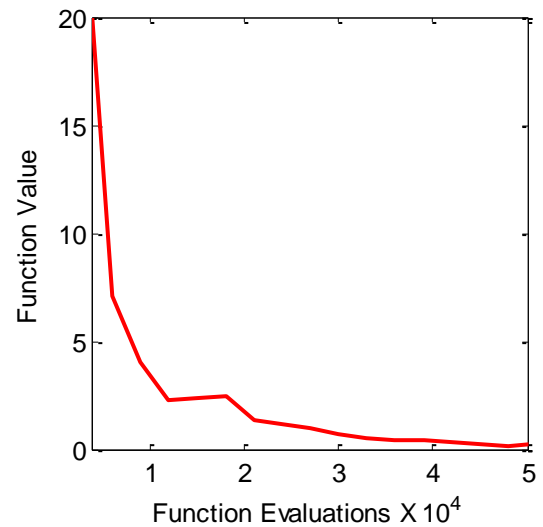


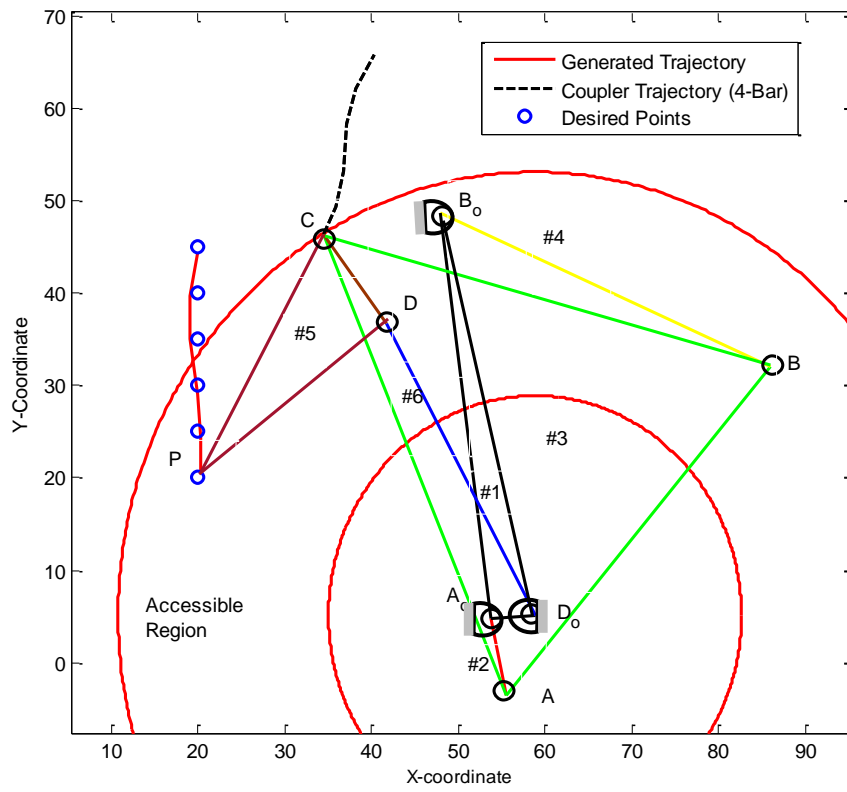
**Fig 5.26** Convergence of algorithm for constrained problem

Obviously, the solution of an unconstrained problem provides a defected mechanism. The two type of defects can be easily identified, namely, circuit and branch in the synthesized mechanism. Figure 5.27a shows the presence of circuit defect in the designed mechanism because the coupler curve of the constituent four-bar lies outside the accessible region between both the concentric circles, that indicates disconnection at point  $C$ . Figure 5.27b demonstrates that the mechanism needs to be dismantled and assemble again outside the accessible region stating that mechanism has circuit defect. Moreover, the links #5 and #6 in Fig 5.27b shows the dead-center configurations of the mechanism, which are represented by points  $B_1$  and  $B_2$ . It is found that all the precision points do not fall on the same branch rather they fall on different branches, namely,  $Branch_1$  and  $Branch_2$ , respectively. This indicates the mechanism suffers from branch defect.

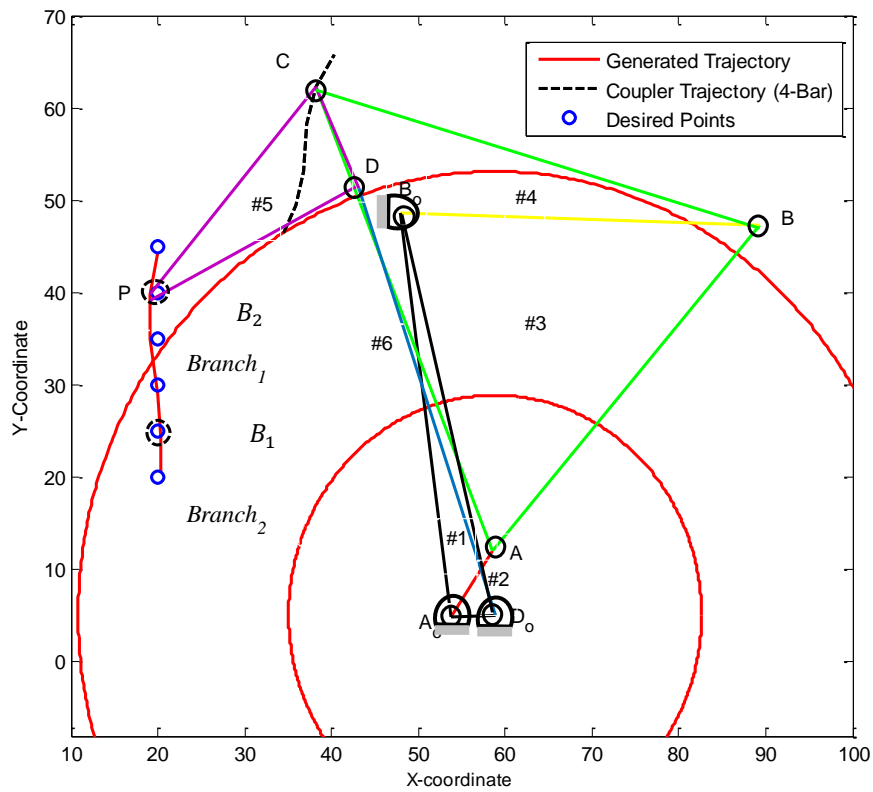
Another case is considered here to demonstrate the branch defect. It occurs when the design positions distribute on different branches. In Fig 5.28 the points  $B_1$  and  $B_2$  represent the configurations (dead-center) of the mechanism where the coupler,  $r_{31}$ , and follower,  $r_{41}$ , of the constituent four-bar become collinear whereas  $B_3$  represents the mechanism configuration where the links  $r_{52}$  and  $r_{62}$  becomes collinear. Accordingly, different branches are formed on the coupler curve corresponding to the design positions. The dash-dot circles on the coupler curve of the constituent four-bar represent the points corresponding to the design positions. In this case, it is found that three dash-dot circles corresponding to the design positions lie on the branch,  $B_1B_3$ , while the remaining three lies on the branch,  $B_2B_3$ , which indicates the presence of branch defect.

*The defects discussed in the preceding paragraph can be avoided by applying the loop-by-loop defect rectification method, proposed in this paper.* Now, the same optimization problem is considered subjected to defect-specific constraints required for the elimination of all the defects. In this method, the constraints are divided into loops, namely, Loop I and Loop II. Loop I represent the constituent four-bar and Eqs (5.26)-(5.29) are used for avoiding Grashof, circuit, branch, and order defects; whereas, Loop II represents a five bar and Eqs (5.30)-(5.32) are used for preventing Grashof, circuit, and branch defects. Lastly, Eq (5.33) is used to bind the design variables within lower and upper limits. All these constraints are applied to synthesize a defect-free Stephenson III six bar mechanism for path generation. In this section, the proposed method is used to synthesize the mechanism for straight line path generation defined in Table 5.1.





a)



b)

**Fig 5.27** Synthesized Stephenson III mechanism demonstrates a) circuit defect b) branch defect

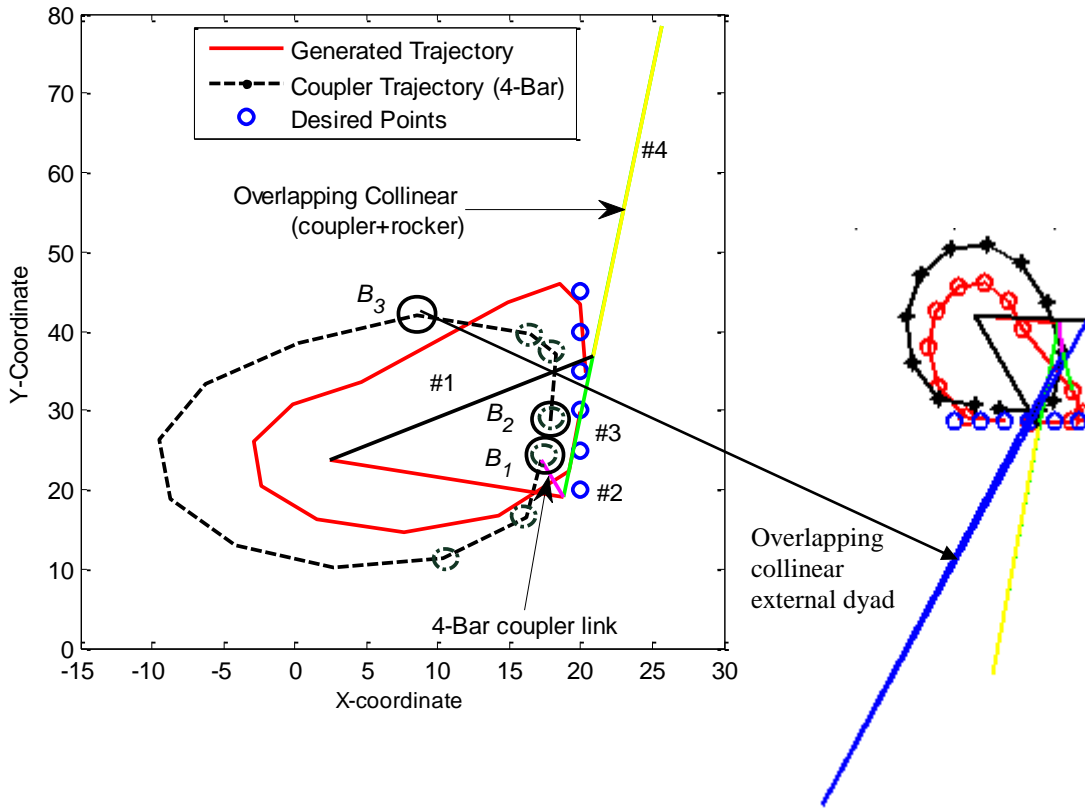


**Fig. 5.28** Synthesized Stephenson III mechanism with branch defect

Table 5.7 shows the comparison of the mechanism synthesized using constrained and unconstrained methodology, presented as “With Constraints (WC)” and “Without Constraints (WOC)”, respectively. The problems are solved using TLBO algorithm discussed in Chapter 4. It is found that the mechanism designed by WOC method satisfy the design requirements but the designed mechanism has defects as shown in Figs 5.27 and 5.28; whereas, the mechanism designed using WC method satisfy design requirements and simultaneously rectify defects during synthesis. Besides, the mechanism designed by WC method generated the mean error of 0.9666 (shown in boldface in Table 5.7) which is less in comparison with, 0.7982, generated by WOC method. It justifies that mechanism designed using the proposed method is defect-free, and it also generates trajectory which can accurately track the desired path as shown in Figs 5.29 and 5.30.

Figure 5.30 demonstrates that the designed Stephenson III mechanism is defect free because the coupler curve of the constituent four-bar mechanism lies within the

accessible region which indicates that circuit defect is not present. Moreover, no dead-center configurations are found for the links,  $r_{31}$  and  $r_{41}$ , of the constituent four-bar

**Table 5.7** The results of Stephenson III mechanism with and without constraints

Design variables	Without constraints	With constraints
$r_{11}$	44.2572	53.3757
$r_{21}$	8.5543	10.5397
$r_{31}$	46.8693	30.5903
$r_{41}$	41.5326	46.4205
$r_{32}$	54.1645	21.5964
$r_{12}$	5.0195	93.2838
$r_{52}$	12.1108	50.5416
$r_{62}$	35.8840	84.2361
$l_{cp}$	29.4668	60.5935
$\alpha_2$	1.1051	0.5807
$\alpha_3$	5.1504	3.7982
$\theta_{11}$	1.7055	4.8401
$\theta_{12}$	0.0539	0.6899
$\theta_{21}^1$	4.9081	4.2964
$\theta_{21}^2$	5.9224	4.9847
$\theta_{21}^3$	3.7497	5.3553
$\theta_{21}^4$	0.5876	5.6561
$\theta_{21}^5$	0.9952	5.9694
$\theta_{21}^6$	1.5417	6.2819
$A_x$	53.8210	71.0487
$A_y$	4.8495	97.1157
$f(\mathbf{x})^*$	0.7982	<b>0.9666</b>

(Loop I) and links,  $r_{52}$  and  $r_{62}$  of the five-bar (Loop II). Besides, the error between the desired and generated trajectories is also displayed in Fig 5.29. The stick diagram (Fig 5.30) is presented to demonstrate that all the positions corresponding to design points lie on the same branch (since no dead configurations are found- one branch circuit); therefore, the mechanism has no branch defect. Figure 5.29 also shows that designed mechanism can track all the design positions without disassembly which indicates that mechanism has no circuit defect due to disassembly of external dyad with Loop I. Lastly, it is observed from Table 5.7 and Fig 5.30 that the driver (crank #2) moves in a sequence which indicates all positions are achieved in order, thereby no order defect. Figure 5.31 demonstrates that  $\mu_1$  follows same sign while decreasing from the first to the last precision point, and same is observed for  $\mu_2$ . Whereas Fig 5.32 shows that  $\theta_{21}$  has an increasing tendency from the first to last precision point that is consistent with the order constraint. It shows constraints to avoid circuit and order defects are

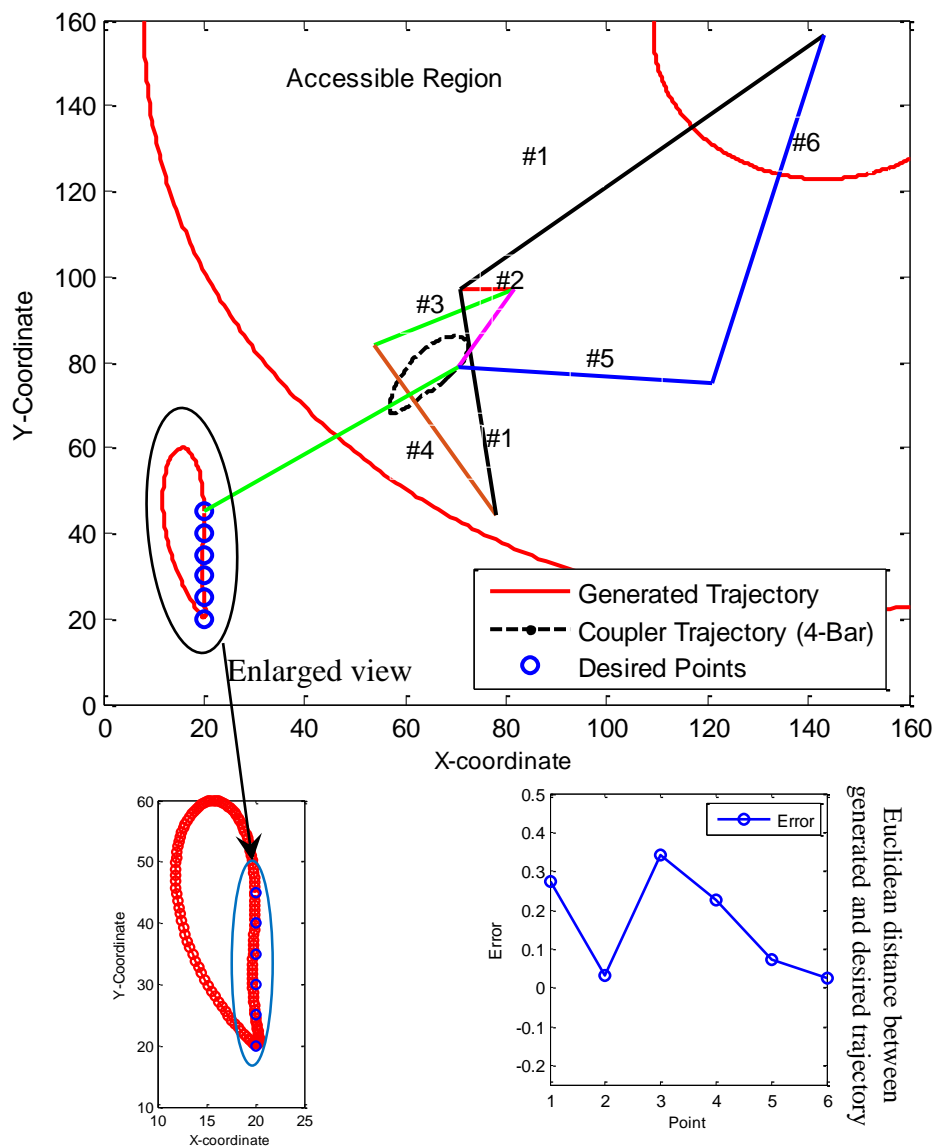


**Fig. 5.29** Defect-free Stephenson III mechanism

satisfied, as demonstrated in Figs 5.31, 5.32. The proposed method simplifies the constraint formulation and enables the designer to synthesize a defect-free Stephenson III six-bar mechanism for path generation. The method can be applied to synthesize a Stephenson III six-bar mechanism for any path.

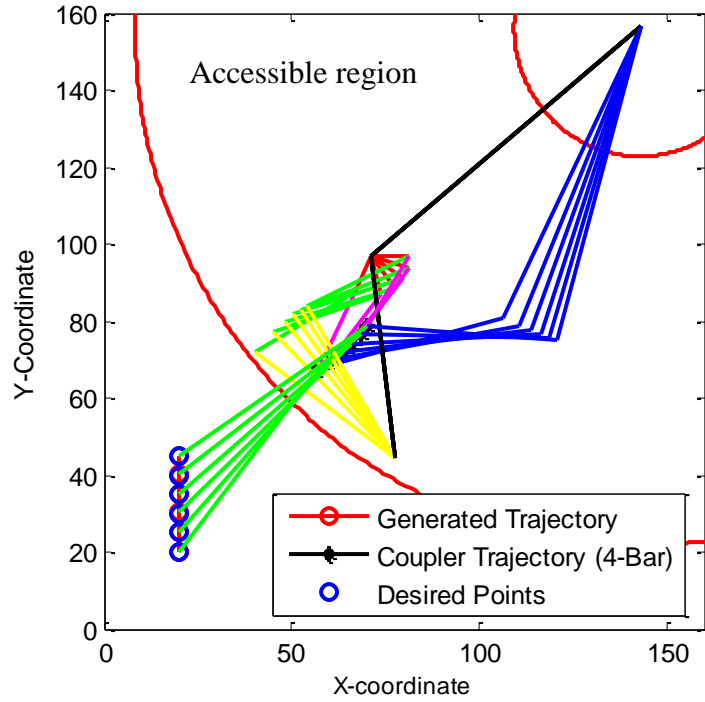


**Fig. 5.30** Stick diagram of Stephenson III mechanism

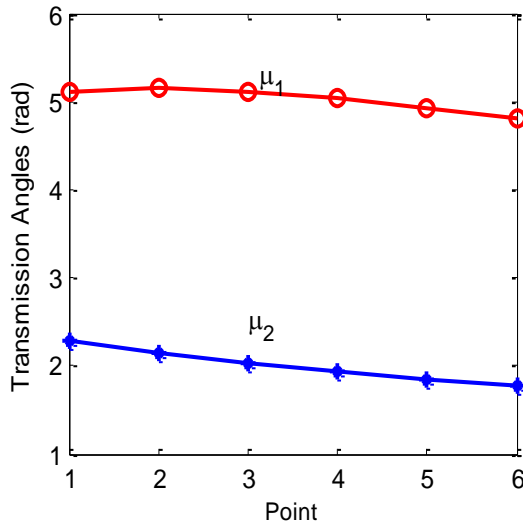


**Fig5.31** Satisfaction of transmission angle constraint

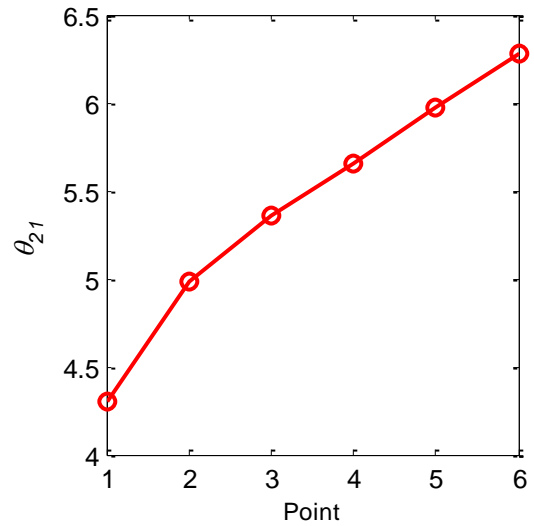


**Fig 5.32** Satisfaction of order constraint

#### 5.4.4 Example 4: Six-Bar for Human Knee Supporting Device

In this example, a Stephenson III six-bar linkage is designed for a knee supporting device using the proposed methodology. The designed linkage is to be designed for predefined positions, shown in Table 5.4. The mechanism is expected to trace a predefined curve having fourteen precision positions. The loop-by-loop method proposed in Section 4.2 can be solved by an optimization algorithm. Here, TLBO is

used in the same way as used in the previous example. The designed Stephenson III linkage for the following range of design variables is presented in Table 5.8

Note that same procedure is followed for example 4, as followed in example 3; therefore convergence is not shown here.

Ranges of design variables:

$$r_{11}, r_{21}, r_{31}, r_{41}, r_{32} \in [20, 200]; \quad \alpha_2 \in [0, 2\pi]; \quad r_{12}, r_{52}, r_{62} \in [20, 200]; \quad \alpha_3 \in [0, 2\pi]; \quad l_{cp} \in [20, 1200]; \quad \theta_{11}, \theta_{12}, \theta_{21}^1, \dots, \theta_{21}^{14} \in [0, 2\pi]; \quad A_x, A_y \in [-500, 500]$$

**Table 5.8** The results of Stephenson III mechanism when constraints are imposed

Design variables	Using TLBO
$r_{11}$	196.935
$r_{21}$	37.8761
$r_{31}$	62.0553
$r_{41}$	176.410
$r_{32}$	50.7329
$r_{12}$	180.0917
$r_{52}$	96.3245
$r_{62}$	172.3972
$l_{cp}$	376.2959
$\alpha_2$	1.4043
$\alpha_3$	5.3832
$\theta_{11}$	4.6199
$\theta_{12}$	2.2736
$\theta_{21}^1$	0.5543
$\theta_{21}^2$	1.6014
$\theta_{21}^3$	1.9879
$\theta_{21}^4$	2.2489
$\theta_{21}^5$	2.5632
$\theta_{21}^6$	2.7506
$\theta_{21}^7$	2.9191
$\theta_{21}^8$	3.0769
$\theta_{21}^9$	3.2311
$\theta_{21}^{10}$	3.4015
$\theta_{21}^{11}$	3.5587
$\theta_{21}^{12}$	3.7026
$\theta_{21}^{13}$	3.8917
$\theta_{21}^{14}$	4.1303
$A_x$	-312.8271
$A_y$	-253.1684
$f(\mathbf{x})^*$	<b>1314.54</b>

Figure 5.33 demonstrates that the designed Stephenson III linkage is defect free because the coupler curve of the constituent four-bar mechanism lies within the accessible region which indicates that circuit defect is not present. Moreover, no dead-

center configurations are found for the links,  $r_{31}$  and  $r_{41}$ , of the constituent four-bar (Loop I) and links,  $r_{52}$  and  $r_{62}$  of the five-bar (Loop II). Besides, the error between the desired and generated trajectories is also displayed in Fig 5.33. The stick diagram (Fig. 5.34) is presented to demonstrate that all the positions corresponding to design points

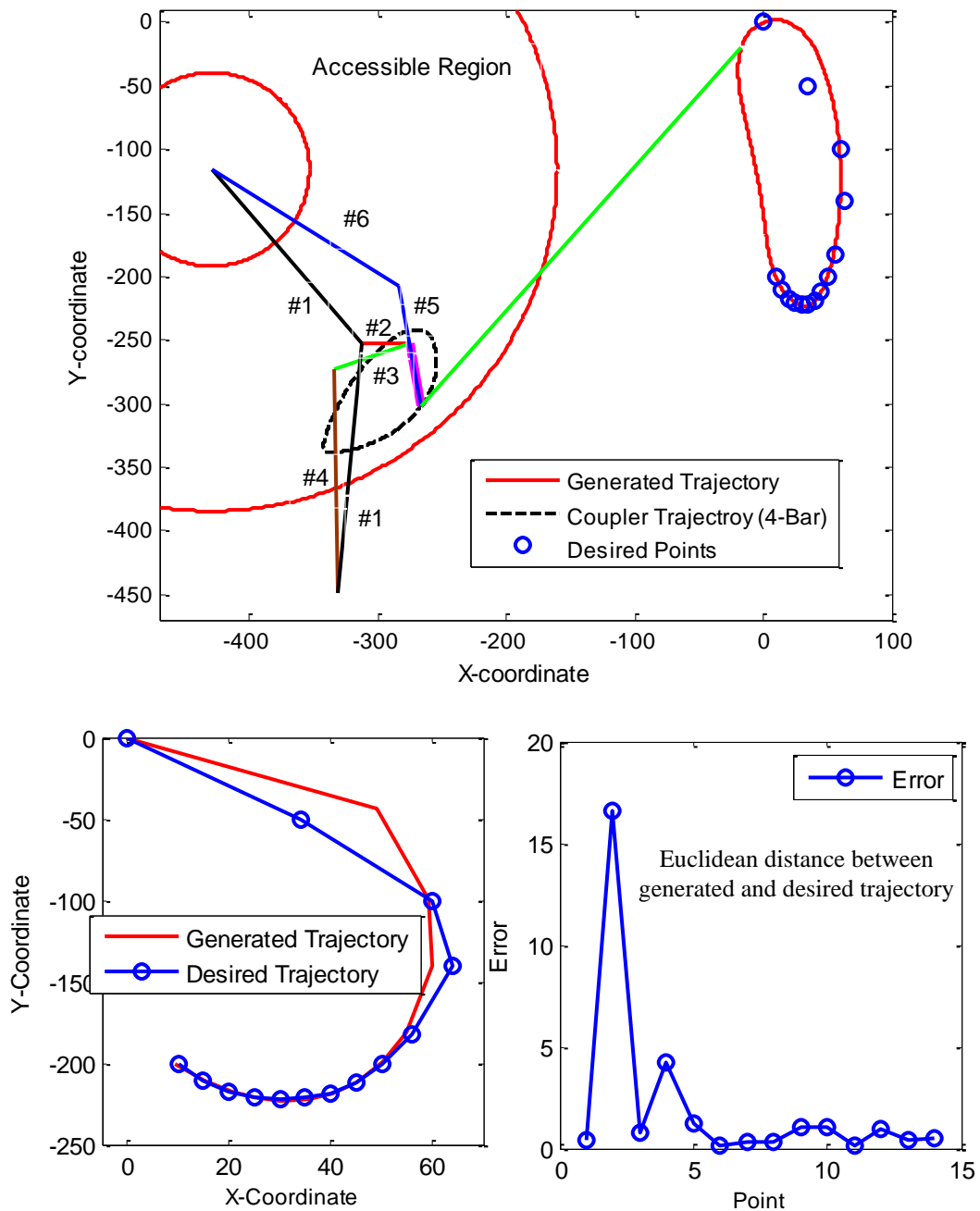


**Fig 5.33** Synthesized defect free Stephenson III linkage

lie on the same branch (since no dead configurations are found- one branch circuit); therefore, the linkage has no branch defect. Figure 5.34 also shows that designed linkage has no circuit defect as it can track all the design positions without disassembly. Lastly, it is observed from Table 5.8 and Fig 5.29 that the driver (crank #2) moves in a sequence and same is observed in Fig 5.36 which indicates linkage is free from order defect. Figure 5.35 depicts that  $\mu_1$  follows same sign while moving from the first to the last precision point, and same is observed for  $\mu_2$ . Figures 5.35 and 5.36 shows that constraints to avoid circuit defect and order defect are satisfied. The proposed method simplifies the constraint formulation and enables the designer to synthesize a defect-free Stephenson III six-bar mechanism for path generation. The method can be applied to synthesize a Stephenson III six-bar mechanism for any path.

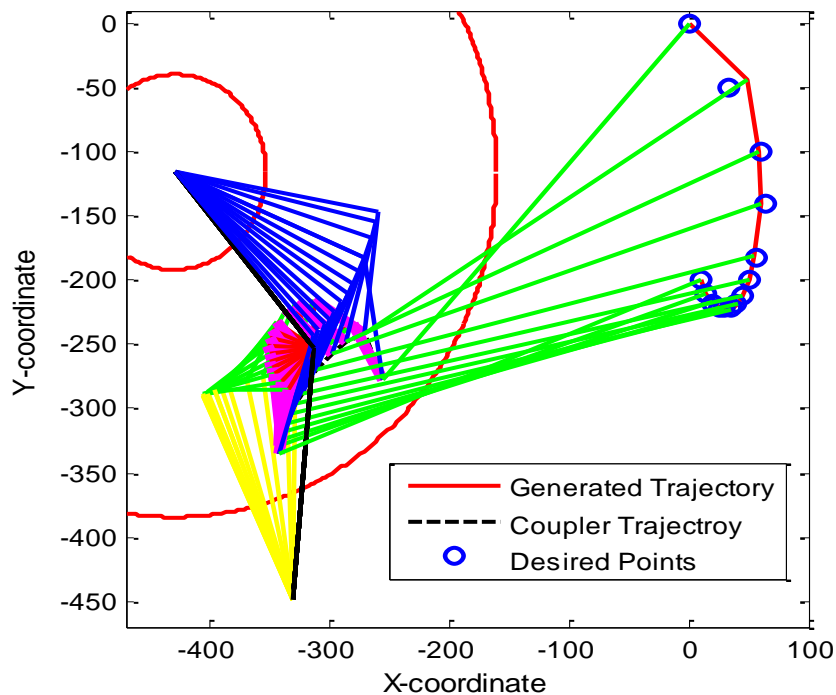


**Fig. 5.34** Stick diagram of Stephenson III mechanism for knee supporting device



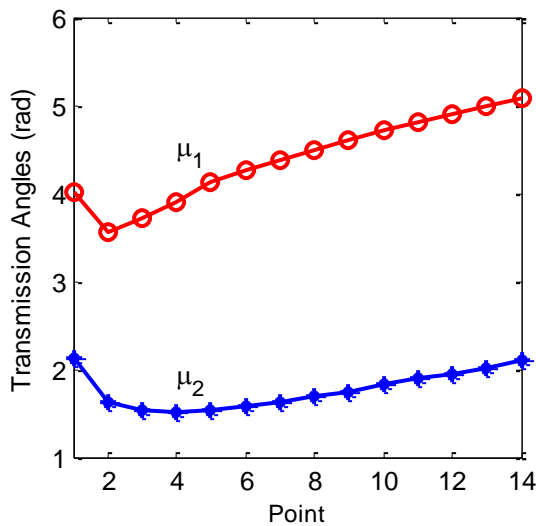


**Fig 5.35** Satisfaction of transmission angle constraint

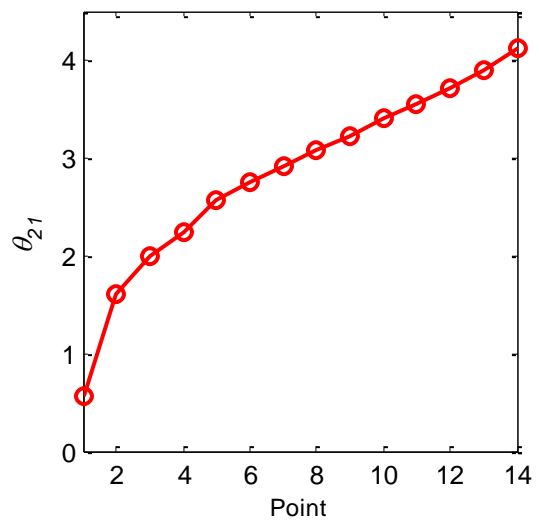


**Fig 5.36** Satisfaction of order constraint

## 5.5 Summary

In this chapter, path synthesis problem of planar linkages is formulated as an optimization problem. The main focus of this chapter is to synthesize the defect-free planar linkages for human knee supporting devices with reduced computational effort and simplified constraint formulation in case of multi-loop linkages. An algorithm based on TLBO philosophy is also refined to solve the highly non-linear constrained optimization problem. The refinement schemes, namely, Grashof- and order-refinement scheme are appended to the well-established TLBO algorithm. The refinement schemes are appended to TLBO for the first time in this study. Using the proposed algorithm, two planar defect-free four-bar linkages are synthesized that can track the prescribed points precisely. A four-bar that can generate the straight line and a new human knee exoskeleton/supporting device using three necessary and sufficient constraints in place of four constraints to synthesize defect-free crank-rocker mechanism is proposed. The design of crank-rocker linkage for human knee exoskeleton which is presented in example 2 is supported by a prototype and experimental validation. The validation is performed for one gait cycle which also confirms that the crank-rocker linkage designed by the defect-free optimal synthesis using proposed refined TLBO can be used for human knee exoskeleton. This also proves that the designed mechanism is not required to assemble and dismantle between the precision points. In addition, this method is preferred over precision point synthesis method, Sec. 3.2.1, because the deviation of the

generated trajectory is negligible as compared to the finite deviation in precision point synthesis method.

The chapter also proposed a new loop-by-loop defect-rectification procedure for the synthesis of Stephenson III six-bar path generator linkage. In the proposed method, the Stephenson III mechanism is divided into Loops; namely, Loop I (four-bar) and Loop II (five-bar) and constraints are formulated for Loop I and Loop II separately. To demonstrate the effectiveness of this method two numerical examples are considered for the synthesis of path generating Stephenson III six-bar linkages. The stick diagrams of Stephenson III linkages are also presented for both cases. Besides, the TLBO, GA, PSO are used as solvers for the path synthesis problem. The TLBO is found to be more efficient than other algorithms used here. It is found that the proposed mechanisms satisfy all the constraints used for defect-elimination.

### Gait-Inspired Linkage Synthesis

In this chapter, two new gait-inspired methodologies for the optimal kinematic synthesis of four-bar linkage are proposed. Typically, mechanisms for gait rehabilitation or assistive devices are synthesized by taking an ankle trajectory in shape of a ‘teardrop.’ This happens by transforming the coordinates of ankle joint relative to the hip joint because it is believed that the synthesis procedure requires the hip joint to be stationary (Tsuge et al., 2016). Various gait rehabilitation and assistive devices have been developed using this theory, for example, UCI gait mechanism (Tsuge and McCarthy, 2016), linkage gait rehabilitation system (Ji and Manna, 2008), linkage gait trainer (LGT) device (Kora et al., 2017), 10-bar linkage to guide gait (Tsuge and McCarthy, 2015) and lower extremity wearable device (Ghosh et al., 2015). In contrast, mechanisms are also synthesized using the flexion/extension trajectory of the human knee (Sancibrian et al., 2016). This concept has been used extensively in the design of prosthetic knee joints and bipeds. However, these conventional synthesis procedures require the solution of complex equations and use less number of precision points. Therefore, the generated trajectory may not be accurate. To address these issues, there is a need to develop a new procedure for the design of gait rehabilitation/ exoskeleton devices by considering  $N$  –precision points which can improve the path tracing ability of mechanism. Since the conventional synthesis procedures require the solution of complex equations and use less number of precision points, which results in inaccurate trajectory tracking. The two novel gait-based mechanism synthesis procedures for  $N$  –precision points are proposed, in this chapter, to design a mechanism which can be embedded in the orthotic and portable gait rehabilitation devices.

As opposed to the conventional linkage synthesis, in the first formulation, gait cycle is divided into two stages, namely, the swing stage and the stance stage, each of which is combined with the optimization techniques to synthesize four-bar linkage for lower limb exoskeleton. The dimensional synthesis is performed in the first stage which is followed by position synthesis of the linkage in the stance stage. This simplifies the problem formulation. Also, the gait trajectory which is considered is not relative to hip joint as used in the conventional procedures. The number of precision points is increased to 20 for one gait cycle which resulted in the accurate tracking of the gait. The stick diagram of the synthesized four-bar linkage is also presented first time to demonstrate the complete gait cycle. Besides, HTLPSO algorithm proposed in Chapter 4 is also used

for the first time to solve the synthesis problem. The synthesized mechanism presented here tracks the gait trajectory precisely and can be used for the portable leg exoskeleton or any rehabilitation device.

In another formulation, the expressions of trajectories are derived, and a two-stage optimization method is proposed to synthesize the four-bar linkage while considering the natural gait trajectories. The two-stage optimization method minimizes the error between generated and desired hip trajectories. The generated hip trajectories can accurately track the path, and the synthesis equations are simplified. In this two-stage method, the first stage deals in linkage synthesis and position synthesis by controlling angles is performed in the second stage.

### **Why Linkage Mechanism?**

It is a prerequisite to comprehending the biomechanics of the knee joint and its coordination with the hip and ankle joints for designing their mechanisms. The anatomy of knee joint varies with age whereas its complex function remains constant. The knee joint is also referred as a gliding hinge joint. It offers six-degrees of freedom range of motion which involves three rotational and three translational movements. Flexion-extension, internal-external, and varus-valgus movements come under rotation whereas anterior-posterior, medial-lateral, and compression-distraction movements come under translation (Hirschmann and Müller, 2015). The experimental trials of the rehabilitation devices such as LOKOMAT clarify the fact that ankle trajectory can be considered as planar in the sagittal plane (Ji and Manna, 2008; Riener et al., 2005). Rolling and gliding are the key motions of the knee joint in the sagittal plane. Also, they are considered as the basic mechanism of movement between femur and tibia as shown in Fig 6.1. This kinematic motion of the knee joint can be achieved through cross four-bar linkage where anterior cruciate (ACL) and posterior cruciate ligaments (PCL) can be considered as rigid links (Menschik, 1974; Sim, 1984). The four-bar linkage allows the combination of rotation and translation motion of the knee joint, in the sagittal plane (Hamon et al., 2014). Also, it has been used for the knee joint of bipedal robots (Hamon and Aoustin, 2009; Hamon and Aoustin, 2010; Aoustin and Hamon, 2013; Hamon et al., 2014) and prosthetic knee joints (Jin, 2003); therefore, to imitate the complex function of the knee joint for creating orthotic and rehabilitation devices, a four-bar mechanism can be used.

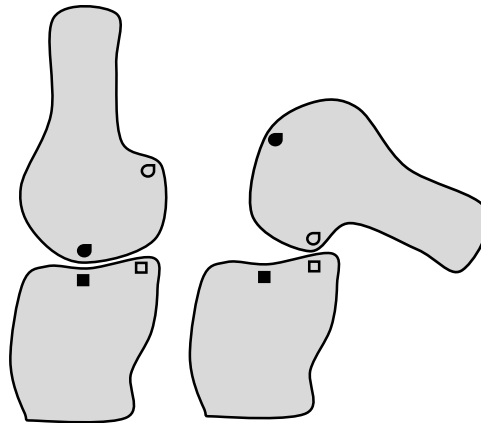


*Fig. 6.1 Contact points generated while rolling and gliding motion, when femur moves relative to tibia*

## **6.1 Gait-Inspired Linkage with Assumed Trajectories**

In this section, a method to synthesize planar four-bar linkage is presented based on the gait cycle. In this method, the foot and hip trajectories are derived using fundamental inverse kinematics (See Appendix D for illustration).

### **6.1.1 Modeling of Exoskeleton Leg**

A complete gait in sagittal plane involves three phases, namely, single support phase (SSP), impact phase (IP), and double support phase (DSP). The SSP is considered as swing phase which begins with the movement of one limb (swing) in the forward direction while another limb (stance) being pivoted to the ground. The SSP phase terminates when the tip of the swing limb strikes the ground (Mu and Wu, 2004). Thereafter, roles of swing and stance limbs are exchanged. For a complete gait cycle, the trajectory of swing limb and trajectory of the hip of the exoskeleton are derived. The hip trajectory is taken when the roles of swing and stance limbs are exchanged. Moreover, only SSP is considered in this chapter.

In this section, lower limb exoskeleton is modeled using four-bar linkage with two extended links and the linkage is restricted to move in the sagittal plane as shown in Fig 6.2. One link extends toward the hip while the other one extends toward the foot. The links are extended to obtain the trajectories of hip joint and foot during walking. The lengths of the extended links are bounded in such a way to maintain the position of the center of the four-bar linkage in synchronization with the healthy human knee joint. The boundary constraints for the extended links, used for thigh and shank, can be considered for a healthy person. These constraints are used for the synthesis of lower limb exoskeleton (LLE). Typically, synthesis procedures (Tsuge et al., 2016; Tsuge and

McCarthy, 2016) require a reference frame,  $\{XOY\}$ , on the LLE which is kept fixed on the walking surface as shown in Fig 6.3. The height of hip from the leveled surface,  $h$ , is assumed as a constant value for the whole gait cycle and the foot is assumed as a point.

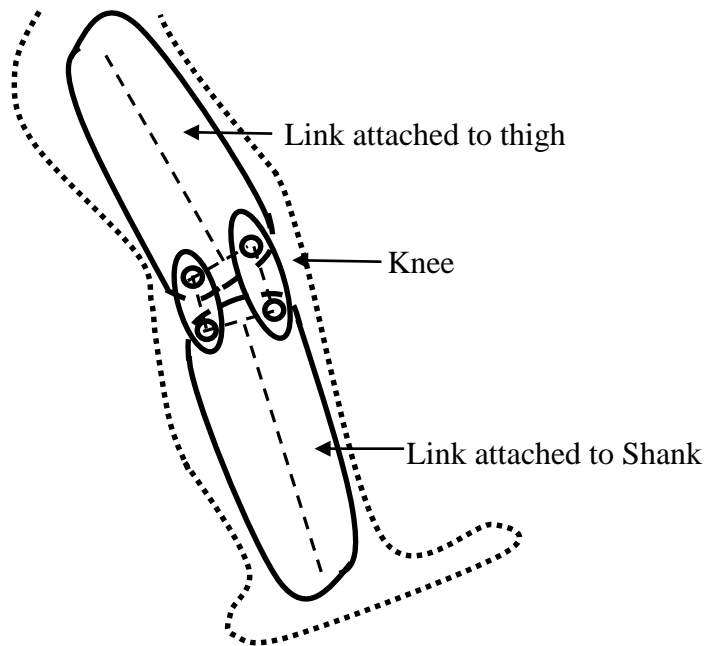


**Fig. 6.2** Lower limb exoskeleton model as four-bar linkage

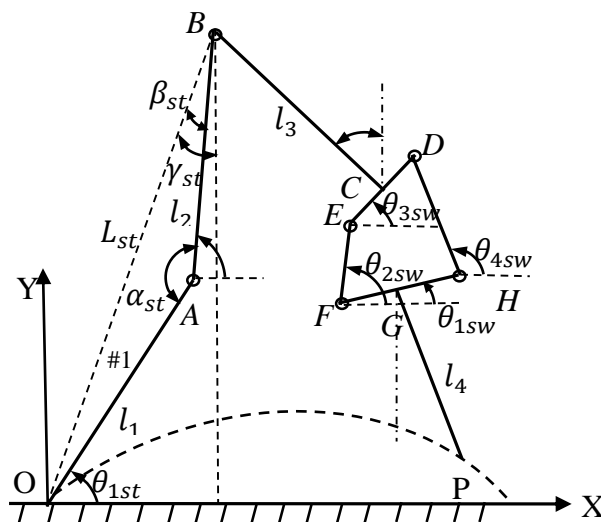


**Fig. 6.3** Various definitions of HLL and LLE, when LLE is in swing phase

Using the defined constraints and assumptions, foot and hip trajectories are derived for LLE. Since the trajectory of the lower limb with a revolute joint is apparent

to the trajectory of healthy lower limb (HLL) without-foot in the sagittal plane (Mu and Wu, 2004), hence, foot and hip trajectories of the lower limb with the revolute joint are derived. Henceforth, lower limb with the revolute joint will be referred as HLL. The foot and hip trajectories are also generated from the derived expression for LLE of the dysfunctional limb.

Various design parameters for the LLE and HLL are shown in Fig 6.3. It represents the swing phase of the LLE and stance phase of the HLL. The frame  $\{XOY\}$  represents a global reference frame. Hip is represented by point  $B$ . The exoskeleton is defined by links  $FE, ED, FH$ , and  $DH$ , wherein,  $CB$  and  $GP$  are extensions of links  $ED$  and  $FH$ , respectively. The Link lengths of  $FH, FE, ED$ , and  $DH$ , are  $r_1, r_2, r_3$ , and  $r_4$ , respectively, and  $\theta_{1sw}, \theta_{2sw}, \theta_{3sw}$ , and  $\theta_{4sw}$  are the orientation of the links  $FH, FE, ED$ , and  $DH$ , respectively, with respect to the X-axis. The subscript  $sw$  represents exoskeleton in swing phase. Lengths of the extended links  $CB$  and  $GP$  are taken as  $l_3$  and  $l_4$ , respectively, and are at  $90^\circ$  to  $r_1$  and  $r_3$ , respectively, at mid of their links. Note that lengths  $l_1$  and  $l_2$  defined by  $OA$  and  $AB$ , respectively, are articulated at point  $A$  through revolute joint, as shown in Fig 6.3. The links  $OA$  and  $AB$  of HLL oriented at an angle of  $\theta_{1st}$  and  $\theta_{2st}$ , respectively, with respect to the axis- X. The subscript  $st$  represents the limb in stance phase. The other parameters which are used for joint profile generation are,  $L_{st}$ , the distance between origin  $O$  and point  $B$ ,  $\gamma_{st}$ , the angle between Y-axis passing through  $B$  and a virtual link  $OB$ ,  $\beta_{st}$ , the angle between links  $AB$  and  $OB$ , and  $\theta_{2sty}$ , the angle between Y-axis passing through  $B$  and link  $AB$ .

Figure 6.4 represents stance phase of LLE and swing phase of HLL, and it also shows various design parameters used for joint profile generation. The reference frame used here is same as used for stance phase of HLL. The point  $O'$  represents the foot-point of HLL. The links  $O'A_e$  and  $A_eB_e$  of HLL are now in swing phase and oriented at an angle of  $\theta_{1swe}$  and  $\theta_{2swe}$ , respectively, with respect to axis -X. The other parameters which are used for joint profile generation are:  $L_{swe}$ , distance between  $O'$  and point  $B_e$ ,  $\gamma_{swe}$ , angle between Y-axis passing through  $B_e$  and a virtual link  $O'B_e$ ,  $\beta_{swe}$ , angle between links  $A_eB_e$  and  $O'B_e$ , and  $\theta_{2swey}$ , angle between Y-axis passing through  $B_e$  and link  $A_eB_e$ . Note that Subscript  $e$  represent exchanged roles whereas  $swe$  represents HLL in swing phase.

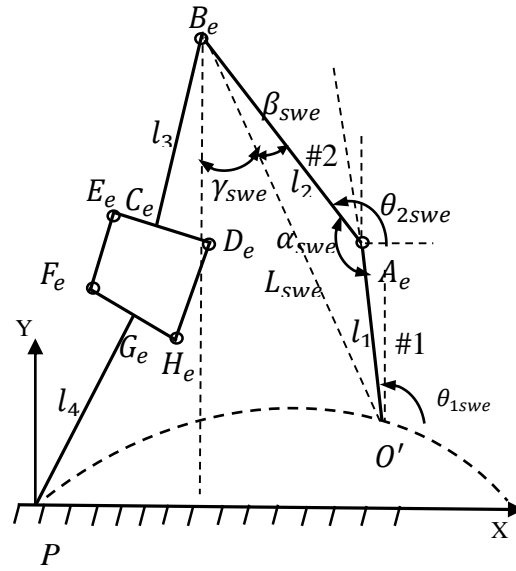


**Fig. 6.4** Various definition of LLE and HLL, when HLL is in swing phase

The joint profile generation of the LLE and HLL is done for one complete gait cycle, since, a gait cycle begins with the reference foot contact to the ground and terminates when the same foot makes contact with the ground again (Perry and Davids, 1992). This covers both the stance and swing phases of the same foot. Hence, trajectory generation of both the exoskeleton leg and the healthy lower limb is performed for stance and swing phases of a gait cycle.

### 6.1.2 Trajectory for LLE in Swing Phase

The lower limb exoskeleton is considered as four-bar linkage. Hence, loop closure equation is required to be solved for finding angles  $\theta_{3sw}$  and  $\theta_{4sw}$ , as in (Norton, 2011), Appendix A can also be used as reference. The coordinates of the hip,  $B_x$  and  $B_y$ , are given as input. Thus coordinates of  $C, E, F,$  and  $G$  derived in the global reference frame XOY using hip coordinates which can be expressed as:

$$C_x = B_x + l_3 \cos\left(\frac{3\pi}{2} + \theta_{3sw}\right) \quad (6.1)$$

$$C_y = B_y + l_3 \sin\left(\frac{3\pi}{2} + \theta_{3sw}\right) \quad (6.2)$$

$$E_x = C_x + \frac{r_3}{2} \cos(\pi + \theta_{3sw}) \quad (6.3)$$

$$E_y = C_y + \frac{r_3}{2} \sin(\pi + \theta_{3sw}) \quad (6.4)$$

$$F_x = E_x + r_2 \cos(\pi + \theta_{2sw}) \quad (6.5)$$

$$F_y = E_y + r_2 \sin(\pi + \theta_{2sw}) \quad (6.6)$$

$$G_x = F_x + \frac{r_1}{2} \cos(\theta_{1sw}) \quad (6.7)$$



$$G_y = F_y + \frac{r_1}{2} \sin(\theta_{1sw}) \quad (6.8)$$

Using Eqs. (6.1)-(6.8), the trajectory of the foot point  $P$  of the LLE is obtained as follows:

$$P_x = G_x + l_4 \cos\left(\frac{3\pi}{2} + \theta_{1sw}\right) \quad (6.9)$$

$$P_y = G_y + l_4 \sin\left(\frac{3\pi}{2} + \theta_{1sw}\right) \quad (6.10)$$

### 6.1.3 Trajectory for HLL in Stance Phase

The trajectories of HLL in stance phase are derived using the input hip trajectory and are expressed as (See Appendix D for detail):

$$L_{st} = \sqrt{(B_x^2) + (B_y^2)} \quad (6.11)$$

$$\gamma_{st} = \tan^{-1}\left(\frac{B_x}{B_y}\right) \quad (6.12)$$

$$\beta_{st} = \cos^{-1}\left(\frac{L_{st}^2 + l_2^2 - l_1^2}{2l_2 L_{st}}\right) \quad (6.13)$$

$$\alpha_{st} = \cos^{-1}\left(\frac{-L_{st}^2 + l_2^2 + l_1^2}{2l_2 l_1}\right) \quad (6.14)$$

$$\theta_{2sty} = \gamma_{st} - \beta_{st} \quad (6.15)$$

$$\theta_{2st} = \frac{\pi}{2} - \theta_{2sty} \quad (6.16)$$

$$\theta_{1st} = \theta_{2st} - (\pi - \alpha_{st}) \quad (6.17)$$

The role of LLE is exchanged with the role of HLL after the completion of, swing phase of LLE, and stance phase of HLL.

### 6.1.4 Trajectory for HLL in Swing Phase

The HLL moves to swing phase after completion of its stance phase and its trajectories are derived using the input hip trajectory as follows (See Appendix D for detail):

$$B_{ex} = P_x - B_x \quad (6.18)$$

$$B_{ey} = P_y - B_y \quad (6.19)$$

$$L_{swe} = \sqrt{(B_{ex}^2) + (B_{ey}^2)} \quad (6.20)$$

$$\gamma_{swe} = \tan^{-1}\left(\frac{B_{ex}}{B_{ey}}\right) \quad (6.21)$$

$$\beta_{swe} = \cos^{-1}\left(\frac{L_{swe}^2 + l_2^2 - l_1^2}{2l_2 L_{swe}}\right) \quad (6.22)$$

$$\alpha_{swe} = \cos^{-1}\left(\frac{-L_{swe}^2 + l_2^2 + l_1^2}{2l_2 l_1}\right) \quad (6.23)$$

$$\theta_{2swey} = \gamma_{swe} + \beta_{swe} \quad (6.24)$$

$$\theta_{2swe} = \frac{\pi}{2} + \theta_{2swey} \quad (6.25)$$

$$\theta_{1swe} = \theta_{2swey} - (\pi - \alpha_{swe}) \quad (6.26)$$

### 6.1.5 Trajectory for LLE in Stance Phase

Here, the new position of  $P_x, P_y$  will become the initial position for the stance phase and that will remain constant for the whole phase. The new coordinates of the foot,  $P_x$  and  $P_y$ , are considered as input. The termination of this phase also completes the gait cycle and the trajectories of the LLE in the stance phase are derived as:

$$G_{ex} = P_x + l_4 \cos\left(\frac{\pi}{2} + \theta_{1ste}\right) \quad (6.27)$$

$$G_{ey} = P_y + l_4 \sin\left(\frac{\pi}{2} + \theta_{1ste}\right) \quad (6.28)$$

$$F_{ex} = G_{ex} + \frac{r_1}{2} \cos(\pi + \theta_{1ste}) \quad (6.29)$$

$$F_{ey} = G_{ey} + \frac{r_1}{2} \sin(\pi + \theta_{1ste}) \quad (6.30)$$

$$E_{ex} = F_{ex} + r_2 \cos(\theta_{2ste}) \quad (6.31)$$

$$E_{ey} = F_{ey} + r_2 \sin(\theta_{2ste}) \quad (6.32)$$

$$C_{ex} = E_{ex} + \frac{r_3}{2} \cos(\theta_{3ste}) \quad (6.33)$$

$$C_{ey} = E_{ey} + \frac{r_3}{2} \sin(\theta_{3ste}) \quad (6.34)$$

$$B_{ex} = C_{ex} + l_3 \cos\left(\theta_{3ste} + \frac{\pi}{2}\right) \quad (6.35)$$

$$B_{ey} = C_{ey} + l_3 \sin\left(\frac{\pi}{2} + \theta_{3ste}\right) \quad (6.36)$$

It is found that normal walking step length of a healthy person varies between 51.1 cm and 93.3 cm, with the mean of 73.6 cm (Jasuja et al., 1997). Hence, a step length of 72 cm is considered. The trajectories of foot and hip can be derived by using polynomial interpolation (Perry, 1992; Mu, 2004). These trajectories may be used for gait synthesis of a person with the dysfunctional lower limb (Mu and Wu, 2004). Now it is a question of how to determine design parameters  $r_1, r_2, r_3, r_4, l_3$ , and  $l_4$  to obtain these desired trajectories for whole gait cycle, for  $N$ -position synthesis. Also, we have to find two sets of independent orientation angles  $\theta_{1m}$  and  $\theta_{2m}$  in which subscript  $m$  becomes  $sw$  for swing phase of the exoskeleton and  $ste$  for the stance phase of the exoskeleton after exchanged roles. In order to find the optimal values of these parameters, a two-stage optimization formulation is proposed in the next section.

### 6.1.6 Optimization Problem Formulation

This section proposes a novel two-stage optimization problem formulation for finding link lengths of a four-bar exoskeleton to walk on the leveled ground. The two stages correspond to the swing and stance phases of an exoskeleton.

### 6.1.6.1 First Stage- When Swing Limb Trajectory of LLE is Considered

The human knee is expected to perform the simple kinematic function of flexion/extension. Hence, the position synthesis of the lower limb is performed in the sagittal plane for leveled walking. For each position of the exoskeleton the unknown parameters  $\theta_{1m}, \theta_{2m}, l_3, l_4, r_1, r_2, r_3,$  and  $r_4$  are taken as design variables. Note that angles  $\theta_{3m}$  and  $\theta_{4m}$  are determined from the loop closure equation of the four-bar linkage. For  $N$  –position synthesis, there will be  $2N$  angle variables,  $\theta_{1m}$  and  $\theta_{2m}$ , and 6 links' dimensions,  $l_3, l_4, r_1, r_2, r_3,$  and  $r_4$ . The  $2N + 6$  design variables constitute a design vector for the optimization problem defined as follows:

$$\mathbf{x} = [\theta_{1m}^1, \dots, \theta_{1m}^N, l_3, l_4, \theta_{2m}^1, \dots, \theta_{2m}^N, r_1, r_2, r_3, r_4]^T \quad (6.37)$$

in which, subscript  $m$  becomes  $sw$  for the swing phase of the exoskeleton while after the exchange of roles between lower limbs, subscript  $m$  becomes  $ste$  for the stance phase of LLE. Note that the  $2N$  positions of the linkage are determined by angles  $\theta_{1m}^1, \dots, \theta_{1m}^N,$  and  $\theta_{2m}^1, \dots, \theta_{2m}^N.$

To synthesize the four-bar linkage, an optimization problem is formulated to minimize the tracking error. Here, the tracking error is the distance between the desired foot trajectory and the path traced by the foot (point  $P$ ) of the LLE shown in Fig 6.3. Then, the objective function of the problem is expressed as follows:

$$f(\mathbf{x}) = \sum_{k=1}^n \sqrt{(P_x^k - P_{xd}^k)^2 + (P_y^k - P_{yd}^k)^2} \quad (6.38)$$

in which,  $P_{xd}, P_{yd}$  are the desired x- and y- coordinates of the foot point and  $P_x, P_y$  are the x- and y- coordinates of points on the path traced by the foot of the exoskeleton. The superscript  $k$  represents the  $k^{th}$  position of the exoskeleton foot, and  $n$  is the number of points of the desired foot/hip trajectory

The four-bar linkage is expected to achieve this objective, such that smallest link ( $EF$ ) can rotate completely, either highest to lowest or vice-versa, and values of design variables should lie within the prescribed range. The following constraints are imposed to get feasible four-bar linkage.

a) Grashof constraint:

$$g_1(\mathbf{x}) = r_1 + r_2 - r_3 - r_4 < 0 \quad (6.39)$$

b) Constant height for gait cycle:

$$g_2(\mathbf{x}) = l_3 + l_4 - h < 0 \quad (6.40)$$

c) Range of variables:

$$L_i \leq x_i \leq U_i$$

in which,  $L_i$  and  $U_i$  are the lower and upper limits for the  $i^{th}$  design variable. Thus using, Eqs. (6.38)-(6.40), the problem is completely stated as:

$$\begin{aligned} \text{minimize} \quad & f(\mathbf{x}) = \sum_{k=1}^n \sqrt{(P_x^k - P_{xd}^k)^2 + (P_y^k - P_{yd}^k)^2} \\ \text{subject to:} \quad & g_1(\mathbf{x}) = r_1 + r_2 - r_3 - r_4 < 0 \quad \text{if } (r_2 < r_3 < r_4 < r_1) \\ & g_2(\mathbf{x}) = l_3 + l_4 - h < 0 \\ & L_i \leq x_i \leq U_i \end{aligned} \quad (41)$$

where  $h$  indicates the constant height of lower limb while walking for one gait cycle. Here,  $h$  is assumed constant but varying  $h$  may be chosen by the linkage designer as per the problem requirements.

### 6.1.6.2 Second Stage- When Roles of Swing- and Stance-Limbs are Exchanged

Once, optimized design of the four-bar linkage is obtained in the first stage, another optimization problem is required to find positions of linkage for stance phase of LLE to complete the gait cycle. Since the links' lengths  $r_1, r_2, r_3, r_4, l_3$ , and  $l_4$  of the linkage are already obtained in the first stage, only new positions are required by the four-bar linkage for tracking the hip trajectory. The position of LLE for the dysfunctional lower limb is obtained by angles  $\theta_{1m}$  and  $\theta_{2m}$ . For the  $N$  –positions, there will be  $2N$  design variables as follows:

$$\mathbf{x} = [\theta_{1m}^1, \dots, \theta_{1m}^N, \theta_{2m}^1, \dots, \theta_{2m}^N]^T \quad (6.42)$$

The positions of the four-bar linkage should be such that they minimize the tracking error. Here, the tracking error is the distance between the desired hip trajectory and the path traced by the hip (point  $B_e$ ) of the designed LLE. It is expressed as follows:

$$f(\mathbf{x}) = \sum_{k=1}^N \sqrt{(B_{ex}^k - B_{exd}^k)^2 + (B_{ey}^k - B_{eyd}^k)^2} \quad (6.43)$$

in which,  $B_{exd}, B_{eyd}$  are the desired x- and y- coordinates of points of the hip after exchanged roles and  $B_{ex}, B_{ey}$  are the x- and y- coordinates of the path traced by the hip of the synthesized LLE. The flowchart shown in Fig 6.5 demonstrates the proposed algorithm for the whole synthesis procedure.

Note: This is an unconstrained optimization problem because positions for the subsequent phase are synthesized for the designed LLE. A new hybrid teaching-learning

particle swarm optimization (HTLPSO) algorithm is presented as a solver for this optimization problem. Chapter 3 presents the detail on HTLPSO algorithm and its MATLAB® code is presented in Appendix C.

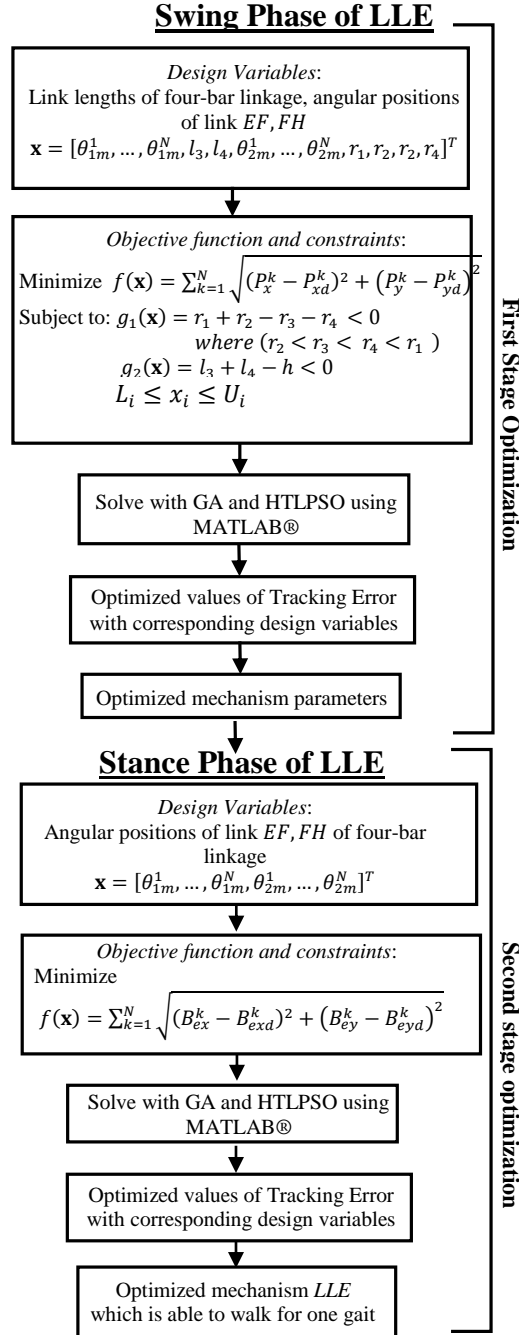


*Fig. 6.5 Two-stage optimization formulation for position synthesis of exoskeleton lower limb*

## 6.2 Gait-Inspired Linkage with Natural Trajectories

In this section, a novel method is proposed to determine the link lengths of a four-bar exoskeleton while using the natural hip and ankle trajectories. The two stages correspond to the linkage design and position synthesis by controlling angles:

### 6.2.1 Kinematic Modeling of Four-Link Exoskeleton

In this section, lower limb exoskeleton is modeled as a four-bar linkage, shown in Fig 6.6 (a), in which, links #1 and #3 are fixed to the shank and the thigh, respectively. Other links #2 and #4 connect links #1 and #3 to form the closed loop  $CDFE$  of the linkage. This exoskeleton four-bar linkage defined by four links #1, #2, #3, and #4 are denoted by  $CD$ ,  $CE$ ,  $EF$ , and  $DF$ , respectively. Note that  $GP$  and  $BA$  are extensions of links  $EF$  and  $CD$  along thigh and shank, respectively. Also, note that points  $P$  and  $A$  represent hip and ankle joints, respectively. The links' lengths and their orientation with respect to the  $X$ -axis are denoted by  $r_1$ ,  $r_2$ ,  $r_3$ , and  $r_4$ , and  $(270^\circ + \theta_1)$ ,  $\theta_2$ ,  $\theta_3$ , and  $\theta_4$ , respectively, as shown in Fig 6.6 (b). Lengths of the extended links  $AB$  and  $GP$  are taken as  $l_1$  and  $l_2$ , respectively, which are oriented  $90^\circ$  to  $CD$  and  $EF$ , respectively, at the center of their links. The ankle and hip trajectories are taken from real *Gait database* (Prakash et al., 2015). The ankle trajectory is used as input to synthesize the linkage

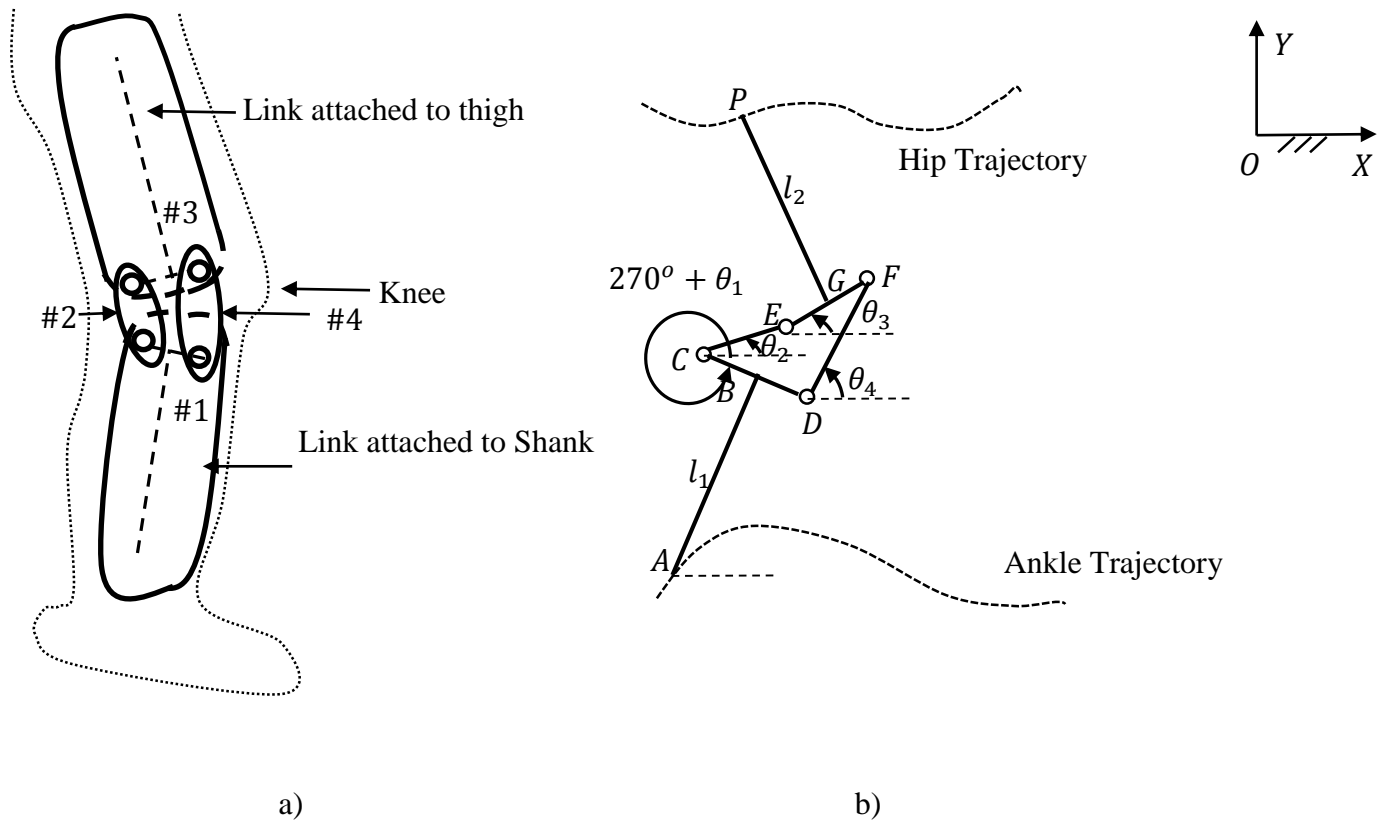


**Fig. 6.6 a) Four-link exoskeleton for lower limb b) Various definitions for four-link exoskeleton**

$\theta_4$ , respectively, as shown in Fig 6.6 (b). Lengths of the extended links  $AB$  and  $GP$  are taken as  $l_1$  and  $l_2$ , respectively, which are oriented  $90^\circ$  to  $CD$  and  $EF$ , respectively, at the center of their links. The ankle and hip trajectories are taken from real *Gait database* (Prakash et al., 2015). The ankle trajectory is used as input to synthesize the linkage

which tracks the given hip trajectory. Here, the linkage is assumed to move in the sagittal plane, as shown in Fig 6.6.

The linkage  $CDFE$  forms a closed loop where  $\theta_1$  and  $\theta_2$  are the unknown angles for one gait cycle. Whereas, the orientations  $\theta_3$  and  $\theta_4$  of links  $EF$  and  $FD$ , respectively can be determined by the loop-closure equation of linkage. Therefore, to obtain the configuration of the four-bar linkage, the loop-closure equation is required to be solved. The details for solving the loop-closure equation are provided in Appendix A. Here, the coordinates of ankle  $A$  ( $A_{xd}, A_{yd}$ ) are taken as input and the coordinates  $C, E, G$ , and  $P$  are derived in global frame  $\{XOY\}$  which can be expressed as:

$$B_x = A_{xd} + l_1 \cos(\theta_1) \quad (6.44)$$

$$B_y = A_{yd} + l_1 \sin(\theta_1) \quad (6.45)$$

$$C_x = B_x + \frac{r_1}{2} \cos\left(\frac{\pi}{2} + \theta_1\right) \quad (6.46)$$

$$C_y = B_y + \frac{r_1}{2} \sin\left(\frac{\pi}{2} + \theta_1\right) \quad (6.47)$$

$$E_x = C_x + r_2 \cos(\theta_2) \quad (6.48)$$

$$E_y = C_y + r_2 \sin(\theta_2) \quad (6.49)$$

$$G_x = E_x + \frac{r_3}{2} \cos(\theta_3) \quad (6.50)$$

$$G_y = E_y + \frac{r_3}{2} \sin(\theta_3) \quad (6.51)$$

The trajectory of the point  $P$  is obtained using Eqs. (6.44)-(6.51), which is expressed as follows:

$$P_x = G_x + l_2 \cos\left(\frac{\pi}{2} + \theta_3\right) \quad (6.52)$$

$$P_y = G_y + l_2 \sin\left(\frac{\pi}{2} + \theta_3\right) \quad (6.53)$$

These trajectories can be used for the dimensional synthesis of the four-bar linkage for the lower limb exoskeleton. The design parameters  $r_1, r_2, r_3, r_4, l_1$ , and  $l_2$  and orientation of extended link  $AB$  and the link  $CE$  with respect to X-axis are unknowns. These parameters can be determined using a two-stage optimization formulation proposed in the next section.

### 6.2.2 Two-Stage Optimization Problem Formulation

This section proposes a novel two-stage optimization problem formulation to find the optimal value of design parameters of four-bar linkage as discussed in kinematic modeling section 6.2.1. Here, four-bar linkage synthesis is formulated as an optimization problem. The four-bar linkage synthesis can be performed by considering a single stage of optimization procedure for  $2N$  precision points with  $4N + 6$  design variables,  $r_1, r_2, r_3, r_4, l_1, l_2, \theta_1^k$  and  $\theta_2^k$  where  $k = 1, \dots, N$  positions. A large number of design variables increase the complexity of the optimization problem to get satisfactory results. Therefore, to reduce the complexity of the optimization and to simplify the linkage synthesis procedure, the linkage synthesis problem is divided into two stages. For  $2N$  precision points synthesis, in the first stage, linkage synthesis is performed by considering  $N$  –precision points with  $2N + 6$  design variables,  $r_1, r_2, r_3, r_4, l_1, l_2, \theta_1^k$  and  $\theta_2^k$  where  $k = 1, \dots, N$  positions. In this stage, link's lengths,  $r_1, r_2, r_3, r_4, l_1, l_2$ , and input angles  $\theta_1^k$  and  $\theta_2^k$  where  $k = 1, \dots, N$  precision points are determined. The next  $N$  –precision points will be obtained by controlling only  $\theta_1^k$  and  $\theta_2^k$  where  $k = N + 1, \dots, 2N$ . These controlling angles are determined in the second stage of optimization. Hence, these two stages reduce the complexity of the linkage synthesis procedure and provide satisfactory results. A complete scheme of the two-stage optimization algorithm is shown in Fig 6.7. The objective functions and design variables involved in both the stages are as follows:

#### *First stage (Linkage Synthesis)*

The first stage is the linkage synthesis stage where the first  $N$  precision points are considered. The goal of the first objective function is to track these  $N$  precision points where each point involves a set of unknown parameters  $\theta_1^k, \theta_2^k, l_1, l_2, r_1, r_2, r_3$ , and  $r_4$ . These independent parameters are considered as design variables in which  $k = 1, \dots, N$ . Note that the angles  $\theta_3^k$  and  $\theta_4^k$  corresponding to each position of  $\theta_1^k$  and  $\theta_2^k$  are determined by the loop-closure equation of the four-bar linkage (Appendix A). For  $N$  –precision points' synthesis, a total of  $2N + 6$  variables is required where  $\theta_1^k$  and  $\theta_2^k$  constitutes  $2N$  variables and links' dimensions constitute six variables.

#### *Design variables (first stage)*

The design vector in the first stage of the optimization problem can be expressed as:

$$\mathbf{x}_1 = [\theta_1^1, \dots, \theta_1^N, \theta_2^1, \dots, \theta_2^N, l_1, l_2, r_1, r_2, r_3, r_4]^T \quad (6.54)$$



Objective function (first stage) and constraint

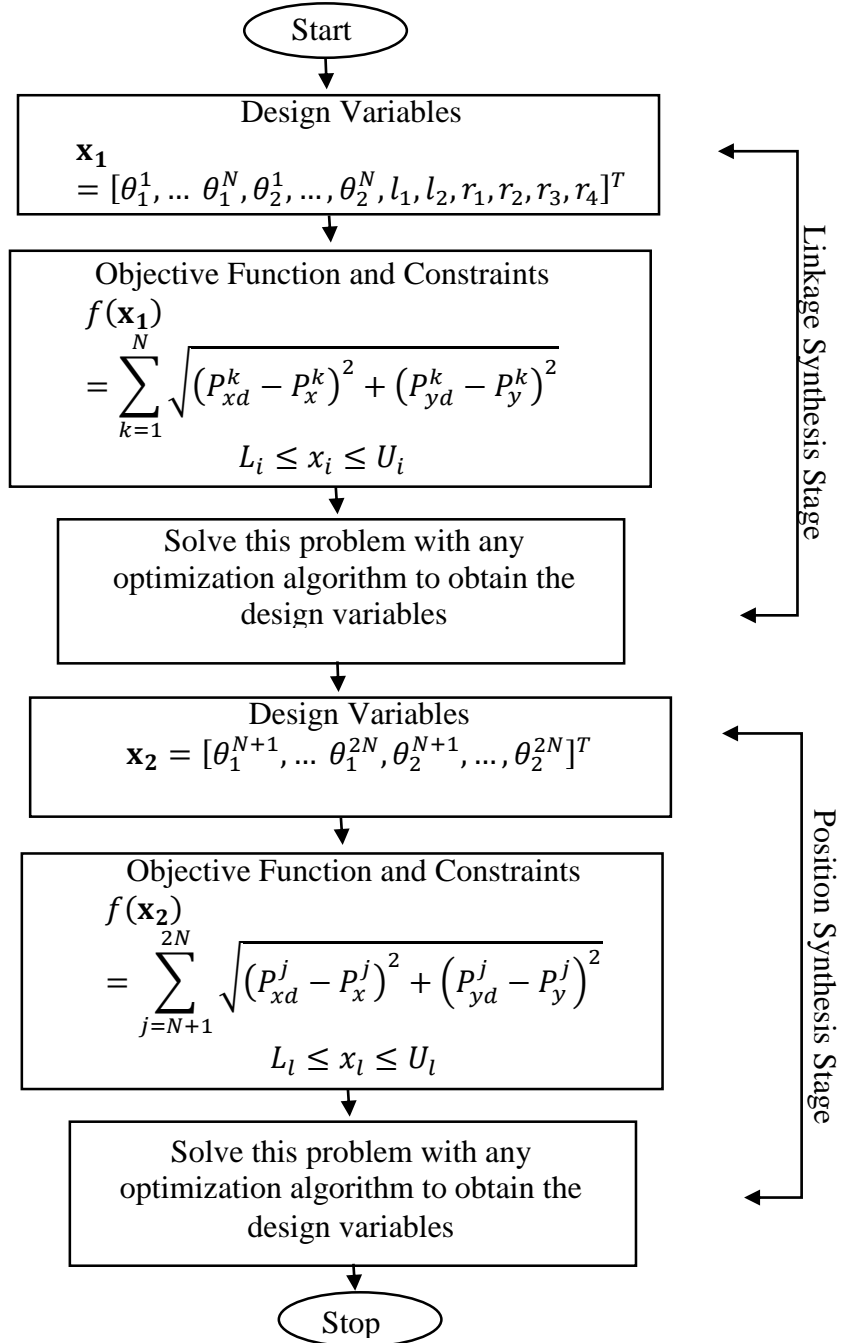


Fig. 6.7 Scheme of two-stage optimization problem

In this stage, the error between generated and desired hip trajectories (point  $P$ ) is considered as the objective function for the input foot trajectory (point  $A$ ). The hip trajectory (generalized) traced by the point  $P$  is shown in Fig 6.6 (b). The error minimization objective between the desired and generated trajectories can be expressed as:

$$f(\mathbf{x}_1) = \sum_{k=1}^N \sqrt{(P_{xd}^k - P_x^k)^2 + (P_{yd}^k - P_y^k)^2} \quad (6.55)$$

The bound constraints are applied to the design variables to get a feasible solution

$$L_i \leq x_i \leq U_i$$

Finally, the optimization problem can be stated as:

$$\begin{aligned} \text{minimize:} \quad & f(\mathbf{x}_1) = \sum_{k=1}^N \sqrt{(P_{xd}^k - P_x^k)^2 + (P_{yd}^k - P_y^k)^2} \quad (6.56) \\ \text{subject to} \quad & L_i \leq x_i \leq U_i \quad i = 1, \dots, n_1 \end{aligned}$$

in which,  $L_i$  and  $U_i$  are the lower and the upper bounds on the  $i^{th}$  design variable,  $n_1$  is the total number of design variables in the first stage,  $k$  is the  $k^{th}$  position achieved by link #3 in the first stage.

The first stage is completed after the determination of the linkage design which can track the hip trajectory with minimum error. Then, the position synthesis for the remaining cycle is performed in the second stage.

#### *Second Stage (Position Synthesis)*

Linkage dimensions are not considered as design variables in the second stage as these are determined in the first stage. If the linkage dimensions are kept as design variables for the second stage, then optimization would result in a new linkage design. Therefore, in this stage, only positions are synthesized by controlling angles  $\theta_1^k$  and  $\theta_2^k$ .

#### *Design variables (second stage)*

The  $2N$  variables  $\theta_1^k, \theta_2^k$  where  $k = N + 1, \dots, 2N$  are considered as design variables and can be expressed as:

$$\mathbf{x}_2 = [\theta_1^{N+1}, \dots, \theta_1^{2N}, \theta_2^{N+1}, \dots, \theta_2^{2N}]^T \quad (6.57)$$

#### *Objective function (second stage) and constraints*

The objective is to synthesize the linkage positions that can track all the precision points with minimum error. Therefore, an error minimization problem is formulated for tracking the desired hip trajectory while using the linkage design obtained in the first stage. Thus, the minimization error function can be expressed as:

$$f(\mathbf{x}_2) = \sum_{j=N+1}^{2N} \sqrt{(P_{xd}^j - P_x^j)^2 + (P_{yd}^j - P_y^j)^2} \quad (6.58)$$

The bound constraints are applied to the design variables to generate the desired hip trajectory with least error.  $L_l \leq x_l \leq U_l$

Finally, the optimization problem can be posed as:

$$\begin{aligned} \text{minimize:} \quad & f(\mathbf{x}_2) = \sum_{j=N+1}^{2N} \sqrt{(P_{xd}^j - P_x^j)^2 + (P_{yd}^j - P_y^j)^2} \quad (6.59) \\ \text{subject to} \quad & L_l \leq x_l \leq U_l \quad l = 1, \dots, n_2 \end{aligned}$$

in which,  $L_l$  and  $U_l$  are the lower and the upper bounds on the  $l^{th}$  design variable,  $n_2$  is the total number of design variables in the second stage,  $j$  is the  $j^{th}$  position achieved by link #3 in the second stage.

### 6.3 Numerical Examples

In this section, two numerical examples are presented that correspond to the two gait-based linkage synthesis procedures proposed in the above sections.

#### 6.3.1 Four-Bar Linkage with Assumed Trajectories

This section presents the effectiveness of the proposed two-stage optimization algorithm by applying it to the realistic non-trivial four-bar linkage synthesis problem defined in Section 6.1. The lower limb measurements for a healthy person change with various factors, namely, sex, age, race, etc. Leg length lies in the range [0.334, 0.424] meters whereas thigh length lies in the range [0.354, 0.450] (Nor et al., 2013). Here, the average leg length (LL) and thigh length (TL) are considered as 0.342m and 0.364m, respectively, for the healthy person, whereas height,  $h$ , of the hip above the ground is constrained to 0.575m while walking on the leveled ground. The desired foot and hip trajectories are shown in Table 6.1. The  $2N + 6$  unknown design variables for the first stage of optimization, Eq. (6.37), and  $2N$  unknown design variables for the second stage of optimization, Eq. (6.42), are optimized. The HTLPSO as presented in Appendix C and an established genetic algorithm (GA) technique is used to solve the problem.

**Table 6.1** Desired foot and hip trajectories (Mu and Wu, 2003; Appendix D for illustration)

Position	1	2	3	4	5	6	7	8	9	10
Coordinates										
$P_{xd}$ (mm)	-360	-335.31	-269.14	-173.34	-59.76	59.74	173.31	269.10	335.2	359.9
$P_{yd}$ (mm)	0	7.803	23.899	39.506	48.77	48.77	39.506	23.899	7.803	0
$B_{exd}$ (mm)	-180	-149.22	-111.52	-68.88	-23.29	23.29	68.88	111.52	149.2	180
$B_{eyd}$ (mm)	575	575	575	575	575	575	575	575	575	575

The following ranges of design variables are set to get the practical solution:

First stage:

$$\begin{aligned} \theta_{1m}^k \in [0, 2\pi], \theta_{2m}^k \in [0, 2\pi], \quad r_1 \in [20, 90], r_2 \in [40, 170], \\ r_3 \in [20, 90], r_4 \in [40, 170], l_3 \in [180, 320], l_4 \in [180, 320] \end{aligned}$$

Second stage:

$$\theta_{1m}^k \in [0, 2\pi], \theta_{2m}^k \in [0, 2\pi]$$

in which, length is mm and angle in radians.

Note: the bounds are as per the anthropometric dimensions of human lower limb

**Table 6.2** Optimized values of design variables of the first stage of optimization

Design Variables	GA	HTLPSO
$r_1$	81.5030	89.5306
$r_2$	45.9870	42.3332
$r_3$	73.5303	73.0147
$r_4$	79.0462	82.8552
$l'_3$	289.097	282.7395
$l'_4$	263.444	284.5872
$\theta_{1sw}^1$	1.2897	1.9538
$\theta_{1sw}^2$	1.7283	2.0972
$\theta_{1sw}^3$	0.3146	0.2024
$\theta_{1sw}^4$	2.8263	3.0222
$\theta_{1sw}^5$	0.0463	3.3189
$\theta_{1sw}^6$	3.2617	3.4576
$\theta_{1sw}^7$	0.5426	3.4102
$\theta_{1sw}^8$	2.9095	3.1559
$\theta_{1sw}^9$	1.5226	2.7332
$\theta_{1sw}^{10}$	1.9654	2.5738
$\theta_{2sw}^1$	5.7489	5.6789
$\theta_{2sw}^2$	5.6952	5.6446
$\theta_{2sw}^3$	5.7331	5.6644
$\theta_{2sw}^4$	5.6005	5.5758
$\theta_{2sw}^5$	5.7996	5.6386
$\theta_{2sw}^6$	5.7903	5.7770
$\theta_{2sw}^7$	6.0985	5.9618
$\theta_{2sw}^8$	6.1842	6.1512
$\theta_{2sw}^9$	3.2548	0.3847
$\theta_{2sw}^{10}$	0.05668	6.2832
$f(\mathbf{x}^*)$	6.836	<b>0.4857</b>

**Table 6.3** Optimized values of design variables of the second stage of optimization

Design Variables	GA	HTLPSO
$\theta_{1ste}^1$	2.5908	1.4033
$\theta_{1ste}^2$	2.7391	1.1536
$\theta_{1ste}^3$	2.8221	2.8543
$\theta_{1ste}^4$	2.9272	2.8997
$\theta_{1ste}^5$	2.8806	2.8793
$\theta_{1ste}^6$	2.7989	2.7977
$\theta_{1ste}^7$	2.6666	2.6597
$\theta_{1ste}^8$	2.4295	2.4693

$\theta_{1ste}^9$	2.2330	2.2311
$\theta_{1ste}^{10}$	1.9790	1.9531
$\theta_{2ste}^1$	6.2814	0.0140
$\theta_{2ste}^2$	6.2056	6.2267
$\theta_{2ste}^3$	6.1189	6.1116
$\theta_{2ste}^4$	6.0068	6.0137
$\theta_{2ste}^5$	5.9204	5.9206
$\theta_{2ste}^6$	5.8392	5.8394
$\theta_{2ste}^7$	5.7728	5.7747
$\theta_{2ste}^8$	5.7376	5.7280
$\theta_{2ste}^9$	5.6969	5.6973
$\theta_{2ste}^{10}$	5.6758	5.6788
$f(\mathbf{x}^*)$	8.3682	<b>1.89E-04</b>

In HTLPSO, the parameter tuning of PSO is required. Therefore, the default parameters are selected for PSO. The population size used in HTLPSO and GA is taken as 200. Both the algorithms are run in succession with the increasing values of the iterations. The best values are found for the 30 independent runs corresponding to each iteration and function values corresponding to function evaluations are compared among themselves. Table 6.2 and 6.3 show the comparison of the optimized values of the design variables obtained after the first and second stages of optimization. The optimized linkage dimensions are  $r_1 = 89.5306$ ,  $r_2 = 42.3332$ ,  $r_3 = 73.0147$ ,  $r_4 = 82.8552$ ,  $l_3 = 282.7395$ , and  $l_4 = 284.5872$ .

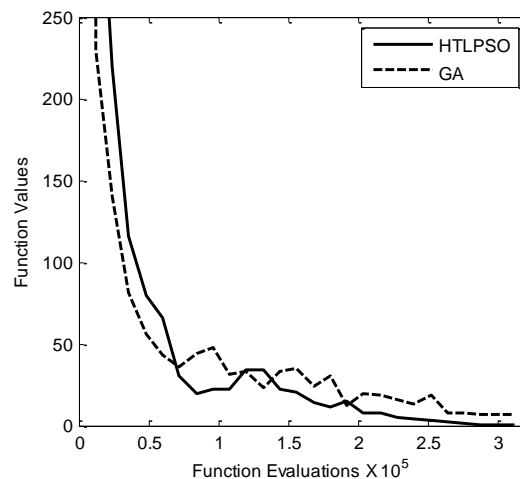


**Fig. 6.8** Convergence of the function value in HTLPSO and GA for swing phase

The converging efficiency of the algorithm is shown by plotting the number of function evaluations v/s function values, Fig 6.8 and Fig 6.9. It is found that HTLPSO reached to the optimum value, 0.4857 and 1.89e-4, for the first and second stage of

optimization in 276000 and 132000 function evaluations, respectively, in comparison to the optimum value, 6.836 and 8.3682, obtained in 288000 and 174000 function evaluations in GA. Table 6.2 and Table 6.3 show the details of the optimized values of design variables and objective function obtained during the first and second stages of optimization, respectively, using both the optimization algorithms. It is found that, the HTLPSO gives better results than that of GA as HTLPSO required 4.17% fewer function evaluation than that of GA for the first stage while it required 24.14% fewer function evaluations than that of GA for the second stage of optimization. The plots of desired and generated foot- and hip-trajectories obtained using HTLPSO and GA are shown in Fig 6.10 and Fig 6.11. From Fig 6.10 and Fig 6.11, it is perceived that the

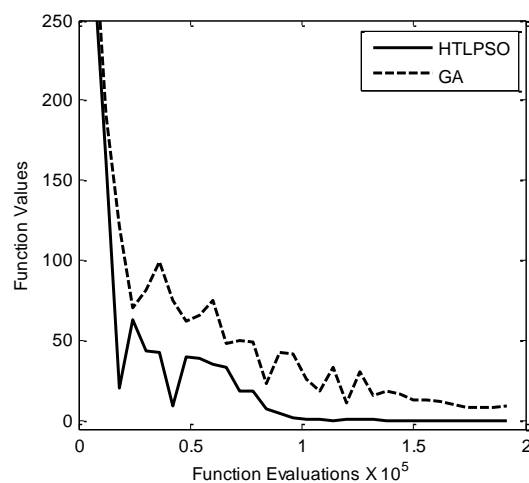


**Fig. 6.9** Convergence of the function value in HTLPSO and GA for support phase

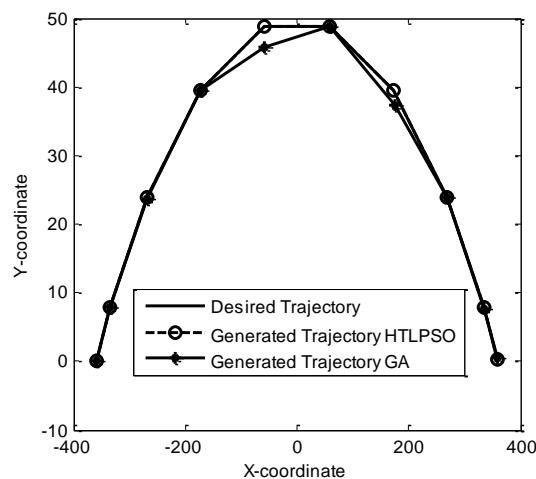


**Fig. 6.10** Comparison of foot trajectories in swing phase

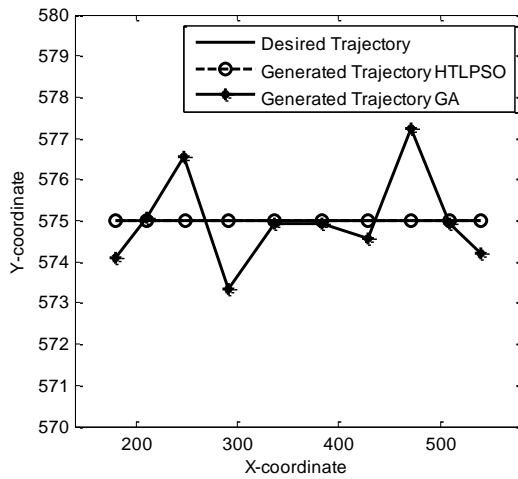


**Fig. 6.11** Comparison of hip-trajectories in support phase

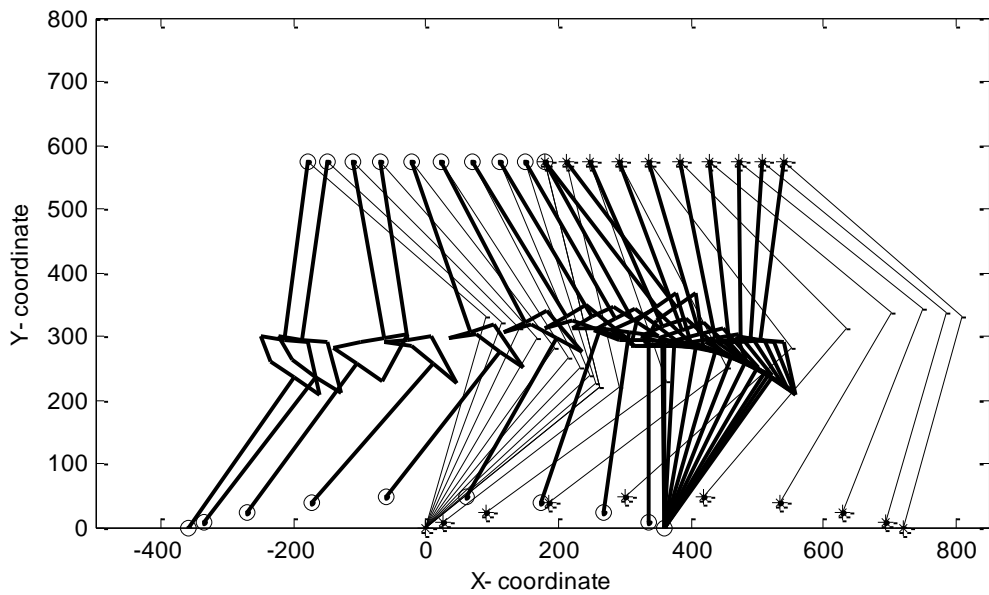


**Fig. 6.12** Stick diagram of a healthy lower limb and exoskeleton lower limb for one gait cycle

foot- and hip-trajectories obtained using the proposed algorithm accurately passes through all the desired precision points during the first and second stages, respectively, while the foot- and hip-trajectories obtained using GA do not accurately pass through all the desired points. It confirms that the proposed gait-inspired synthesis procedure can track all the desired points of the gait more accurately.

Furthermore, the healthy lower limb and lower limb exoskeletons are simulated in MATLAB® for one complete gait cycle which is shown as a stick diagram in Fig. 6.12. The stick diagram demonstrates the position of the whole lower limb at all the

desired points for a complete gait cycle. Besides, a solid model (scaled with a factor 0.6) of the proposed lower limb exoskeleton designed using the proposed gait-inspired four-bar linkage synthesis algorithm is presented. Figure 6.13 shows the concept design and CAD model of the designed linkage during flexion for different poses.

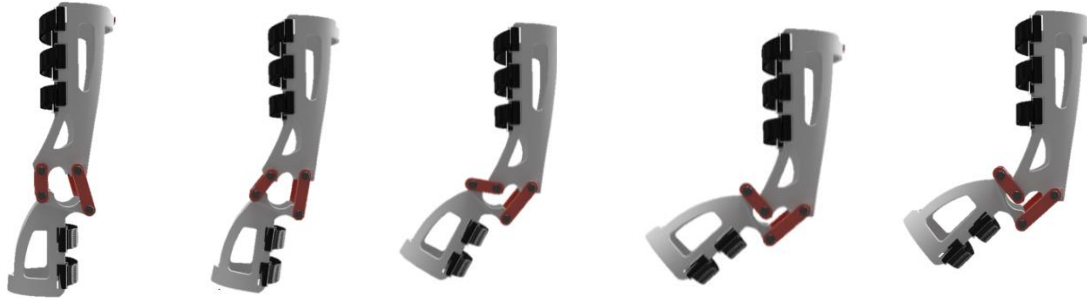


*Fig. 6.13 CAD model of the designed linkage when embedded in an orthotic device*

### **6.3.2 Four-Bar Linkage with Natural Trajectories**

In this section, a realistic numerical example is included to demonstrate the effectiveness of the two-stage algorithm as defined in the preceding section. A four-bar linkage exoskeleton is synthesized using the proposed design procedure for lower limb of the subject of age 20yrs, height 1.70 m, weight 54kg, and leg length of 0.92 m. The foot and hip trajectories of the healthy subject are taken from gait database (Prakash et al., 2015), and ten precision points are selected on one gait cycle. The detailed procedure for selection of the precision points on the desired and input trajectories is illustrated below.

#### *Selection of Precision Points*

A set of data points of the hip and ankle joints of a healthy subject walking on a levelled surface is taken from the *MNIT gait database* (Prakash et al., 2015). The dataset marks the hip and ankle joints' positions for two gait cycles of the same lower limb as shown in Fig 6.14 (a). The position coordinates are collected in the global reference frame where hip joint is moving. In the conventional synthesis procedures, the hip joint requires to be stationary, and the data is transformed relative to the hip joint. In contrast, here the trajectories are taken with respect to the global reference frame. The x-direction is taken as positive towards the right of the origin, and the y-direction, i.e., from shoulder to ankle is taken as negative. The original data are taken in pixel and are calibrated to millimeters (mm). The red markers in Fig 6.14 (b) indicate the positions of ankle and hip joints. The hip positions (x-coordinate) indicate that subject moves from 3685.9 mm towards 525.4545 mm, i.e., from the positive right towards origin as



shown in Fig 6.13. However in this work, to comprehend the mathematical model with ease, the linkage is moved from the negative left towards origin as shown in Fig 6.6 (b). Therefore, x-coordinates are transformed accordingly and are presented in Table 6.4. ‘Best-Fit’ curves which fit 68 data points for desired and input trajectories of hip and ankle joints, respectively, are identified using MATLAB®.

It is difficult to use all the 68 data points as precision points to synthesize the linkage. Therefore, ten precision points are selected (Table 6.4) out of 68 data points, using scheme presented in Fig 6.15, for one gait cycle to synthesize a mechanism. To select the precision points, parametric equations of Best-Fit curves for the ankle ( $A_{xd}, A_{yd}$ ) and the hip joints ( $P_{xd}, P_{yd}$ ) are formed using MATLAB®. The equations are evaluated at an equal interval of 166.3397mm and 165.933 mm for hip and ankle joints, respectively, for 20 precision points of two gait cycle. These intervals are selected based on the start and end points of the X-coordinate which are, 3685.9mm and 525.4545 mm for the hip joint, and 3685.9 mm and 533.1818 mm for ankle joint, respectively. The scheme for selection of the precision points is shown in Fig 6.15.

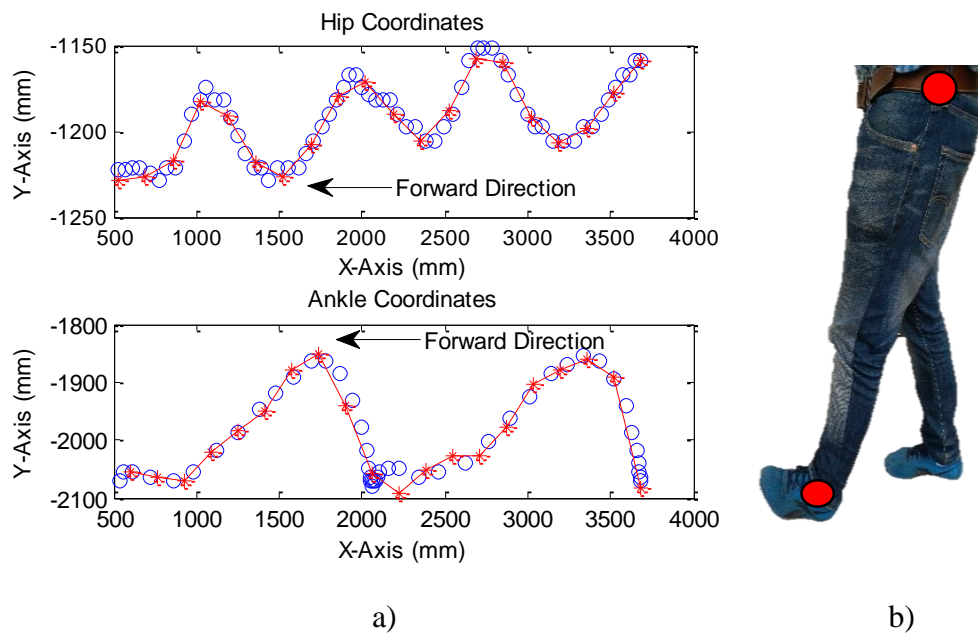


**Fig. 6.14 a)** Curve fitting of the Trajectory Data

**b)** Marker indicating hip and ankle positions

**Table 6.4** Selected precision points on the fitting curve

Positions	$P_{xd} * 1000$	$P_{yd} * 1000$	$A_{xd} * 1000$	$A_{yd} * 1000$
1	-3.6859	-1.1590	-3.6859	-2.0826
2	-3.5196	-1.1775	-3.5236	-1.8906
3	-3.3532	-1.1981	-3.3614	-1.8590

4	-3.1869	-1.2071	-3.1991	-1.8783
5	-3.0206	-1.1919	-3.0368	-1.9024
6	-2.8542	-1.1600	-2.8745	-1.9767
7	-2.6879	-1.1577	-2.7123	-2.0273
8	-2.5215	-1.1878	-2.5500	-2.0288
9	-2.3552	-1.2052	-2.3877	-2.0509
10	-2.1889	-1.1900	-2.2255	-2.0918

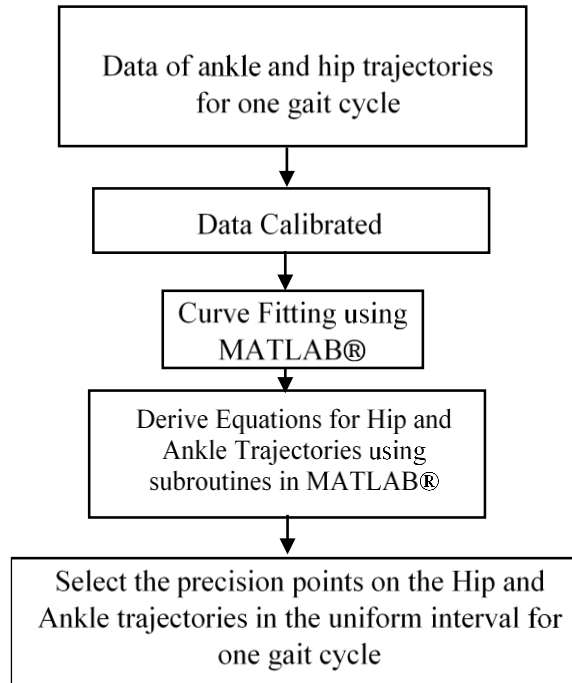


**Fig. 6.15** Scheme for selection of precision points

The first five precision points are taken in the first stage synthesis in which  $\theta_1^k$  and  $\theta_2^k$  where  $k = 1, \dots, 5$  and  $r_1, r_2, r_3, r_4, l_1$  and  $l_2$  are design variables. The bounds on the design variables which are taken as follows:

*First Stage:*

$$\theta_1^k \in \left[0, \frac{\pi}{2}\right], \theta_2^k \in [0, 2\pi], r_1, r_2, r_3, r_4 \in [40, 170], l_1 \in [280, 500], l_2 \in [280, 400]$$

*Second Stage:*

$$\theta_1^k \in \left[0, \frac{\pi}{2}\right], \theta_2^k \in [0, 2\pi]$$

*Note angle is in radian and length is in mm.*

To obtain a feasible solution, the two well-established algorithms, namely, TLBO and PSO are used. The purpose of using two-nature inspired algorithms is not to compare their performance but to validate their results, which should be near

approximate of the global minimum. Since both these nature-inspired algorithms are stochastic in nature, therefore, each algorithm is run 25 times, and the best solution with minimum error is selected which is as follows:

$\mathbf{x}_1$

$$= \begin{bmatrix} 1.2374, 0.7530, 0.6750, 0.6825, 0.7323, 1.6622, 2.4527, 2.6601, \\ 2.6131, 2.4457, 471.0019, 374.0438, 72.4620, 104.4731, 123.6035, 119.0642 \end{bmatrix}^T$$

Figure 6.16 shows that PSO converges faster and gives less error in comparison with TLBO in the first stage of the algorithm. The best linkage obtained by PSO tracks all five precision points accurately as shown in Figs 6.17 and 6.18.

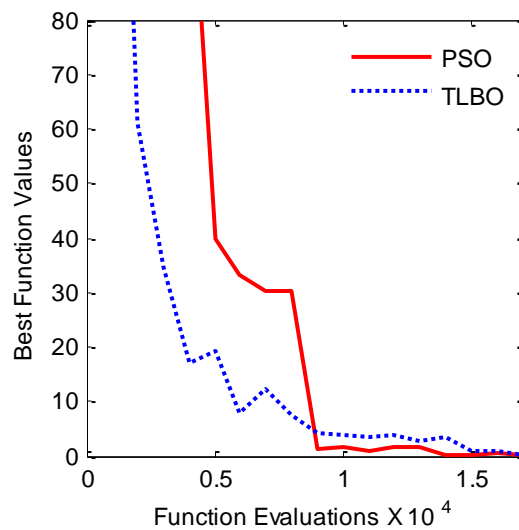


**Fig. 6.16** Convergence of best objective function v/s number of function evaluations

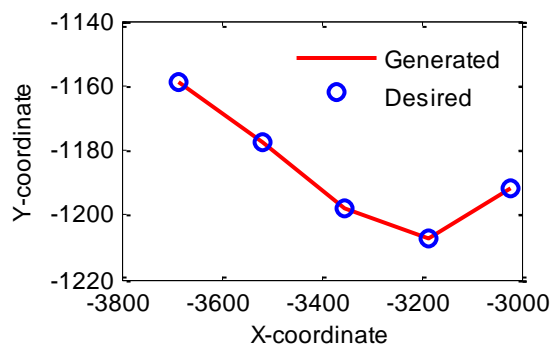


**Fig. 6.17** Generated trajectory and desired points of hip joint P during the first stage using PSO

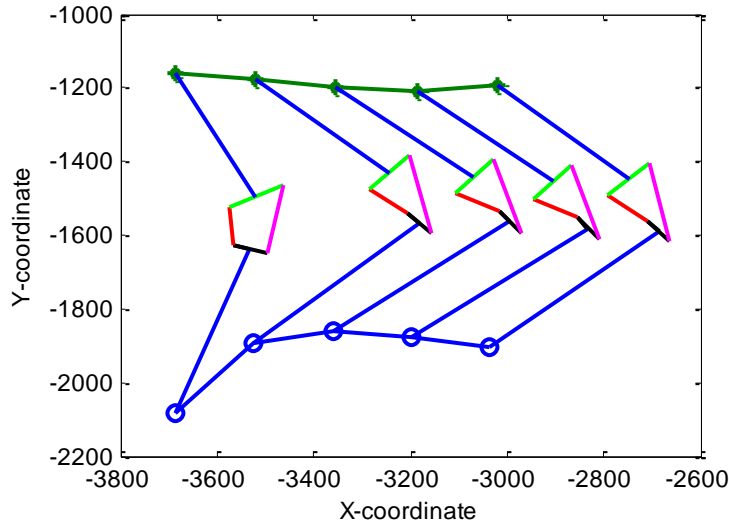


**Fig. 6.18** Tracking of precision points on the hip trajectory

Thereafter, the designed linkage is used further to track the remaining five precision points on the hip trajectory. The position (configuration) synthesis is performed during the second stage of the algorithm. The same procedure is used for solving the optimization algorithm as used in the first stage. Figure 6.19 shows that PSO converges faster than TLBO in the second stage. The design vector of the synthesized positions for the linkage is obtained using PSO in the second stage. The resulted design vector is as follows:

$$\mathbf{x}_2 = [0.9179, 1.0401, 0.9637, 0.9705, 1.1220, 1.9755, 1.7669, 1.8648, 1.8414, 1.6623]^T$$

Figure 6.20 shows the trajectory generated by designed linkage tracks the remaining five precision points accurately. Also, the configuration of the designed linkage while moving is shown in Fig 6.21. Lastly, the stick diagram in Fig 6.22 shows that the four-bar linkage designed using the proposed synthesis procedure can track all the precision points for one gait cycle. Moreover, it also demonstrates the configurations of the lower limb (four-bar linkage) at each desired precision point. If this linkage is fixed to a user, their lower limb can generate the appropriate trajectories required for one gait cycle. Therefore, the designed linkage can be used for any application which requires walking.

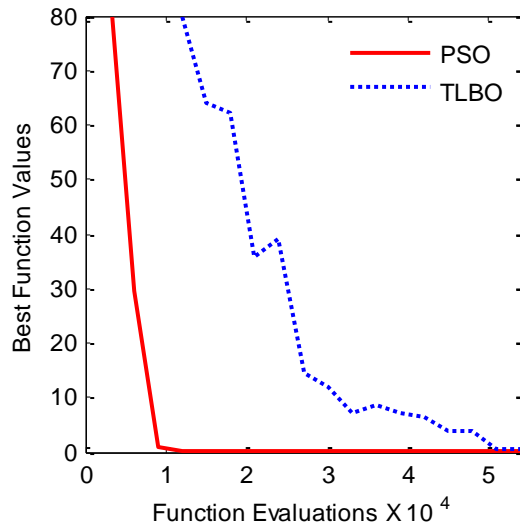


**Fig. 6.19** Convergence of best objective function v/s number of function evaluations

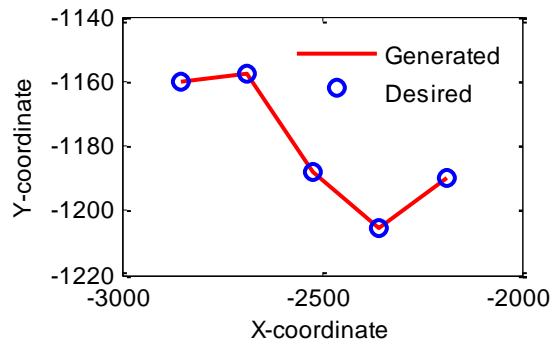


**Fig. 6.20** Generated trajectory and desired points of hip point P during the second stage using PSO

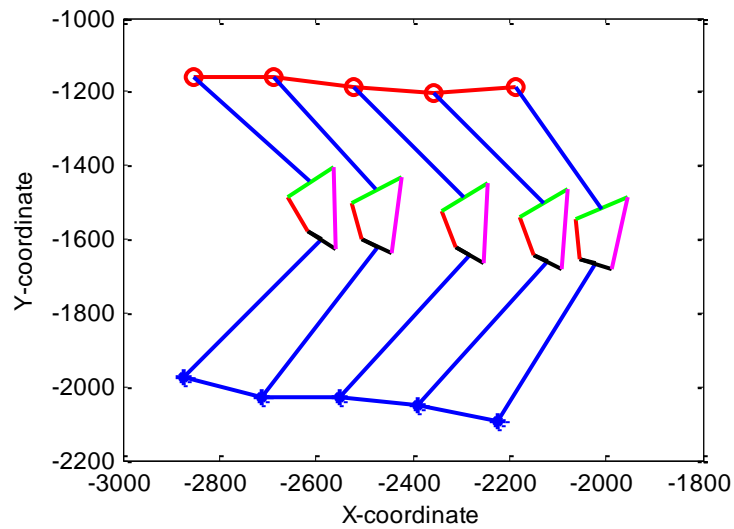


**Fig. 6.21** Four-bar linkage lower limb tracking 5 precision points on the hip trajectory

A four-bar mechanism is also proposed in this example which can be used to replace the single-axis revolute joint in the knee-ankle-foot, hip-knee-ankle-foot, and knee orthoses. Thus, the design obtained using the simplified gait-based mechanism synthesis procedure can be embedded in the orthotic and portable gait rehabilitation devices. The novel gait-based four-bar linkage synthesis procedure can be used to synthesize any mechanism which involves human walking. The real trajectories are taken with respect to a global reference frame. A total of ten precision points is selected out of 68 points available on the foot and hip trajectories for the synthesis. The ankle trajectory is taken as input while the linkage is designed for tracking the hip trajectory. The synthesis procedure divides the problem into two stages. The first stage is devoted to the linkage design in which five precision points are considered to obtain the linkage parameters. The parameters obtained in the first stage are used as input to the second stage for determining the linkage positions for the remaining five precision points. A two-stage optimization problem is formulated to minimize the tracking error between the generated and desired hip trajectories. To solve this optimization problem, two nature-inspired optimization algorithms, namely, TLBO and PSO are used. It is found that minimum error of  $5.2 \times 10^{-2}$  and  $9.92 \times 10^{-8}$  are obtained during first and second stages, respectively. The designed linkage is simulated in MATLAB® for one gait cycle which is shown in stick diagram (Fig 6.22).

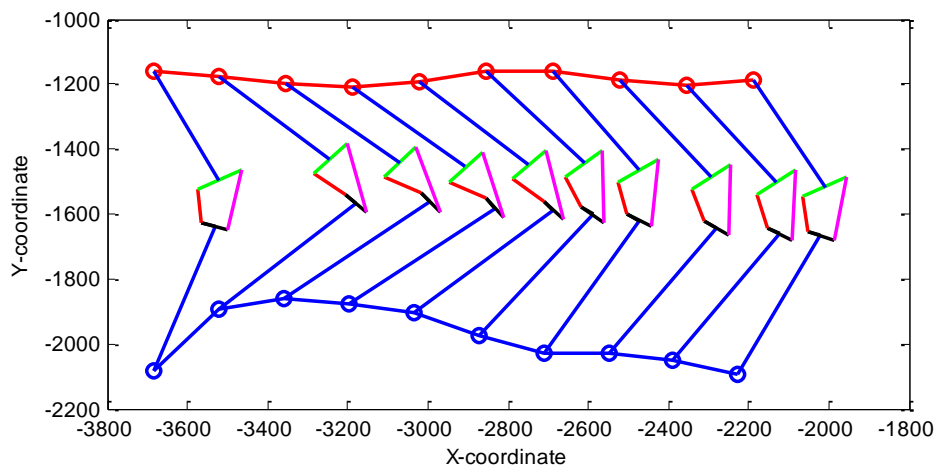


**Fig. 6.22** Stick diagram of four-bar linkage lower limb exoskeleton for one gait cycle

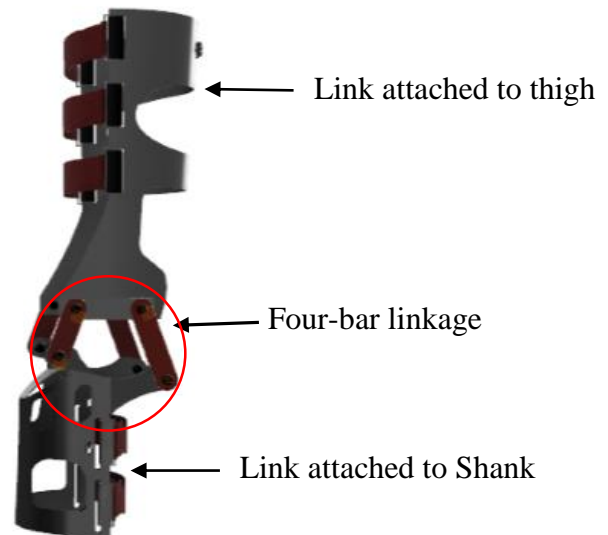


**Fig. 6.23** Conceptual design of four-bar knee exoskeleton

Figure 6.23 shows the conceptual design of an exoskeleton device which demonstrates the assembly of the four-bar linkage. The thigh and shank link lengths in the exoskeleton can be varied to obtain another variant of the exoskeleton; however, these lengths should not exceed the design lengths proposed in this section. This way the proposed mechanism can be embedded in other orthotic/exoskeleton and gait rehabilitation devices. The work can be extended by, considering compliant links in place of rigid links, considering adjustable four-bar linkage, and use of control technology to embed the designed mechanism in the gait rehabilitation device.

#### **6.4 Summary**

In this chapter, two gait-inspired four-bar linkage synthesis procedures are proposed while considering the assumed and natural trajectories, respectively. The first procedure divides the gait in swing and the stance stages and the foot and hip trajectories are derived in the frame fixed to the ground. The synthesis problem is posed as a two-stage optimization algorithm. In the first stage, minimization of the Euclidean distance between the desired and generated swing limb trajectories of exoskeleton lower limb is considered as the objective function. In the second stage, minimization of the Euclidean distance between the desired and generated stance limb trajectories is taken as the objective function. The synthesis of four-bar linkage is illustrated with a realistic non-trivial numerical example of exoskeleton lower limb. To obtain a feasible solution, HTLPSO algorithm is used and its results are compared with the well-established algorithm (GA). It is found that the HTLPSO optimization algorithm converges to an

optimum value in 4.17% fewer function evaluations for the first stage, and 24.14% fewer function evaluations for the second stage, in comparison to the GA. Hence, HTLPSO is computationally more efficient algorithm compared to GA, for this problem. A solid model is also presented to demonstrate the poses of linkage during flexion. In order to verify gait of lower limb for one complete gait cycle, simulation of the synthesized linkage is also performed in MATLAB®, and the stick diagram of the lower limb while walking is also presented. In another case, the proposed gait-based synthesis procedure has been applied on the real trajectories for the first time. This synthesis procedure develops a generalized walking mechanism for use in the lower limb of exoskeletons, bipeds, prosthesis, rehabilitation devices etc. The designed mechanism can be integrated with the control technology for its application in gait rehabilitation devices, exoskeleton, bipeds, etc., wherever walking like humans, is needed. Besides, this mechanism can also be applied to any body weight support- or portable- rehabilitation devices. The designed linkage can achieve all the orientations required during walking which is demonstrated by stick diagram.



## Topology Optimization of Supporting Device

Robotic knee exoskeletons have been used increasingly in the rehabilitation community; which assists the patients with gait disorder and those with spinal cord injuries. These systems could be attached to the patients' knee for assisting or control technology could be embedded into it in order to provide controlled movement and recover mobility. The assistive knee device is used to assist the surrounding ligaments, tendons, and muscles of the injured knee joint. Various knee exoskeletons have been discussed; however, their shape synthesis is not reported. Rather, a standard frame is used for knee-ankle-foot orthosis which is controlled using pneumatic cylinders (Skelton et al., 2013). This chapter aims to present the shape synthesis of the assistive/supporting knee device. Moreover, four-bar linkage is used for the knee exoskeleton, in this chapter. Assistive knee exoskeleton devices proved to be an important tool for providing support to injured knee joints. Typically single axis joints are observed in the lower limb exoskeletons which can be replaced with linkage mechanisms to obtain the desired range of motion. In this chapter, four-bar linkages are used for the knee exoskeleton in which cranks and rockers are connected to the lateral and medial sides of the knee joint, for connecting shank and thigh attachments. Furthermore, in this chapter, a novel assistive knee device is proposed using shape synthesis. The device consists of a four-bar linkage in which thigh and shank are the extended links. The device is modeled in FUSION software for simulation. The components are assembled to form an assistive knee exoskeleton which can be used by any person with injured knee joint.

### 7.1 Design Specifications

It is necessary to comprehend gait biomechanics for providing assistance and facilitating walk. Therefore, gait data are collected from the clinical gait analysis (CGA) database (Yu et al., 2013), and it is used in the force analysis of four-bar linkage. Dimensions of four-bar linkage are adapted from chapter 5 and links' lengths are scaled 0.7 of their original lengths.

Gait data for a healthy subject of 70 kg, 0.9 m leg-length walking at 1m/s are collected and normalized to the percentage of the gait cycle (1-100%). The data are taken, for one gait cycle starting from the heel strike of the right leg and terminates with the heel strike of the same leg. Figure 7.1 illustrates the biomechanics of knee joint of a healthy human subject for one gait cycle in which Fig 7.1 (a) represents the knee

flexion/extension, and Fig 7.1 (b) represents the knee joint torque for one gait cycle. It is observed that knee flexion is restricted to about  $60^\circ$  while walking; whereas, the peak torque attains 30 N-m at the beginning of the gait cycle.

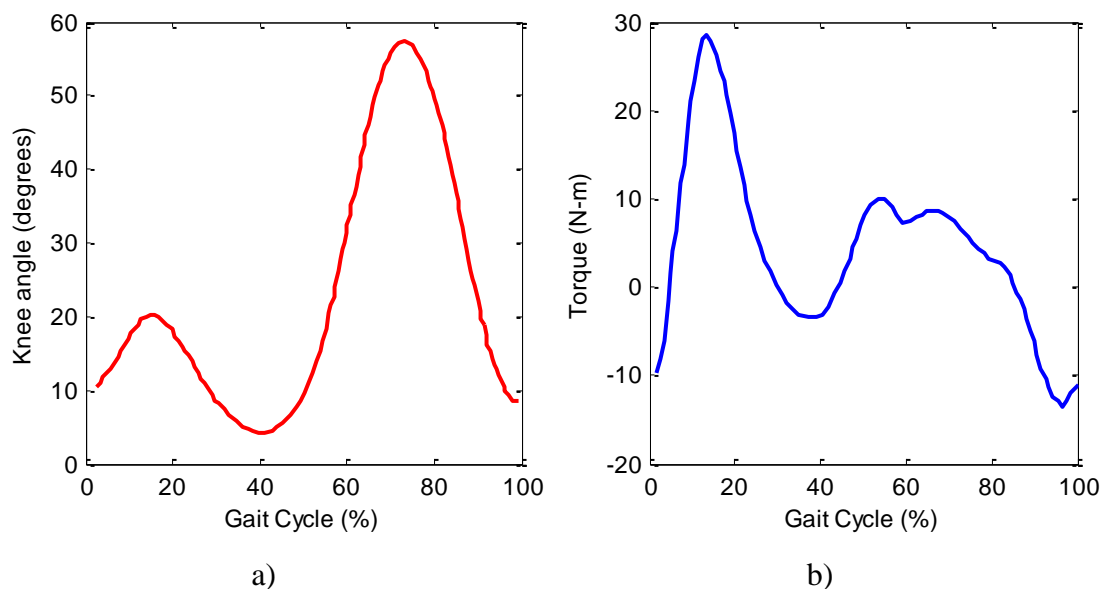


**Fig. 7.1** Biomechanics of human knee joint **a)** joint angle **b)** joint torque

*Note- The above data will be utilized in determining the force required in one gait cycle.*

## 7.2 Mechanism Analyses

In this section, position and static force analyses of the four-bar linkage designed in chapter 5, is performed.

### 7.2.1 Position Analysis

Figure 7.2 shows the schematic diagram of the four-bar linkage of knee supporting device in which links #1 and #3 are fixed to shank and thigh, respectively. Other links, i.e., #2 and #4 act as a connection between shank and thigh.  $\{XOY\}$  represents a global reference frame; links' lengths are represented by  $r_1$ ,  $r_2$ ,  $r_3$ , and  $r_4$ , and orientations of the links' with respect to the X-axis are represented by  $\theta_1$ ,  $\theta_2$ ,  $\theta_3$  and  $\theta_4$ , shown in Fig 7.3.

The biomechanical data collected from CGA normalized database, as shown in Figs 7.1 (a) and 7.1 (b), are utilized for the position and static force analyses of the four-bar linkage. Dimensions of the four-bar linkage are adapted from chapter 5 and scaled to 0.7 of their original dimensions. Table 7.1 shows the scaled dimensions of the four-bar linkage.

Position analysis of the four-bar linkage can be performed for one gait cycle using knee joint angle  $\theta_{knee}$  and link #1 angle,  $\theta_1$ , as inputs. Wherein, other angles of

the four-bar, i.e.,  $\theta_2$  and  $\theta_4$  can be obtained by solving the loop-closure equation (Kinzel, 1999). Appendix A.3 provides the detail for finding the unknowns  $\theta_2$  and  $\theta_4$  in the linkage. This enables us to determine the joints' trajectories of the four-bar linkage. Thereafter, static force analysis of the four-bar linkage is performed by using the knee joint torque data, presented in Fig 7.1 (b).

### 7.2.2 Static Force Analysis

A local non-rotating body coordinate system (LNRBCS) is set up at the center of gravity (CG) of each link to carry out the static force analysis of the four-bar linkage. Free body diagram of the four-bar linkage is shown in Fig 7.4 where LNRBCS is fixed at CG of each link.

*Note: CG is assumed to lie on the line joining two joints which connects two other links.*

**Table 7.1** Dimensions of four-bar linkage

Link parameters	Adapted dimensions (Chapter 5)	Scaled dimensions
$r_1$	81.7145	57.20
$r_2$	49.0499	34.34
$r_3$	64.1500	44.91
$r_4$	73.1816	51.23
$\theta_1$	25.3925°	

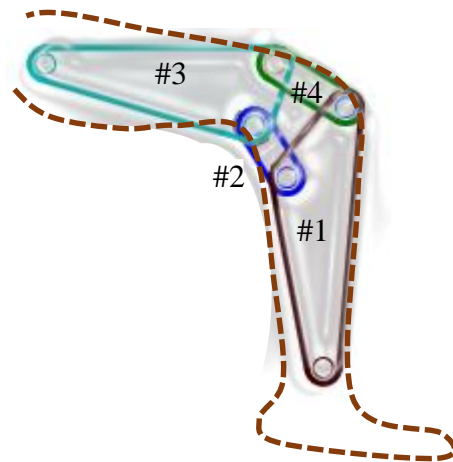


**Fig. 7.2** Schematic diagram of the four-bar linkage for the knee exoskeleton

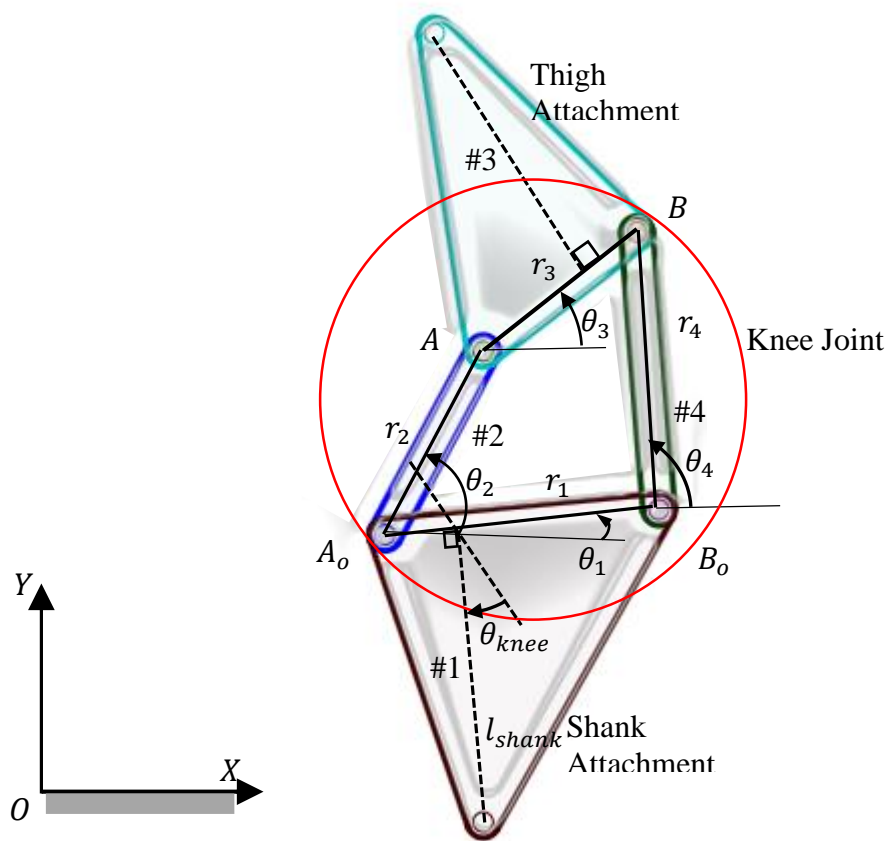


**Fig. 7.3** Various definitions of four-bar linkage

The reaction forces are denoted by  $\mathbf{F}_{ij}$  in which subscripts  $i$  and  $j$  represent the links' numbers.  $\mathbf{F}_{ij}$  represents the reaction force of the link  $\#i$  on link  $\#j$ , and its Cartesian components are denoted by  $\mathbf{F}_{ijx}$  and  $\mathbf{F}_{ijy}$ . The force required to actuate the knee exoskeleton is represented by  $\mathbf{F}_{req}$ . The position vector  $\mathbf{R}_{kl}$  is the vector which locates the joint with respect to the CG. The subscript  $k$  denotes the adjoining link, whereas, the subscript  $l$  denotes the parent link, for example, in case of link  $\#1$ , the subscript 2 in position vector,  $\mathbf{R}_{21}$ , represents the adjoining link  $\#2$ , whereas, subscript 1 represents the parent link  $\#1$ . The position vector in the link  $\#1$  point towards the link end,  $A_o$ , from CG of the link. Similarly, other position vectors are defined.

Note  $\mathbf{F}_{ij} = -\mathbf{F}_{ji}$

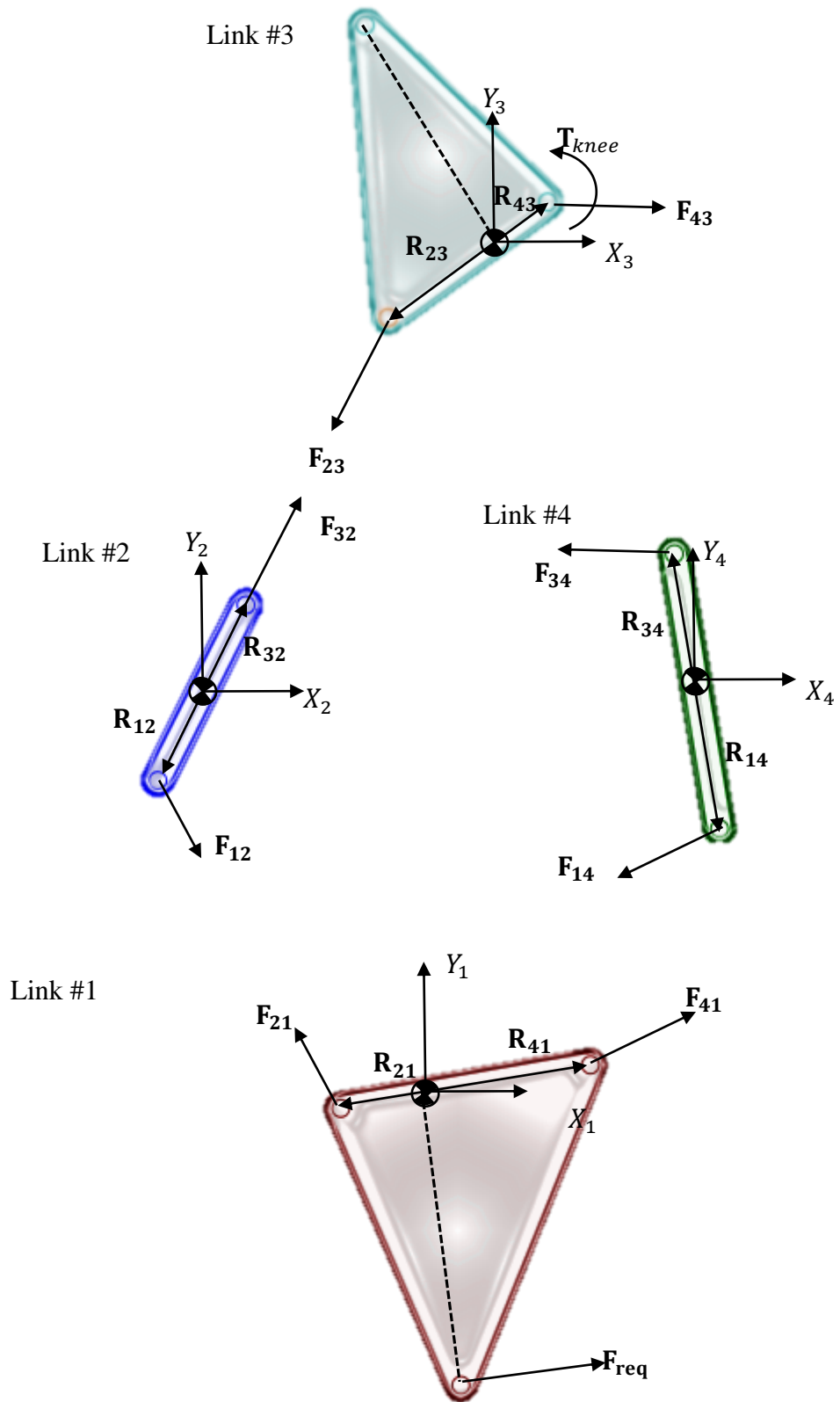


Fig. 7.4 Free body diagram of four-bar linkage

Three equations are formed for each moving body, two of which are separate force summations in  $X$  and  $Y$  directions, whereas, third is for the torques in the  $Z$  direction. These equations form a set of simultaneous equations for the any system which can be solved by matrix method (Norton, 2011) as follows:

$$\mathbf{F} = \begin{bmatrix} F_{21x} \\ F_{21y} \\ F_{32x} \\ F_{32y} \\ F_{43x} \\ F_{43y} \\ F_{14x} \\ F_{14y} \\ F_{req} \end{bmatrix} = \begin{bmatrix} 1 & 0 & 0 & 0 & 0 & 0 & -1 & 0 & \cos \theta_1 \\ 0 & 1 & 0 & 0 & 0 & 0 & 0 & -1 & \sin \theta_1 \\ -R_{21y} & R_{21x} & 0 & 0 & 0 & 0 & R_{41y} & -R_{41x} & K \\ 0 & 0 & -1 & 0 & 1 & 0 & 0 & 0 & 0 \\ 0 & 0 & 0 & -1 & 0 & 1 & 0 & 0 & 0 \\ 0 & 0 & R_{23y} & -R_{23x} & -R_{43y} & R_{43x} & 0 & 0 & 0 \\ 0 & 0 & 0 & 0 & -1 & 0 & 1 & 0 & 0 \\ 0 & 0 & 0 & 0 & 0 & -1 & 0 & 1 & 0 \\ 0 & 0 & 0 & 0 & R_{34y} & -R_{34x} & -R_{14y} & R_{14x} & 0 \end{bmatrix} \begin{Bmatrix} 0 \\ 0 \\ 0 \\ 0 \\ 0 \\ -T_{knee} \\ 0 \\ 0 \\ 0 \end{Bmatrix} \quad (7.1)$$

in which,  $\theta_{1k} = \theta_1 - \frac{\pi}{2}$ ,  $K = l_{shank}(\cos \theta_{1k} \sin \theta_1 - \sin \theta_{1k} \cos \theta_1)$

$$R_{21x} = R_{21}(\cos(\theta_1 + \pi))$$

$$R_{21y} = R_{21}(\sin(\theta_1 + \pi))$$

$$R_{41x} = R_{41}(\cos \theta_1)$$

$$R_{41y} = R_{41}(\sin \theta_1)$$

$$R_{23x} = R_{23}(\cos(\theta_3 + \pi))$$

$$R_{23y} = R_{23}(\sin(\theta_3 + \pi))$$

$$R_{43x} = R_{43}(\cos \theta_3)$$

$$R_{43y} = R_{43}(\sin \theta_3)$$

$$R_{34x} = R_{34}(\cos \theta_4)$$

$$R_{43y} = R_{34}(\sin \theta_4)$$

$$R_{14x} = R_{14}(\cos(\theta_4 + \pi))$$

$$R_{14y} = R_{14}(\sin(\theta_4 + \pi))$$

### 7.3 Topology Optimization of Supporting Device

Base models are prepared from anthropometric measurements of a healthy human lower limb. The models of the crank, rocker, thigh attachment, and shank attachment are utilized to perform shape synthesis of the knee exoskeleton. The links' lengths that are used in the base models are presented in Table 7.1, while the width and thickness of both links are taken as 15 mm and 5 mm, respectively. The thigh attachment is extended to a length of 215.9 mm while the shank attachment is extended to a length of 165.1 mm. The base models have been designed to don and doff easily by a person of leg length 900 mm. Figures 7.5 through 7.8 show the base models for synthesizing shapes of all components, namely, thigh attachment, crank, rocker, and shank attachment, of the knee exoskeleton.

The reaction forces and the force required to actuate the exoskeleton are determined through static force analysis. These forces are applied to the joints of the base models using a CAD/CAE software (FUSION 360®); after that, models are promoted to the shape optimization section of the simulation module in FUSION 360®. Simulation is performed for these models while preserving the regions which cannot be removed. Consequently, tentative regions are obtained that are no longer required or can be removed. Figure 7.9 shows the schematic diagram for shape synthesis of knee exoskeleton.



*Fig. 7.5 Base model of thigh attachment used for shape synthesis of knee exoskeleton*



*Fig. 7.6 Crank model for knee exoskeleton*



*Fig. 7.7 Rocker model for knee exoskeleton*

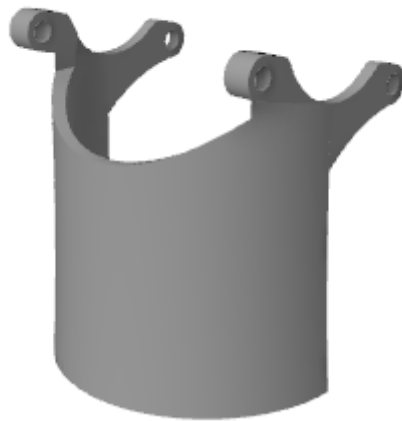


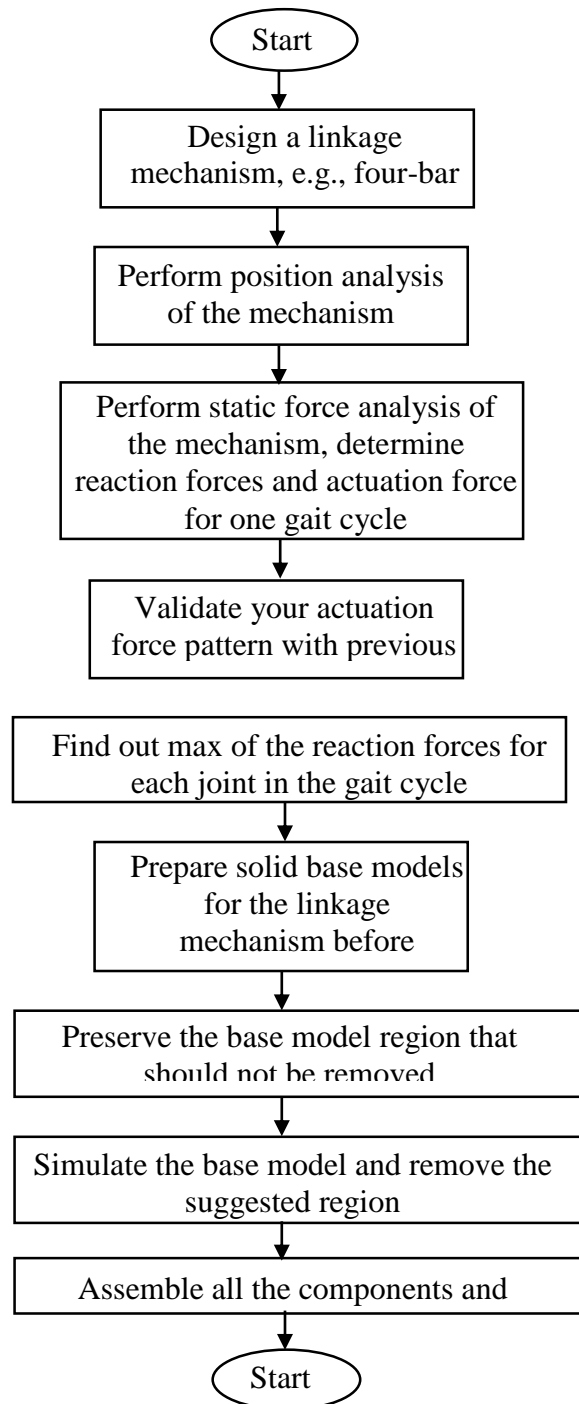
*Fig. 7.8 Base model of shank attachment used for shape synthesis of knee exoskeleton*

#### **7.4 Results**

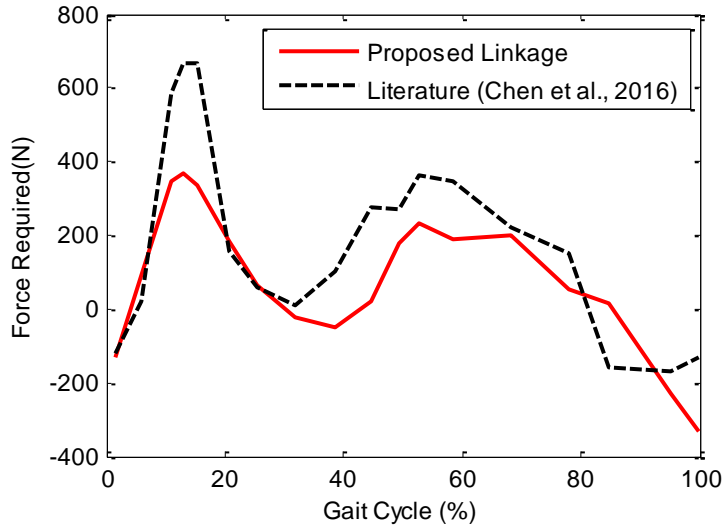
The supporting knee exoskeleton is designed using the methodology discussed in Section 7.3. Since available supporting device contains single-axis knee joint that cannot imitate natural human gait; therefore, in this work, scaled dimensions of four-bar linkage for knee joint are taken, shown in Table 7.1. As discussed in Section 7.2, positions analysis of the four-bar linkage is performed for one gait cycle using the biomechanics of knee joint angle. From the position analysis, unknowns in the four-bar linkage,  $\theta_2$  and  $\theta_4$  are determined. It is a prerequisite for performing the static force analysis. Utilizing the biomechanics of knee joint angle, torque, and procedure discussed in Section 7.3, the reaction, and actuating forces are evaluated. Figure 7.10



depicts the comparison between required actuating forces of proposed linkage with the literature (Chen et al., 2016) while walking.

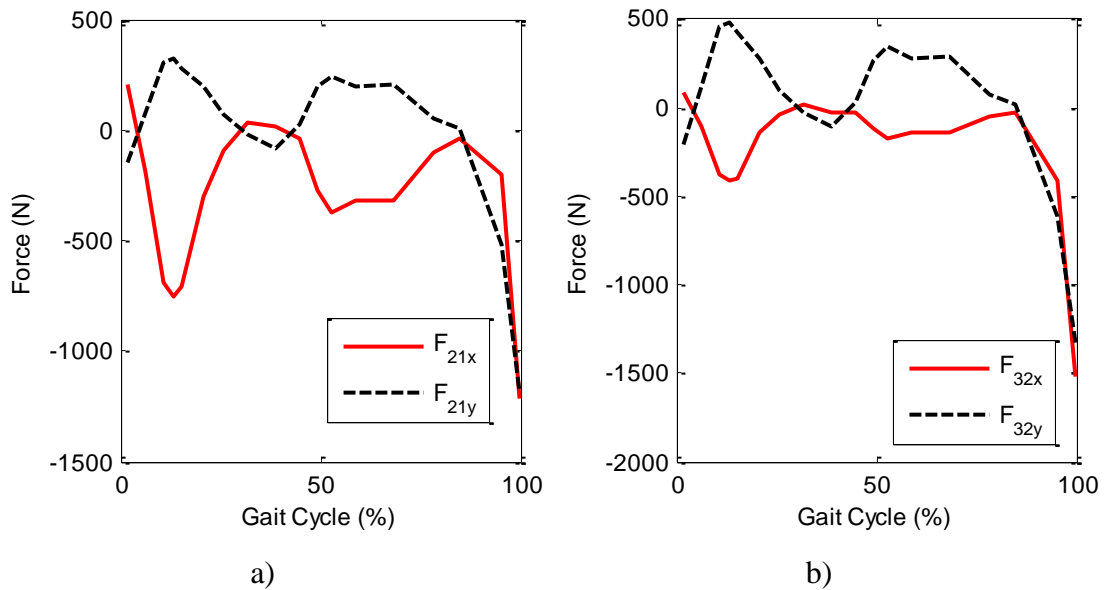


*Fig. 7.9 Schematic diagram for shape synthesis of knee exoskeleton*



**Fig. 7.10** Comparison between required actuating force of proposed knee linkage with literature

It is found that the required force pattern for one gait cycle follows the reported result in which the actuating peak force required is 668.36 N (Chen et al., 2016); whereas it is 370.28 N for the proposed linkage. Hence, a reduction of 45% is observed in the required peak force. Figure 7.11 (a) through (d) shows the reaction forces in the proposed knee exoskeleton for one gait cycle. The maximum of reaction forces from one gait cycle is taken for simulation and presented in Table 7.2.



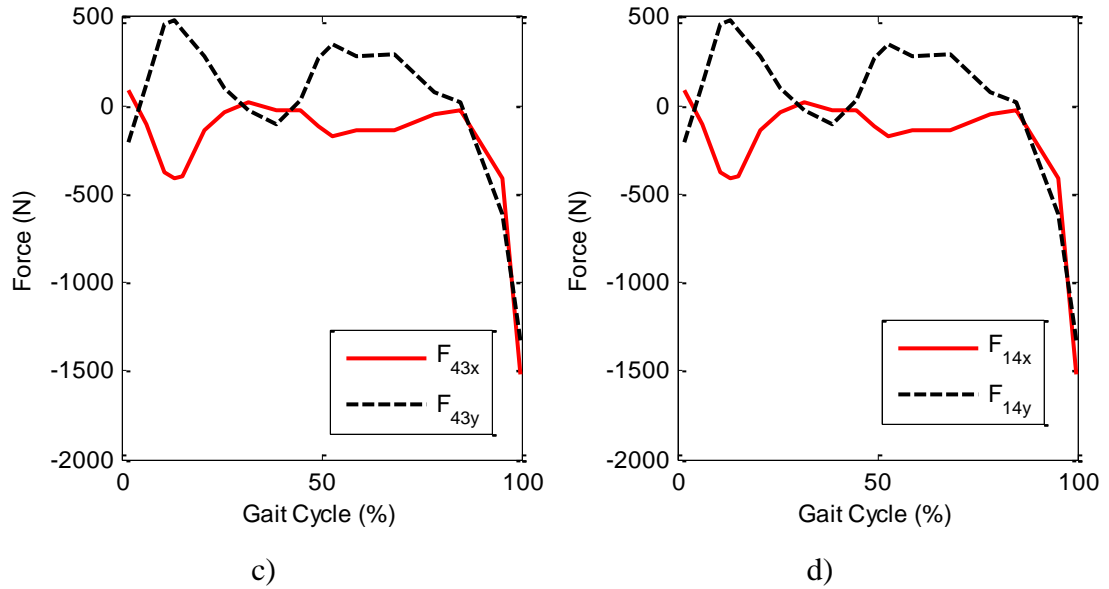


**Fig. 7.11** Reaction forces in the knee exoskeleton for one gait cycle **a)**  $F_{21x}$  and  $F_{21y}$  **b)**  $F_{32x}$  and  $F_{32y}$  **c)**  $F_{43x}$  and  $F_{43y}$  **d)**  $F_{14x}$  and  $F_{14y}$

**Table 7.2** Max value of forces in one gait cycle

Force parameters	Max Force (N)
$F_{21x}$	1215.3
$F_{21y}$	1184.8
$F_{32x}$	1516.2
$F_{32y}$	1327.6
$F_{43x}$	1516.2
$F_{43y}$	1327.6
$F_{14x}$	1516.2
$F_{14y}$	1327.6
$F_{req}$	-370.2

Stainless steel and aluminum are the typically preferred metals for the knee joint exoskeleton/orthotics (Stills, 1987). Therefore in this work, steel is used for knee exoskeleton during simulation. The base models are moved to shape optimization module in simulation section of FUSION 360®, where the reaction and actuating forces are applied to the knee exoskeleton. The simulation is performed for the individual components rather than on the assembly. The regions which cannot be removed are preserved prior to solving the simulation problem. Figures 7.12 through 7.15 show the simulation models of all the components of the four-bar in which their required regions are preserved, while reaction and actuating forces are applied to them. Besides, it shows the specified target mass for the components that allows material removal below the

marked threshold. After that, all the components are promoted to model module followed by sketch module where allowable blue colored<sup>4</sup> regions are removed from them.

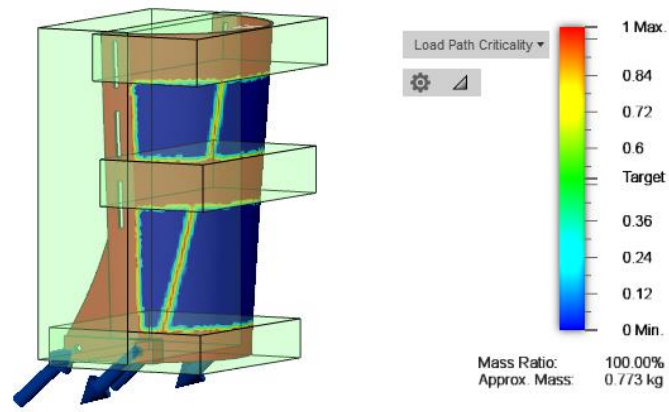


*Fig. 7.12 Simulated model of thigh attachment*

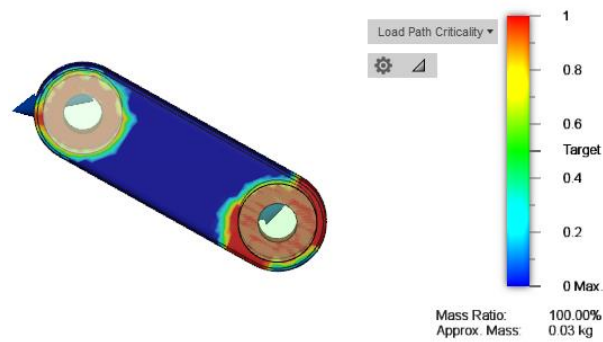


*Fig. 7.13 Simulated model of crank*

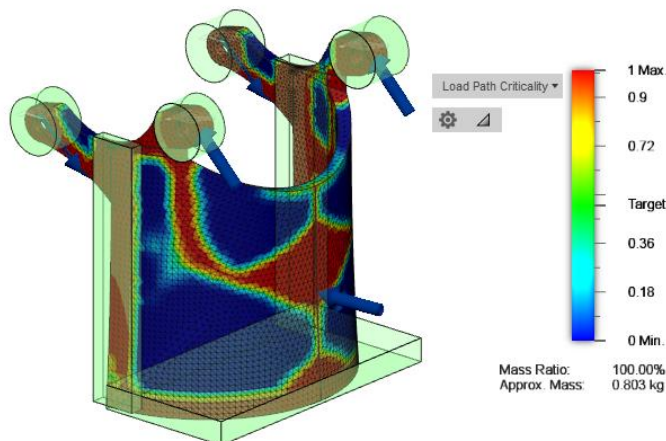


*Fig. 7.14 Simulated model of shank attachment*

<sup>4</sup> Visible in web version of chapter

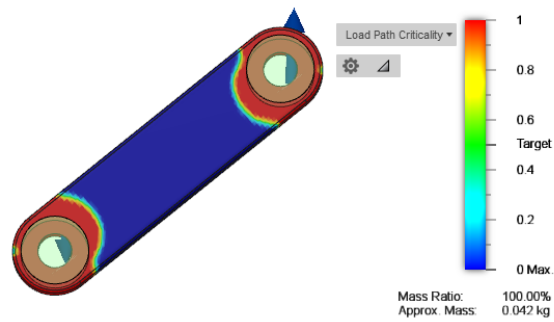


**Fig 7.15** Simulated model of rocker

Initial masses of the components of the four-bar (knee exoskeleton) are 0.773 kg, 0.803 kg, 0.03 kg, and 0.042 kg, for thigh attachment, shank attachment, crank, and rocker, respectively. The masses of these components are reduced after shape synthesis. Table 7.3 shows a total reduction of 21 % in the masses is achieved after shape synthesis.

**Table 7.3** Weight of the components of knee supporting device

Component	Initial Mass (kg)	Obtained masses(kg)	Percentage reduction in mass
Thigh attachment	0.773	0.526	32
Shank attachment	0.803	0.694	14
Crank	0.03X2	0.03 X2	0
Rocker	0.042X2	0.042 X2	0
<b>Total</b>	<b>1.72</b>	<b>1.364</b>	<b>21</b>

*Note: masses of Velcro, bolts, and clamps are not taken*

Following the shape synthesis, all the components are assembled using bolts and clamps; whereas, Velcros are attached to the thigh and shank attachments for tightly holding the lower leg. Figure 7.16 shows an assembled model of the knee exoskeleton in which four-bar linkage is embedded.

### 7.5 Summary

This chapter presented shape synthesis of the supporting knee joint device for persons with injured knee and stroke patients to rehabilitate gait. In this chapter, the four-bar linkage is used on the lateral and the medial sides of the knee joint in which thigh and shank attachments are common to both the linkages. Static force analysis is performed for the four-bar linkage to determine the reaction and actuating forces. It is found that

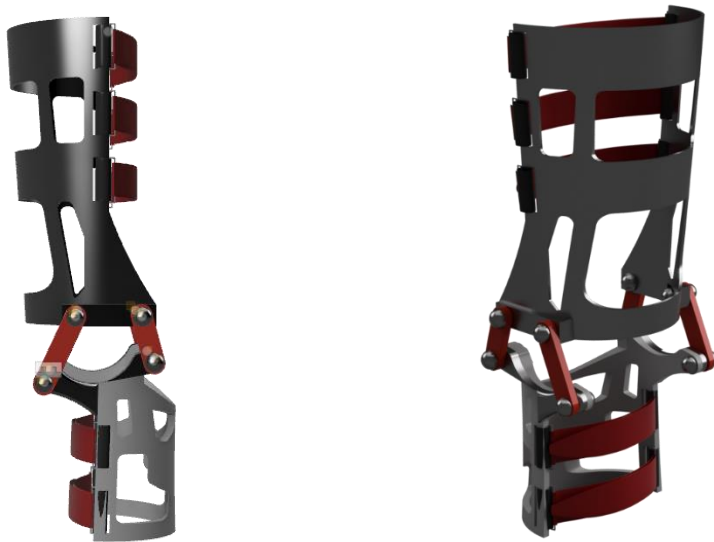


*Fig 7.16 CAD model of the supporting device with four-bar linkage*

the obtained actuating force is consistent with the reported literature, for one gait cycle. Moreover, the peak actuating force required in the presented linkage is reduced 45% in comparison with the linkage reported in the literature. Solid models are created for the knee joint supporting device. Based on the reaction and actuation forces, shapes of the solid models of the individual components of the knee exoskeleton are synthesized in FUSION 360®. A reduction of 32 % mass is observed in the thigh attachment while 14 % is observed in the shank attachment. Finally, a knee exoskeleton of 1.364 kg is developed which consists of one thigh attachment, two cranks, two rockers, and one shank attachment. The developed knee joint supporting device can be used for providing biomechanical assistance to support the surrounding ligaments, tendons, and muscles of the injured knee. Furthermore, control technology can be used to make the device an aid for the stroke patients.

## Conclusions

This thesis presents an optimization methodology for the synthesis of planar defect-free linkages, a hybrid algorithm to solve the optimization problem and gait-inspired synthesis of planar linkages besides other contributions. The analytical synthesis techniques are discussed in chapter 3. The syntheses of planar four-bar linkages are presented in detail for three and four precision points to generate the path. The two distinct real-life applications are considered to demonstrate the syntheses methods for three and four precision points, respectively.

In chapter 4, a new hybrid teaching-learning particle swarm optimization (HTLPSO) algorithm is proposed, which is the combination of teaching-learning-based optimization (TLBO) and particle swarm optimization (PSO) algorithms. The proposed algorithm is validated by utilizing the five constrained benchmark functions, and three cases of four-bar linkage synthesis for path generation task. Besides TLBO and PSO, the WOA, MFO and APSO are among others which are used for comparison with HTLPSO. It is found that HTLPSO algorithm performs better than PSO, MFO, WOA, APSO, and TLBO for all the five benchmark functions. The algorithm also finds the better solution for the synthesis of the four-bar linkage without prescribed timing in path generation tasks and the same cannot find near optimal solution in prescribed timing cases. However, HTLPSO finds reasonable optimal solutions in comparison to the other algorithms. Hence, HTLPSO is found to be an important tool for a variety of problems including planar linkage synthesis. In chapter 5, optimization problems are formulated to minimize the tracking error between the generated and the desired trajectories for the synthesis of the four- and six-bar linkages. The defect-free planar linkages for human knee supporting devices are synthesized using optimization algorithms. Refinements schemes, namely, Grashof and order are applied to TLBO algorithm for reducing the computational effort and solving the highly non-linear constrained optimization problems. Using the proposed algorithm and three necessary and sufficient constraints, a four-bar linkage for knee supporting device is designed which is supported by a prototype and experimental validation. The validation confirms that the designed linkage is defect-free and ready to be applied to the rehabilitation device. Besides a novel loop-by-loop defect-rectification procedure for the synthesis of Stephenson III six-bar path generator linkage is also proposed. In the proposed method, constraints are formulated for Loop I and Loop II separately. The effectiveness of this method is

demonstrated by two numerical examples. The stick diagrams of Stephenson III linkages are also presented for validation.

A two-stage optimization methodology for the synthesis of linkages is proposed in chapter 6. The method is inspired by gait; hence, it is named as gait-inspired linkage synthesis. The two methods are proposed which utilize the assumed and natural gait trajectories, respectively. In the first procedure, gait is divided into the swing and the stance stages and the foot and hip trajectories are derived in the frame fixed to the ground. In this stage, the Euclidean distance between the desired and generated swing limb trajectories is minimized; whereas, the Euclidean distance between the desired and generated stance limb trajectories is minimized in the second stage. The method is demonstrated with a realistic example, and HTLPSO algorithm developed in chapter 4 is used to solve the optimization problem. On comparing it with GA, it is found that the HTLPSO optimization algorithm converges to an optimum value in 4.17% fewer function evaluations for the first stage and 24.14% fewer function evaluations for the second stage. In another synthesis procedure, instead of assumed, natural gait trajectories are utilized for linkage synthesis. A two-stage optimization problem is formulated in which the first stage is used for linkage synthesis and positions are synthesized by controlling angles in the second stage. Furthermore, CAD models are also presented. The gait of synthesized linkages is simulated in MATLAB®, and the stick diagram of the whole synthesized linkage while walking is also presented. The proposed synthesis method is quite general and is equally applicable for synthesizing walking linkages to use in the lower limb of exoskeletons, bipeds, prosthesis, rehabilitation devices etc. The designed linkages can be combined with control theory for its use in gait rehabilitation devices, exoskeleton, bipeds, etc., wherever walking like humans, is required. In summary, the following conclusions are drawn:

- 1) The analytical techniques for the synthesis of linkages can be used; however, the number of precision points are restricted to 9 and 11 for four- and six-bar linkages, respectively.
- 2) Optimal synthesis methods proposed in this work can be used for the defect-free synthesis of the four- and six-bar linkages. The methodology can be applied for path as well as motion generation tasks.
- 3) The proposed use of the reduced number of necessary and sufficient constraints can support in synthesizing a defect-free crank-rocker four-bar linkage. Besides to reduce the computational effort the proposed refinement



scheme can be used in any optimization algorithm which is appended to TLBO for the first time.

- 4) The Stephenson III six-bar linkage can be synthesized using the proposed loop-by-loop method. Also, the constraints are formulated in the simplified form for defect-free rectification.
- 5) The gait-inspired methodologies can be utilized for linkage synthesis while using simplified mathematical model during linkage synthesis.
- 6) For synthesizing linkage using the gait-inspired method, the proposed two-stage optimization method can be used, and the stick diagram can be used to portray the orientations of the linkage during the gait cycle.
- 7) The presented shape synthesis methodology can be used for embedding the designed linkage in the supporting device.
- 8) The proposed HTLPSO algorithm can be utilized for synthesis of linkages to generate path. However, it can be used for wide range of applications. The algorithm is tested on several constrained benchmark functions and path synthesis problems. Besides, it is used as a solver in chapter 6 while using proposed gait-inspired synthesis.
- 9) Various results available in literature are proved in this work. For instance, in chapter 5, benchmarks problems are solved using the proposed methodologies.

### **Future Scope of the Work**

This research has disclosed several intuitive directions that form the scope for future work, which is outlined as follows:

- 1) In this research work, single objective functions are considered. The use of multiobjective functions may render useful results.
- 2) The defect-free synthesis, which has been performed for path generation task in the present work, may be performed for hybrid tasks.
- 3) Other inversions of six-bar and higher order linkages may be used to improve the results.
- 4) The eight or ten order linkage may be synthesized for the whole lower limb rehabilitation device, using the proposed methodology.
- 5) An active device may be developed using the proposed linkages and control theory.

- 6) Besides above, use of adjustable linkage in rehabilitation devices is another interesting area to explore.
- 7) Synthesis of anthropomorphic linkages using polynomials is another interesting work that could be done.

## References

- Acharyya SK, Mandal M. Performance of EAs for four-bar linkage synthesis. *Mechanism and Machine Theory*. 2009 Sep 30;44(9):1784-94.
- Al-Araidah O, Batayneh W, Darabseh T, BaniHani SM. Conceptual design of a single DoF human-like eight-bar leg mechanism. *JJMIE*. 2011 Aug;5(4).
- Alexandridis A, Chondrodima E, Sarimveis H. Cooperative learning for radial basis function networks using particle swarm optimization. *Applied Soft Computing*. 2016 Dec 31;49:485-97.
- Allemand Y, Stauffer Y, Clavel R, Brodard R. Design of a new lower extremity orthosis for overground gait training with the WalkTrainer. In *Rehabilitation Robotics, 2009. ICORR 2009. IEEE International Conference on* 2009 Jun 23 (pp. 550-555). IEEE.
- Almandeel A, Murray AP, Myszka DH, Stumph HE. A function generation synthesis methodology for all defect-free slider-crank solutions for four precision points. *Journal of Mechanisms and Robotics*. 2015 Aug 1;7(3):031020.
- Angeles J, Alivizatoss A, Akhras R. An unconstrained nonlinear least-square method of optimization of RRRR planar path generators. *Mechanism and Machine Theory*. 1988 Jan 1;23(5):343-53.
- Angeles J, Bernier A. The global least-square optimization of function-generating linkages. *Journal of mechanisms, transmissions, and automation in design*. 1987 Jun 1;109(2):204-9.
- Angeles J, Callejas M. An Algebraic Formulation of Grashof's Mobility Criteria with Application to Linkage Optimization Using Gradient Dependent Methods. *ASME Journal of Mechanisms, Transmissions, and Automation in Design*. 1984 Dec;106(3):327-32.
- Aoustin Y, Hamon A. Human like trajectory generation for a biped robot with a four-bar linkage for the knees. *Robotics and Autonomous Systems*. 2013 Dec 1;61(12):1717-25.
- Arora J. *Introduction to optimum design*. Elsevier; 2004 Jun 2.
- Balli SS, Chand S. Defects in link mechanisms and solution rectification. *Mechanism and Machine Theory*. 2002 Sep 30;37(9):851-76.
- Banala SK, Agrawal SK, Scholz JP. Active Leg Exoskeleton (ALEX) for gait rehabilitation of motor-impaired patients. In *Rehabilitation Robotics, 2007. ICORR 2007. IEEE 10th International Conference on* 2007 Jun 13 (pp. 401-407). IEEE.

- Banala SK, Kim SH, Agrawal SK, Scholz JP. Robot assisted gait training with active leg exoskeleton (ALEX). *IEEE Transactions on Neural Systems and Rehabilitation Engineering*. 2009 Feb;17(1):2-8.
- Bataller A, Cabrera JA, Clavijo M, Castillo JJ. Evolutionary synthesis of mechanisms applied to the design of an exoskeleton for finger rehabilitation. *Mechanism and Machine Theory*. 2016 Nov 30;105:31-43.
- Batayneh W, Al-Araidah O, Malkawi S. Biomimetic design of a single DoF Stephenson III leg mechanism. *Mechanical Engineering Research*. 2013 Jul 17;3(2):43.
- Bawab S, Li H. A new circuit identification method in four-position four-bar linkages. *Journal of Mechanical Design*. 1997 Sep 1;119(3):417-9.
- Berkelman P, Rossi P, Lu T, Ma J. Passive orthosis linkage for locomotor rehabilitation. In *Rehabilitation Robotics, 2007. ICORR 2007. IEEE 10th International Conference on 2007 Jun 13* (pp. 425-431). IEEE.
- Blechsmidt JL, Uicker JJ. Linkage synthesis using algebraic curves. *ASME J. Mech., Transm., Autom. Des.* 1986 Dec 1;108:543-8.
- Bouri M, Stauffer Y, Schmitt C, Allemand Y, Gnemmi S, Clavel R, Metrailler P, Brodard R. The WalkTrainer: a robotic system for walking rehabilitation. In *Robotics and Biomimetics, 2006. ROBIO'06. IEEE International Conference on 2006 Dec 17* (pp. 1616-1621). IEEE.
- Brake DA, Hauenstein JD, Murray AP, Myszka DH, Wampler CW. The complete solution of alt-burmester synthesis problems for four-bar linkages. *Journal of Mechanisms and Robotics*. 2016 Aug 1;8(4):041018.
- Bulatović RR, Miodragović G, Bošković MS. Modified krill herd (MKH) algorithm and its application in dimensional synthesis of a four-bar linkage. *Mechanism and Machine Theory*. 2016 Jan 31;95:1-21.
- Bulatovic RR, Orđević SR. Optimal synthesis of a path generator six-bar linkage. *Journal of mechanical science and technology*. 2012 Dec 1;26(12):4027.
- Burmester L. *Lehrbuch der Kinematik*. Felix Verlag, Leipzig, 1888.
- Buśkiewicz J. A method for optimal path synthesis of four-link planar mechanisms. *Inverse Problems in Science and Engineering*. 2015 Jul 4;23(5):818-50.
- Butler PB, Evans GA, Rose GK, Patrick JH. A review of selected knee orthoses. *Rheumatology*. 1983 Jan 1;22(2):109-20.
- Cabrera JA, Simon A, Prado M. Optimal synthesis of mechanisms with genetic algorithms. *Mechanism and Machine theory*. 2002 Oct 31;37(10):1165-77.

- Chase TR, Erdman AG, Riley DR. Improved Centerpoint Curve Generation Techniques for Four-Precision Position Synthesis Using the Complex Number Approach. *Journal of Mechanisms, Transmissions, and Automation in Design*. 1985 Sep 1;107(3):370-6.
- Chase TR, Erdman AG, Riley DR. Triad synthesis for up to five design positions with application to the design of arbitrary planar mechanisms. *Journal of mechanisms, transmissions, and automation in design*. 1987 Dec 1;109(4):426-34.
- Chase TR, Fang WE. Order rectification for complex number based Burmester curves. *Journal of Mechanical Design*. 1991 Sep 1;113(3):239-47.
- Chase TR, Mirth JA. Circuits and branches of single-degree-of-freedom planar linkages. *Journal of mechanical design*. 1993 Jun 1;115(2):223-30.
- Chase TR. A Note on the Waldron Construction for Transmission Angle Rectification. *Journal of Mechanical Design*. 2006 Mar 1; 128(2):509-12.
- Chaudhary K, Chaudhary H. Optimal design of planar slider-crank mechanism using teaching-learning-based optimization algorithm. *Journal of Mechanical Science and Technology*. 2015 Dec 1;29(12):5189-98.
- Chaudhary K, Chaudhary H. Optimal dynamic design of planar mechanisms using teaching-learning-based optimization algorithm. *Proceedings of the Institution of Mechanical Engineers, Part C: Journal of Mechanical Engineering Science*. 2016 Dec;230(19):3442-56.
- Chen G, Chan CK, Guo Z, Yu H. A review of lower extremity assistive robotic exoskeletons in rehabilitation therapy. *Critical Reviews™ in Biomedical Engineering*. 2013;41(4-5).
- Chen G, Qi P, Guo Z, Yu H. Mechanical design and evaluation of a compact portable knee-ankle-foot robot for gait rehabilitation. *Mechanism and Machine Theory*. 2016 Sep 30; 103:51-64.
- Chevallereau C, Bessonnet G, Abba G, Aoustin Y, editors. *Bipedal robots: Modeling, design and walking synthesis*. John Wiley & Sons; 2013 Mar 1.
- Chi-Yeh H. A general method for the optimum design of mechanisms. *Journal of Mechanisms*. 1966 Sep 1;1(3-4):301-13.
- Colombo G, Joerg M, Reinhard Schreier BN, Dietz V. Treadmill training of paraplegic patients using a robotic orthosis. *Development*. 2000 Nov;37(6):693-700.

- Daniali HM, Varedi SM, Dardel M, Fathi A. A novel algorithm for kinematic and dynamic optimal synthesis of planar four-bar mechanisms with joint clearance. *Journal of Mechanical Science and Technology*. 2015 May 1;29(5):2059-65.
- De A, Awasthi A, Tiwari MK. Robust formulation for optimizing sustainable ship routing and scheduling problem. *IFAC-PapersOnLine*. 2015 Jan 1;48(3):368-73.
- De A, Kumar SK, Gunasekaran A, Tiwari MK. Sustainable maritime inventory routing problem with time window constraints. *Engineering Applications of Artificial Intelligence*. 2017 May 31;61:77-95.
- De A, Mamanduru VK, Gunasekaran A, Subramanian N, Tiwari MK. Composite particle algorithm for sustainable integrated dynamic ship routing and scheduling optimization. *Computers & Industrial Engineering*. 2016 Jun 30;96:201-15.
- Dollar AM, Herr H. Lower extremity exoskeletons and active orthoses: challenges and state-of-the-art. *IEEE Transactions on robotics*. 2008 Feb; 24(1):144-58.
- Dong Y, Tang J, Xu B, Wang D. An application of swarm optimization to nonlinear programming. *Computers & Mathematics with Applications*. 2005 Jun 1;49(11-12):1655-68.
- Draganich L, Reider B, Rimington T, Piotrowski G, Mallik K, Nasson S. The effectiveness of self-adjustable custom and off-the-shelf bracing in the treatment of varus gonarthrosis. *JBJS*. 2006 Dec 1;88(12):2645-52.
- Eiben ÁE, Hinterding R, Michalewicz Z. Parameter control in evolutionary algorithms. *IEEE Transactions on evolutionary computation*. 1999 Jul;3(2):124-41.
- Erdman AG, Sandor GN. *Advanced mechanism design: analysis and synthesis (Vol. 2)*. Prentice-Hall, Inc.; 1984.
- Erdman AG. Three and four precision point kinematic synthesis of planar linkages. *Mechanism and Machine Theory*. 1981 Dec 31;16(3):227-45.
- Ettefagh MM, Abbasi M, Emdadi H. Path synthesis of the four-bar mechanism using ABC algorithm and comparing with BGA. In *Innovations in Intelligent Systems and Applications (INISTA)*, 2013 IEEE International Symposium on 2013 Jun 19 (pp. 1-5). IEEE.
- Fallahi B, Hall AS, Ragsdell KM. Application of the generalized reduced gradient method to selected mechanisms synthesis problems. In *Presented at the ASME Des Eng Tech Conf 1981*. ASME.

- Fernández-Bustos I, Aguirrebeitia J, Avilés R, Angulo C. Kinematical synthesis of 1-dof mechanisms using finite elements and genetic algorithms. *Finite elements in analysis and design*. 2005 Sep 30;41(15):1441-63.
- Filemon E. In addition to the Burmester theory. In *Proceedings of Third World Congress for Theory of Machines and Mechanisms* 1971 Sep (pp. 63-78).
- Filemon E. Useful ranges of centerpoint curves for design of crank-and-rocker linkages. *Mechanism and Machine Theory*. 1972 Mar 1;7(1):47-53.
- Freivogel S, Mehrholz J, Husak-Sotomayor T, Schmalohr D. Gait training with the newly developed 'LokoHelp'-system is feasible for non-ambulatory patients after stroke, spinal cord and brain injury. A feasibility study. *Brain Injury*. 2008 Jan 1;22(7-8):625-32.
- Freudenstein F. Approximate synthesis of four-bar linkages. *Resonance*. 2010 Aug 1;15(8):740-67.
- Gao H, Xu W. Particle swarm algorithm with hybrid mutation strategy. *Applied soft computing*. 2011 Dec 1;11(8):5129-42.
- Ghosh S, Robson N, McCarthy JM. Geometric design of a passive mechanical knee for lower extremity wearable devices based on anthropomorphic foot task geometry scaling. In *ASME 2015 International Design Engineering Technical Conferences and Computers and Information in Engineering Conference 2015 Aug 2* (pp. V05BT08A069-V05BT08A069). American Society of Mechanical Engineers.
- Giesbrecht D, Wu CQ, Sepehri N. Design and optimization of an eight-bar legged walking mechanism imitating a kinetic sculpture, "wind beast". *Transactions of the Canadian Society for Mechanical Engineering*. 2012 Nov;36(4):343-55.
- Giridhar G. *Caring for Our Elders: Early Responses India Ageing Report 2017*, 2017 June 19, UNFPA India.
- Gogate GR, Matekar SB. Optimum synthesis of motion generating four-bar mechanisms using alternate error functions. *Mechanism and Machine Theory*. 2012 Aug 31;54:41-61.
- Greenfield JR, Hwang HF, Davies C, McDaid AJ. Soft-stop knee brace for rehabilitation from ligament injuries: Design and pilot trial. In *Rehabilitation Robotics (ICORR), 2017 International Conference on* 2017 Jul 17 (pp. 352-357). IEEE.

- Guo H, Hung AS, Liao WH, Fong DT, Chan KM. Gait analysis for designing a new assistive knee brace. In *Robotics and Biomimetics (ROBIO)*, 2011 IEEE International Conference on 2011 Dec 7 (pp. 1990-1995). IEEE.
- Guo XN, Chu JK. Mobility of Stephenson Six-Bar Chains—Part I: Circuit and Circuit Defect. In *Proceedings of the DETC '04 ASME 2004a Design Engineering Technical Conferences and Computers and Information in Engineering Conference 2004a* Sep 28.
- Guo XN, Chu JK. Mobility of Stephenson Six-Bar Chains—Part II: The Motion Order. *Proceedings of ASME DETC'04*. 2004b Sep 28.
- Guo Z, Fan Y, Zhang J, Yu H, Yin Y. A New 4M Model-Based Human-Machine Interface for Lower Extremity Exoskeleton Robot. In *International Conference on Intelligent Robotics and Applications 2012* Oct 3 (pp. 545-554). Springer, Berlin, Heidelberg.
- Guo Z, Yu H, Yin YH. Developing a mobile lower limb robotic exoskeleton for gait rehabilitation. *Journal of Medical Devices*. 2014 Dec 1;8(4):044503.
- Ha KH, Murray SA, Goldfarb M. An approach for the cooperative control of FES with a powered exoskeleton during level walking for persons with paraplegia. *IEEE Transactions on Neural Systems and Rehabilitation Engineering*. 2016 Apr;24(4):455-66.
- Haghighi HE, Nekoui MA. Inverse kinematic for an 8 degrees of freedom biped robot based on cubic polynomial trajectory generation. In *Control, Instrumentation and Automation (ICCIA)*, 2011 2nd International Conference on 2011 Dec 27 (pp. 935-940). IEEE.
- Hamon A, Aoustin Y, Caro S. Two walking gaits for a planar bipedal robot equipped with a four-bar mechanism for the knee joint. *Multibody System Dynamics*. 2014 Mar 1;31(3):283-307.
- Hamon A, Aoustin Y. Cross four-bar linkage for the knees of a planar bipedal robot. In *Humanoid Robots (Humanoids)*, 2010 10th IEEE-RAS International Conference on 2010 Dec 6 (pp. 379-384). IEEE.
- Hamon A, Aoustin Y. Study of different structures of the knee joint for a planar bipedal robot. In *Humanoid Robots, 2009. Humanoids 2009. 9th IEEE-RAS International Conference on 2009* Dec 7 (pp. 113-120). IEEE.
- Hangalur G, Bakker R, Tomescu S, Chandrashekar N. New Adjustable Unloader Knee Brace and Its Effectiveness. *Journal of Medical Devices*. 2018 Mar 1;12(1):015001.



- Hartenberg RS, Denavit J. Kinematic synthesis of linkages. McGraw-Hill; 1964.
- Hesse S, Uhlenbrock D. A mechanized gait trainer for restoration of gait. *Journal of rehabilitation research and development*. 2000 Nov 1; 37(6):701-8.
- Hirschmann MT, Müller W. Complex function of the knee joint: the current understanding of the knee. *Knee Surgery, Sports Traumatology, Arthroscopy*. 2015 Oct 1;23(10):2780-8.
- Hrones JA. Analysis of the Four-bar Linkage. Published Jointly by the technology Press of the Massachusetts Institute of Technology, and Wiley; 1951.
- Hussain S, Xie SQ, Jamwal PK, Parsons J. An intrinsically compliant robotic orthosis for treadmill training. *Medical engineering & physics*. 2012 Dec 31;34(10):1448-53.
- Hutter M, Remy CD, Hoepflinger MA, Siegwart R. Scarleth: Design and control of a planar running robot. In *Intelligent Robots and Systems (IROS), 2011 IEEE/RSJ International Conference on* 2011 Sep 25 (pp. 562-567). IEEE.
- Hwang WM, Chen YJ. Defect-free synthesis of Stephenson-III motion generators. *Proceedings of the Institution of Mechanical Engineers, Part C: Journal of Mechanical Engineering Science*. 2008 Dec 1;222(12):2485-94.
- International Organization for Standardization, <https://www.iso.org/standard/15800.html>
- Jasuja OP, Harbhajan S, Anupama K. Estimation of stature from stride length while walking fast. *Forensic science international*. 1997 May 5;86(3):181-6.
- Ji Z, Manna Y. Synthesis of a pattern generation mechanism for gait rehabilitation. *Journal of Medical Devices*. 2008 Sep 1;2(3):031004.
- Jin D, Zhang R, Dimo HO, Wang R, Zhang J. Kinematic and dynamic performance of prosthetic knee joint using six-bar mechanism. *Journal of rehabilitation research and development*. 2003 Jan 1;40(1):39.
- Jonathan Kofman PE, PhD. Engineering design review of stance-control knee-ankle-foot orthoses. *Journal of rehabilitation research and development*. 2009 Feb 10;46(2):257.
- Kafash SH, Nahvi A. Optimal synthesis of four-bar motion generator linkages using circular proximity function. *Proceedings of the Institution of Mechanical Engineers, Part C: Journal of Mechanical Engineering Science*. 2015 Dec 11:0954406215621586.

- Kawamoto H, Hayashi T, Sakurai T, Eguchi K, Sankai Y. Development of single leg version of HAL for hemiplegia. In *Engineering in Medicine and Biology Society, 2009. EMBC 2009. Annual International Conference of the IEEE 2009 Sep 3* (pp. 5038-5043). IEEE.
- Kawasaki S, Ohata K, Tsuboyama T, Sawada Y, Higashi Y. Development of new rehabilitation robot device that can be attached to the conventional Knee-Ankle-Foot-Orthosis for controlling the knee in individuals after stroke. In *Rehabilitation Robotics (ICORR), 2017 International Conference on 2017 Jul 17* (pp. 304-307). IEEE.
- Khorshidi M, Soheilypour M, Peyro M, Atai A, Panahi MS. Optimal design of four-bar mechanisms using a hybrid multi-objective GA with adaptive local search. *Mechanism and Machine Theory*. 2011 Oct 31;46(10):1453-65.
- Kim JH, Shim M, Ahn DH, Son BJ, Kim SY, Kim DY, Baek YS, Cho BK. Design of a knee exoskeleton using foot pressure and knee torque sensors. *International Journal of Advanced Robotic Systems*. 2015 Aug 20;12(8):112.
- Kim JW, Jeong S, Kim J, Seo T. Numerical hybrid Taguchi-random coordinate search algorithm for path synthesis. *Mechanism and Machine Theory*. 2016 Aug 31;102:203-16.
- Kim JW, Seo T, Kim J. A new design methodology for four-bar linkage mechanisms based on derivations of coupler curve. *Mechanism and Machine Theory*. 2016 Jun 30;100:138-54.
- Kinzel G, Waldron K. *Kinematics, Dynamics, and Design of Machinery*. Jone Wiley & Sons. 1999.
- Kong K, Jeon D. Design and control of an exoskeleton for the elderly and patients. *IEEE/ASME Transactions on mechatronics*. 2006 Aug;11(4):428-32.
- Kong K, Moon H, Hwang B, Jeon D, Tomizuka M. Impedance compensation of SUBAR for back-drivable force-mode actuation. *IEEE Transactions on Robotics*. 2009 Jun;25(3):512-21.
- Kora K, Stinear J, McDaid A. Design, Analysis, and Optimization of an Acute Stroke Gait Rehabilitation Device. *Journal of Medical Devices*. 2017 Mar 1;11(1):014503.
- Krishnamurty S, Turcic DA. A general method of determining and eliminating branching in planar multiloop mechanisms. *ASME J. Mech. Des.* 1988 Dec 1;110(4):414-22.

- Krishnamurty S, Turcic DA. Optimal synthesis of mechanisms using nonlinear goal programming techniques. *Mechanism and machine Theory*. 1992 Sep 1;27(5):599-612.
- Kubo K, Miyoshi T, Kanai A, Terashima K. Gait rehabilitation device in central nervous system disease: a review. *Journal of Robotics*. 2011;2011.
- Kunjur A, Krishnamurty S. Genetic algorithms in mechanism synthesis. *Journal of Applied Mechanisms and Robotics*. 1997;4(2):18-24.
- Lai X, Zhang M. An efficient ensemble of GA and PSO for real function optimization. In *Computer Science and Information Technology, 2009. ICCSIT 2009. 2nd IEEE International Conference on 2009 Aug 8* (pp. 651-655). IEEE.
- Lee WT, Russell K. Developments in quantitative dimensional synthesis (1970-present): four-bar motion generation. *Inverse Problems in Science and Engineering*. 2017 Apr 7:1-6.
- Lin WY. A GA–DE hybrid evolutionary algorithm for path synthesis of four-bar linkage. *Mechanism and Machine Theory*. 2010 Aug 31;45(8):1096-107.
- Liu CH, Lin MH, Huang YC, Pai TY, Wang CM. The development of a multi-legged robot using eight-bar linkages as leg mechanisms with switchable modes for walking and stair climbing. In *Control, Automation and Robotics (ICCAR), 2017 3rd International Conference on 2017 Apr 24* (pp. 103-108). IEEE.
- Low KH, Yin Y. Providing assistance to knee in the design of a portable active orthotic device. In *Automation Science and Engineering, 2006. CASE'06. IEEE International Conference on 2006 Oct 8* (pp. 188-193). IEEE.
- Mao Y, Agrawal SK. Design of a cable-driven arm exoskeleton (CAREX) for neural rehabilitation. *IEEE Transactions on Robotics*. 2012 Aug;28(4):922-31.
- Mariappan J, Krishnamurty S. A generalized exact gradient method for mechanism synthesis. *Mechanism and Machine Theory*. 1996 May 1;31(4):413-21.
- Martínez-Alfaro H. Four-bar mechanism synthesis for n desired path points using simulated annealing. In *Advances in Metaheuristics for Hard Optimization 2007* (pp. 23-37). Springer Berlin Heidelberg.
- Masiero S, Mastrocostas M, Musumeci A. Orthoses in Older Patients. In *Rehabilitation Medicine for Elderly Patients 2018* (pp. 133-145). Springer, Cham.
- Masrom S, Moser I, Montgomery J, Abidin SZ, Omar N. Hybridization of particle swarm optimization with adaptive genetic algorithm operators. In *Intelligent*

- Systems Design and Applications (ISDA), 2013 13th International Conference on 2013 Dec 8 (pp. 153-158). IEEE.
- McCarthy JM. Geometric Design of Linkages. Springer Science & Business Media; (Vol 11) 2000 Apr 26.
- McKendry J, Brown B, Westervelt ER, Schmiedeler JP. Design and analysis of a class of planar biped robots mechanically coordinated by a single degree of freedom. *Journal of Mechanical Design*. 2008 Oct 1;130(10):102302.
- Menschik A. Mechanik des kniegelenkes. *Z Orthop*. 1974 Jun;112:481-95.
- Mirjalili S, Lewis A. The whale optimization algorithm. *Advances in Engineering Software*. 2016 May 31;95:51-67.
- Mirjalili S. Moth-flame optimization algorithm: A novel nature-inspired heuristic paradigm. *Knowledge-Based Systems*. 2015 Nov 30;89:228-49.
- Mirth JA, Chase TR. Circuit rectification for four precision position synthesis of Stephenson six-bar linkages. *Transactions-american society of mechanical engineers journal of mechanical design*. 1995a Dec 1;117:644-5.
- Mirth JA, Chase TR. Circuit rectification for four precision position synthesis of four-bar and Watt six-bar linkages. *Journal of Mechanical Design*. 1995b Dec 1;117(4):612-9.
- Mirth JA. The application of geometric constraint programming to the design of motion generating six-bar linkages. In *Proceedings of the 2012 ASME International Design Engineering Technical Conferences, Chicago, IL (August 2012)* 2012 Aug 12.
- Motorika, ReoAmbulator, Motorika, Mount Laurel, NJ, USA, 2017, <http://www.motorika.com/?categoryId=90004>.
- Mu X, Wu Q. Sagittal gait synthesis for a five-link biped robot. In *American Control Conference, 2004. Proceedings of the 2004* 2004 Jun 30 (Vol. 5, pp. 4004-4009). IEEE.
- Mu X, Wu Q. Synthesis of a complete sagittal gait cycle for a five-link biped robot. *Robotica*. 2003 Oct;21(5):581-7.
- Mu X. Dynamics and motion regulation of a five. Link biped robot walking in the sagittal pi. 2004 Ane (Doctoral dissertation, The University of Manitoba).
- Mundo D, Gatti G, Dooner DB. Optimized five-bar linkages with non-circular gears for exact path generation. *Mechanism and Machine Theory*. 2009 Apr 30;44(4):751-60.
- Mundo D, Liu JY, Yan HS. Optimal synthesis of cam-linkage mechanisms for precise path generation. *Journal of Mechanical Design*. 2006 Nov 1;128(6):1253-60.

- Nariman-Zadeh N, Felezi M, Jamali A, Ganji M. Pareto optimal synthesis of four-bar mechanisms for path generation. *Mechanism and Machine Theory*. 2009 Jan 31;44(1):180-91.
- Nishad SS, Dutta A, Saxena A. Design and control of a three finger hand exoskeleton for translation of a slender object. In *Ubiquitous Robots and Ambient Intelligence (URAI)*, 2014 11th International Conference on 2014 Nov 12 (pp. 179-184). IEEE.
- Nokleby SB, Podhorodeski RP. Optimization-based synthesis of Grashof geared five-bar mechanisms. *Journal of mechanical design*. 2001 Dec 1;123(4):529-34.
- Nor FM, Abdullah N, Mustapa AM, Wen LQ, Faisal NA, Nazari DA. Estimation of stature by using lower limb dimensions in the Malaysian population. *Journal of forensic and legal medicine*. 2013 Nov 1;20(8):947-52.
- Norton RL. *Kinematics and Dynamics of Machinery*. McGraw-Hill Higher Education; 2011 May 19.
- Ohta Y, Yano H, Suzuki R, Yoshida M, Kawashima N, Nakazawa K. A two-degree-of-freedom motor-powered gait orthosis for spinal cord injury patients. *Proceedings of the Institution of Mechanical Engineers, Part H: Journal of Engineering in Medicine*. 2007 Jun 1;221(6):629-39.
- Paluska SA, McKeag DB. Knee braces: current evidence and clinical recommendations for their use. *American family physician*. 2000 Jan; 61(2):411-8.
- Paradis MJ, Willmert KD. Optimal mechanism design using the gauss constrained method. *Journal of Mechanisms, Transmissions, and Automation in Design*. 1983 Jun 1;105(2):187-96.
- Parrish B, McCarthy JM. Identification of a usable six-bar linkage for dimensional synthesis. In *New Trends in Mechanism and Machine Science 2013* (pp. 255-262). Springer, Dordrecht.
- Pathak VK, Singh AK, Singh R, Chaudhary H. A modified algorithm of Particle Swarm Optimization for form error evaluation. *tm-Technisches Messen*. 2017 Apr 20;84(4):272-92.
- Penunuri F, Peón-Escalante R, Villanueva C, Pech-Oy D. Synthesis of mechanisms for single and hybrid tasks using differential evolution. *Mechanism and Machine theory*. 2011 Oct 31;46(10):1335-49.
- Perry J, Davids JR. Gait analysis: normal and pathological function. *Journal of Pediatric Orthopaedics*. 1992 Nov 1;12(6):815.

- Peshkin M, Brown DA, Santos-Munné JJ, Makhlin A, Lewis E, Colgate JE, Patton J, Schwandt D. KineAssist: A robotic overground gait and balance training device. In *Rehabilitation Robotics, 2005. ICORR 2005. 9th International Conference on* 2005 Jun 28 (pp. 241-246). IEEE.
- Plecnik MM, McCarthy JM. Design of Stephenson linkages that guide a point along a specified trajectory. *Mechanism and Machine Theory*. 2016 Feb 29;96:38-51.
- Plecnik MM, McCarthy JM. Kinematic synthesis of Stephenson III six-bar function generators. *Mechanism and Machine Theory*. 2016 Mar 31;97:112-26.
- Prakash C, Gupta K, Mittal A, Kumar R, Laxmi V. Passive marker based optical system for gait kinematics for lower extremity. *Procedia Computer Science*. 2015 Jan 1;45:176-85.
- Quintero H, Farris R, Hartigan C, Clesson I, Goldfarb M. A powered lower limb orthosis for providing legged mobility in paraplegic individuals. *Topics in spinal cord injury rehabilitation*. 2011 Jul 1;17(1):25-33.
- Rao R, Patel V. An elitist teaching-learning-based optimization algorithm for solving complex constrained optimization problems. *International Journal of Industrial Engineering Computations*. 2012;3(4):535-60.
- Rao RV, Savsani VJ, Vakharia DP. Teaching-learning-based optimization: a novel method for constrained mechanical design optimization problems. *Computer-Aided Design*. 2011 Mar 31;43(3):303-15.
- Rao RV, Savsani VJ. Mechanical design optimization using advanced optimization techniques. *Springer Science & Business Media*; 2012 Jan 15.
- Rao RV. Teaching-Learning-Based Optimization Algorithm. In *Teaching Learning Based Optimization Algorithm 2016* (pp. 9-39). Springer International Publishing.
- Reinkensmeyer D, Wynne JH, Harkema SJ. A robotic tool for studying locomotor adaptation and rehabilitation. In *Engineering in Medicine and Biology, 2002. 24th Annual Conference and the Annual Fall Meeting of the Biomedical Engineering Society EMBS/BMES Conference, 2002. Proceedings of the Second Joint 2002 Oct 23* (Vol. 3, pp. 2353-2354). IEEE.
- ReWalk Robotics, Inc., 200 Donald Lynch Boulevard Marlborough, MA 01752, USA, <http://rewalk.com/>
- Riener R, Lunenburger L, Jezernik S, Anderschitz M, Colombo G, Dietz V. Patient-cooperative strategies for robot-aided treadmill training: first experimental results.

- IEEE transactions on neural systems and rehabilitation engineering. 2005 Sep;13(3):380-94.
- Robson NP, McCarthy JM. Planar four-bar linkages using task velocity specifications. *International Journal of Engineering Research & Innovation*. 2010;33.
- Rosen JB. The gradient projection method for nonlinear programming. Part I. Linear constraints. *Journal of the society for industrial and applied mathematics*. 1960 Mar;8(1):181-217.
- Roth B. On the screw axes and other special lines associated with spatial displacements of a rigid body. *Journal of Engineering for Industry*. 1967 Feb 1;89(1):102-10.
- Russell K, Shen Q, Sodhi RS. *Mechanism design: visual and programmable approaches*. CRC Press; 2013 Dec 2.
- Ruthenberg BJ, Wasylewski NA, Beard JE. An experimental device for investigating the force and power requirements of a powered gait orthosis. *Journal of rehabilitation research and development*. 1997 Apr 1;34(2):203.
- Sancibrian R, García P, Viadero F, Fernandez A. A general procedure based on exact gradient determination in dimensional synthesis of planar mechanisms. *Mechanism and Machine Theory*. 2006 Feb 28;41(2):212-29.
- Sancibrian R, Sarabia EG, Sedano A, Blanco JM. A general method for the optimal synthesis of mechanisms using prescribed instant center positions. *Applied Mathematical Modelling*. 2016 Feb 1;40(3):2206-22.
- Santra D, Mukherjee A, Sarker K, Chatterjee D. Hybrid PSO-ACO algorithm to solve economic load dispatch problem with transmission loss for small scale power system. In *Intelligent Control Power and Instrumentation (ICICPI), International Conference on* 2016 Oct 21 (pp. 226-230). IEEE.
- Sardashti A, Daniali HM, Varedi SM. Optimal free-defect synthesis of four-bar linkage with joint clearance using PSO algorithm. *Meccanica*. 2013 Sep 1;48(7):1681-93.
- Saremi S, Mirjalili S, Lewis A. Grasshopper optimisation algorithm: Theory and application. *Advances in Engineering Software*. 2017 Mar 31;105:30-47.
- Schmiedeler JP, Westervelt ER, Dunki-Jacobs AR. Integrated design and control of a biped robot. In *Proceedings of the 2005 ASME International Design Engineering Technical Conference* 2005 Jan 1 (pp. 24-28).
- Selvi Ö, Yavuz S. Design and Dimensional Optimization of a Novel Walking Mechanism with Firefly Algorithm. In *International Workshop on Computational Kinematics* 2017 May 22 (pp. 67-75). Springer, Cham.

- Seo KH, Park Y, Yun S, Park S, Jeon KW, Jun J, Kim DH. Robotic gait rehabilitation system on treadmill. In *Ubiquitous Robots and Ambient Intelligence (URAI)*, 2014 11th International Conference on 2014 Nov 12 (pp. 116-120). IEEE.
- Sheba JK, Elara MR, Martínez-García E, Tan-Phuc L. Synthesizing reconfigurable foot traces using a Klann mechanism. *Robotica*. 2017 Jan;35(1):189-205.
- Shen Q, Lee WT, Russell K. On Adjustable Planar Four-Bar Motion Generation With Order, Branch and Circuit Defect Rectification. *Journal of Mechanisms and Robotics*. 2015 Aug 1;7(3):034501.
- Shen Z, Allison G, Cui L. An Integrated Type and Dimensional Synthesis Method to Design One Degree-of-Freedom Planar Linkages With Only Revolute Joints for Exoskeletons. *Journal of Mechanical Design*. 2018 Sep 1;140(9):092302.
- Sim FH. The Knee: Form, Function, and Ligament Reconstruction. In *Mayo Clinic Proceedings* 1984 Jan 1 (Vol. 59, No. 1, p. 55). Elsevier.
- Skelton J, Wu SK, Shen X. Design of a Powered Lower-Extremity Orthosis for Sit-to-Stand and Ambulation Assistance. *Journal of Medical Devices*. 2013 Sep 1;7(3):030910.
- Smaili A, Diab N. Optimum synthesis of hybrid-task mechanisms using ant-gradient search method. *Mechanism and Machine Theory*. 2007 Jan 31;42(1):115-30.
- Smit-Anseeuw N, Gleason R, Vasudevan R, Remy CD. The Energetic Benefit of Robotic Gait Selection—A Case Study on the Robot RAMone. *IEEE Robotics and Automation Letters*. 2017 Apr;2(2):1124-31.
- Soh GS, Pérez Gracia A, McCarthy JM. The kinematic synthesis of mechanically constrained planar 3R chains. In *Proceedings of EuCoMeS, the first European Conference on Mechanism Science Obergurgl (Austria), February 21–26 2006* 2006 (pp. 1-17).
- Sohoni VN, Haug EJ. A state space technique for optimal design of mechanisms. *Journal of Mechanical Design*. 1982 Oct 1;104(4):792-8.
- Soleimani H, Kannan G. A hybrid particle swarm optimization and genetic algorithm for closed-loop supply chain network design in large-scale networks. *Applied Mathematical Modelling*. 2015 Jul 15;39(14):3990-4012.
- Sonawale KH, McCarthy JM. A design system for eight-bar linkages as constrained 4r serial chains. *Journal of Mechanisms and Robotics*. 2016 Feb 1;8(1):011016.



- Sreenath K, Park HW, Poulakakis I, Grizzle JW. A compliant hybrid zero dynamics controller for stable, efficient and fast bipedal walking on MABEL. *The International Journal of Robotics Research*. 2011 Aug;30(9):1170-93.
- Stauffer Y, Allemand Y, Bouri M, Fournier J, Clavel R, Métrailler P, Brodard R, Reynard F. The WalkTrainer—a new generation of walking reeducation device combining orthoses and muscle stimulation. *IEEE Transactions on neural systems and rehabilitation engineering*. 2009 Feb;17(1):38-45.
- Stegall P, Winfree K, Zanotto D, Agrawal SK. Rehabilitation exoskeleton design: Exploring the effect of the anterior lunge degree of freedom. *IEEE Transactions on Robotics*. 2013 Aug;29(4):838-46.
- Stills ML, Knee Joint Materials and Components. *Clinical prosthetics and orthotics*. 1987; 11(2): 91-94.
- Subbian T, Flugrad DR. Six and seven position triad synthesis using continuation methods. *Journal of Mechanical Design*. 1994 Jun 1;116(2):660-5.
- Suh CH, Radcliffe CW. *Kinematics and mechanisms design*. Wiley; 1978.
- Suh CH, Radcliffe CW. Synthesis of plane linkages with use of the displacement matrix. *Journal of Engineering for Industry*. 1967 May 1;89(2):206-14.
- Suh CH. Design of space mechanisms for rigid body guidance. *Journal of Engineering for Industry*. 1968 Aug 1;90(3):499-506.
- Tian F, Hefzy MS, Elahinia M. State of the Art Review of Knee–Ankle–Foot Orthoses. *Annals of biomedical engineering*. 2015 Feb 1;43(2):427-41.
- Ting KL. Five-bar Grashof criteria. *Journal of Mechanisms, Transmissions, and automation in Design*. 1986 Dec 1;108(4):533-7.
- Tinubu SO, Gupta KC. Optimal synthesis of function generators without the branch defect. *Journal of Mechanisms, Transmissions, and Automation in Design*. 1984 Sep 1;106(3):348-54.
- Tsuge BY, McCarthy JM. An Adjustable Single Degree-of-Freedom System to Guide Natural Walking Movement for Rehabilitation. *Journal of Medical Devices*. 2016 Dec 1;10(4):044501.
- Tsuge BY, McCarthy JM. Synthesis of a 10-bar linkage to guide the gait cycle of the human leg. In *Proceeding of ASME 2015 International Design Engineering Technical Conferences and Computers and Information in Engineering Conference* 2015 Aug 2 (pp. 2-5).

- Tsuge BY, Plecnik MM, McCarthy JM. Homotopy directed optimization to design a six-bar linkage for a lower limb with a natural ankle trajectory. *Journal of Mechanisms and Robotics*. 2016 Dec 1;8(6):061009.
- Tzafestas S, Raibert M, Tzafestas C. Robust sliding-mode control applied to a 5-link biped robot. *Journal of Intelligent & Robotic Systems*. 1996 Jan 1;15(1):67-133.
- Ullah I, Kota S. Optimal synthesis of mechanisms for path generation using Fourier descriptors and global search methods. *Journal of Mechanical Design*. 1997 Dec 1;119(4):504-10.
- Unluhisarcikli O, Pietrusinski M, Weinberg B, Bonato P, Mavroidis C. Design and control of a robotic lower extremity exoskeleton for gait rehabilitation. In *Intelligent Robots and Systems (IROS), 2011 IEEE/RSJ International Conference on* 2011 Sep 25 (pp. 4893-4898). IEEE.
- Veneman JF, Kruidhof R, Hekman EE, Ekkelenkamp R, Van Asseldonk EH, Van Der Kooij H. Design and evaluation of the LOPES exoskeleton robot for interactive gait rehabilitation. *IEEE Transactions on Neural Systems and Rehabilitation Engineering*. 2007 Sep;15(3):379-86.
- Waldron KJ, Stevensen EN. Elimination of Branch, Grashof, and Order Defects in Path-Angle Generation and Function Generation Synthesis. *Journal of Mechanical Design*. 1979 Jul 1;101(3):428-37.
- Waldron KJ. Graphical solution of the branch and order problems of linkage synthesis for multiply separated positions. *Journal of Engineering for Industry*. 1977 Aug 1;99(3):591-7.
- Waldron KJ. Elimination of the branch problem in graphical Burmester mechanism synthesis for four finitely separated positions. *Journal of Engineering for Industry*. 1976 Feb 1;98(1):176-82.
- Wampler CW, Morgan AP, Sommese AJ. Complete solution of the nine-point path synthesis problem for four-bar linkages. *Journal of Mechanical Design*. 1992 Mar 1;114(1):153-9.
- Wang P, Low KH, Tow A. Synchronized walking coordination for impact-less footpad contact of an overground gait rehabilitation system: NaTUre-gaits. In *Rehabilitation Robotics (ICORR), 2011 IEEE International Conference on* 2011 Jun 29 (pp. 1-6). IEEE.

- Watanabe K, Funabashi H. Kinematic Analysis of Stephenson Six-Link Mechanisms: 1st Report, Discrimination of Composition Loops. Bulletin of JSME. 1984;27(234):2863-70.
- Watanabe K, Katoh H. Identification of motion domains of planar six-link mechanisms of the Stephenson-type. Mechanism and Machine Theory. 2004 Oct 31;39(10):1081-99.
- West RG, inventor; Healthsouth Corporation, assignee. Powered gait orthosis and method of utilizing same. United States patent US 6,689,075. 2004 Feb 10.
- Wilhelm SR, Sullivan T, Van de Ven JD. Solution rectification of slider-crank mechanisms with transmission angle control. Mechanism and Machine Theory. 2017 Jan 31;107:37-45.
- Wolpert DH, Macready WG. No free lunch theorems for optimization. IEEE transactions on evolutionary computation. 1997 Apr;1(1):67-82.
- Yan HS, Chiou ST. An algorithm for the optimal synthesis of complex function generators. Engineering Optimization+ A35. 1987 Aug 1;12(1):75-88.
- Yang T, Westervelt ER, Schmiedeler JP, Bockbrader RA. Design and control of a planar bipedal robot ERNIE with parallel knee compliance. Autonomous robots. 2008 Nov 1;25(4):317-30.
- Yogesh CK, Hariharan M, Ngadiran R, Adom AH, Yaacob S, Berkai C, Polat K. A new hybrid PSO assisted biogeography-based optimization for emotion and stress recognition from speech signal. Expert Systems with Applications. 2017 Mar 1;69:149-58.
- Yu H, Cruz MS, Chen G, Huang S, Zhu C, Chew E, Ng YS, Thakor NV. Mechanical design of a portable knee-ankle-foot robot. In Robotics and Automation (ICRA), 2013 IEEE International Conference on 2013 May 6 (pp. 2183-2188). IEEE.
- Zeilig G, Weingarden H, Zwecker M, Dudkiewicz I, Bloch A, Esquenazi A. Safety and tolerance of the ReWalk™ exoskeleton suit for ambulation by people with complete spinal cord injury: A pilot study. The journal of spinal cord medicine. 2012 Mar 1;35(2):96-101.
- Zhang C, Norton PR, Hammonds T. Optimization of parameters for specified path generation using an atlas of coupler curves of geared five-bar linkages. Mechanism and machine theory. 1984 Jan 1;19(6):459-66.
- Zhang X, Zhou J, Ye Y. Optimal mechanism design using interior-point methods. Mechanism and Machine Theory. 2000 Jan 31;35(1):83-98.

- Zhang Y, Arakelian V, Le Baron JP. Design of a Legged Walking Robot with Adjustable Parameters. In *Advances in Mechanism Design II 2017* (pp. 65-71). Springer International Publishing.
- Zhou H, Cheung EH. Optimal synthesis of crank–rocker linkages for path generation using the orientation structural error of the fixed link. *Mechanism and Machine Theory*. 2001 Aug 31;36(8):973-82.
- Zimmerman RA. Planar Linkage Synthesis for Mixed Motion, Path and Function Generation Using Poles and Rotation Angles. In *ASME 2017 International Design Engineering Technical Conferences and Computers and Information in Engineering Conference 2017 Aug 6* (pp. V05AT08A047-V05AT08A047). American Society of Mechanical Engineers.

## Position Analysis of Planar Linkages

Loop-closure equation plays an important role in the kinematic analysis of planar linkages. In this appendix, the loop-closure equation is solved.

### A.1 Position Analysis of Four-Bar Linkage

In this section, the loop-closure equations are solved for four-bar linkages presented in chapter 5 (Fig 5.1).

The loop closure equation for four-bar can be rewritten in the scalar form as:

$$r_2 \cos \theta_2 + r_3 \cos \theta_3 - r_1 \cos \theta_1 - r_4 \cos \theta_4 = 0 \quad (\text{A.1})$$

$$r_{21} \sin \theta_2 + r_3 \sin \theta_3 - r_1 \sin \theta_1 - r_4 \sin \theta_4 = 0 \quad (\text{A.2})$$

Squaring and adding Eqs. (A.1) and (A.2), gives  $\theta_{41}$ .in terms of  $\theta_{11}$  and  $\theta_{21}$

$$A_1 = 2(r_1 r_4 \cos \theta_1 - r_2 r_4 \cos \theta_2)$$

$$B_1 = 2(r_1 r_4 \sin \theta_1 - r_2 r_4 \sin \theta_2)$$

$$C_1 = r_1^2 + r_2^2 + r_4^2 - r_3^2 - 2r_1 r_2 (\cos \theta_1 \cos \theta_2 + \sin \theta_1 \sin \theta_2)$$

$$\theta_4 = 2 \tan^{-1} \left( \frac{-B_1 + \sigma \sqrt{(B_1^2 - C_1^2 + A_1^2)}}{C_1 - A_1} \right)$$

$$\sigma = \mp, \text{ for open and cross assembly mode}$$

Rearranging and dividing Eqs (A.1) and (A.2) gives  $\theta_{31}$  as follows:

$$\theta_{31} = \tan^{-1} \frac{r_{11} \sin \theta_{11} + r_{41} \sin \theta_{41} - r_{21} \sin \theta_{21}}{r_{11} \cos \theta_{11} + r_{41} \cos \theta_{41} - r_{21} \cos \theta_{21}}$$

### A.2 Position Analysis of Six-Bar Linkage

In this section, the loop-closure equations are solved for four-bar linkages presented in chapter 5 (Fig 5.3). The loop closure equation for Loop I can be rewritten in the scalar form as:

$$r_{21} \cos \theta_{21} + r_{31} \cos \theta_{31} - r_{11} \cos \theta_{11} - r_{41} \cos \theta_{41} = 0 \quad (\text{A.3})$$

$$r_{21} \sin \theta_{21} + r_{31} \sin \theta_{31} - r_{11} \sin \theta_{11} - r_{41} \sin \theta_{41} = 0 \quad (\text{A.4})$$

On squaring and adding Eqs. (A.3) and (A.4) gives  $\theta_{41}$ .in terms of  $\theta_{11}$  and  $\theta_{21}$

$$\theta_{41} = 2 \tan^{-1} \left( \frac{-B_1 + \sigma \sqrt{(B_1^2 - C_1^2 + A_1^2)}}{C_1 - A_1} \right)$$

$$\sigma = \mp, \text{ for open and cross assembly mode}$$

$$A_1 = 2(r_{11} r_{41} \cos \theta_{11} - r_{21} r_{41} \cos \theta_{21})$$

$$B_1 = 2(r_{11} r_{41} \sin \theta_{11} - r_{21} r_{41} \sin \theta_{21})$$

$$C_1 = r_{11}^2 + r_{21}^2 + r_{41}^2 - r_{31}^2 - 2r_{11} r_{21} (\cos \theta_{11} \cos \theta_{21} + \sin \theta_{11} \sin \theta_{21})$$

Rearranging and dividing Eqs (A.3) and (A.4) gives  $\theta_{31}$  as follows:

$$\theta_{31} = \tan^{-1} \frac{r_{11} \sin \theta_{11} + r_{41} \sin \theta_{41} - r_{21} \sin \theta_{21}}{r_{11} \cos \theta_{11} + r_{41} \cos \theta_{41} - r_{21} \cos \theta_{21}}$$

The loop closure equation for Loop II can be rewritten in the scalar form as:

$$r_{22} \cos \theta_{22} + r_{32} \cos \theta_{32} + r_{52} \cos \theta_{52} - r_{12} \cos \theta_{12} - r_{62} \cos \theta_{62} = 0 \quad (\text{A.5})$$

$$r_{22} \sin \theta_{22} + r_{32} \sin \theta_{32} + r_{52} \sin \theta_{52} - r_{12} \sin \theta_{12} - r_{62} \sin \theta_{62} = 0 \quad (\text{A.6})$$

On squaring and adding Eqs. (A.5) and (A.6) generates the expression for  $\theta_{62}$ . Dividing Eqs. (A.5) and (A.6) generates the expression for  $\theta_{52}$ .

$$\theta_{62} = 2 \tan^{-1} \frac{-B_2 + \sigma \sqrt{(B_2^2 - C_2^2 + A_2^2)}}{C_2 - A_2}$$

$$A_2 = 2(r_{62}r_{12} \cos \theta_{12} - (r_{62}r_{22} \cos \theta_{22} - r_{62}r_{32} \cos \theta_{32}))$$

$$B_2 = 2(r_{62}r_{12} \sin \theta_{12} - (r_{62}r_{22} \sin \theta_{22} - r_{62}r_{32} \sin \theta_{32}))$$

$$C_2 = r_{62}^2 + r_{12}^2 + r_{22}^2 + r_{32}^2 - r_{52}^2 +$$

$$2r_{22}r_{32}(\cos \theta_{22} \cos \theta_{32} + \sin \theta_{22} \sin \theta_{32}) -$$

$$2r_{12}r_{22}(\cos \theta_{12} \cos \theta_{22} + \sin \theta_{12} \sin \theta_{22}) -$$

$$2r_{12}r_{32}(\cos \theta_{12} \cos \theta_{32} + \sin \theta_{12} \sin \theta_{32})$$

$$\theta_{52} = \tan^{-1} \frac{r_{62} \sin \theta_{62} + r_{12} \sin \theta_{12} - r_{22} \sin \theta_{22} - r_{32} \sin \theta_{32}}{r_{62} \cos \theta_{62} + r_{12} \cos \theta_{12} - r_{22} \cos \theta_{22} - r_{32} \cos \theta_{32}}$$

### A.3 Solution of loop closure equation when $\theta_{knee}$ and $\theta_1$ are known:

The loop-closure equation (See Fig 7.3 for illustration) can be used to determine unknown angles of the four-bar linkage, namely,  $\theta_2$  and  $\theta_4$ , as follows:

$$\mathbf{r}_2 + \mathbf{r}_3 = \mathbf{r}_1 + \mathbf{r}_4$$

$$\theta_3 = \theta_{knee} + \theta_1$$

$$A \cos \theta_4 + B \sin \theta_4 + C = 0$$

$$A = 2r_1r_4 \cos \theta_1 - 2r_3r_4 \cos \theta_3$$

$$B = 2r_1r_4 \sin \theta_1 - 2r_3r_4 \sin \theta_3$$

$$C = r_1^2 + r_3^2 + r_4^2 - r_2^2 - 2r_1r_3(\cos \theta_1 \cos \theta_3 + \sin \theta_1 \sin \theta_3)$$

$$\theta_4 = 2 \tan^{-1} \left( \frac{-B + \sigma \sqrt{B^2 + A^2 - C^2}}{C - A} \right)$$

$$\theta_2 = \tan^{-1} \left( \frac{r_1 \sin \theta_1 + r_4 \sin \theta_4 - r_3 \sin \theta_3}{r_1 \cos \theta_1 + r_4 \cos \theta_4 - r_3 \cos \theta_3} \right)$$

## Refinement Scheme for TLBO

The teaching-learning-based optimization is a well-established nature-inspired algorithm that is used for distinct applications. In this Appendix, a refinement scheme is proposed to reduce the computational effort during synthesis of linkages for path generation.

### B.1 Teaching-learning-based optimization algorithm

This algorithm is based on the philosophy of teaching and learning. In this algorithm, the two basic modes of the learning, i.e., through teacher (known as teaching phase) and through interaction with the other learners (known as learning phase) are considered. These modes are modelled mathematically and implemented for the optimization process. In TLBO, the group of learners is considered as population, and different courses offered to the learners are considered as design variables. The numeric values of design variables are considered as the course marks. The Learners' result is akin to fitness function value of the optimization method. The TLBO algorithm works in two phases, namely, teaching phase and learning phase for each iteration.

#### B.1.1 Teacher phase

Teaching phase is the first part of the TLBO algorithm where the learners learn through the teacher. Since, the teacher is considered as the highly learned, knowledgeable, and experienced person who shares knowledge with the learners. Thus, the best learner of the entire population is identified as 'teacher'. A good teacher can increase the level of learners up to his or her own level. Hence, the teacher tries to increase the mean result of the class of learners that depends on the teacher and learners' qualities. In this phase, course marks of all learners are updated by of best course marks, i.e., of the teacher as shown in Fig B.1. Then, initial and updated course marks of learners are compared while course marks of the learner corresponding to the better result is stored for the new class of learners. The teacher phase ends with the creation of new class of learners. This new class of learners is considered as the initial population for the 'Learner phase.'

#### B.1.2 Learner phase

Through two ways, learners can improve their knowledge: one from the input given by the teacher and the other through interaction among themselves. Here learner improves his/her knowledge through discussions, presentations, and interaction with other learners. Each learner interacts randomly with at least one other learner of his class to improve his/her marks. The course marks of the learner are updated if the other learner

has the better result in the corresponding courses, as shown in the Learning phase of Fig B.1. Then, each of the initial and updated learners' result corresponding to the course marks is compared similar to the Teaching phase. The learner with the better result corresponding to the course marks are collected for the final class of learners (population). This marks the end of the Learning phase of the algorithm. The completion of one teaching-learning cycle represents one iteration. The process of the algorithm continues until the termination criteria is achieved. The scheme of TLBO algorithm is shown in Fig B.1.

Notations used in the TLBO algorithm are defined as follows:

$p$  = Number of learners, i.e., population size

$L_i, U_i$  = Lower and upper bounds for the  $i^{th}$  course marks

$x_i$  =  $i^{th}$  design variable, i.e., course offered to learner

$n$  = Number of design variables

$x_{ij}$  = Marks in the  $i^{th}$  course for  $j^{th}$  learner

$t$  =  $t^{th}$  iteration, i.e., a teaching-learning cycle

$\mu_i$  = Mean of the  $i^{th}$  course for whole class of learners

$M_i$  = Marks of the  $i^{th}$  course whose objective function value is minimum

$f_j$  = Objective function value of the  $j^{th}$  learner

$rand$  = Any random number in range of 0 and 1

The probability of obtaining the feasible solution which satisfies the constraints is minimal with the initial random population. Hence, refinement scheme is applied after initial population generation to reduce the computational effort. The scheme modifies the chosen initial population as per the feasibility to make an effective mechanism. This refinement scheme is applied to well-established TLBO algorithm before the initial calculation of objective function, after that, constraints are applied. The refinement scheme for TLBO is presented here in two stages- for Grashof constraint and order constraint. In Grashof refinement scheme, first four design variables in design vector  $\mathbf{x}^*$  are rearranged such that it follows Grashof condition, Eq.(5.6), whereas order scheme



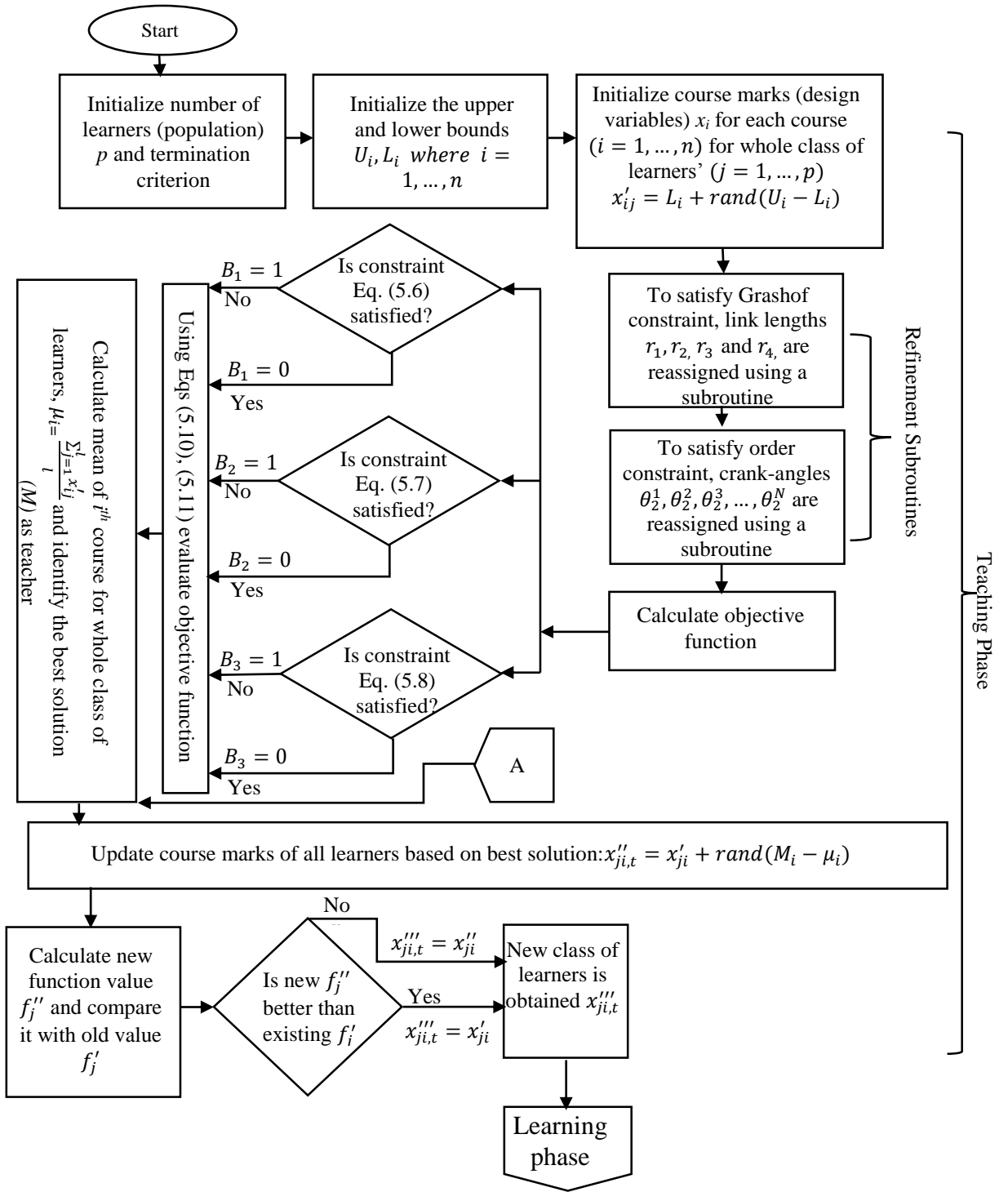
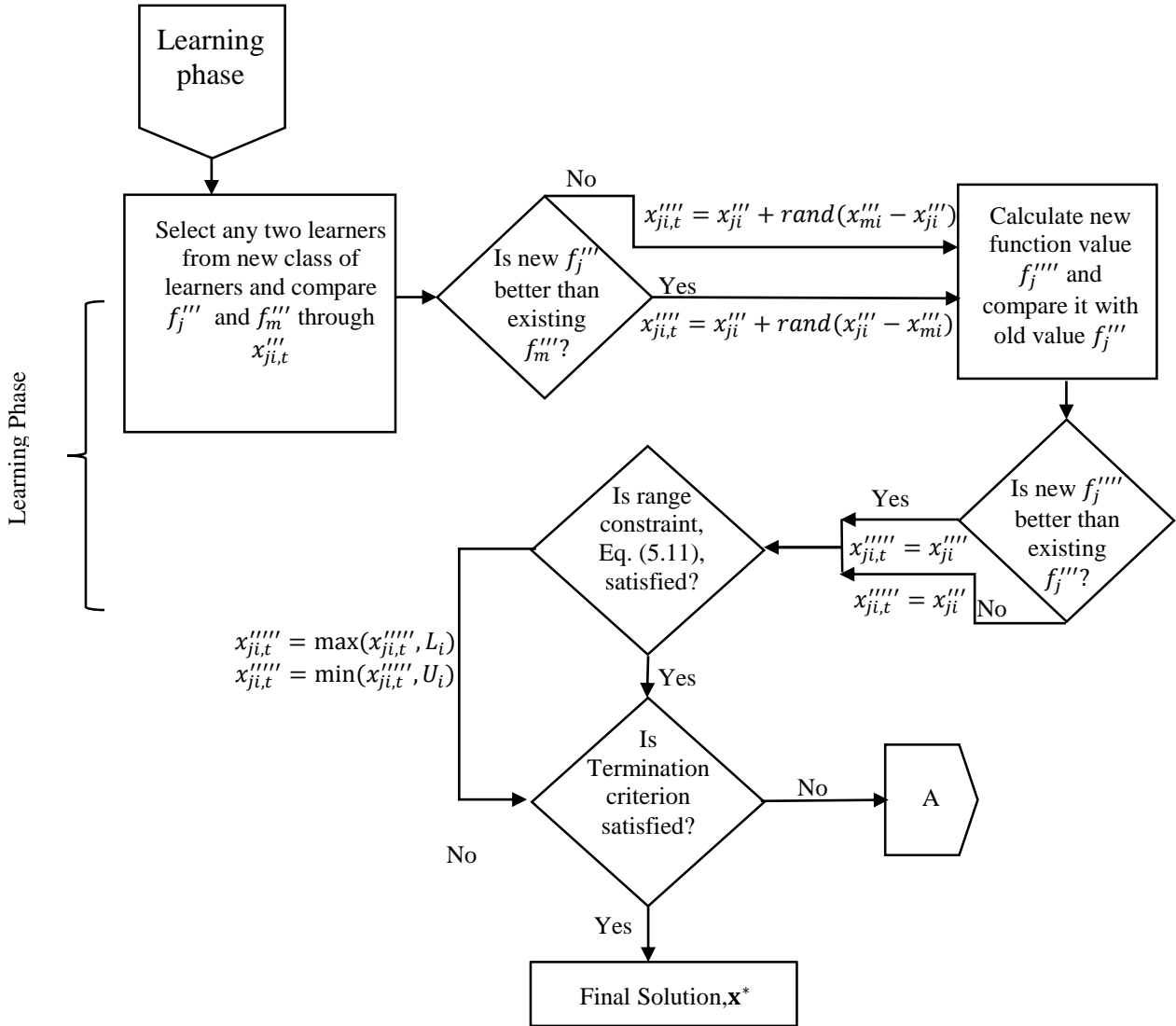


Fig. B.1 Continued



**Fig. B.1** Scheme of the TLBO algorithm for defect-free synthesis of crank-rocker mechanism

rearranges  $\theta_2^1, \theta_2^2, \theta_2^3, \dots, \theta_2^N$  according to the constraint in Eq.(5.7). Note that  $x_{ij}', x_{ij}''$  and  $x_{ij}'''$  represent the course marks updations in Teaching phase whereas  $x_{ij}''''$  and  $x_{ij}'''''$  represent course marks updations in Learning phase. Five classes of learners are formed in each iteration. The fifth class of learners obtained at the end of Learning phase of the current iteration is treated as initial population (class of learner) for Teaching phase of the next iteration. Here, the termination criterion for TLBO algorithm is considered as the number of function evaluations or the number of iterations. The number of function evaluations depends on the number of iterations and population size (learners' class size). The number of function evaluations is equal to double the product of the number of iterations and class size (or population size). Therefore, the number of design

variables (courses) do not affect the function evaluations but may affect the computational effort of the algorithm. This algorithm has been used effectively for the optimization of the mechanical design of disc clutch brake, step cone pulley, Belleville spring, hydrostatic thrust bearing and robot gripper (Rao et al., 2011). However, it is implemented with modification to the synthesis of the crank-rocker mechanism for defect-free path generation, for the first time in this study.



### MATLAB® code for HTLPSO algorithm

A HTLPSO algorithm is hybridized by merging TLBO and PSO algorithms. The MATLAB® code of the HTLPSO algorithms is presented here.

#### C.1 HTLPSO algorithm

```

clc; close all; clear all;
tic % Start Stopwatch
population_size=[]; % size of population
variables=[]; % number of design variables
iteration=[]; % number of iterations
ll=[];
ul=[];
lower_limit=ll; % lower limit on design variables
upper_limit=ul; upper limit on design variables
population_sizeTLBO=ceil(population_size*0.5);
%% RUNS
maxrun=10;
for run=1:maxrun
run;
%% TLBO STARTS HERE
%% Start of Teacher Phase
%% Step 1:Initialize population and result (Table 1)
for j=1:population_size
for k=1:variables
mark(k)=(ll(k))+((ul(k)-ll(k))*rand);
end
pop1(j,:)=mark;
pop1_result(j)=objective_function(pop1(j,:));
end
for i=1:iteration
%% Step 2:Calculating mean for variables
mean_pop1=mean(pop1);
%% Step 3:Identify best solution
[r1 r2]=sort(pop1_result);

```

```

best=pop1(r2(1,:));
%% Step 4:Modify solution based on best solution (Table 2)
for j=1:(population_sizeTLBO)
for k=1:variables
pop2(j,k)=pop1(j,k)+((best(k)-mean_pop1(k))*rand);
end
pop2_result(j)=objective_function(pop2(j,:));
%% Step 5:selection of better solution (Table 3)
if pop2_result(j)<pop1_result(j)
pop3(j,:)=pop2(j,:);
pop3_result(j)=pop2_result(j);
elseif pop2_result(j)>pop1_result(j)
pop3(j,:)=pop1(j,:);
pop3_result(j)=pop1_result(j);
end
end
%% For N/2 best

[rt1 rt2]=sort(pop3_result);
for i=1:(population_sizeTLBO*0.5)
for j=1:variables
best_pop3(i,j)=pop3(rt2(i),j);
end
best_result_pop3(i)=rt1(1,i);
end
%% End of Teacher Phase
%% PSO to obtain best N/2
m=variables; % number of variables
n=ceil(population_size*0.5); % population size
wmax=0.9; %inertia weight
wmin=0.4;
w=0.7; %inertia weight
c1=2; % acceleration factor
c2=2; % acceleration factor

```

```

LB=ll;
UB=ul;
%% PSO main program
% %pso initialization-----
% for i=1:n
%     for j=1:m
%         x0(i,j)=round(LB(j)+rand()*(UB(j)-LB(j)));
%     end
% end
% for j=1:(n)
% for k=1:variables
% mark(k)=(ll(k))+((ul(k)-ll(k))*rand);
% end
% pop_pso(j,:)=mark;
% pop_pso_result(j)=objective_function(pop_pso(j,:));
% end
x0=pop1;
x=x0;          % initial population
v=0.1*x0;      % initial velocity
for i=1:n
    f0(1,i)=objective_function(x0(i,:));
end
[fmin0,index0]=min(f0);

pbest=x0;      % initial pbest
gbest=x0(index0,:);
%% PSO initialization-----
%% PSO velocity update
    for i=1:n
        for j=1:m
            v(i,j)=w*v(i,j)+c1*rand()*(pbest(i,j)-x(i,j))...
                +c2*rand()*(gbest(1,j)-x(i,j));
        end
    end
end

```

**%% PSO position update**

```
for i=1:n
    for j=1:m
        x(i,j)=x(i,j)+v(i,j);
    end
end
```

**%% handling boundary violations**

```
% for i=1:n
%     for j=1:m
%         if x(i,j)<LB(j)
%             x(i,j)=LB(j);
%         elseif x(i,j)>UB(j)
%             x(i,j)=UB(j);
%         end
%     end
% end
```

```
for j=1:n
for k=1:variables
x(j,k)=max(x(j,k),ll(k));
x(j,k)=min(x(j,k),ul(k));
end
f(j)=objective_function(x(j,:));
end
```

```
% for i=1:n
%     f(1,i)=objective_function(x(i,:));
% end
```

**%% updating pbest and fitness**

```
for i=1:n
    if f(1,i)<f0(1,i)
        pbest(i,:)=x(i,:);
        f0(1,i)=f(1,i);
    end
```

```
end
```

```
[fmin,index]=min(f0);
```



```

% updating gbest and best fitness
    if fmin<fmin0
        gbest=pbest(index,:);
        fmin0=fmin;
    end

%% Combined population of TLBO teacher's phase and PSO total N
%% For N/2 best
    [rp1 rp2]=sort(f0');
    for i=1:(n*0.5)
        for j=1:variables
            best_pso_pop(i,j)=pbest(rp2(i),j);
        end
        best_result_pso(i)=rp1(i,1);
    end

% COMBINED POPULATION N
pop3T=[best_pop3; best_pso_pop];
pop3T_result=[best_result_pop3';best_result_pso'];

%% Start of Learner Phase
%% Step 6: Selection of any two solutions (learners) randomly
    for j=1:population_size*0.5
        hh=ceil(population_size*0.5*rand);
        while hh==j
            hh=ceil(population_size*0.5*rand);
        end

%% Step 7: Comparison of two solutions (learners) (Table 4)
        if pop3T_result(j)<pop3T_result(hh)
            for k=1:variables
                pop4(j,k)=pop3T(j,k)+((pop3T(j,k)-pop3T(hh,k))*rand);
            end
        else
            for k=1:variables
                pop4(j,k)=pop3T(j,k)+((pop3T(hh,k)-pop3T(j,k))*rand);
            end
        end
    end

```

```

end
pop4_result(j)=objective_function(pop4(j,:));
%% Step 8:Comparison of results (learners) (Table 5)
if pop4_result(j)<pop3T_result(j)
pop5(j,:)=pop4(j,:);
pop5_result(j)=pop4_result(j);
elseif pop3T_result(j)<pop4_result(j)
    pop5(j,:)=pop3T(j,:);
pop5_result(j)=pop3T_result(j);
end
end
%% Check for within bound (Handling Constraints)
for j=1:population_size*0.5
for k=1:variables
pop5(j,k)=max(pop5(j,k),ll(k));
pop5(j,k)=min(pop5(j,k),ul(k));
end
pop5_result(j)=objective_function(pop5(j,:));
end
pop1=pop5;
pop1_result=pop5_result;
end
[r1 r2]=sort(pop1_result);
best_result(run)=pop1_result(r2(1));
best_design(run,:)=pop1(r2(1),:);
end
%% To obtain best result and design from all runs
[best_results_all_runs index]=min(best_result);
mean_all_results=sum(best_result(1:run))/run;
best_design_allruns=best_design(index,:);
standard_deviation=std(best_result);
toc

```

### Sagittal Position Analysis of Five-Link Robot: A Case Study

Biped robots are the class of walking machines that imitate the human locomotion (Tzafestas et al., 1996) when moving on rugged terrain, steep slopes, a flat path with obstacles and industrial fields. It has always been mesmerizing for a man to create the mechanical system in his own image. Since 18th century (Chevallereau et al., 2009) the researchers have been working in this area which resulted in the creation of bipeds from Leonardo da Vinci humanoid robot to ASIMO, HONDA, SONY, iROBOT, etc. Locomotion is an important aspect of bipeds, and its trajectory planning would be required under different situations. Alternating repetition of same elementary movement from one leg to another is walking. Biped is expected to walk on the leveled ground, inclined, rough plane, etc. Walking step is composed of two kinematically distinct phases: swing phase or single support phase (SSP) and double support phase (DSP) (Chevallereau et al., 2009). Walking trajectory plays an important role in the linkage synthesis of the knee or whole lower limb. In this Appendix, a five-link robot is modeled to imitate the human walk, and stick diagram of walking robot is presented to validate the results.

#### D.1 Trajectory Generation

A five-link planar biped model as shown in Fig D.1. is taken for sagittal position analysis. All the joints between the links are pinned joints and are actuated.

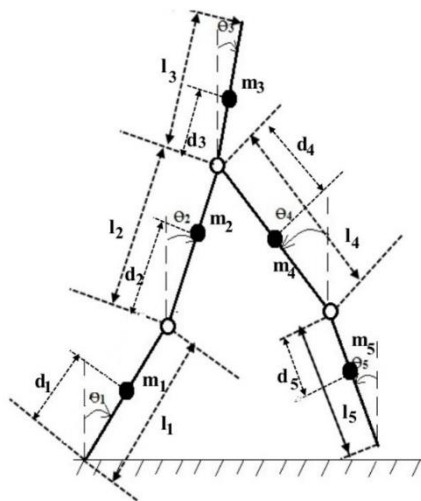


*Fig. D.1 Five-link biped*

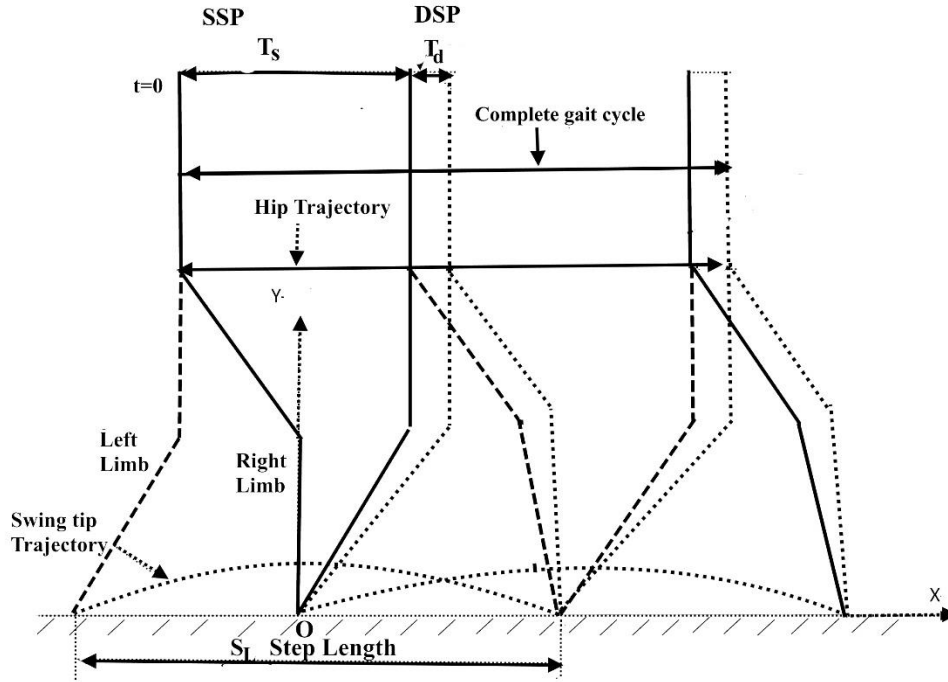


*Fig. D.2 Complete gait cycle*

Each walking step is divided into two kinematically distinct phases SSP and DSP as shown in Fig D.2. SSP is the single support phase which begins with the movement of one limb (swing) in the forward direction while another limb (stance) is pivoted on the ground and terminates with the tip of the swing limb touching the ground. DSP is the double support phase which begins when the heel of the swing limb strikes the ground while stance limb being on the ground. In the subsequent step, the support exchange takes place. Swing limb and hip trajectories are required for obtaining the biped joint profiles (Haghighi et al., 2011 and Mu et al., 2004). These trajectories must satisfy configuration of the biped.

### **D.1.1 Foot Trajectory**

For a planar five-link biped robot, the trajectory of swing limb during SSP can be generated using polynomial interpolation as:

$$x_a(t) = a_0 + a_1t + a_2t^2 + a_3t^3 \quad (D.1)$$

$$y_a(t) = b_0 + b_1t + b_2t^2 + b_3t^3 + b_4t^4 + b_5t^5 \text{ for } 0 \leq t \leq T_s \quad (D.2)$$

Where  $x_a(t)$  and  $y_a(t)$  are coordinates of the tip of the swing limb at time  $t$ . The SSP will finish at  $t=T_s$ . Origin of coordinate frame is fixed at the tip of the supporting limb.

There is a total of ten unknown coefficients  $a_0, a_1, a_2, a_3$  and  $b_0, b_1, b_2, b_3, b_4, b_5$ . Therefore ten constraint equations are required to find them. In SSP, phase begins with lift off of the tip of swing limb and ends when it lands back on the ground. Mathematical constraint relations (Xiuping Mu and Qiong Wu., 2004) are as follows:

Geometrical constraints:

$$y_a(0) = 0 \quad (D.3)$$

$$y_a(T_s) = 0 \quad (D.4)$$

Maximum clearance of swing limb from ground:

$$y_a(T_m) = H_m \quad (D.5)$$

$$\dot{y}_a(T_m) = 0 \quad (D.6)$$

$$x_a(T_m) = S_m \quad (D.7)$$

Minimizing impact effect:

$$\dot{y}_a(T_s) = 0 \quad (D.8)$$

$$\dot{x}_a(T_s) = 0 \quad (D.9)$$

Gait repeatability:

$$x_a(0) = -\frac{S_L}{2} \quad (D.10)$$

$$x_a(T_s) = \frac{S_L}{2} \quad (D.11)$$

$$\dot{x}_a(0) = 0 \quad (D.12)$$

$$\dot{y}_a(0) = 0 \quad (D.13)$$

Where  $T_m$  is the time instant when the tip of the swing limb reaches to maximum clearance from the ground,  $H_h$  is the maximum clearance (y-axis) of swing limb from the ground,  $S_m$  is the location of maximum clearance (x-axis), and  $S_L$  is the step length. The above Eqs. (D.1)-(D.13) can be used for determining polynomial coefficients which are as follows:

$$a_0 = -0.36, \quad a_1 = 0, \quad a_2 = 6, \quad a_3 = -6.667$$

$$b_0 = 0, \quad b_1 = 0, \quad b_2 = 2.22, \quad b_3 = -7.4074, \quad b_4 = 6.1728, \quad b_5 = 0$$

### D.1.2 Hip Trajectory

Hip trajectory plays a significant role on biped stability. Hip trajectory is designed separately for SSP and DSP. A third order polynomial is used to define its x-coordinate while y-coordinate maintains constant. Thus trajectory of hip in SSP and DSP are as follows:

$$x_{hs}(t) = c_0 + c_1t + c_2t^2 + c_3t^3 \quad 0 \leq t \leq T_s \quad (D.14)$$

$$x_{hd}(t) = d_0 + d_1t + d_2t^2 + d_3t^3 \quad 0 \leq t \leq T_d \quad (D.15)$$

$$y_{hs}(t) = H_h \quad 0 \leq t \leq T_s \quad (D.16)$$

$$y_{hd}(t) = H_h \quad 0 \leq t \leq T_d \quad (D.17)$$

At time  $t$ ,  $x_{hs}$  and  $x_{hd}$  denote x coordinates of hip during SSP and DSP, respectively, whereas  $y_{hs}$  and  $y_{hd}$  are y- coordinates. There are 8 unknown polynomial coefficients  $c_0, c_1, \dots, c_3$  in Eq. (D.14) and  $d_0, d_1, \dots, d_3$  in Eq. (D.15).  $H_h$  is the height of hip which is kept constant for whole gait cycle. Mathematically, the constraints (Mu and Wu., 2004) are presented as follows:

Gait repeatability (SSP and DSP):

$$x_{hs}(0) = -S_{so} \quad (D.18)$$

$$\dot{x}_{hs}(0) = V_{h1} \quad (D.19)$$

$$\dot{x}_{hd}(T_d) = V_{h1} \quad (D.20)$$

$$x_{hd}(T_d) = 0.5S_L - S_{so} \quad (D.21)$$

Gait continuity (SSP and DSP):

$$x_{hd}(0) = S_{do} \quad (D.22)$$

$$x_{hs}(T_s) = S_{do} \quad (D.23)$$

$$\dot{x}_{hs}(T_s) = V_{h2} \quad (D.24)$$

$$\dot{x}_{hd}(0) = V_{h2} \quad (D.25)$$

Where  $S_{so}$  and  $S_{do}$  represents position of the hip at the beginning of SSP and DSP respectively. The above Eqs. (D.18)-(D.25) can be used for determining unknown polynomial coefficients which are as follows:

$$c_0 = -0.18, \quad c_1 = 0.4, \quad c_2 = 1.1667, \quad c_3 = -1.3889$$

$$d_0 = 0.18, \quad d_1 = 0.3, \quad d_2 = 0.8, \quad d_3 = -2.0$$

## D.2 Joint Profile Generation

The joint angle profiles can be derived from designed trajectories of swing limb and hip using geometric solution approach of inverse kinematics.

### Joint Trajectory in DSP

Simple geometric relations are desired for the SSP and DSP which are presented in Table D.1.

**Table D.1:** SSP and DSP geometric relations

SSP (Haghighi et al.,2011)	DSP
<b>For Swing Leg</b>	<b>For Swing Leg</b>

---

$x \text{ coordinate} = x_{hs}$ $y \text{ coordinate} = y_{hs}$ $L_s^2 = x_{hs}^2 + y_{hs}^2$ $\gamma_1 = \tan^{-1} \frac{x_{hs}}{y_{hs}}$ $\beta_1 = \sin^{-1} \frac{l_2 \sin \alpha}{L_s}$ $\alpha_1 = \cos^{-1} \frac{-L_s^2 + l_1^2 + l_2^2}{2l_1 l_2}$ $\theta_2 = \gamma_1 - \beta_1$ $\theta_1 = \theta_2 + \pi - \alpha_1$ $\theta_3 = 0$	$x_{diffs} = x_{hd}$ $y_{diffs} = y_{hs}$ $L_{ds} = \sqrt{x_{diffs}^2 + y_{diffs}^2}$ $\gamma_{ds} = \tan^{-1} \frac{x_{hd}}{y_{hs}}$ $\beta_{ds} = \cos^{-1} \frac{L_s^2 + l_2^2 - l_1^2}{2L_{ds} l_2}$ $\alpha_{ds} = \cos^{-1} \frac{-L_{ds}^2 + l_1^2 + l_2^2}{2l_2 l_1}$ $\theta_{2d} = \gamma_{ds} - \beta_{ds}$ $\theta_{1d} = \theta_{2d} + (\pi - \alpha_{ds})$ $\theta_{3d} = 0$
---	--

---

<p style="text-align: center;"><b>For Support Leg</b></p> $x_{diff} = x_a - x_{hs}$ $y_{diff} = y_{hs} - y_a$ $L_p^2 = x_{diff}^2 + y_{diff}^2$ $\gamma_2 = \tan^{-1} \frac{x_{diff}}{y_{diff}}$ $\beta_2 = \sin^{-1} \frac{l_5 \sin \alpha_2}{L_p}$ $\alpha_2 = \cos^{-1} \frac{-L_p^2 + l_4^2 + l_5^2}{2l_4 l_5}$ $\theta_4 = \gamma_2 + \beta_2$ $\theta_5 = \theta_4 - (\pi - \alpha_2)$	<p style="text-align: center;"><b>For Support Leg</b></p> $x_{diffdsp} = 0.5S_L - x_{hd}$ $y_{diffdsp} = y_{hs}$ $L_{dsp} = \sqrt{x_{diffdsp}^2 + y_{diffdsp}^2}$ $\gamma_{dsp} = \tan^{-1} \frac{x_{diffdsp}}{y_{diffdsp}}$ $\beta_{dsp} = \cos^{-1} \frac{L_{dsp}^2 + l_4^2 - l_5^2}{2L_{dsp} l_4}$ $\alpha_{dsp} = \cos^{-1} \frac{-L_{dsp}^2 + l_4^2 + l_5^2}{2l_4 l_5}$ $\theta_{4d} = \gamma_{dsp} + \beta_{dsp}$ $\theta_{5d} = \theta_{4d} - (\pi - \alpha_{dsp})$
---	---

---

*Note the swing and stance phase models are utilized to generate the foot trajectory for the gait-inspired synthesis, in Chapter 6.*

The notations are defined in Fig D.3 and similar diagram can be used for modeling in SSP. The above method is useful for generating the joint trajectory for steady walking on the leveled ground.

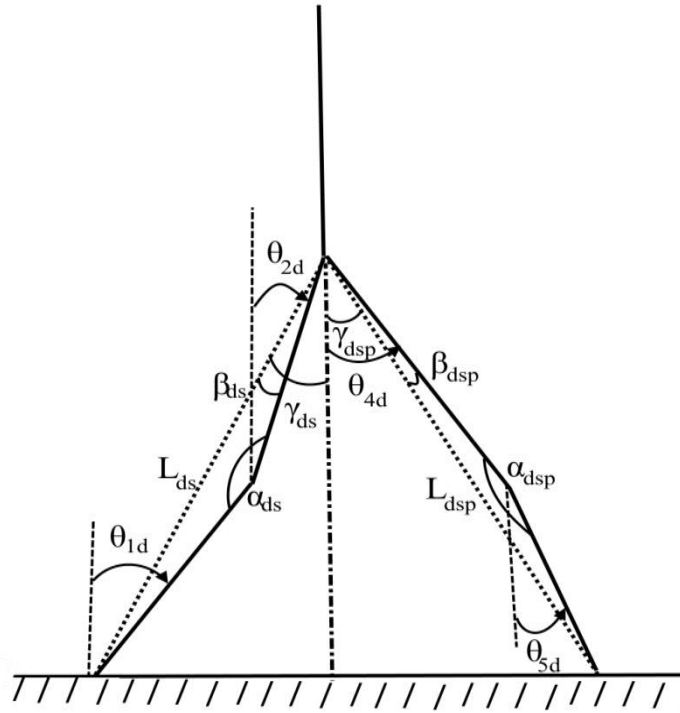


**Fig. D.3** Various definitions for five-link biped in DSP

### D.3 Numerical Example

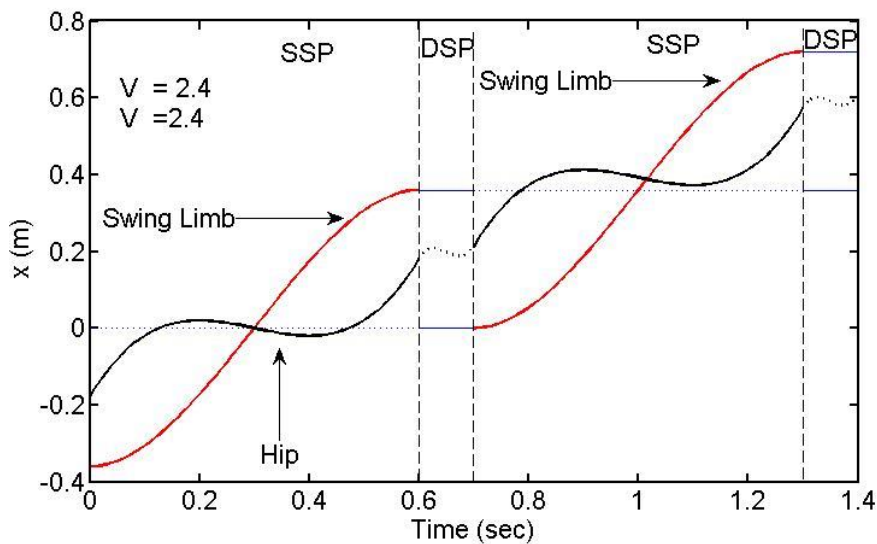
A planar five-link biped model is used here for sagittal position analysis. The values physical parameters (links) of biped are  $l_1=0.332$ ,  $l_2=0.302$ ,  $l_3=0.486$ ,  $l_4=0.302$ ,  $l_5=0.332$ ,  $d_1=0.189$ ,  $d_2=0.236$ ,  $d_3=0.282$ ,  $d_4=0.236$ ,  $d_5=0.189$ . All dimensions are in meter. While other variables are  $S_L=0.72$ ,  $T_s=0.6$ ,  $T_d=0.1$ ,  $H_m=0.05$ ,  $S_m=0$ ,  $T_m=0.3$ ,  $H_h=0.575$ ,  $S_{so}=0.18$ ,  $S_{do}=0.18$ . Several hip trajectories corresponding to  $V_{h1}$  and  $V_{h2}$  are obtained, and two are shown in Fig D.4. From the series of values of  $V_{h1}$  and  $V_{h2}$ , those values are selected for which smooth hip trajectory is obtained in SSP and DSP. The smooth hip trajectory shown in Fig D.5. is obtained when  $V_{h1}=0.4$  and  $V_{h2}=0.3$ . This smooth trajectory is selected for deriving the joint profiles.

### D.4 Discussion

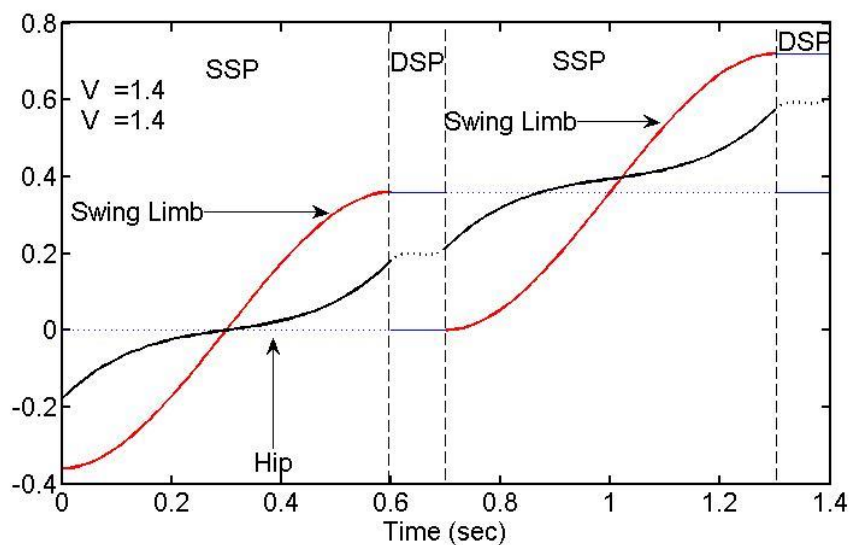
The horizontal displacements of hip, swing limb tip and stance limb with respect to time is shown in Fig D.5. Figure D.6. shows the path traced by the left and right limb for complete gait cycle. Joint profiles derived by inverse kinematics for all the joints are shown in Fig D.7. It is observed from Fig D.7. that trajectories are smooth and repeatable. Figure D.8 shows the stick diagram of the five-link bipedal robot. It shows the overall motion of biped for one complete gait cycle. Torso is represented by blue colour, red colour represents left limb and right limb is represented by black colour, it is observed that initial and final posture of biped is same.



This appendix presents a systematic geometrical method for determining joints angle profiles for a five-link bipedal robot with attention being focused on DSP. As most of the previous works have focused on SSP and DSP is often neglected. This model includes both SSP and DSP but only DSP diagram is used to explain geometric relations. To demonstrate the effectiveness of this method computer simulation was carried out. It was found that gait pattern appears natural. This research provides a tool for generating walking patterns. This work can be extended to a 7 link model on different planes with stability check.



a)



b)

**Fig. D.4** *x*-displacement of hip and feet a) When  $V_{h1}=V_{h2} =2.4$  m/s b) When  $V_{h1}=V_{h2} = 1.4$  m/s

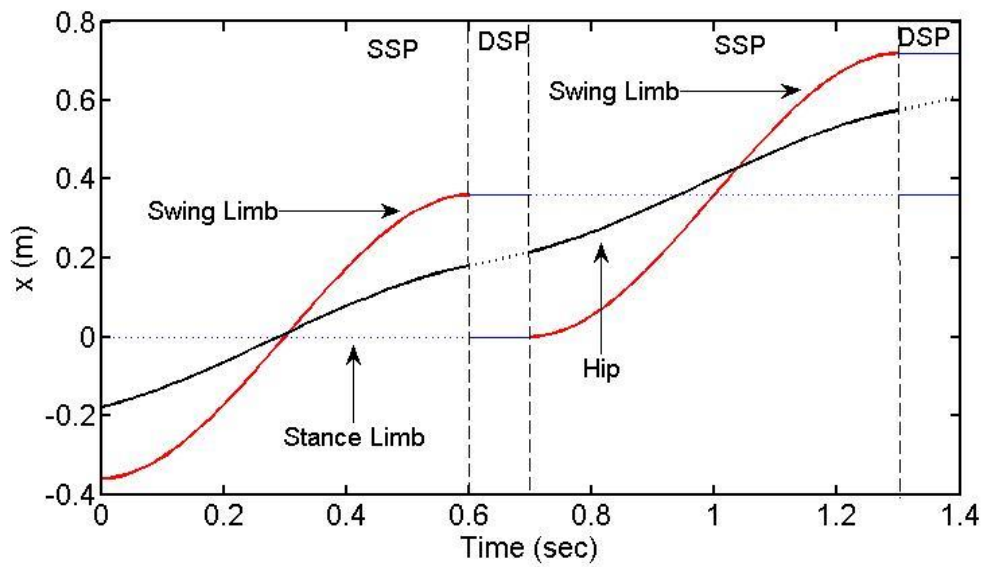


*Fig. D.5 Hip and lower limb trajectories when  $V_{h1}=0.4$  and  $V_{h2}=0.3$  m/s*

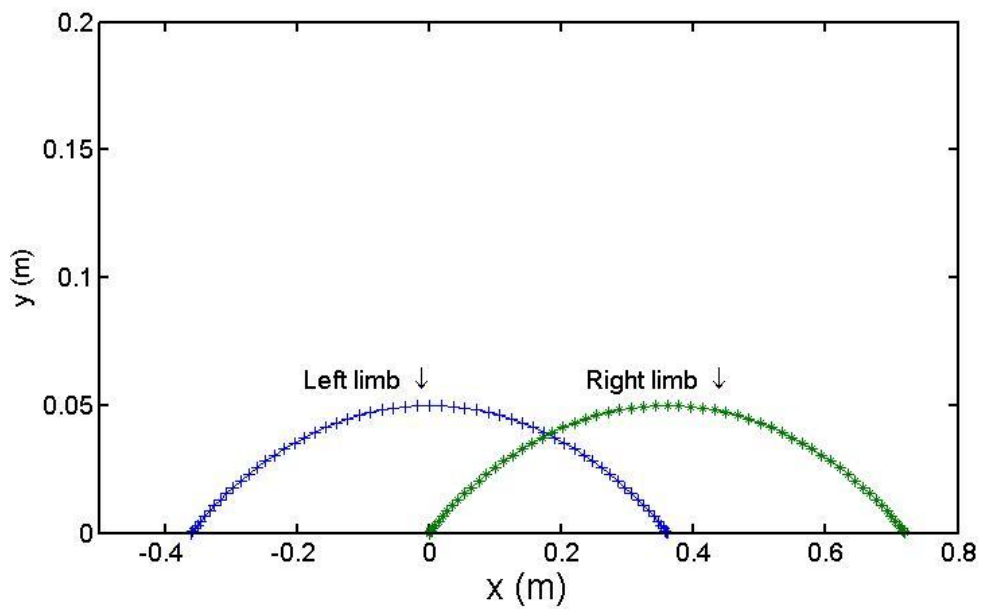


*Fig. D.6 Lower limb trajectories*

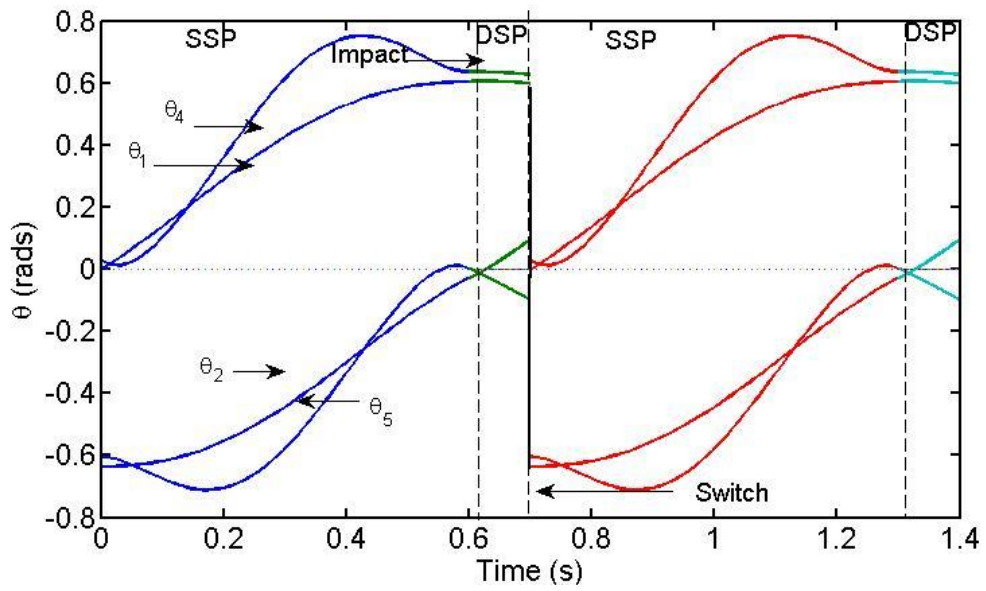


**Fig. D.7** Joint angle profiles

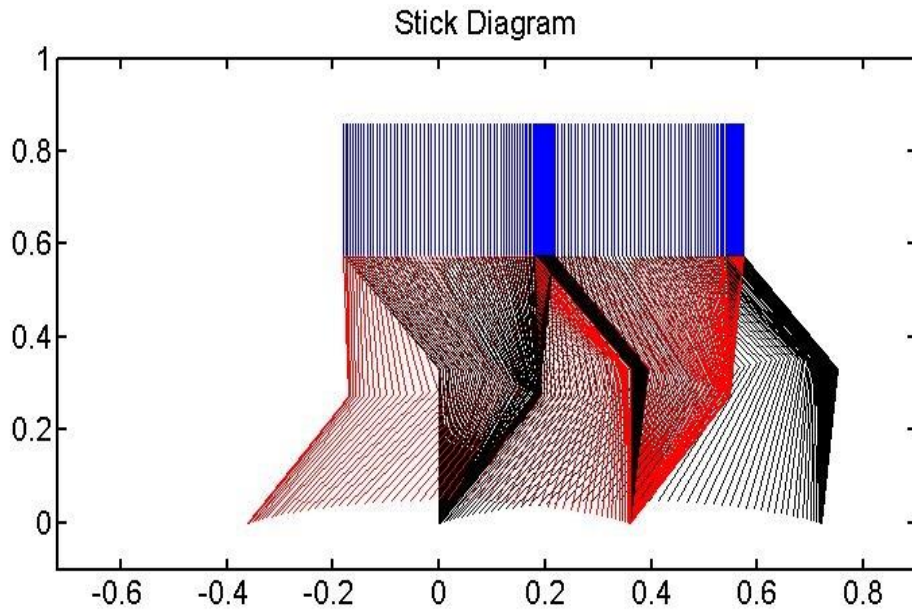


**Fig. D.8:** Stick diagram



## **Papers Published/Submitted/Presented Based On This Work**

### **SCI Journals**

1. Singh R, Chaudhary H, Singh AK. Defect-free optimal synthesis of crank-rocker linkage using nature-inspired optimization algorithms. *Mechanism and Machine Theory*. 2017 Oct 1;116:105-22.
2. Singh R, Chaudhary H, Singh AK. A novel gait-based synthesis procedure for the design of 4-bar exoskeleton with natural trajectories. *Journal of Orthopaedic Translation*. 2018 Jan 1;12:6-15.
3. Singh R, Chaudhary H, Singh AK. A new hybrid teaching–learning particle swarm optimization algorithm for synthesis of linkages to generate path. *Sādhanā*. 2017 Nov 1;42(11):1851-70.
4. Singh R, Chaudhary H, Singh AK. A loop-by-loop defect rectification procedure for optimal synthesis of Stephenson III path generators. Submitted to *Mechanism and Machine Theory*, November 2017.
5. Singh R, Chaudhary H, Singh AK. A Novel Gait-Inspired Four-Bar Lower Limb exoskeleton to Guide the Walking Movement. Submitted to *Journal of Mechanics in Medicine and Biology*, July 2017.

### **SCOPUS Journal**

1. Singh R, Chaudhary H, Singh AK. Shape synthesis of an assistive knee exoskeleton device to support knee joint and rehabilitate gait. *Disability and Rehabilitation: Assistive Technology*. 2018 Jul 16:1-9.

### **Refereed Conference Proceedings**

1. Singh R, Chaudhary H, Singh AK. Sagittal Position Analysis of Gait Cycle for a Five Link Biped Robot. In *CAD/CAM, Robotics and Factories of the Future 2016* (pp. 387-396). Springer, New Delhi.
2. Singh R, Chaudhary H, Singh AK. Optimal synthesis of crank-rocker linkage for exoskeleton knee. In *Recent Advances and Innovations in Engineering (ICRAIE)*, 2016 International Conference on 2016 Dec 23 (pp. 1-5). IEEE.



## Brief Bio-data of the Author

Name : **Ramanpreet Singh**  
 Date of birth : December 27, 1986  
 Address for correspondence : H.N. 43, Chandi Ki Taksal,  
 Jaipur (Rajasthan), India - 302002

### Education:

Degree	Discipline	Institute	Board/University	Percentage	Year	Division
Secondary	--	Saint Soldier Public School Jaipur	CBSE	77.4	2002	First
Senior Secondary	PCM	Saint Soldier Public School Jaipur	CBSE	75.8	2004	First
B.E.	Mechanical Engineering	Manipal Institute of Technology, Manipal	Manipal University, Manipal, Karnataka	86.2	2009	First
M.Tech.	Mechanical Engineering (Design)	Lovely Professional University	Lovely Professional University, Punjab		2014	First
Ph.D.	Mechanical Engineering	Malaviya National Institute of Technology Jaipur	Autonomous	---	Thesis submitted in February 2018	---

### Teaching Experience:

Organisation	Designation	Service Period
Poornima Institute of Engineering and Technology, Jaipur	Lecturer	July,2009-December,2009
Poornima Group of Institutions, Jaipur	Lecturer	September, 2010-May,2011
Lovely Professional University, Punjab	Lecturer	July, 2011-April, 2014
Manipal University Jaipur	Assistant Professor	August, 2018-Present

### Industrial Experience:

Organisation	Designation	Service Period
TCS, Bangalore	ASE(Trainee)	December, 2009-July, 2010
C21 Mall Indore	Maintenance Manager	May, 2011-July, 2011

Membership of Professional Society: Association for Machines and Mechanisms

India

Awards and achievements

- Fellowship for Ph. D., granted by Ministry of Human Resources and Development India. (2014-2018).
- Honored with Academic Achievers Award by the Honorable Chancellor of Lovely Professional. (2015).
- University Gold Medalist in M.Tech. (2015).
- Editor-in-Chief article choice award for “A Novel Gait-Based Synthesis Procedure for the Design of 4-Bar Exoskeleton with Natural Trajectories” by Journal of Orthopaedic Translation (SCI Journal) (2017)
- Recognized Reviewer Award by Mechanism and Machine Theory Journal, June 2018
- Outstanding Reviewer Award by Mechanism and Machine Theory Journal, Elsevier, August, 2018